The Case for Stainless Steel Reinforcing Bars

by

Colin Bradley Van Niejenhuis

A thesis
presented to the University of Waterloo
in fulfilment of the
thesis requirement for the degree of
Master of Applied Science
in
Civil Engineering

Waterloo, Ontario, Canada, 2015

I hereby declare that I am the sole author of this thesis. This is a true copy of the thesis including any required final revisions, as accepted by my examiners.

I understand that my thesis may be made electronically available to the public.

Abstract

As Canada's ever expanding transportation network continues to age, the costs associated with rehabilitating and replacing structural elements, such as bridges, continues to grow. This rehabilitation is often required because the structural reinforcing has begun to corrode, producing corrosion product with a larger volume than the initial reinforcing steel, which leads to cracking and de-bonding of the concrete. In the past, most departments of transportation have used low cost, carbon steel. Now, as the Ministry of Transportation of Ontario looks for alternative materials with longer service lives, the use of stainless steel reinforcing bars in critical structural locations has become increasingly financially feasible.

Thus, at the request of the Ministry of Transportation of Ontario, an experimental and analytical projected was undertaken to compare the corrosion resistance of six stainless steels and two corrosion resistant reinforcements: S31653, S32205, S32101, S30403, S24100, S32304, MMFX, and galvanized steel with that of the traditional low carbon 400W reinforcement. There are two objective of the project, first to experimentally compare the corrosion resistance of the different reinforcements in both sound and cracked concrete while being exposed to a 21.1% chloride brine, while the second is to create a model for the corrosion-limited service life of reinforced concrete, which includes both sound and cracked concrete.

The experimental monitoring included comparing the corrosion resistance of the different reinforcements in: sound (non-cracked) concrete, concrete with a crack transverse to the reinforcement, and concrete with a longitudinal crack above, and parallel to, the reinforcement. After the concrete was cured for 28 days, the cracks were induced, and the sides that did not contain the cracks were coated with epoxy to ensure unidirectional chloride diffusion through the exposed area and the cracked region. The specimens were then monitored by conducting galvanostatic pulse (GP) tests weekly and linear polarization resistance (LPR) tests monthly. The resulting corrosion current density (i_{corr}) and open circuit potentials (E_{corr}) values were monitored over a 600 day exposure period. Both the i_{corr} and E_{corr} data indicate that the reinforcement in the sound concrete specimens remained passive over this period and, therefore, monitoring will continue until active corrosion initiates. In the longitudinal and transversely cracked concrete, the i_{corr} and E_{corr} values indicated that corrosion had initiated in a number of specimens, so all the specimens

were removed from their chloride baths, autopsied, inspected, and ranked. The ranking of reinforcement from most resistant to least corrosion resistant is as follows: S32205, S32101, S32304, S30403, S31653, S24100, galvanized, MMFX, and 400W.

The corrosion modelling expanded upon two models from the literature, Hartt et al. [1] and Lu et al. [2], by using Fick's second law to model the ingress of chloride in both sound and cracked concrete. Once the model was created, a Monte Carlo simulation was performed to statistically determine the effects of: crack width, crack density, concrete cover, chloride threshold concentration, surface chloride concentration, and chloride diffusion on the expected life of a concrete structure with both a 100 and 300 year service life. This allowed a critical cost ratio (CCR) to be computed, solely on the value of the reinforcement without taking into account any other owner or social costs. The CCR is defined as how much an owner would be willing to pay for corrosion resistant steel compared with 400W steel over the life of the structure. The results of this analysis can be summarized in three ways. First, this procedure has determined that the parameters that have the greatest effect on the service life of the structure from least to greatest are: surface chloride concentration, crack width and density, chloride diffusion rate of the concrete, and the chloride threshold level of the proposed alternative stainless steel. If the structural designer actively designs to limit the first three parameters, the financial feasibility of corrosion resistant reinforcing dramatically decreased. Second, 15 design curves have been created to help designers quickly assess the financial feasibility of corrosion resistant reinforcement based on the specific requirements of their highway structure. Third, if the design curves suggest corrosion resistant reinforcement is viable, it is recommended that the analysis be re-run for the proposed reinforcement once the chloride threshold for the specific corrosion resistant rebar grade and local surface chloride accumulations have been determined. This will allow the designers to have site specific critical cost ratios, allowing them to determine if the owner or societal costs must be included in the feasibility study.

Both the experimental and modelling data strongly suggest that corrosion resistant steel, especially S32205 and S32101, are financially viable replacements for traditional 400W reinforcement, especially in critical structural applications where access or user delay costs prohibit frequent replacement or rehabilitation.

Acknowledgements

I would like to sincerely thank Dr. Scott Walbridge, and Dr. Carolyn Hansson, without whom my pursuit of graduate studies would never have been possible. The advice they have given has shaped the way I view research, and has increased my passion for discovery. I would like to thank our lab group: Brad Bergsma, Matt Hunt, James Cameron and Tim Bandura as well as the structural lab group: Doug Hirst and Richard Morrisson for the help provided along the way.

Without the financial support of the Ministry of Transportation of Ontario and materials supplied by: Holcim Canada, Valbruna, Otukompu, Talley, and Harris Rebar Ltd. this project would not have been possible.

Finally, I would like to thank my parents and family for standing behind my higher education, and pushing me excel in everything I do. Last but not least I would like to thank my loving wife Lindsay for being patient and always supporting and inspiring me.

Table of Contents

List of Figures

List of Tables

List of Equations

List of Variables

Variable	Units	Definition
A	$\frac{m^2}{m^2}$	Total area of sound concrete per metre squared of deck area
A_{cr}	$\frac{m^2}{m^2}$	Total area of cracks per metre squared of deck area
B	mV	Stearn-Geary constant (typically taken as 26mV for the passive state, or 52 mV for the active state)
CCR	-	Critical cost ratio: the ratio of how much more an owner is will to pay for stainless steel compared with black steel
$C(x,T)$	$\frac{kg}{m^3}$	Free chloride concentration at a depth x at a time T
C_s	$\frac{kg}{m^3}$	Surface chloride content
CR_{AVG}	$\frac{\mu m}{year}$	Average corrosion rate over the whole rebar surface
Cost_{bb}	$\frac{\$}{kg}$	Current cost of the black bar
Cost_{ss}	$\frac{\$}{kg}$	Cost of stainless steel required to make the net present value of the structure with the black steel and stainless steel equal
D_a	$\frac{m^2}{s}$	Apparent diffusion coefficient of the sound concrete
D_{cc}	$\frac{m^2}{s}$	Combined chloride diffusion coefficeint
D_{cr}	$\frac{m^2}{s}$	Apparent chloride diffusion coefficient of the cracked concrete
ERF	-	Gaussian error function
E_{corr}	V or mV	Open circuit potential
f'_c	MPa	Compressive strength of a standard cylinder (MPa)

i_{corr}	$\frac{A}{m^2}$	Corrosion current density
L	m	Bar length
m	-	Number of replacements of the structure using stainless steel
n	-	Number of replacements of the structure using black steel
NPV_{bb}	$	Net present value of the structure using black bar
R_p	-	Polarization resistance
t	Years	Number of years since the installation of the 1st structure
t_i	Years	Time to corrosion initiation
t_p	Years	Propogation time from corrosion initiation until concrete spalling renders the structure unusable
t_s	Years	Total service life
x	m	Concrete cover
W_k	m	Crack width
ø	mm	Diameter
ϕ	m	Bar diameter
γ	%	*D*iscount rate
χ_{Crit}	mm	Critical corrosion section loss required to crack the concrete

Chapter 1 Introduction

1.1. Background

Concrete structures make up a significant percentage of the aging national infrastructure system. As a result, the durability and life cycle costs associated with the maintenance of these structures has never been of higher importance. Concrete structures play a pivotal role in: buildings, highway and utility networks, national defence, and marine applications. These structures often play a critical role in public safety (e.g. bridges on major transportation links, hospitals, dams, etc.) Although concrete would appear to be a very durable, long lasting building material, concrete structures are extremely susceptible to deterioration in harsh environments, such as those where repetitive freeze thaw cycles and high chloride levels are present.

What makes concrete such a durable material is that fact that it is: resistant to water ingress (limiting shrinkage and warping seen in timber), stable in the natural environment, and extremely strong in compression. The low strength of concrete in tension, on the other hand, is a challenge that must be overcome in the design of concrete structures. With the exception of dome and arch structures, which carry primarily compressive forces, tensile forces will invariably be induced. These tensile forces can be resisted by embedding steel reinforcing bars (rebar) in the concrete, creating a relatively durable composite material, but one that is susceptible to another form of deterioration – corrosion of the reinforcing bars.

In the production of steel, the base materials are altered from a lower energy state, to a higher energy state. Reversing this change is the driving force for corrosion as the steel wants to return to its lower free energy state. Although the concrete initially protects the steel by forming a passive film on the surface, corrosion will eventually initiate [3].The two most common causes for corrosion of rebar in concrete are carbonation and chloride ingress. Carbonation is a chemical reaction of carbon dioxide, and the calcium-silicate-hydrate in the concrete. This reaction produces calcium carbonate and water, which reduces the pH and changes the permeability of the surface concrete [4]. As the pH decreases, the passive film that was protecting the steel from actively corroding breaks down and the steel becomes susceptible to rapid corrosion. Chloride ingress is the more common cause for corrosion, especially in marine environments and for highway infrastructure subjected to de-icing salts. As salt concentrations build up on the surface, the

chlorides begin to diffuse through the concrete, eventually reaching the surface of the rebar. Once the chloride concentration surpasses a threshold value, typically believed to be 0.4% - 0.5% by weight of cementitious material for standard black rebar, active corrosion is likely to initiate [5].

Traditional carbon steel reinforcing bars (black rebar) in Canada are used in most regular concrete applications because of the metal's low cost and its passivity in high pH environments. These bars typically consist of low alloy steel with a yield strength of 400 to 500 MPa, which conforms to CSA G30.18 [6]. These reinforcing bars, can be either weldable or non-weldable. Depending on the structural application and geometry, bar diameters from 10 mm to 55 mm can be specified and are readily available (see Table 1-1).

Table 1-1: Properties of deformed reinforcing bars [6]

Properties of Deformed Reinforcing Bars				
Bar Designation	Nominal Dimension			Mass Per Unit Length (kg/m)
	Diameter (mm)	Area (mm^2)	Perimeter (mm)	
10	11.3	100	35.5	0.785
15	16	200	50.1	1.57
20	19.5	300	61.3	2.355
25	25.2	500	79.2	3.925
30	29.9	700	93.9	5.495
35	35.7	1000	112.2	7.85
45	43.7	1500	137.3	11.775
55	56.4	2500	177.2	19.625

Corrosion of machinery and infrastructure in general has a detrimental effect on all sectors of society including: transportation, infrastructure, utilities, manufacturing, and government. A 2002 report by the US Department of Transportation Federal Highway Administration [7] stated that the direct cost of corrosion in that industry was approximately $137.9 billion/year. When this was

extrapolated to include indirect costs, it exceeded $279 billion/year, or 3.1% of the US gross domestic product (GDP) in 1998 when the data was collected (see Figure 1-1).

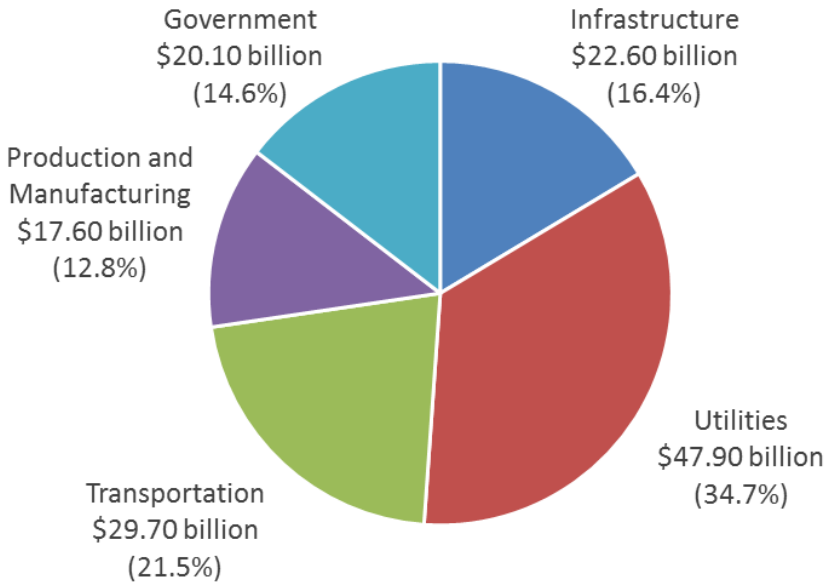

Figure 1-1: Cost of corrosion in industry categories [7]

Highway bridges fall under the infrastructure category, and comprise 37% of the initial estimate of $22.6 billion/year (see Figure 1-2). This was broken down into four categories: $3.8 billion to replace structurally deficient bridges, $2 billion for maintenance and capital costs of concrete bridge decks, $2 billion for concrete substructure, and $0.5 billion for maintenance of steel bridge structures [7]. Although the direct annual cost of corrosion here is assumed to be $8.3 billion, it is estimated that the indirect costs (eg. user delays, environmental disturbances, elevated noise levels, increased accidents [8, 9]) can run up to 10 times more than the direct costs.

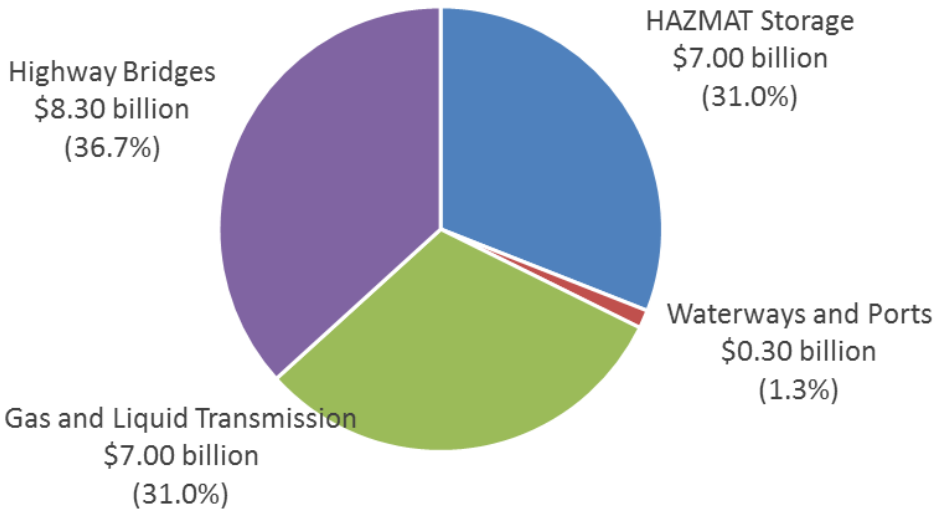

Figure 1-2: Infrastructure cost of corrosion [7]

If it is assumed that, although the infrastructure has aged, the percentage of GDP remains the same, the direct cost of corrosion would be approximately 520 billion dollars annually, based on 16.8 the trillion GDP in 2013 [10].

To compare Ontario's infrastructure with that of the United States, a study by statistics Canada [11], which finished in 2007, determined that the average age of Ontario's bridge and overpass infrastructure was 24.1 years, which is slightly lower than the all-time high of 24.5 years. This means that the 2600 bridges under MTO's jurisdiction in the year 2000 [12], had reached an average of 56 percent of their useable service life, which changed from a 50 year to a 75 year design life when CSA-S6-00 was introduced [13, 14]. By comparison, Transportation for America reported in 2013 [15] that American bridges average 43 years of age. The report also suggests that 11% of American bridges are deficient, with an average age of 65 years for these bridges.

1.2. Research Objectives

As the Ministry of Transportation of Ontario (MTO) continues to strive to improve the state of the highway infrastructure in Ontario, the need to provide structures with increased service lives is paramount. As such, the MTO now requires bridge designs to comply with a 75 – 100 year service life, ideally without major rehabilitation. With the harsh Canadian climate, many freeze thaw

cycles, and exposure to heavy application of de-icing and anti-icing agents, there are a number of ways to reach this goal, including the use of more corrosion resistant reinforcing steels.

Against this background, the objectives of this thesis are as follows:

1) to perform corrosion tests on both sound and cracked concrete specimens to evaluate six grades of stainless steel (UNS 31603, UNS S24100, UNS 32205, UNS 32304, UNS 32101, and UNS 30403) and two grades of corrosion resistant steel (galvanized and MMFX) and compare their performance to traditional carbon steel reinforcing;
2) to develop a probabilistic model for predicting the service lives of reinforced concrete structures subjected to corrosion of the reinforcing steel, which considers the effect of cracks on the rate of chloride diffusion and the effect of the reinforcing steel grade; and
3) to use the probabilistic model, as well as a comprehensive literature review, to determine the optimal steel grade for areas of high corrosion in highway bridge structures, from the point of view of minimizing direct and indirect life-cycle costs.

1.3. Scope

As this study is limited in duration and content breadth, the scope is limited as follows:

- The experimental procedure has utilized electrochemical test methods to determine the corrosion rates of the reinforcing steel in the three different concrete environments. These measured corrosion currents are averaged over the whole exposed area of the steel to give the corrosion rates, while likely only local corrosion has initiated. Thus the electrochemical data can only be used to comparatively view the corrosion resistance of the different steels.
- The stainless steels used do not encompass all commercially available grades. This study has utilized the most common forms of steel reinforcement currently being used by departments of transportation around North America.
- By wet curing the concrete for twenty-eight days, the quality of the concrete likely exceeds that of field concrete. The results of time to corrosion initiation should be scaled back based on known black bar corrosion initiation in different concrete environments.
- The definition of failure used for the life cycle monitoring was that, once concrete spalling has occurred, the structure has come to the end of its service life, although field data

demonstrate that this is not the case. As such, the critical cost ratios demonstrate a worst case scenario.

- The assumption of averaging the chloride diffusion rate in the cracked and uncracked regions can overestimate the concrete service life because corrosion in the cracked region will occur more quickly than the program estimates, leading to higher failure rates than the analysis has suggested.

Chapter 2 Literature Review

2.1. Traditional Corrosion Resistant Concrete Reinforcement

In concrete applications which are highly susceptible to cracking and chloride attack, (highway or marine infrastructure), corrosion resistant rebar has been utilized in locations of the structure that have historically demonstrated the highest corrosion potential. For highway bridges, these areas include: bridge deck top reinforcing layers, regions around expansion joints, the bases of bridge piers subject to chloride splashing, as well as barrier walls, Figure 2-1. Knudsen et al. [16] suggest that although the initial cost of corrosion resistant or stainless steel rebar is much higher than that of black rebar, savings incurred through: increased service life, reduced reinforcement cover, and fewer social impacts through road closers make the costs comparable over an 80 year bridge design life [16]

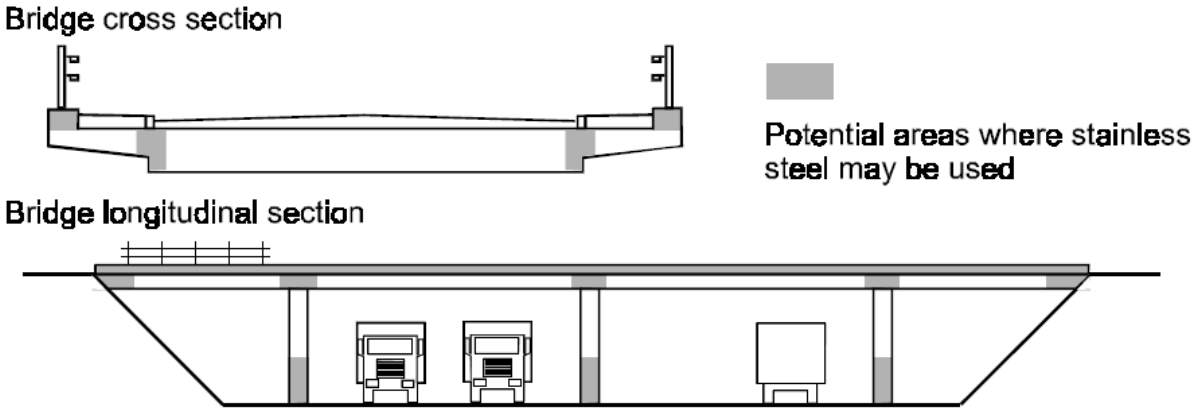

Figure 2-1: Potential cost saving region with use of corrosion resistant reinforcing [16]

Traditionally, corrosion resistant reinforcement has included products such as galvanized and epoxy coated rebar, but have grown to include glass fibre reinforced polymers (GFRP), carbon fibre reinforced polymers (CFRP), stainless steel, and proprietary products such as MMFX.

2.1.1. Epoxy Coated Rebar

Epoxy coated rebar was introduced in the 1970's, as a method of protecting black rebar from chloride ions, thereby increasing the time to corrosion initiation. The process of coating a bar in epoxy is a four part fusion bonding process. First the rebar must be cleaned of surface contamination, and all sharp and rough edges removed. Next, a chromated primer is applied to the

surface, then the bar must be heated to meet the epoxy supplier's recommendation before the epoxy coating is applied electrostatically [8]. Once an even coating has been applied, between 175 to 300 μm for straight bars [17], the coating is cured, after which the bars are cut to the required length and a patch is applied to seal the exposed ends. Until March 2013, epoxy coated rebar was a recommended corrosion resistant reinforcement in Ontario, but has since been removed from new highway infrastructure. Manning [18] concluded that research has shown that epoxy coatings fail for a number of reasons including: loss of adhesion when moisture gets under the coating, failure of coating in bend locations, and surface induced damage from improper transportation and installations practices. This has led to instances of corrosion initiation ranging between ten and thirty-five years, a limited result considering the premium paid for the product.

2.1.2. GFRP Rebar

Although fibre reinforced polymers (FRP) have been commercially available since the mid 1930's, glass fibre reinforced polymers have only been used for concrete reinforcing since the late 1970's. As the name suggests, the main constituent of a GFRP bar is a bundle of glass fibres which account for approximately 60-80% by volume of the final product [19]. The rest of the volume is made up of a resin matrix consisting of either: polyester, epoxy, or vinyl ester, depending on the mechanical properties required. The glass fibres are formed by extruding molten glass and, once drawn through the resin, the strands are oriented and compressed together then heated and pulled through shaping rollers, Figure 2-2.

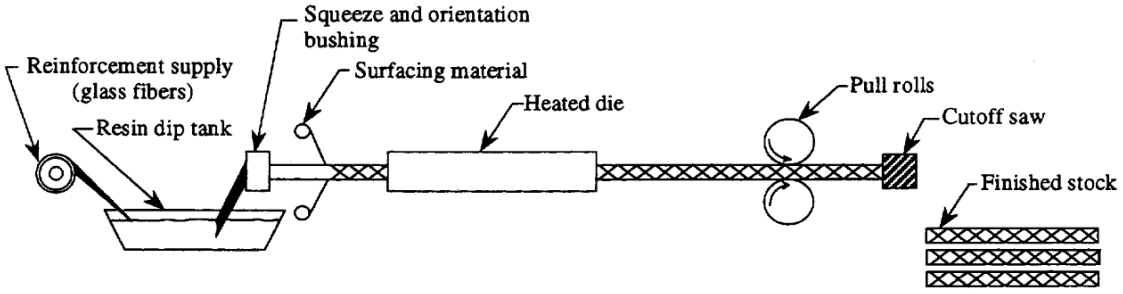

Figure 2-2: Pultrusion process of GFRP [19]

The main advantage of using GFRP instead of traditional black rebar is its non-metallic properties. These properties include: high tensile strength, no corrosion susceptibility, as well as being non-magnetic, a valuable property when used for structures housing magnetic resonance imaging

(MRI) equipment [20]. Although it seems like a prime candidate for highly corrosive environments, it also suffers from a number of durability issues that ACI Committee 440 describes in Table 2-1.

Table 2-1: Advantages and disadvantages of FRP reinforcement [20]

Advantages of FRP Reinforcement	Disadvantages of FRP Reinforcement
-High longitudinal tensile strength (varies with sign and direction of loading relative to fibres)	-No yielding before brittle rupture
-Corrosion Resistance (not dependent on a coating)	- Low transverse strength (varies with sign and direction of loading relative to fibres)
-Nonmagnetic	-Low modulus of elasticity (varies with type of reinforcing fibre)
-High fatigue endurance (varies with type of reinforcing fibres)	-Susceptibility of damage to polymeric resins and fibers under ultraviolet radiation exposure
-Lightweight (about 1/5 to 1/4 the density of steel)	-Low durability of glass fibers in a moist environment
-Low thermal and electric conductivity (for glass and aramid fibres)	-Low durability of some glass and aramid fibers in an alkaline environment
	-High coefficient of thermal expansion perpendicular to the fibers, relative to concrete
	-May be susceptible to fire depending on matrix type and concrete cover thickness

The disadvantages, alongside the limited long term data available, require extreme care to be taken when designing with GFRP.

2.1.3. Galvanized Rebar

Over the last 70-80 years, galvanized rebar has been an option for the replacement of traditional black steel in reinforced concrete due to: its stability in the lower pH environment produced by concrete carbonation, and a higher chloride threshold value than that of black steel [21]. Galvanizing utilizes the corrosion resistant attributes of zinc in concrete and is applied by hot dipping, flame spraying, or electroplating. Each process includes multiple surface preparation

stages where oxidized iron and mill scale are removed before the molten zinc layer is applied, Figure 2-3.

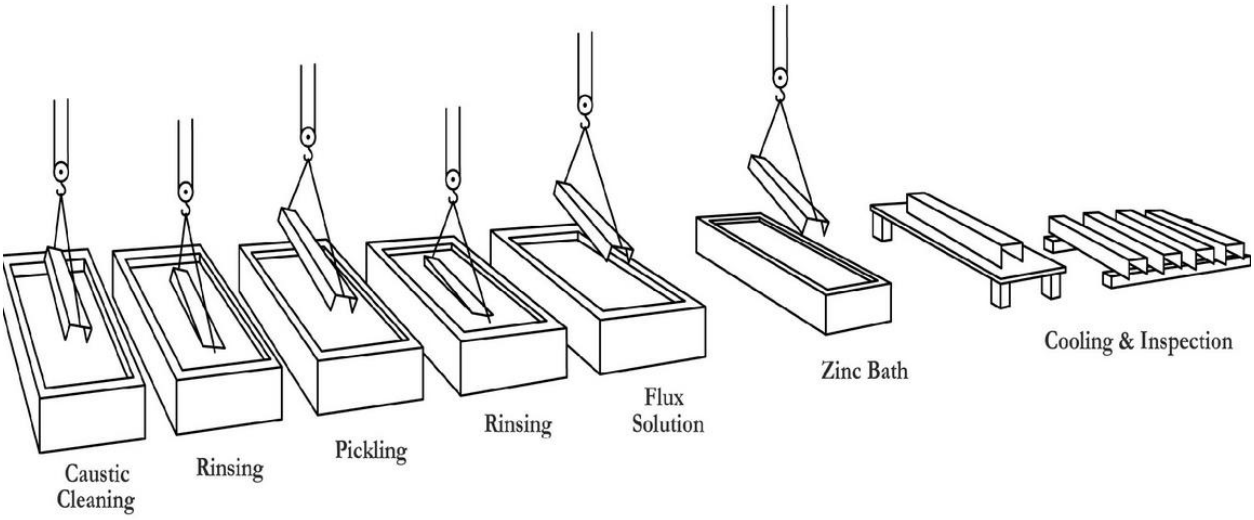

Figure 2-3: Hot dipped galvanizing process [22]

The zinc layer acts to protect the steel in two ways. First, Andrade and Macias [23] found that in solutions simulating that of concrete pores (12+/- 0.1< pH <13.3 +/- 0.1) that the galvanized steel produced a protective layer of calcium hydroxyzincate ($Ca(Zn(OH)_3)_2$), which reduces the corrosion rate of the zinc. Second, it can act as a sacrificial anode which will corrode instead of the base steel material, but after a higher chloride threshold has been surpassed. Bautista and Gonzalez [24] suggest that once active corrosion of the zinc has begun, the total thickness can be lost in less than five years, and corrosion of the black steel can commence, making galvanized steel ideal for moderately aggressive chloride concentrations .

2.1.4. Stainless Steel Concrete Reinforcement

The use of stainless steel for reinforcement has often been seen as a last resort due to the high initial cost. It is thought to have first been used between 1937 and 1941 to create a 2100 meter long pier in the Port of Progreso, Mexico [25]. In 1999, Arminox Stainless [26] conducted both a physical inspection and chloride penetration analysis, and determined that the UNS32304 stainless steel in sound concrete had exhibited little corrosion over the first 60 years of its service life. In comparison, a second pier build in the early 1970's using plain carbon steel had already completely deteriorated by 1999 and was no longer useable, Figure 2-4.

Figure 2-4: Progreso Pier, Mexico [26]

Three groups of stainless steel are typically available in today's construction market including: austenitic, duplex, and ferritic. Both the austenitic and ferritic, as their names suggest, are single phase austenite and ferrite, respectively. Austenitic stainless is often considered to have the best corrosion resistance due to its high nickel content, which comes at a price premium. Comparatively, the duplex and ferritic stainless steel have approximately half the nickel and no nickel respectively [27].

Table 2-2: Comparison of composition and mechanical properties of austenitic, duplex and ferritic stainless steel [27]

Group of Stainless Steel	Grade		Composition (EN 10088)			Ductility (% elongation)
	EN	ASTM	Cr	Ni	Mo	
Austenitic	1.4301	UNS S30403	17.5-19.5	8.0-10.5	-	45
	1.4401	UNS S31603	16.5-18.5	10.0-13.0	2.0-2.5	40
Duplex	1.4162	UNS S32101	21	1.5	0.3	30
	1.4362	UNS S32304	22.0-24.0	3.5-5.5	0.1-0.5	20
	1.4462	UNS S32205	21.0-23.0	4.5-6.5	2.5-3.5	20
Ferritic	1.451	UNS S43035	16.0-18.0	-	-	23
	1.4509	UNS S44100	17.5-18.5	-	-	18
	1.5421	UNS S44400	17.0-20.0	-	1.8-2.5	20

When comparing the prices of the different grades of stainless, it is important to look at the percentages of both molybdenum and nickel as the price per unit of these components can range from eight to thirty times as much as chromium and manganese, making 316 and 2205 the most expensive stainless steel options from a raw materials perspective, Figure 2-5.

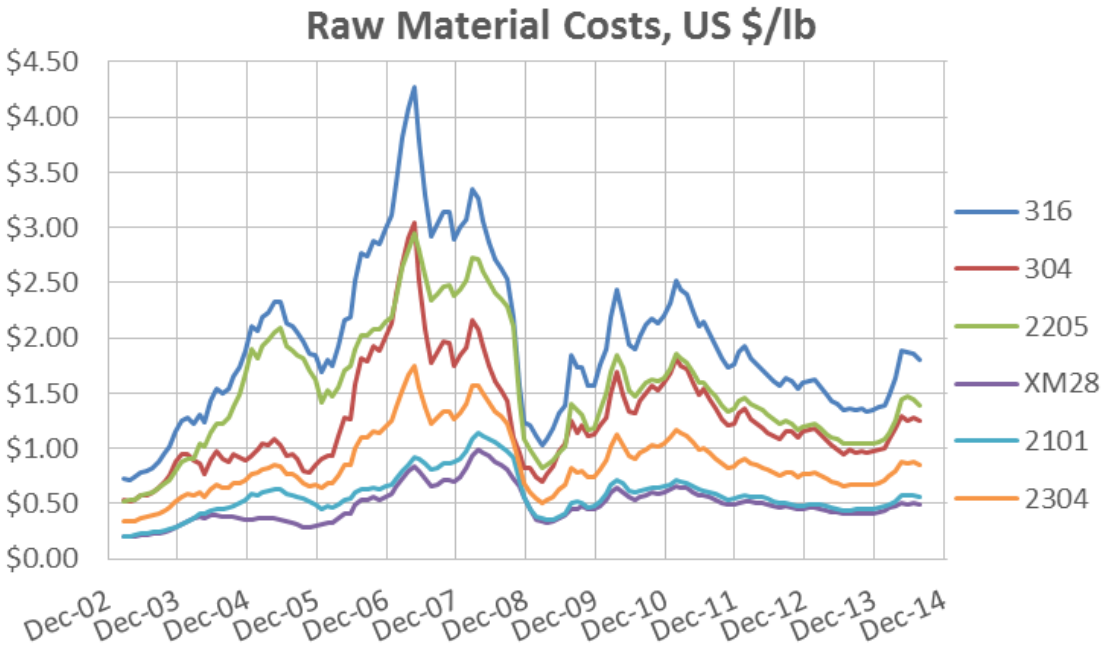

Figure 2-5: Raw material cost comparison

2.2. Chloride Threshold Values

When evaluating the corrosion resistance of steel in concrete, the chloride threshold level (CTL) is of particular interest. The chloride threshold level is the chloride concentration at which the passive layer of the steel is likely to break down and active corrosion is initiated. This concentration can be presented as either total chloride by weight % of cementitious material (weight % cement) or free (non-chemically bound) chloride (weight % cement). In order to determine these levels, a number of tests have been employed including: rebar specimens in synthetic pore solution [28, 29], rebar specimens in concrete or mortar with known amounts of admixed chlorides [30], and rebar samples removed from field applications such as bridges or piers. Although many researchers use the CLT to compare the corrosion resistance of different materials, the levels can vary significantly in single experiments, and when comparing results with many studies. Randström et al. [31] demonstrate this when comparing their own results for 2101 with those of Hurley and Scully, with values varying from 1.1-1.4 wt % to 5.7-10.6 wt %.

Table 2-3: CCLT values in wt % chlorides for the investigated stainless steel rebar grades. Comparison with other groups using a similar method have also been added. Numbers in brackets represent the number of rebar tested [31].

Stainless Steel Product	Randström et al. 2010 [31]	Bertolini et al. 1996 [32]	Bertolini et al. 2009 [33]	Hurley and Scully 2006 [34]
pH (after test)	12.8-13.3	12.6	12.6	12.6
304L	2.8-10.6	5	6.5-10	-
316L	5.7-6.8	5.5	>10	2.8-11.29
LDX 2101	5.7-10.6	-	3.5-6	1.1-1.4
2304	4.6-10.6	>10	7.5-8	-

Glass and Buenfeld [5] present Hansson and Sørensens [35] data for black steel in such a way as to emphasize how slightly differing concrete mixture designs, curing regimes and black steel surface conditions will vary the CCLT from 0.4 to 2.70 wt%, Figure 2-6.

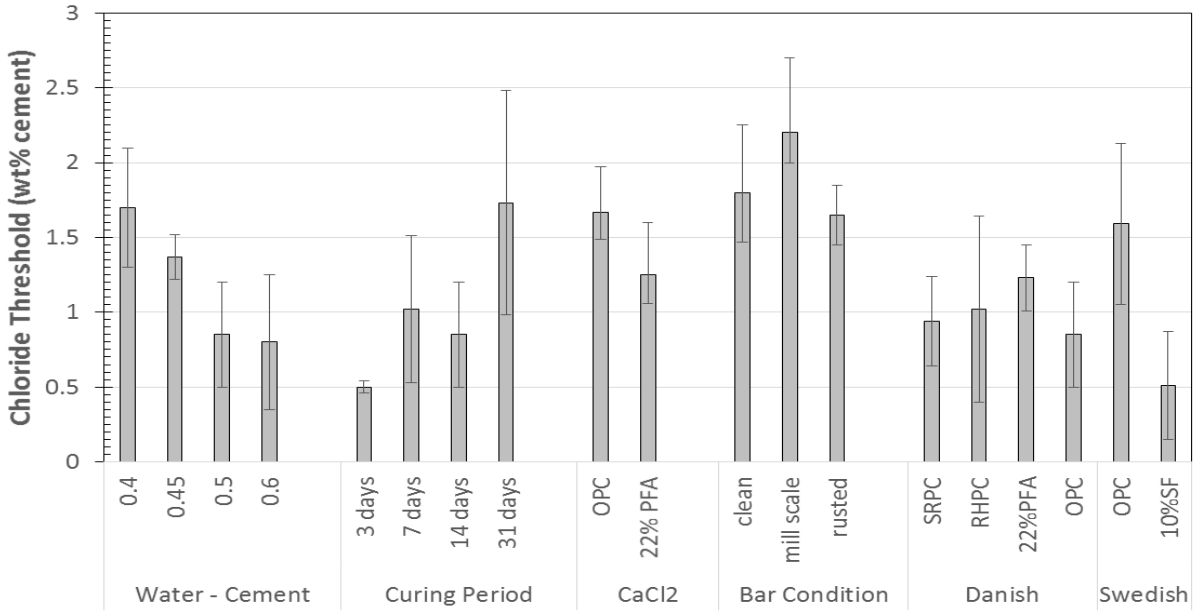

Figure 2-6: An analysis of published data giving the mean and standard deviation of the chloride threshold levels determined for six replicate mortar specimens in a range of experimental conditions [5].

2.3. Life Cycle Cost Analysis

Although corrosion of steel in concrete continues to be a large problem, federal and provincial infrastructure managers continue to fiercely debate the merits of stainless steel relative to other expensive replacement options. Without an analysis of the complete life of the structure including user costs, the up-front costs are hard to justify for materials that do not have long term service records. With the Ministry of Transportation of Ontario and other departments of transportation mandating 75-100 year life cycles for highway bridges, following the recommendation of the Canadian Bridge Design code [36], a number of studies, procedures, and programs have been completed or are ongoing. These programs aim to model: the diffusion of chlorides through both sound and cracked concrete, corrosion initiation times for numerous material types, and crack propagation and structural failure periods based on user input data.

2.4. Chloride Transportation Modelling

Since the primary cause of reinforcement corrosion is via chloride ingress, many researchers have attempted to create models that adequately explain the transportation methods of chlorides through different types of concrete. Poulsen and Moejbro [37] suggest that this transportation takes place via: diffusion, permeation, migration, or convection, with diffusion and convection being the most common.

2.5. Sound Concrete

To model diffusion many authors [1, 2, 38] use an extension of Fick's second law, which states:

$$C(x,T) = C_s \cdot \left(1 - \mathrm{ERF}\left(\frac{x}{2\sqrt{D \cdot T}}\right)\right) \qquad \text{Equation 1}$$

Where: $C(x,T)$ is the free chloride concentration (kg/m^3) at a depth x at a time T; C_s is the surface chloride content (kg/m^3), ERF is the Gaussian error function, and D is the apparent diffusion coefficient (m^2/s). Although Equation 1 appears to be straight forward if the parameters are known, determining these parameters for different environments and materials is extremely difficult. For instance, the concrete mix design, the placing, compacting and curing conditions and temperatures, and the use of water reducers, accelerators and other admixtures will drastically vary the diffusivity

of the concrete. This equation is also meant for homogeneous materials and one-dimensional diffusion, so additional considerations are needed for cracked or deteriorated concrete.

2.6. Life-365

In 1998, ACI's strategic development council specified the need for a life cycle cost analysis model, and with the funding of Master Builders Inc, Grace Construction Products, and the Silica Fume Association, the initial Life-365 program was created by Michael Thomas and Evan Bentz at the University of Toronto, and released in October of 2000 [39]. The initial program required user defined: geographic location, type of structure, type of exposure, corrosion prevention strategies, and the concrete cover. In 2008, Bentz and Ehlen were tasked with updating the software, with updates including: improved time to corrosion initiation, estimated construction costs, present worth life cycle costs, and concrete design constituents for diffusion reduction [40]. This update also takes into account the varying chloride build up rates for different regions in North America, based on local climates and de-icing techniques [41], Figure 2-7. It should be noted that for the Ontario chloride buildup range of 0.06 to 0.08 wt. % of concrete per year translates into a chloride buildup rate of between 0.35 and 0.45 wt. % cementitious material per year

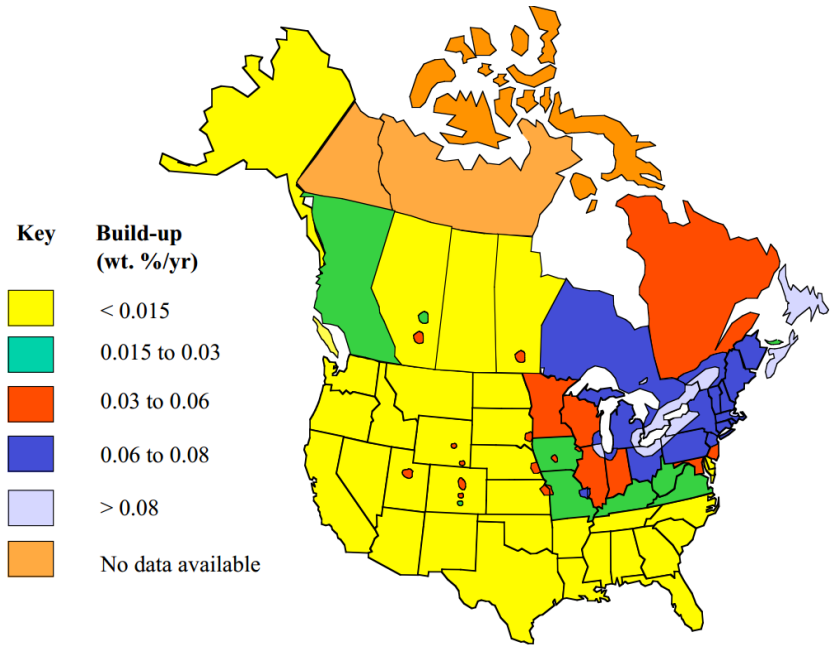

Figure 2-7: Chloride buildup rate (wt. % concrete per year) by North American Region [41]

This version of the software allows the user to analyze the financial effects of using corrosion mediation techniques such as: black vs. epoxy coated vs. stainless steel rebar, or sealers and membranes vs. supplementary cementitious materials for reducing chloride diffusion.

Although Life-365 2.0 is a very vigorous and effective tool, a number of limitations were noted which include: (i) given propagation periods for black and epoxy coated steel of 6 and 20 years, respectively, instead of a statistical or mathematical modeling approach, (ii) not including concrete cracking parameters to increase effective diffusion coefficient and (iii) utilizing a chloride threshold value for all stainless steels of 10 times that of black steel (0.5% by weight of cementitious material) instead of a grade comparison technique.

2.7. Concrete Cover

Concrete cover for structural members is designed to limit the chloride ingress and the time to corrosion initiation. The concrete cover requirements vary drastically based on exposure condition (sea water, de-icing solutions, sulphate exposure, freeze thaw etc.), or the application of the member. An example of this is the CSA [6] requirements for black rebar in: beams, girders, columns, and piles not exposed to chlorides or freeze thaw cycles versus structurally reinforced concrete exposed to chlorides and extreme environments with high durability requirements, which require 30mm and 60mm of concrete cover respectively. When used in highway structure design, the minimum concrete cover increases, Table 2-4, due to the high costs associated with the repair or replacement.

Table 2-4: Minimum concrete covers and tolerances, Canadian Highway Bridge Design Code [36]

Environmental exposure		Component	Reinforcement/ steel ducts	Concrete cover and tolerances	
				Cast-in-place, mm	Precast concrete, mm
De-icing chemicals; spray or surface runoff containing de-icing chemicals; marine spray	(1)	Top of bottom slab for rectangular deck	-reinforcing steel	40 +/- 10	40 +/- 10
			-Pretensioning	----	55 +/- 5
			-Post-tensioning	60 +/- 10	60 +/- 10
	(3)	Top surface of structural component	-reinforcing steel	70 +/- 20	55 +/- 10
			-Pretensioning	----	70 +/- 5
	(10)	Precast T-,I, or box girder	-reinforcing steel	----	35 +10/- 5
			-Pretensioning	----	50 +/- 5
			-Post-tensioning	----	55 +/- 10

Alternatively, if stainless steel is introduced into these exposure conditions, the concrete cover could logically be decreased due to the largely increased chloride threshold of stainless. The United Kingdom's Department of Transportation has recently recommended an amendment to the design manual for roads and bridges [42] which allows for stainless steel to be used with a concrete cover of 30mm, if contractors can ensure exceptionally rigid tolerances are met. Alternatively, Bergmann and Schnell [43] suggest that a reduction of concrete cover from 75mm to 50mm can have a concrete deck volume reduction of 10.5%, which can reduce the total factored load on the girders by up to 4%.

Chapter 3 Experimental Procedure

3.1. Rebar Grades

The experiments were designed and organized in order to compare the corrosion resistance of a number of stainless and corrosion resistant steels under similar conditions. As such, six different grades of stainless (with two suppliers of one grade), two corrosion resistant, and regular 400w grade steels were chosen, Table 3-1. The reinforcing steels, which were provided by a number of manufacturers, were 15M and came in 1220mm (4ft) sections, the exception being the 20M 304L stainless steel provided by Valbruna in both 1220 (4ft) and 610mm (2ft) sections for a previous study. These steels were chosen at the request of the Ministry of Transportation of Ontario to compare currently used stainless steel (S31653, S24100), with new less expensive grades of stainless steel.

Table 3-1: Steel rebar tested

UNS Designation	Type	Supplier	Bar Designation
S30403	304L	Valbruna	20M
S31653	316LN	Valbruna	15M
S32101	XM-26	Outokumpu	15M
S32205	XM-26	Valbruna	15M
S32304	XM-26	North American Stainless	15M
S24100	XM-28	Talley	15M
S24100	XM-28	Valbruna	15M
400W	Black	Harris Rebar	15M
	Galvanized	International Zinc Association	15M
ASTM A1035M	MMFX	MMFX Steel	15M

According to the American Society for Testing and Materials, each grade must meet certain chemical requirements, outlined in Table 3-2. This ensures the quality and consistency across the manufacturing process.

Table 3-2 Stainless steel chemical composition requirements [44]

UNS Designation	Type	Chemical Composition, %								
		Carbon	Manganese	Phosphorus	Sulfur	Silicon	Chromium	Nickle	Molybdenum	Nitrogen
S30403	304L	0.03	2	0.045	0.03	1	18.0-20.0	8.0-12.0	-	-
S31653	316LN	0.03	2	0.045	0.03	1	16.0-18.0	10.0-13.0	2.00-3.00	0.10-0.16
S32101	2101	0.04	4.0-6.0	0.04	0.03	1	21.0-22.0	1.35-1.70	0.10-0.80	0.20-0.25
S32205	2250	0.03	2	0.03	0.02	1	22.0-23.0	4.5-6.5	3.0-3.5	0.14-0.20
S32304	2304	0.03	2.5	0.04	0.03	1	21.5-24.5	3.0-5.5	0.05-0.60	0.06-0.20
S24100	XM-28	0.15	11.0-14.0	0.045	0.03	1	16.5-19.0	0.5-2.50	-	0.20-0.45

3.2. Salt Solution

In Ontario there are a number of anti-icing agents that are applied to the highway infrastructure including: sodium chloride (NaCl), magnesium chloride ($MgCl_2$), calcium chloride ($CaCl_2$), and a multi-chloride, which is a combination of the three. All four are used in different parts of the province of Ontario based on local availability and local temperature (ie. requiring lower eutectic freezing points). A sample of the four chloride solutions was analyzed by Activation Labs, and the chloride levels were determined, Table 3-3.

Table 3-3 Chemical compositions and chloride concentrations of de-icing agents

Solution	Percentage of Solution			
	NaCl	$MgCl_2$	$CaCl_2$	Total Cl^-
NaCl	25	1	0	15.7
$MgCl_2$	0	32	0	23.3
$CaCl_2$	1	0	37	24.5
Multi Cl^-	12	4	16	21.1

Although all the salt solutions were available, the multi chloride brine was used in the present experiments due to local availability, and relatively lower cost than the other brines.

3.3. Rebar Preparation

The rebar were cut into 356 mm (14 inch) lengths with a band saw and the cut edges were ground to remove burs. A 4.5mm ø hole was drilled to a depth of 10 mm, into which a 20 gauge copper wire was soldered to create an electrical connection. Each specimen type had wire with a specific colour coating, in order to easily differentiate the different steel grades while embedded in concrete. The ends were then sealed with varying lengths of epoxy lined shrink tube (25mm (1 inch) to 76 mm (3 inches)), allowing between 204 mm (8 inches) and 255 mm (10 inches) of exposed length. The ends were filled with hot glue to fully seal the end of the bar and limit end effects, Figure 3-1.

Figure 3-1: Rebar preparation

3.4. Concrete

3.4.1. Concrete Mixture Design

The concrete mix design, Table 3-4, follows the MTO guidelines for concrete bridge mixtures with two exceptions being: the wet curing time and the size of the large aggregate.

Table 3-4: Ontario bridge mix design

Ontario Bridge Mix Design		
Constituent	Amount (m^3)	
Gravel (14mm)	1045	kg
Sand	705	kg
GU Cement	297	kg
Slag	98	kg
Euclid Air Extra	237	mL
Superplasticizer	900	mL
Water	155	L + abs
w/c	0.40	ratio

The difference in curing time being that the specimens were cured in the humidity chamber for 28 days compared with the minimum 4 days of wet curing specified by the Ontario Provincial

Standard Specification (OPSS) 904 for concrete structures, when the curing temperature is above zero degrees Celsius [45]. The large aggregate in the concrete was 14mm, slightly smaller than the 19mm aggregate specified by OPSS 1002 [46] to ensure even aggregate distribution in the small laboratory specimens.

3.4.2. Concrete Casting

Due to difficulties in determining the optimal design for the longitudinal cracks, the initial casting plan was to cast the specimens in two separate casts. The first cast included: stainless steel sound concrete specimens, and stainless steel transversely cracked specimens. The second cast included: black and corrosion resistant sound concrete specimens, black and corrosion resistant transversely cracked specimens, and the longitudinally cracked specimens. Due to preparation errors in the black and non stainless steel sound concrete specimens, a third casts was required.

3.5. Specimen Design

The three specimen designs used to evaluate the corrosion resistance of the different rebar grades correspond to three different field surface conditions: sound concrete above and around reinforcing bars, concrete with cracks oriented transversely to the reinforcement, and concrete with cracks oriented longitudinally to, and above, the reinforcement. The sound concrete represents the ideal conditions, which are often not present in the field, but is typical of laboratory specimens. The transversely and longitudinally cracked specimens represent more realistic field conditions, with cracking occurring due to shrinkage, loading, and thermal variations.

3.5.1. Sound Concrete Specimens

The concrete beam specimens, Figure 3-2, were designed to represent sound concrete (not cracked) with a single steel reinforcement mat. The top bar of the mat was positioned 25mm (1 inch) below the surface of a 38mm (1.5 inch) deep ponding well to be filled with multi chloride brine. The cover of 25mm, differed from the 60mm – 75mm for structural concrete members exposed to chlorides in the field, in order to limit the time required for chloride ingress to reach the surface of the reinforcement [6].

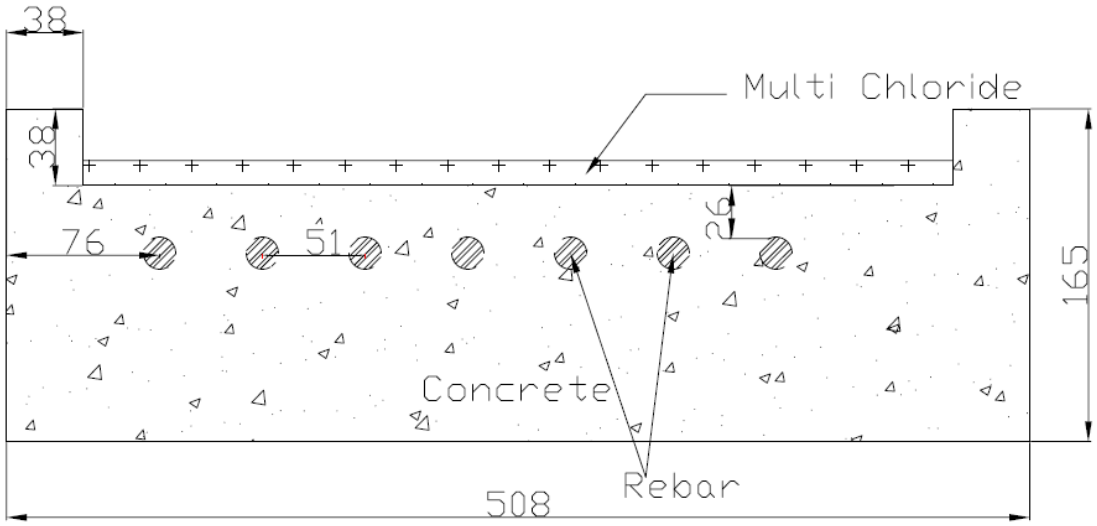

Figure 3-2: Sound concrete beam

Eight different sound concrete specimens were cast, following the basic layout shown in Figure 3-2 and Figure 3-3. The different specimens include:

- four beams, each with one of each of seven stainless steel bars described in Table 3-1 with a short section of transverse rebar (Figure 3-3);
- two beams, each with 2 of each of the three none stainless bars tested (galvanized, MMFX, and Black); and
- two beams, each with two of each of the three non stainless bars tested without the transverse rebar shown in Figure 3-3.

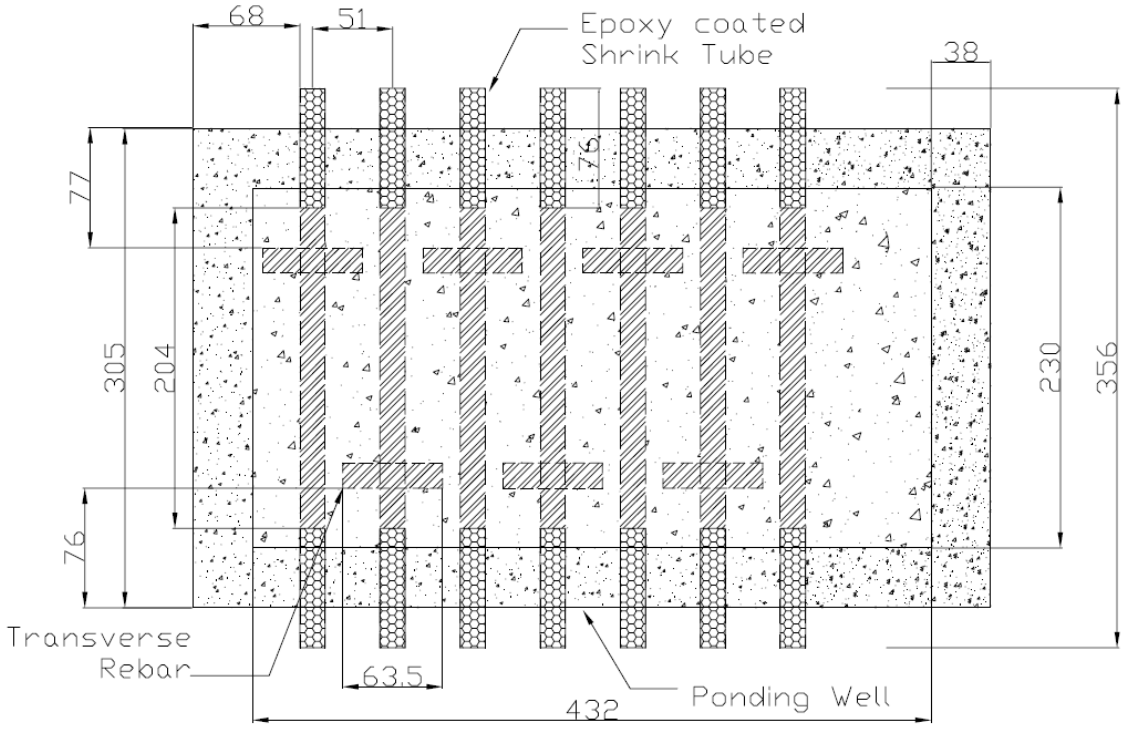

Figure 3-3: Sound concrete plan view

To ensure a consistent ponding well, and for ease of construction the specimens were cast upside down on top of a 38 mm (1.5 inch) extruded polystyrene insulation board, Figure 3-4. This also allowed for the 64 mm (2.5 inch) transverse rebar to be tied to the bottom side of the 204 mm (8 inch) exposed section of test specimen using UNS S31653 stainless steel tie wire.

Figure 3-4: Sound concrete formwork

3.5.2. Transversely Cracked Concrete

The specimens used to simulate cracks transverse (perpendicular) to the rebar were cast individually in concrete prisms measuring: 67 mm (~2.75 inches) square by 356 mm (14 inches) long Figure 3-5. This allowed for a 255 mm (10 inch) long exposed surface. Similar to the sound concrete specimens, a 25 mm cover was used to allow timely chloride diffusion. To ensure that the rebar was approximately centred in the concrete prism, formwork was created which centred the exposed epoxy coated end, while fishing line was utilized to support the fully embedded end of the specimen.

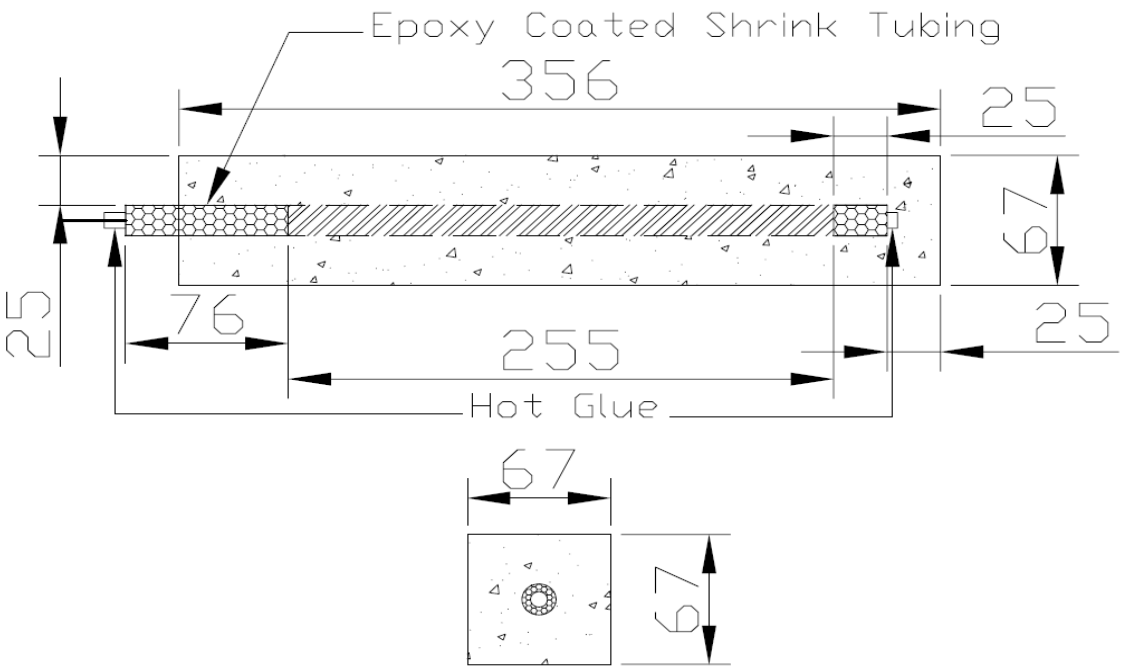

Figure 3-5: Transverse cracked specimen

Once the specimens had been cured in the humidity chamber for twenty-eight days, a transverse crack was induced in each prism by 3-point bending. Thereafter, an epoxy coating was applied to the four (left, right, base, and bottom) sides of the prism to simulate deck continuity and try to limit the chloride ingress to only the cracked region, Figure 3-6.

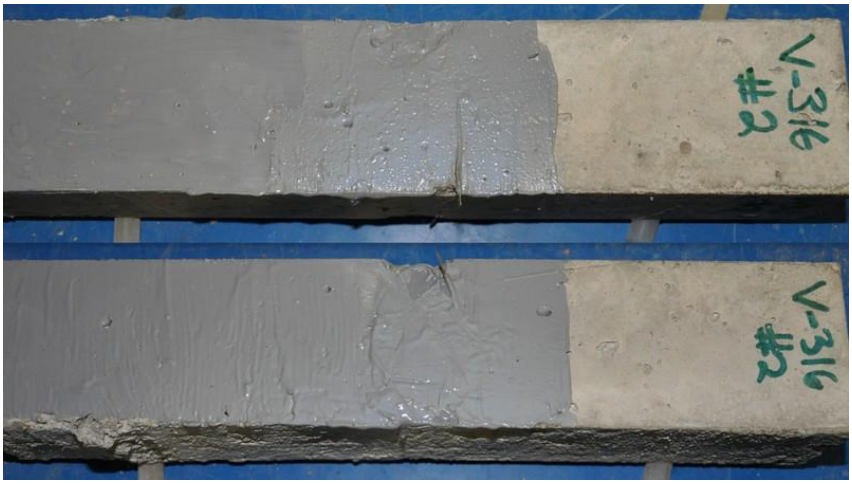

Figure 3-6: Epoxy coating on two sides of the beam cracked perpendicular to the rebar

3.5.3. Longitudinally Cracked Specimens

These specimens were prepared to represent the cracks which often form above, and parallel to, the lateral bars of a bridge deck. Eight bars with a 255 mm exposed length were cast into concrete beams measuring: 966 mm (~38 inches) long by 114 mm (~4.5 inches) tall by 356 mm (14 inches) wide, Figure 3-7. The specimen was cast upside down with the bars located above a 6.4 mm (1/4 inch) deep plexiglass triangular prism. This created a notch in the surface of the beam to create an area of higher stress when inducing the crack parallel to the rebar. This provided a 25 mm cover between the root of the notch and the surface of the rebar.

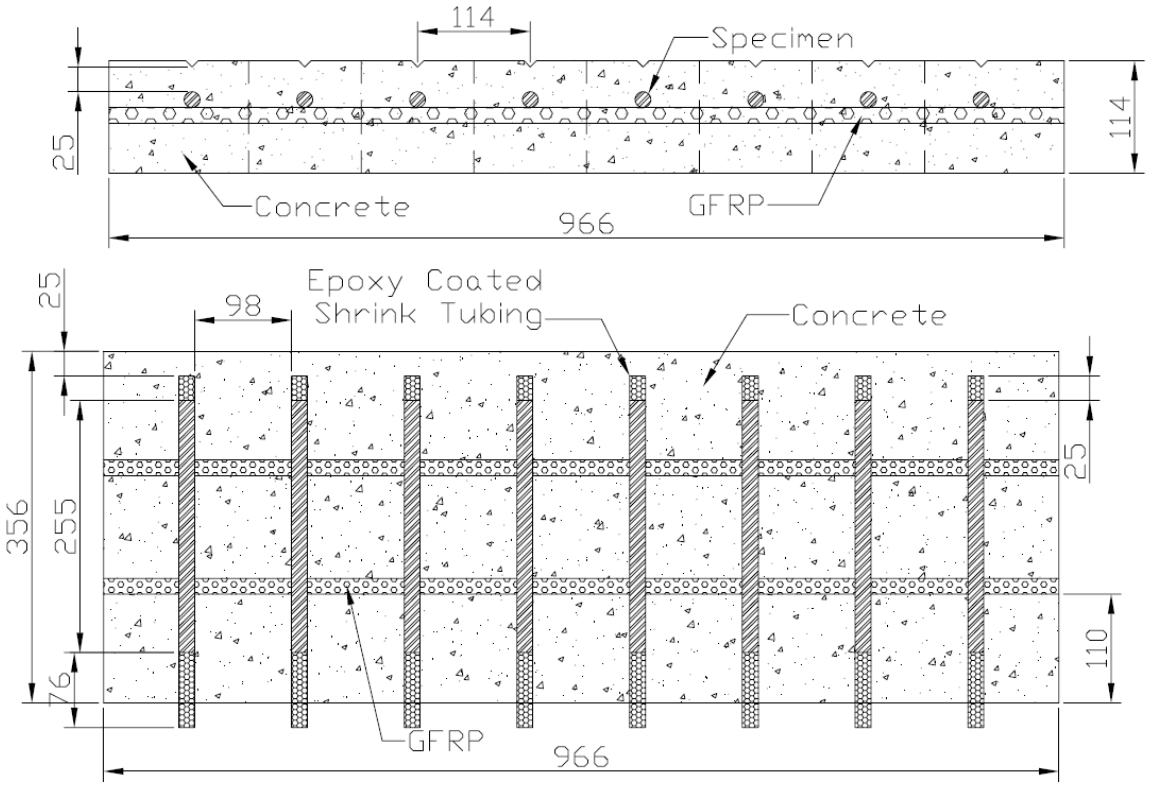

Figure 3-7: Longitudinal specimen beam

The bars were supported by two 15 mm Glass Fibre Reinforced Polymer (GFRP) bars in order to reinforce the concrete while the cracks were induced. The GFRP was used because it is an effective electrical insulator and prevented shorting between bars during subsequent electrochemical testing, Figure 3-8.

Figure 3-8: Formwork and bars for longitudinally cracked specimens

Once the cracks were induced, as described below, the specimens were cut in half, the exposed GFRP was removed, and then epoxied the prisms were coated with epoxy on four (left, right, bottom and base) sides to limit chloride ingress to only the cracked region. Two specimens, each with four bars, were then placed upright in a container and the multi chloride brine solution was added to approximately 25 mm (1 inch) below the top concrete surface, Figure 3-9.

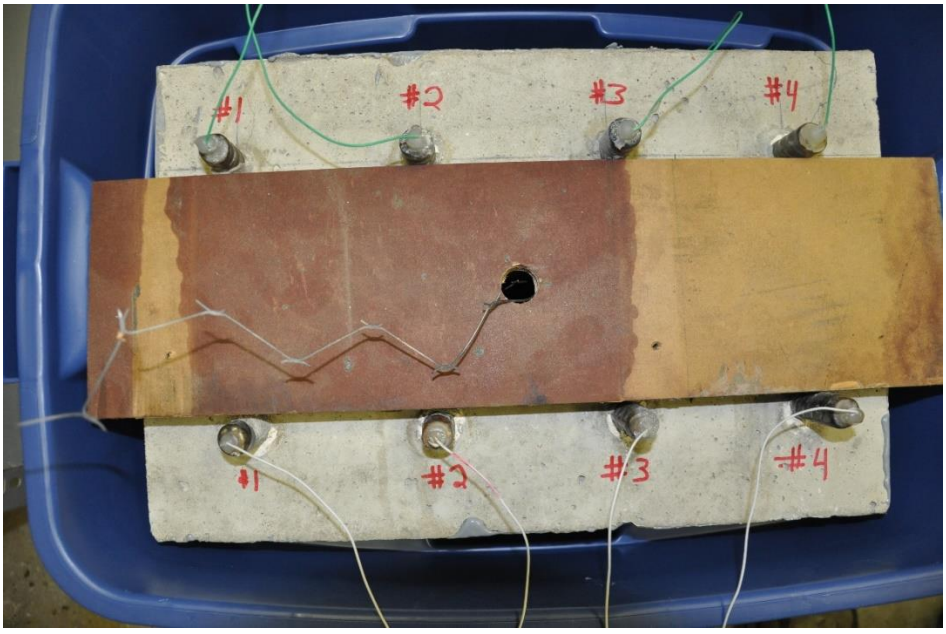

Figure 3-9: Longitudinally cracked specimen soaking in anti-icing solution

3.6. Inducing Longitudinal and Transverse Cracks

The cracks for both the longitudinal and transverse specimens were induced by placing the specimens in three point bending, Figure 3-10. Once the cracks had been induced, a 304 stainless steel shim (10mm wide by 10mm long by 0.26mm thick) was placed in the crack to prevent the crack from closing. This was done to simulate worst case bridge deck conditions, of approximately 0.3mm, the crack opening level above which the Ministry of Transportation of Ontario requires the crack be sealed, [47].

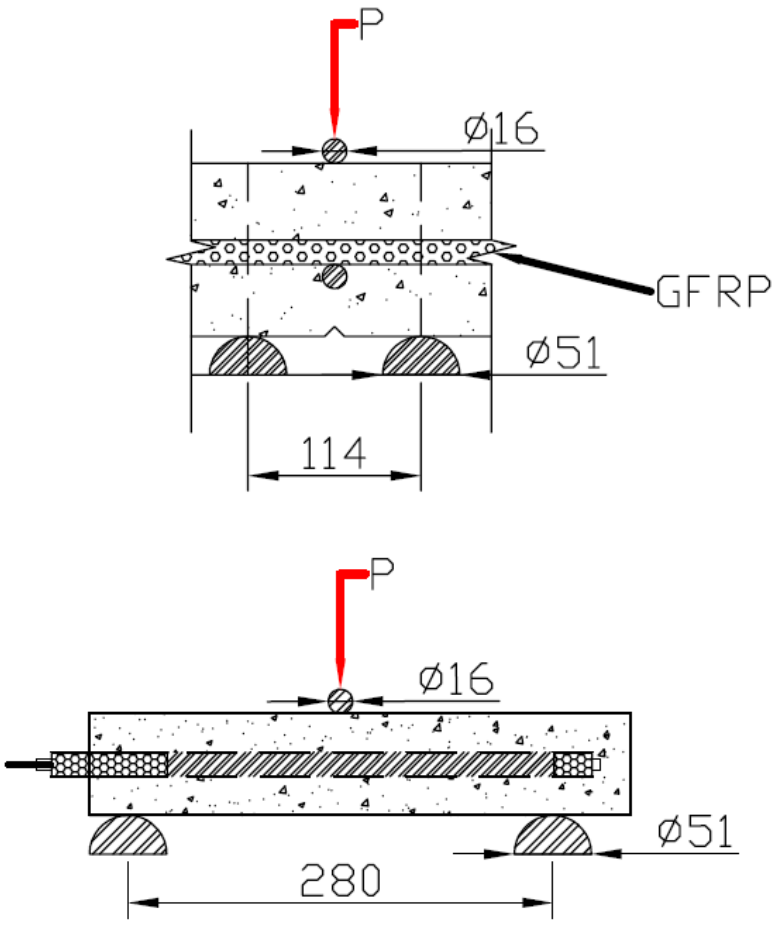

Figure 3-10: Three point bending - longitudinal specimens

3.7. Electrochemical Testing

In order to determine the comparative corrosion resistance of the steels in the three different environments micro-cell corrosion monitoring techniques were used. These techniques included: galvanostatic pulse (GP), linear polarization resistance (LPR), and cyclic polarization (CP). These

three techniques were employed with different test frequencies of weekly, monthly, and a single test respectively, with GP and LPR allowing for polarization resistance (R_p) to be determined.

3.7.1. Galvanostatic Pulse Technique

The galvanostatic pulse technique [48] requires the application of a constant current, 10μA in this experiment, to the rebar and measuring the resulting potentials. In the case of specimens in concrete it allows for both the polarization resistance and the concrete resistance to be determined, assuming a steady state is reached, Figure 3-11. If the potential or potential step between measurements are low, or the specimen is not shielded (eg Faraday Cage) the data will be susceptible to noise which can result in data that is difficult to analyze.

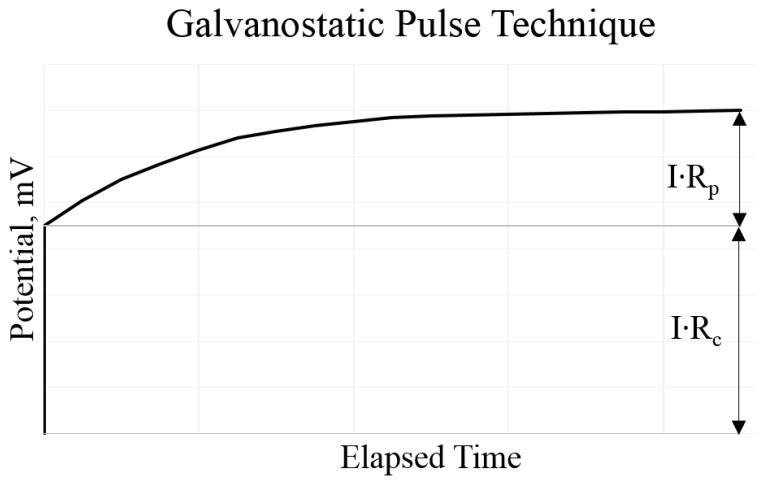

Figure 3-11: Galvanostatic pulse technique

3.7.2. Linear Polarization Resistance Technique

The potentiostatic linear polarization resistance technique [49] requires the application of a constant potential and the resulting current response is measured, Figure 3-12. This technique requires two scans, +/- 20mV vs open circuit potential (ΔE) in this experiment, of 150 seconds to allow the current response (Δi) to enter the linear region. Once the current response is determined, the polarization resistance can be determined using Equation 2, and, once combined with the taffel constant (β), and the exposed area (A), can be used to determine the corrosion current density (i_{corr}), Equation 3.

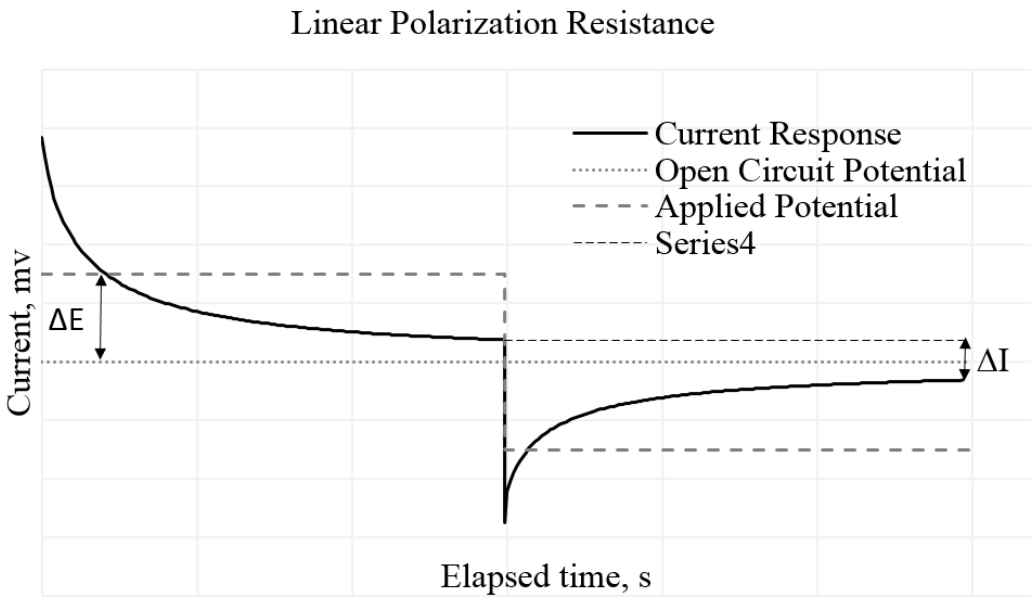

Figure 3-12: Linear polarization resistance

$$R_p = \frac{\Delta E}{\Delta i} \qquad \text{Equation 2}$$

$$i_{corr} = \frac{B}{R_p \cdot A} \qquad \text{Equation 3}$$

3.7.3. Cyclic Polarization Technique

For the potentiodynamic cyclic polarization technique [50], a larger range of potentials is applied at a constant scan rate. During the current testing, a scan rate of 0.01mv/S, was applied from open circuit potential to +500mV and then reversing to -900mV, Figure 3-13. The curve below demonstrates both a stable (not corroding) and non-stable (corroding) sample in black and red curve respectively, Figure 3-13. As the potential is increased, the passive film impedance decreases and, depending on the material composition, a new film may be created. In the case of the passive bar, when the potential is decreased, the impedance of the film slowly increases and is greater than the original (exhibiting a lower current density at each potential and a more anodic open circuit potential). In the case of the active bar, the passive film has broken down and, when the potential

scan reverses, the bar is not stable enough to reform the passive film (resulting in a higher current density at each potential and a more cathodic open circuit potential).

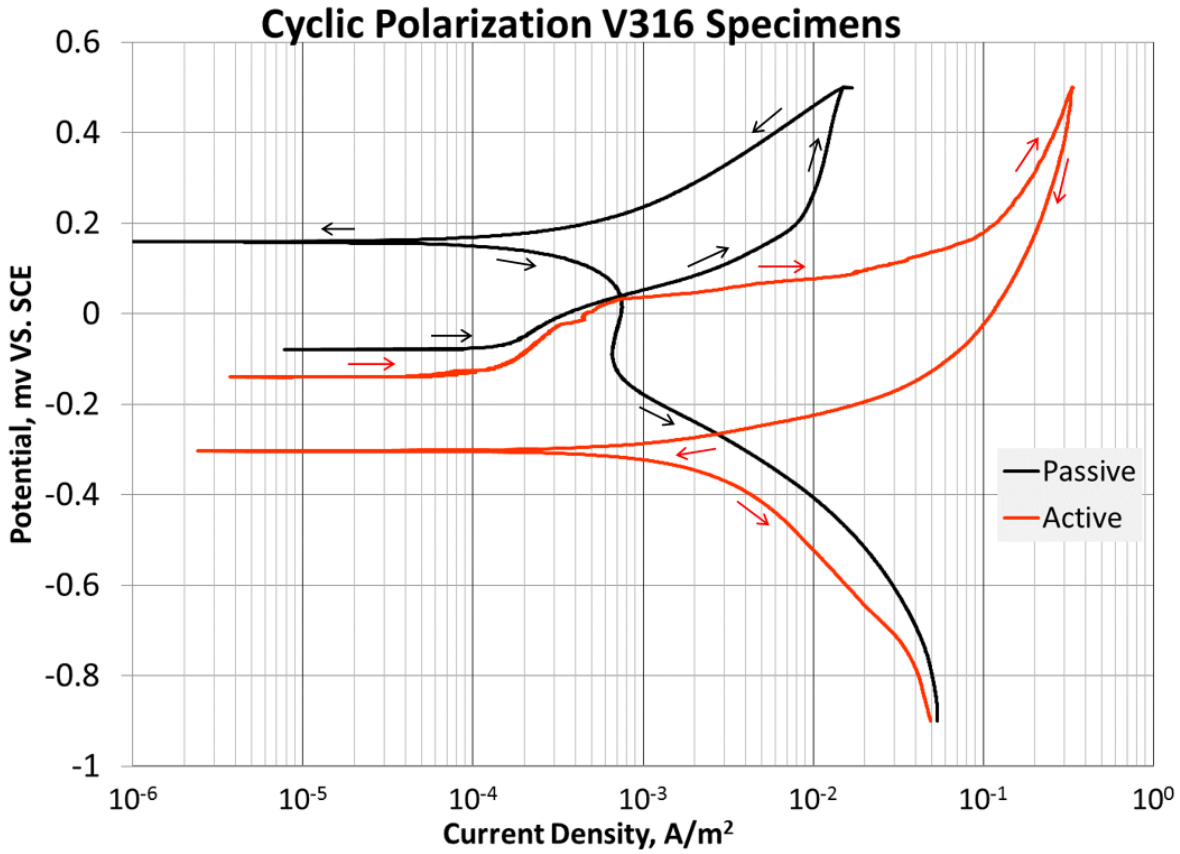

Figure 3-13: Cyclic polarization curve for passively and actively corroding steel

Chapter 4 Experimental Results and Discussion

The following sections describe the physical properties of the materials tested as well as the current results from the ongoing experimental program.

4.1. Concrete

To ensure that the concrete exceeded the 35 MPa compressive strength required for Ontario highway bridges, compression tests were completed at 28 days after casting, the results of which are presented in Table 4-1 . What can be noted is that the average compressive strength of the tested cylinders is 9-35% higher than the required 35 MPa specified strength. This is common and due to the risks assessed by the contractor. It is much cheaper to provide mixes with strengths much higher than the required strength, then to have to remove the concrete if the strength it too low.

Table 4-1: Average concrete compressive strength (MPa)

Cast	Date	Air Content	Average Compression Strength (Mpa)			
			7 Day	14 Day	21 Day	28 Day
#1	19-Dec-12	4.50%	-	-	48.17	47.16
#2	24-Jan-13	6.00%	32.3	39.07	-	45.38
#3	27-Feb-13	6.10%	-	-	-	38.13

4.2. Chemical Composition of the Alloys

The composition of the steels used in the experimental program are presented in Table 4-2. These data were collected using X-ray fluorescence, and it should be noted that all the different steels fall within acceptable ranges for chemical composition. Also note that this technique cannot determine the lighter elements (eg. carbon, nitrogen) because it cannot accurately detect elements with atomic mass less than aluminum.

4.3. Electrochemical Testing

The following sections discuss the results of the electrochemical tests that were performed on: fifty-two bars in sound concrete specimens, fifty longitudinally cracked specimens, and fifty

transversely cracked specimens. From these test the: corrosion current density (i_{corr}), open circuit potential (E_{corr}), and the concrete resistance (R_c) were able to be determined. The following sections discuss the results of the electrochemical testing by breaking the specimens into three categories which are: black and corrosion resistant reinforcement, recently developed stainless steel grades, and traditional stainless steel grades.

4.3.1. Corrosion Potential (E_{corr}) and Corrosion Current Density (I_{corr})

In order to interpret the corrosion potential of uncoated reinforcing steel in field concrete, ASTM C876 was established, [51]. The standard suggests potentials to compare the collected open circuit potentials against in order to determine the possibility of corrosion, graphically depicted in Figure 4-1. It should be noted that the recommended interpretations of this test were designed for black steel, based on years of experimental results, thus these interpretations are not applicable for the stainless or galvanized steel. If the sound concrete data in Figure 4-2 is compared to those presented in Figure 4-14 and Figure 4-8 it can be noted how much variation the corrosion potential of stainless steel has compared with traditional black reinforcement. While the black reinforcement stays relatively constant at a potential of -0.1 mV vs saturated calomel electrode, well within the low probability of corrosion region of Figure 4-1, the stainless steels vary from -0.125 mV to -0.275 mV vs saturated calomel electrode under passive corrosion conditions. Thus, in order to use a method similar to that presented in ASTM C876, a different chart should be created for each stainless steel, which compares the open circuit potential vs probability of corrosion. For the current experiment, both linear polarization resistance and galvanostatic polarization techniques were used with average Ecorr values presented in Appendix A.

Table 4-2: Chemical composition of experiment steel determined by XRF (note this technique cannot determine carbon and nitrogen contents).

UNS Designation	Type	Actual Chemical Composition, % (XRF)							
		Carbon	Manganese	Phosphorus	Sulfur	Silicon	Chromium	Nickel	Molybdenum
S30403	304L	<LOD	1.32	<LOD	<LOD	<LOD	18	8.6	0.49
S31653	316LN	<LOD	1.24	0.082	0.3	0.85	17.64	10.4	2.14
S32101	2101	<LOD	4.87	<LOD	<LOD	0.87	21.07	1.46	0.165
S32205	2205	<LOD	1.56	0.14	0.38	0.89	21.7	4.94	2.91
S32304	2304	<LOD	1.63	<LOD	<LOD	0.54	22.36	3.94	0.21
S24100	Valbruna XM-28	<LOD	12.03	<LOD	<LOD	0.53	17.62	2.31	<LOD
S24100	Talley XM-28	<LOD	12.15	<LOD	<LOD	0.63	16.83	0.73	0.17

* Areas marked "<LOD" mean element levels fall below level of detection.

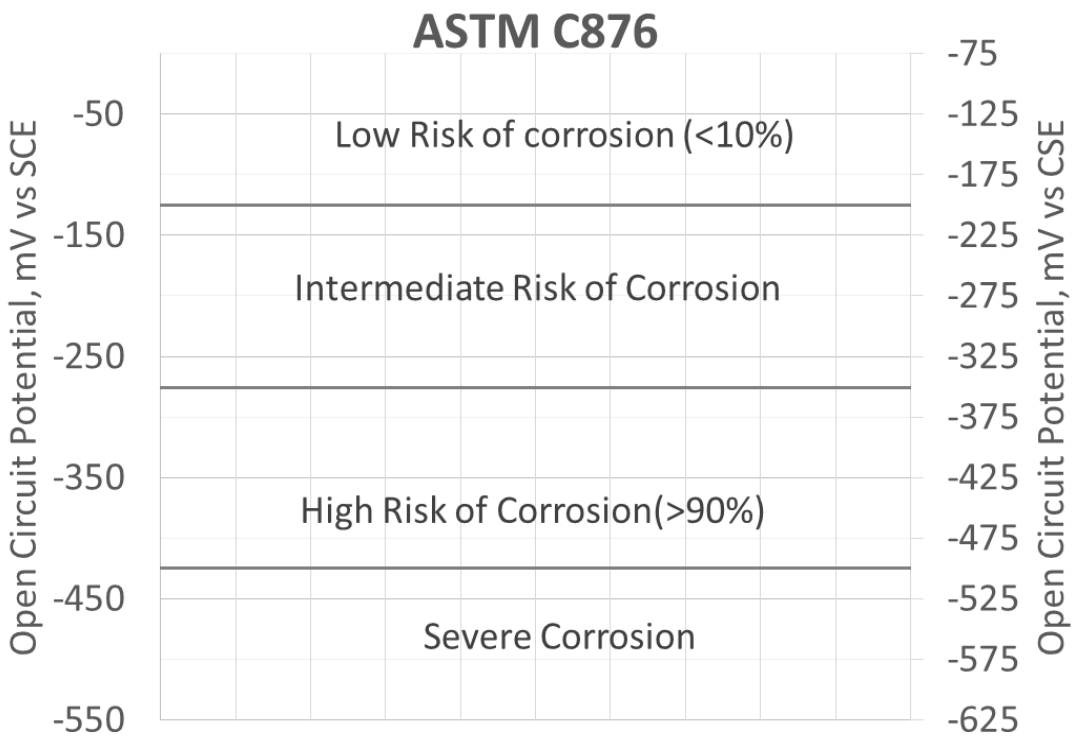

Figure 4-1: ASTM C876: Corrosion potential of uncoated black reinforcing steel in concrete

4.3.1.1. Black and Corrosion Resistant Reinforcement

4.3.1.1.1. Sound Concrete

From both the E_{corr} and i_{corr} data, Figure 4-2 and Figure 4-3 respectively, the black and corrosion resistant rebar in sound concrete specimens currently do not appear to be corroding because the E_{corr} values are in the low risk of corrosion region for the black steel, and the i_{corr} values fall below 0.001 A/m^2, which equates to an average corrosion depth loss of approximately 1μm per year. Note however, how anodic the galvanized rebar is, between -350mV and -225mV, compared with the -950mV to -400mV (Figure 4-4), and -1000mv to – 500mv (Figure 4-6) for the transversely and longitudinally cracked bars respectfully. It should also be noted that the i_{corr} data from the LPR tests all fall well below the values determined by the GP technique because the concrete resistance cannot directly be removed by the polarization resistance of the system.

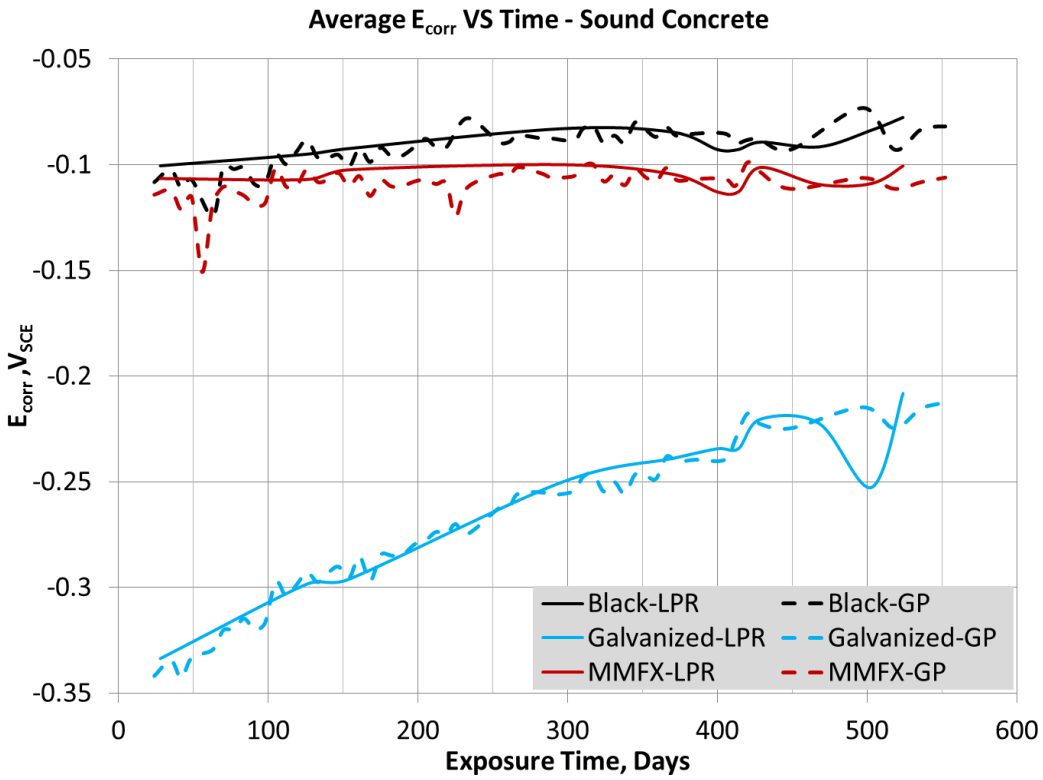

Figure 4-2: Average E_{corr} – Corrosion resistant rebar in sound concrete

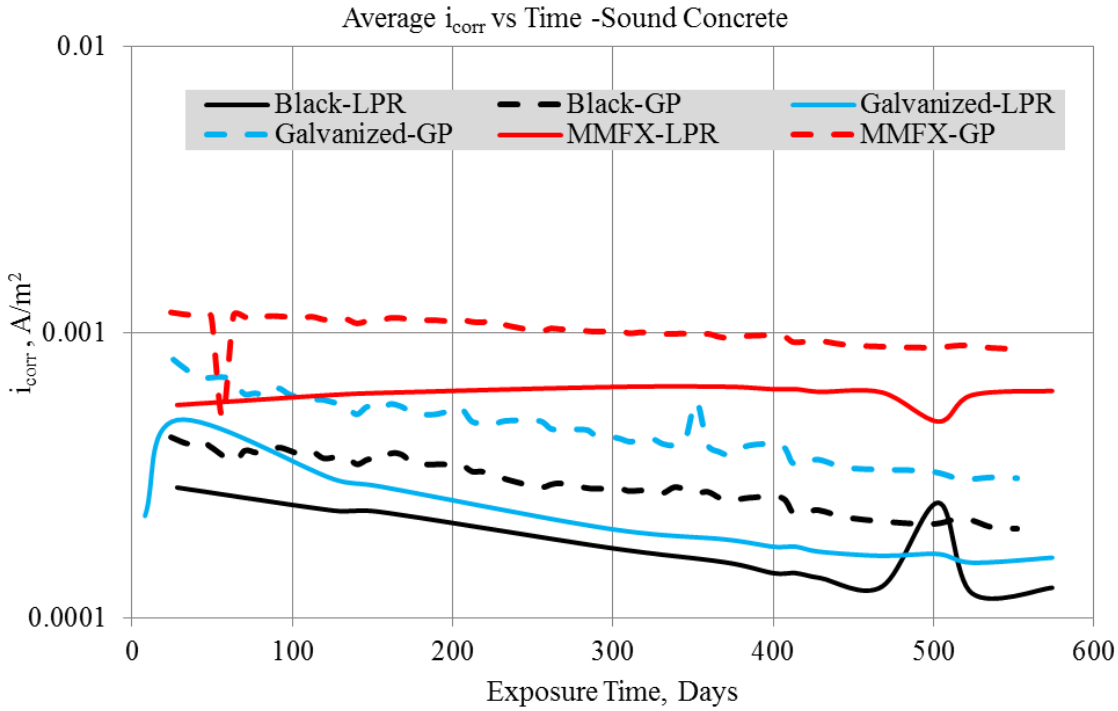

Figure 4-3: Average i_{corr} - Corrosion resistant rebar in sound concrete

4.3.1.1.2. Transverse and Longitudinally Cracked Concrete

The open circuit potentials of the bars in the cracked concrete are significantly more cathodic than those in the sound concrete, indicating that they are actively corroding. From both the LPR and the GP curves, Figure 4-4 to Figure 4-7 , it appears that corrosion initiated almost as soon as the specimens were exposed to the multi chloride brine. Although the data from the LPR is almost an order of magnitude lower than the GP values, because the concrete resistance cannot be determined from the LPR technique, both sets of data show that the large crack widths allowed the chloride direct access to the steel surface. For both the longitudinal and transversely cracked specimens, the corrosion potential and corrosion current density decreased with time, potentially due to the oxygen limiting the reaction, seen in the second half of Equation 4. Another possibility is that the corrosion products have built up on the surface of the bars, and seeped into the cracks, blocking the cracks and limiting the transportation of more chlorides to the rebar surface.

$$Fe \rightarrow Fe^{2+} + 2e^{-}$$

$$2e^{-} + \frac{1}{2}O_2 + H_2O \rightarrow 2(OH^{-})$$

Equation 4

For the transversely cracked concrete the average value of the corrosion potential appears to become more anodic and, similarly, the corrosion current density decreases around day 375 of exposure to chlorides. This is because the specimen exhibiting the highest corrosion rate for each of the black, galvanized and MMFX bars was removed and autopsied at this time. Therefore the data collected after this time were the average values for the four bars exhibiting the lower corrosion rates.

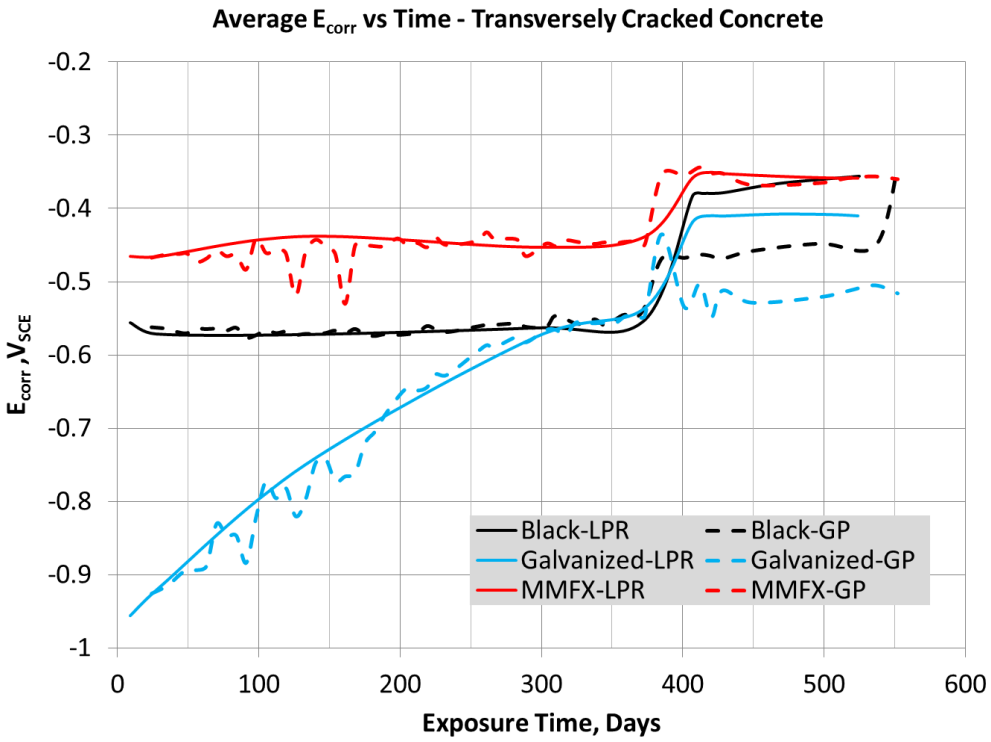

Figure 4-4: Average E_{corr} – Corrosion resistant rebar in transversely cracked concrete

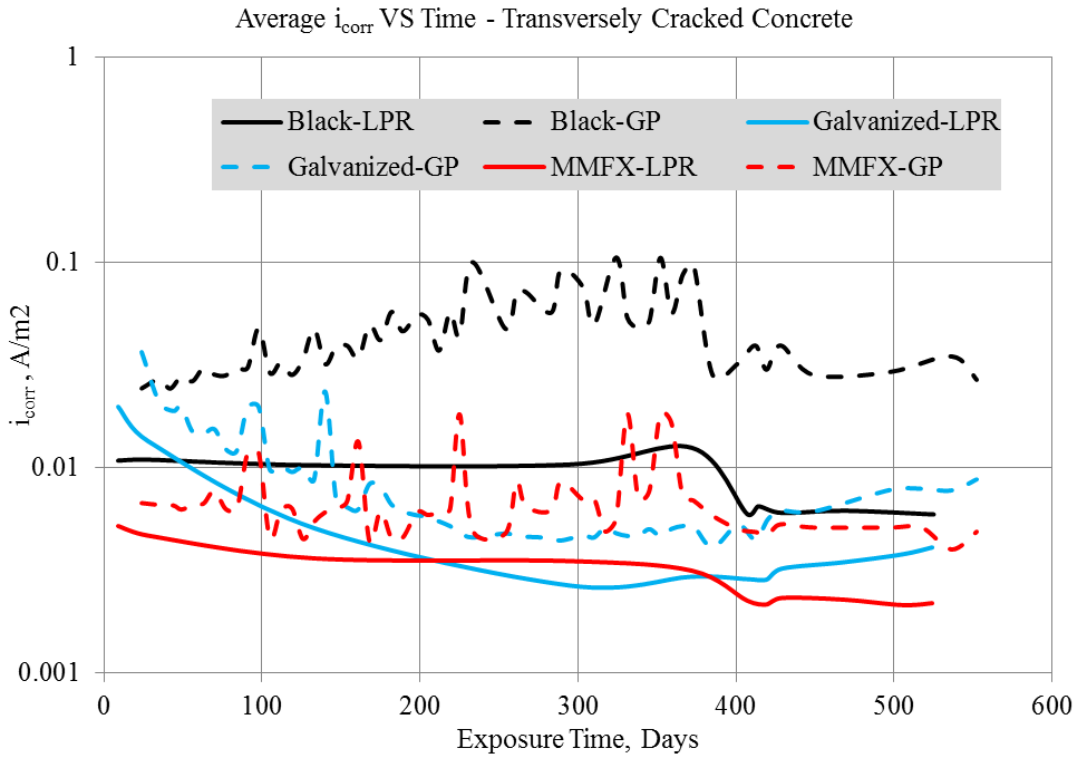

Figure 4-5: Average i_{corr} – Corrosion resistant rebar in transversely cracked concrete

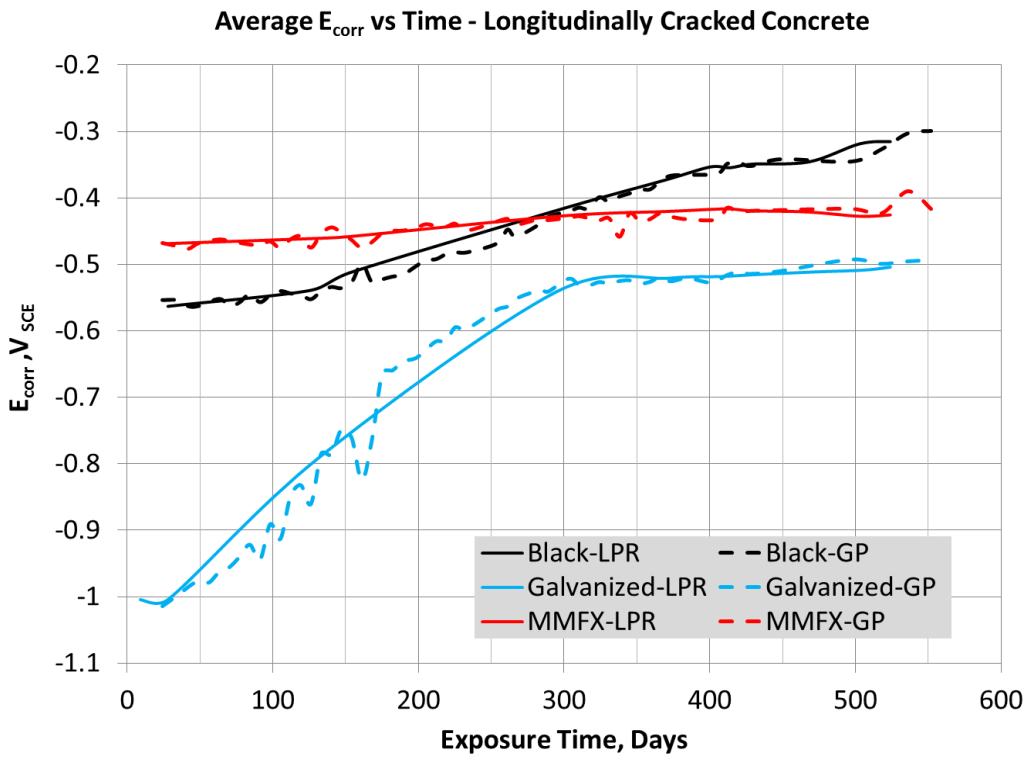

Figure 4-6: Average E_{corr} - Corrosion resistant rebar in longitudinally cracked concrete

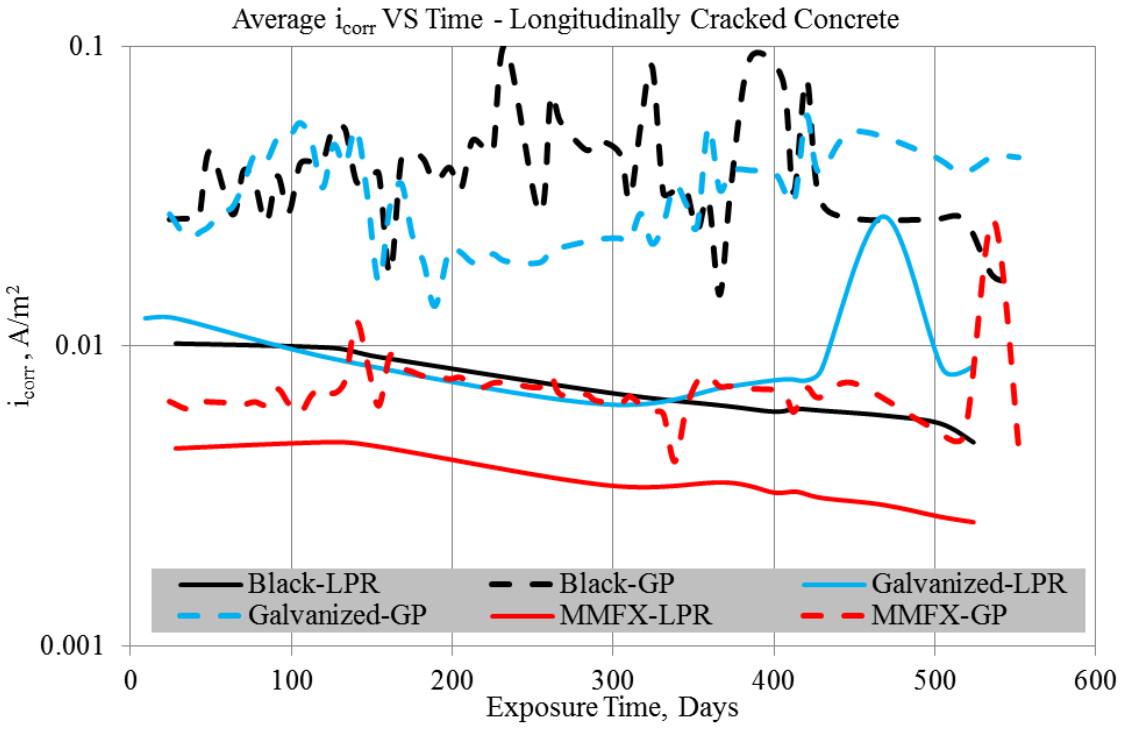

Figure 4-7: Average i_{corr} - Corrosion resistant rebar in longitudinally cracked concrete

4.3.1.2. Traditional Stainless Steel Grades

4.3.1.2.1. Sound Concrete

From the data presented in Figure 4-8 and Figure 4-9, again it is assumed that the steel is not corroding.

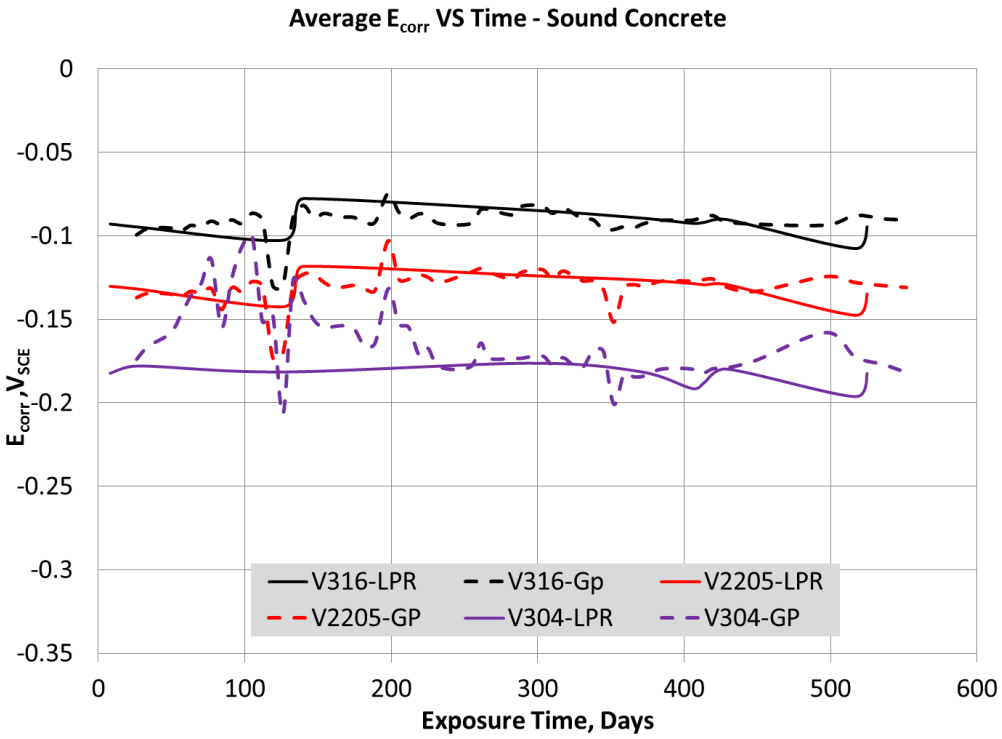

Figure 4-8: Average E_{corr} - 304L, 316LN, and 2205 stainless steel rebar in sound concrete

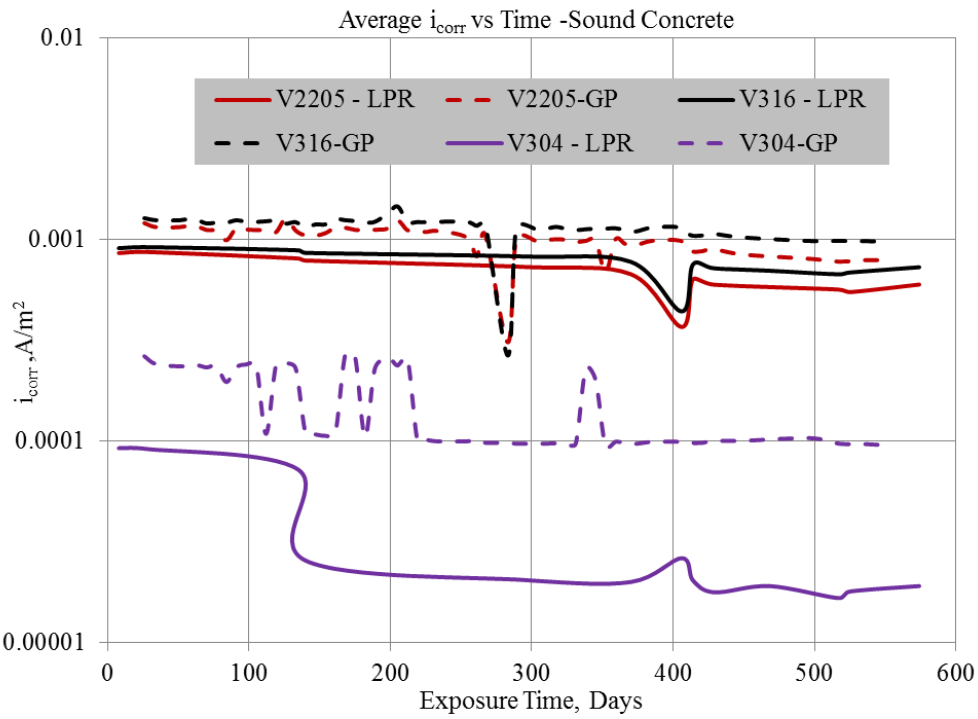

Figure 4-9: Average i_{corr} - 304L, 316LN, and 2205 stainless steel rebar in sound concrete

4.3.1.2.2. Transverse and Longitudinally Cracked Concrete

Analysis of the data for the transverse and longitudinally cracked specimens, Figure 4-10 to Figure 4-13 and the individual data in Appendix A, electrochemically indicates that chloride has reached the surface of all the stainless steels. When the single bars of each specimen are analysed, the 304L and 2205 appear to confirm what the averages suggested. When the individual 316LN bars in the longitudinally cracked specimens E_{corr} and i_{corr} data are analyzed, it looks as if specimen 1 and 5 have begun to actively corrode, but when the specimens were autopsied only specimen 1 exhibited corrosion product on the exposed surface, appendix C. To determine the full extent of the corrosion, the bars have been removed from the concrete and photographed with the results of the longitudinal autopsy presented in Appendix C.

.

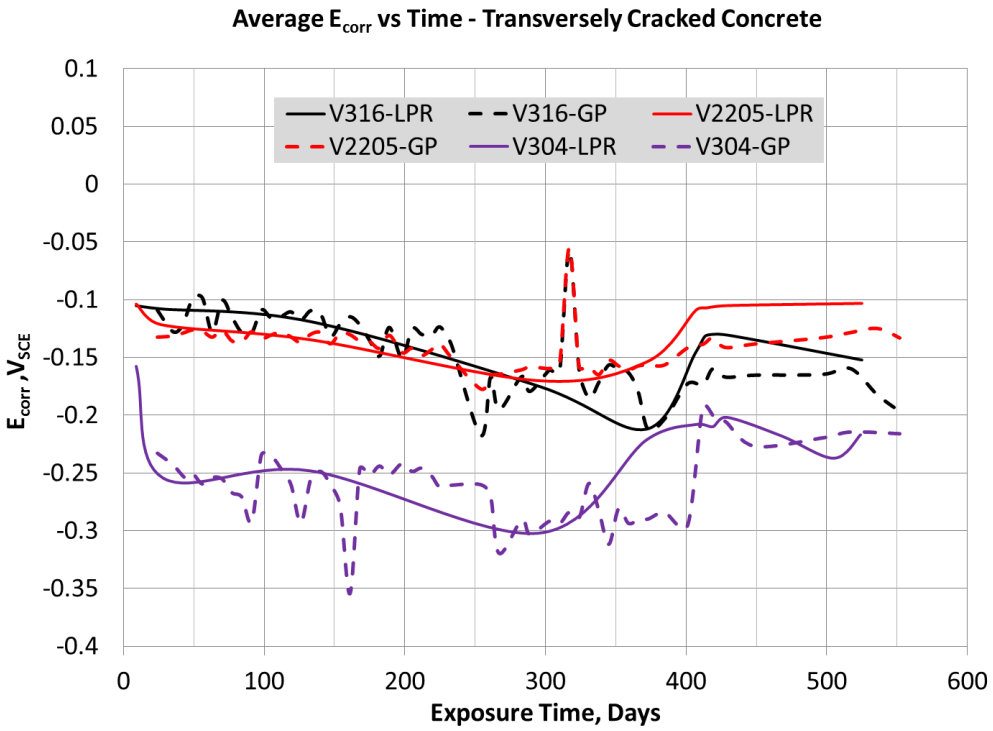

Figure 4-10: Average E_{corr} - 304L, 316LN, and 2205 stainless steel rebar in transversely cracked concrete

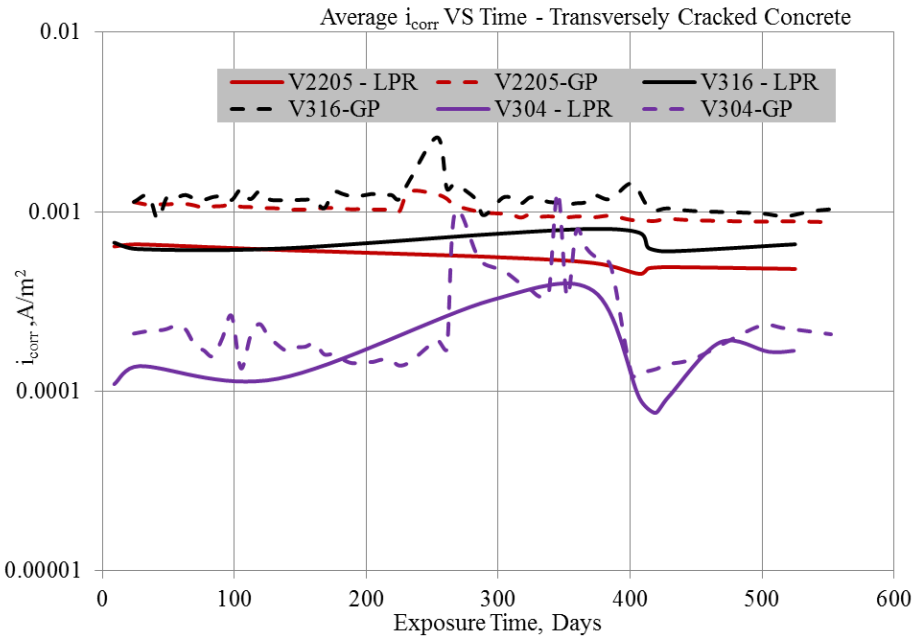

Figure 4-11: Average i_{corr} - 304L, 316LN, and 2205 stainless steel rebar in transversely cracked concrete

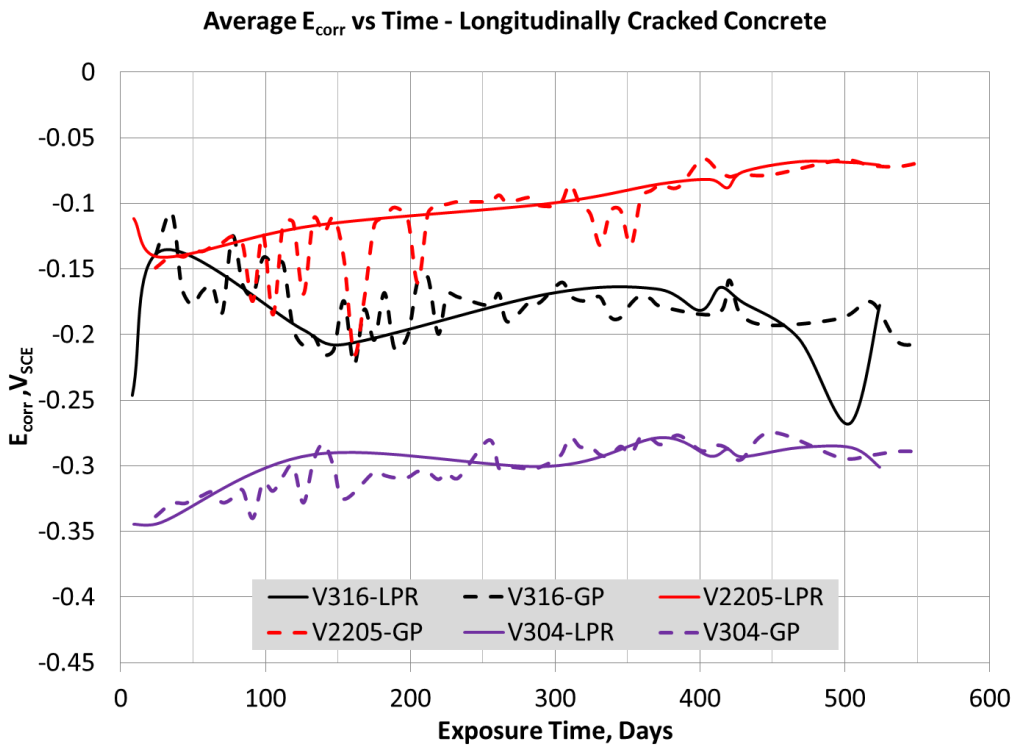

Figure 4-12: Average E_{corr} - 304L, 316LN, and 2205 stainless steel rebar in longitudinally cracked concrete

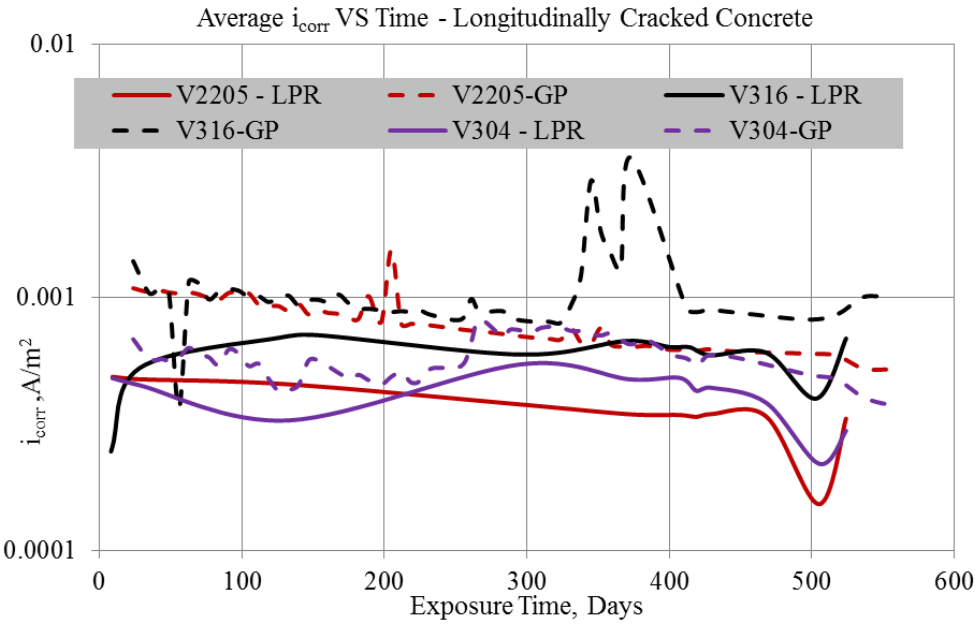

Figure 4-13: Average i_{corr} - 304L, 316LN, and 2205 stainless steel rebar in longitudinally cracked concrete

4.3.1.3. Recently developed Stainless Steel Grades

4.3.1.3.1. Sound Concrete

From the data presented in Figure 4-14 and Figure 4-15, it can be assumed that the steel is not corroding for a two reasons. First, the black and corrosion resistant rebar in the same environment did not exhibit corroded material properties. Second, the i_{corr} values are well into what is considered a passive state (ie depth loss of less than 1µm per year). The XM28 provided by both Talley and Valbruna have open circuit potentials between -150mV SCE and -125mV SCE, which remained relatively consistent throughout the ongoing tests. The data also demonstrates that the open circuit potentials of passive Outokumpu 2101 and American Arminox 2304 are more cathodic, ranging between -250mV and -190mV SCE and -270mV and -220mV SCE, respectively. This is interesting as both 2101 and 2304 are lower than that of Valbruna's 316, 2205, and 304 (Figure 4-8.

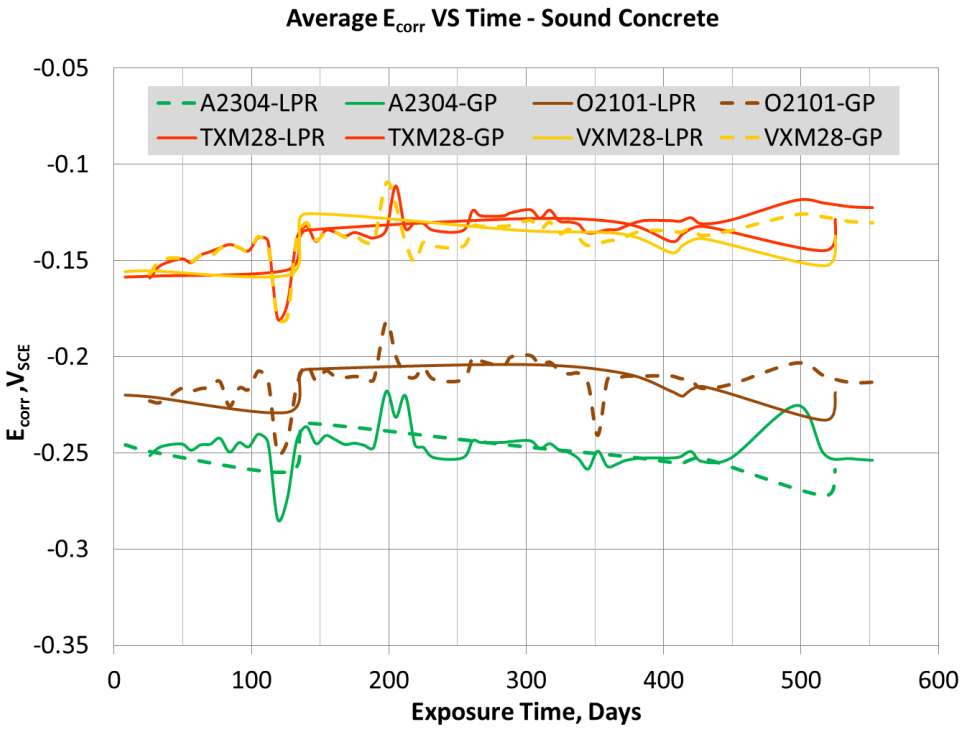

Figure 4-14: Average E_{corr} - Stainless steel rebar in sound concrete

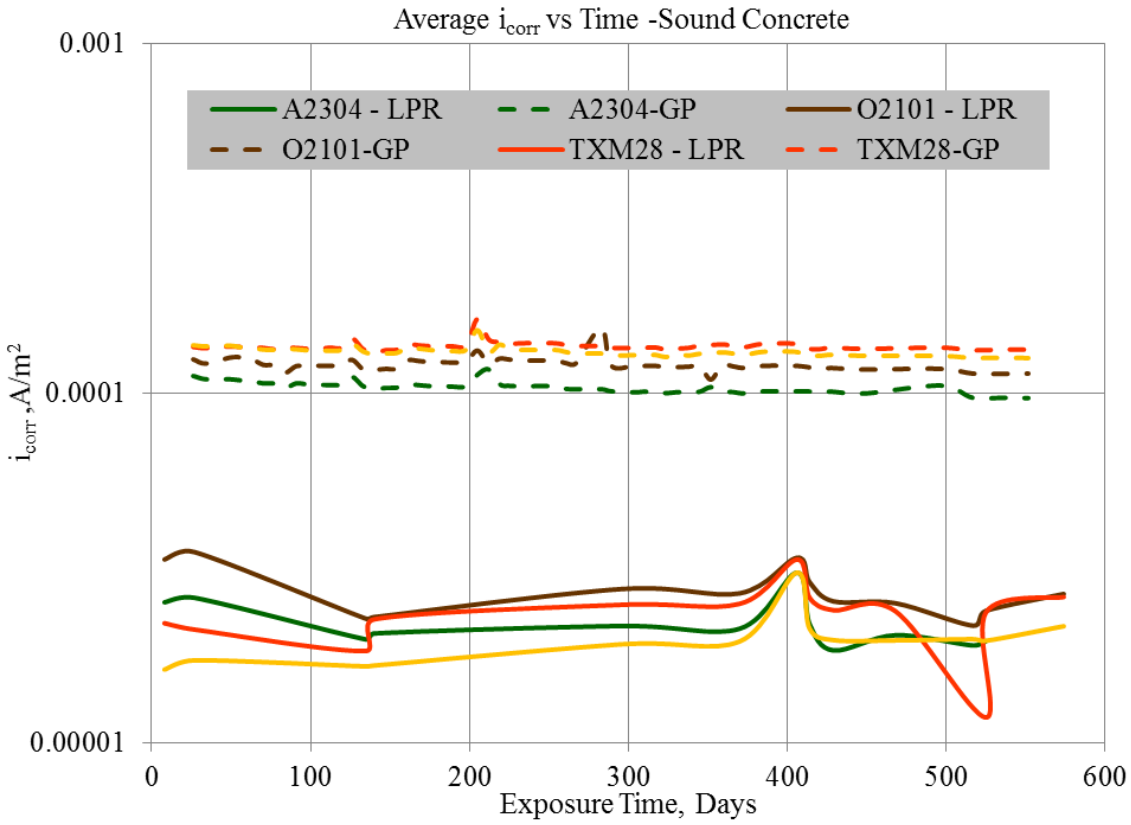

Figure 4-15: Average i_{corr} - Stainless steel rebar in sound concrete

4.3.1.3.2. Transversely and Longitudinally Cracked Concrete

Comparing the average open circuit potentials of the bar in transversely and longitudinally cracked specimens to those of the bars in sound concrete, the data suggests that chloride has reached the surface of the bar, and has begun to break down the passive film. This is best shown in the XM28 specimens as the open circuit potential dropped from approximately -150mV in the sound concrete to -350mV in the longitudinally cracked specimens. Although the average corrosion current density values all appear to be in the passive range, when the individual specimen results are viewed, Appendix A, it appears as though a number of specimens have begun to actively corrode, examples of which are given in Figure 4-20 and Figure 4-21. It should also be noted that corrosion current density values given in the plots are determined using the entire exposed area of the bar (steel not covered by end capping) whereas, if only the area of localized corrosion is accounted for, more bars may exhibit active corrosion tendencies (have corrosion current densities above 0.01 A/m^2).

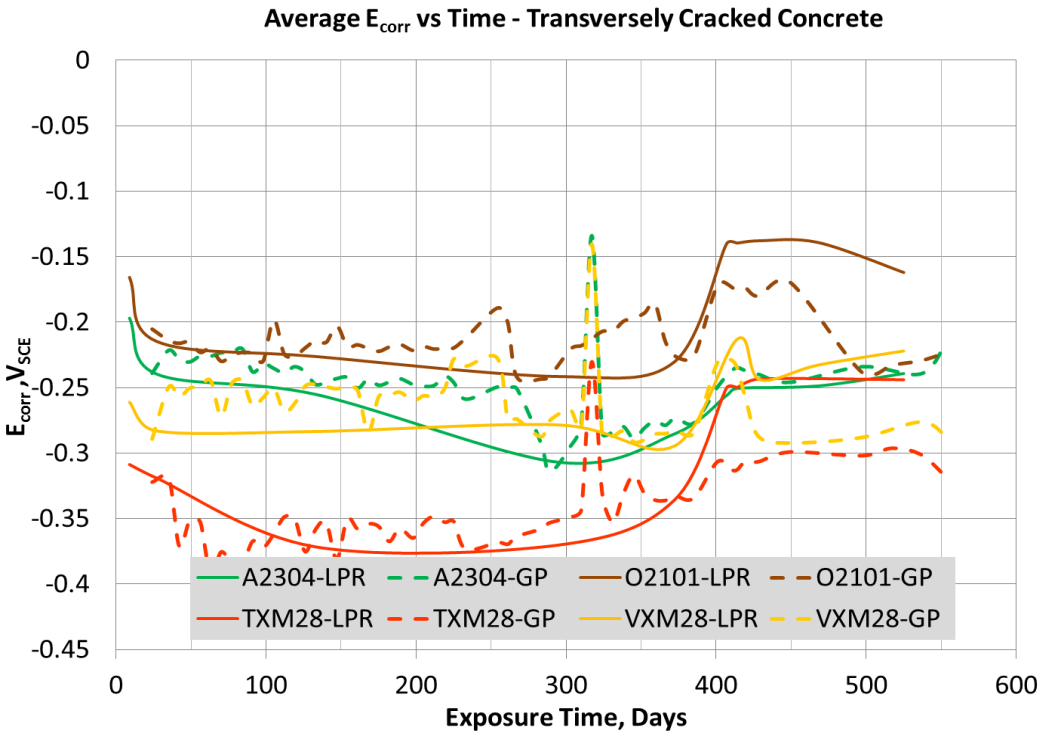

Figure 4-16: Average E_{corr} - Stainless steel rebar in transversely cracked concrete

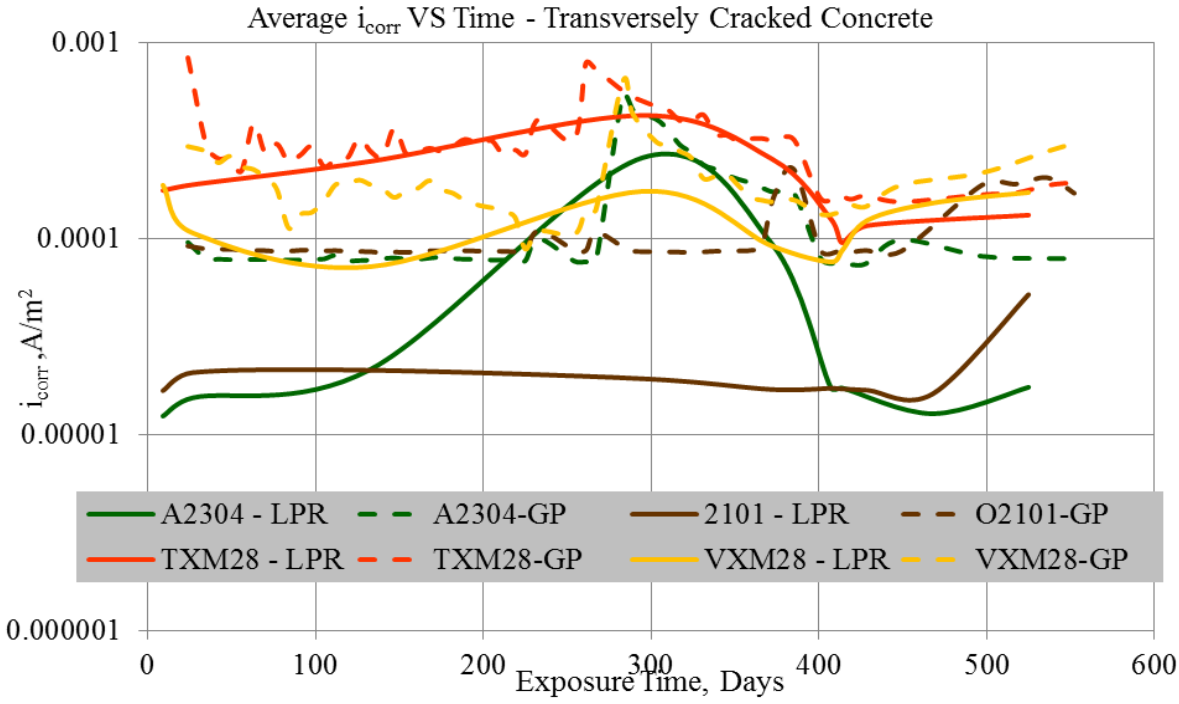

Figure 4-17: Average i_{corr} - Stainless steel rebar in transversely cracked concrete

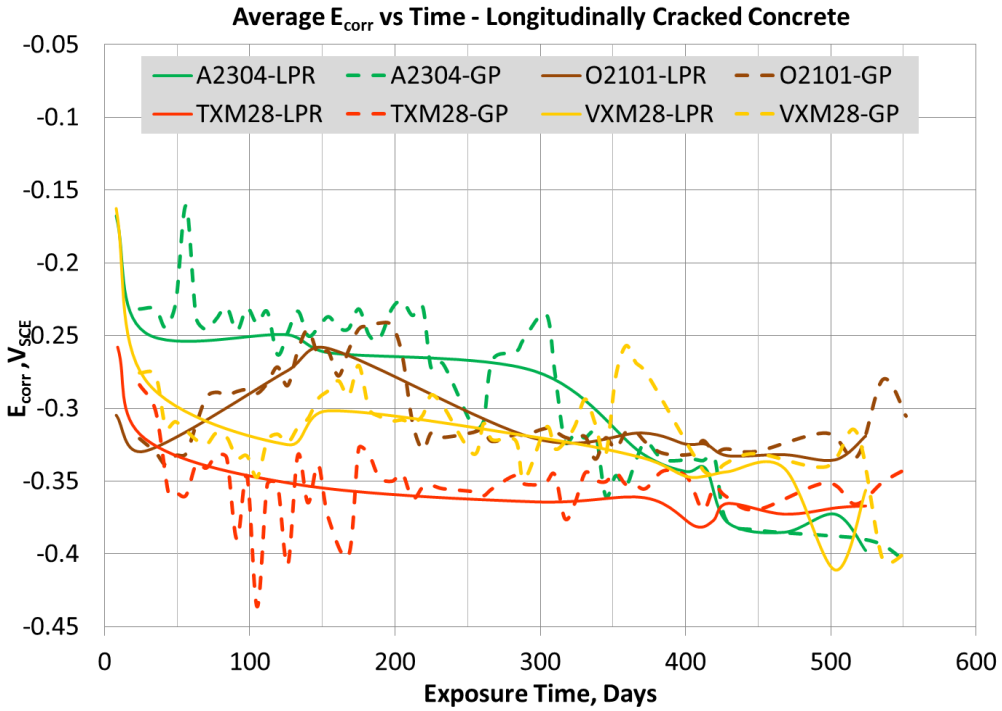

Figure 4-18: Average E_{corr} - Stainless steel rebar in longitudinally cracked concrete

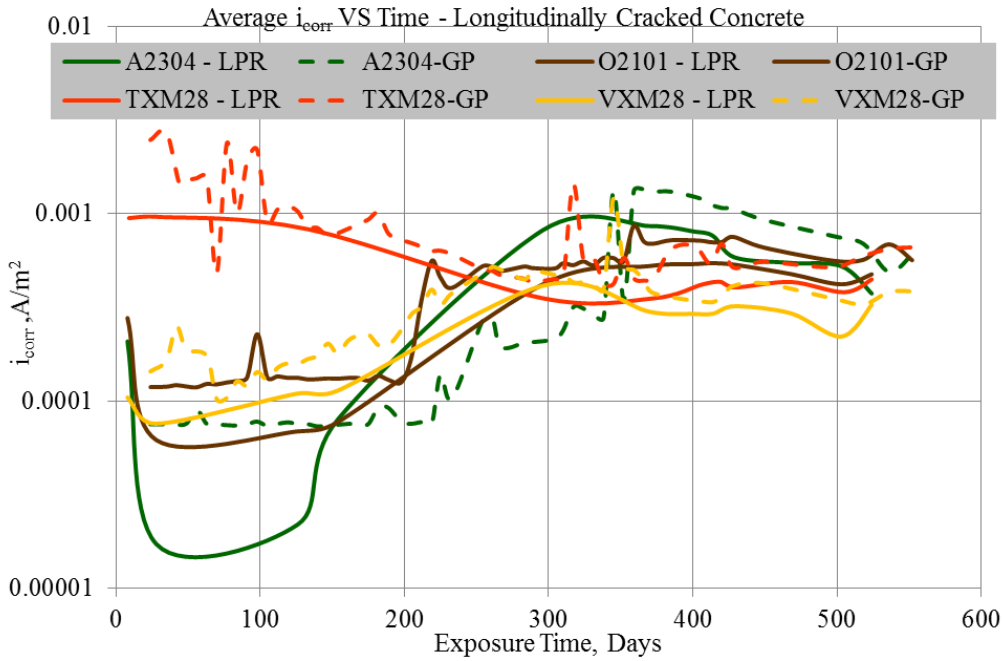

Figure 4-19: Average i_{corr} - Stainless steel rebar in longitudinally cracked concrete

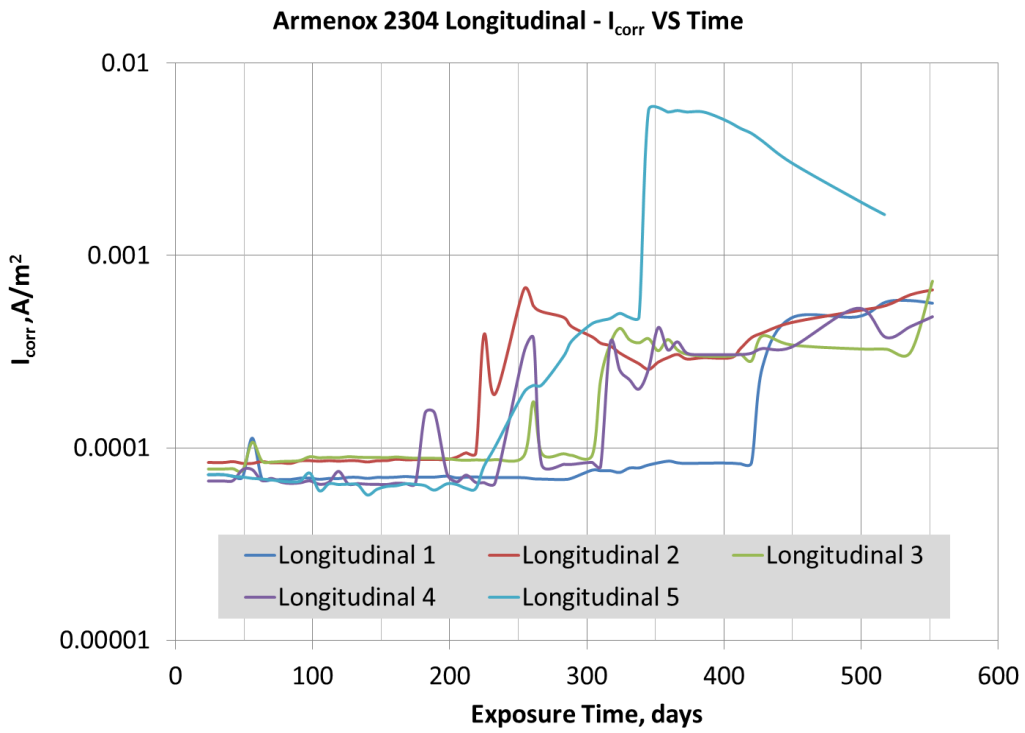

Figure 4-20: Individual i_{corr} values for A2304 in longitudinally cracked specimens

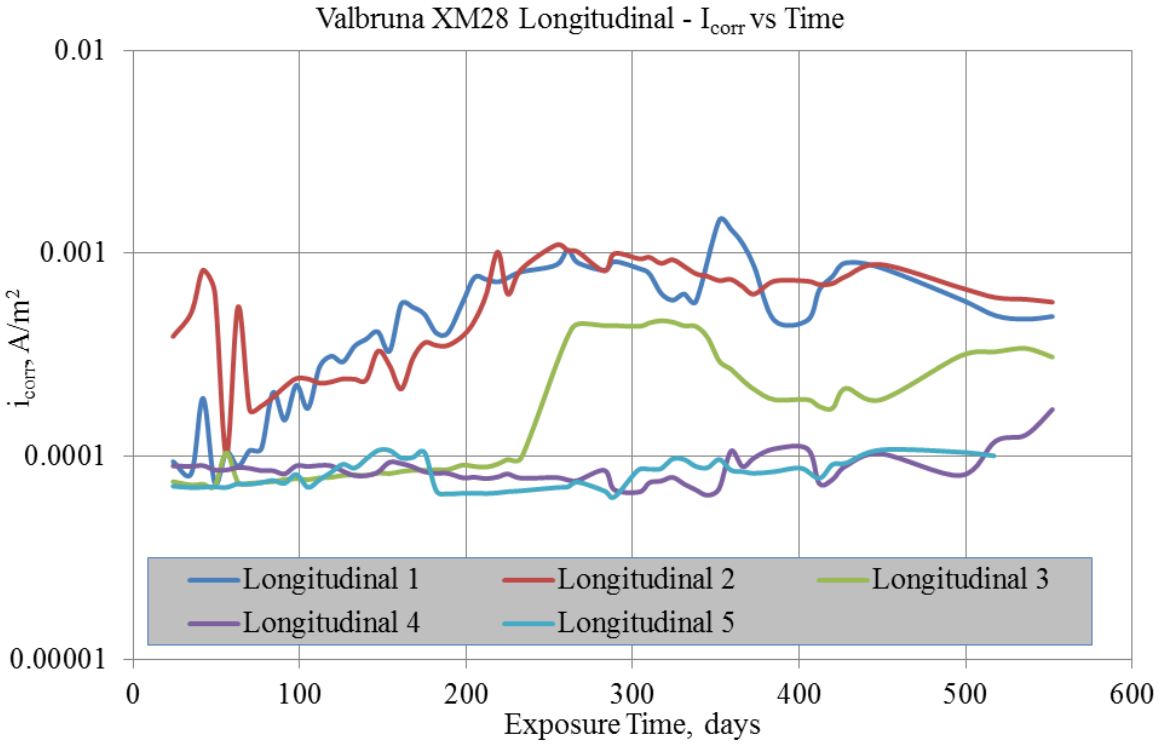

Figure 4-21: Individual i_{corr} values for VXM28 in longitudinally cracked specimen

4.3.2. Cyclic Polarization

4.3.2.1. Black and Corrosion Resistant Rebar

4.3.2.1.1. Sound Concrete

From the cyclic polarization curves, Figure 4-22 to Figure 4-24, it can be seen that the black, galvanized, and MMFX specimens all exhibit passive corrosion (on the reverse anodic potential sweep, the corrosion current density is at lower values than those in the initial curve).

4.3.2.1.2. Longitudinally and Transversely Cracked Concrete

For both the bars in longitudinally and transversely cracked specimens the open circuit potential is significantly more negative than those of the bars in sound concrete. The exponential shape of the curves and the data for the return potentials sweep being at higher current density values are typical of metals exhibiting active corrosion.

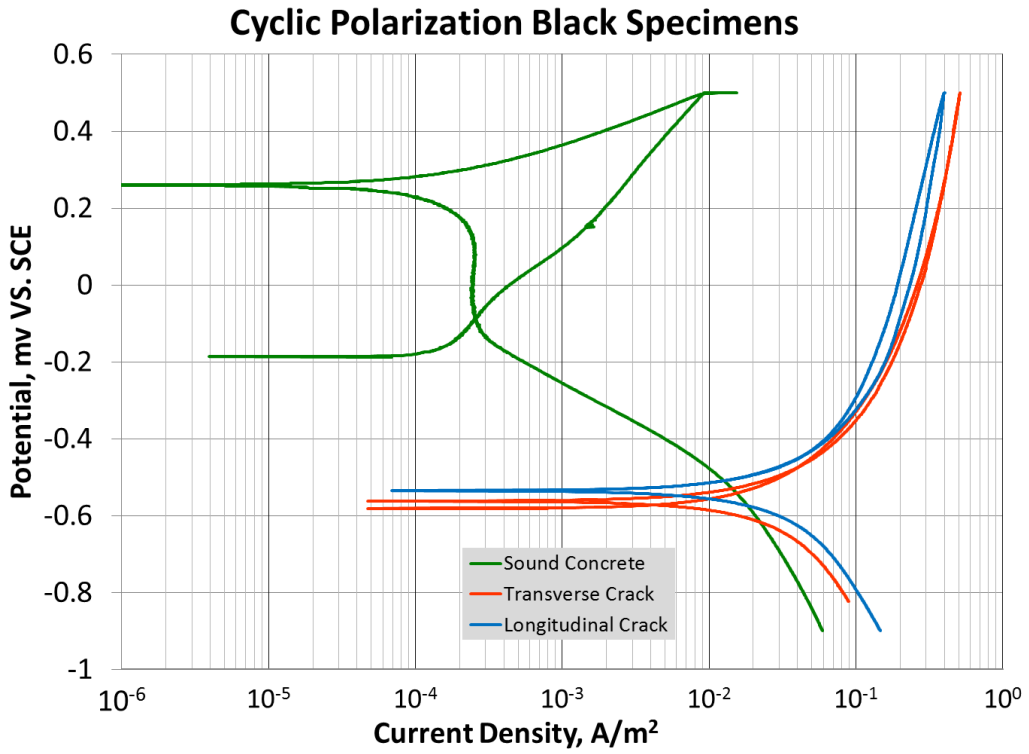

Figure 4-22: Cyclic polarization black

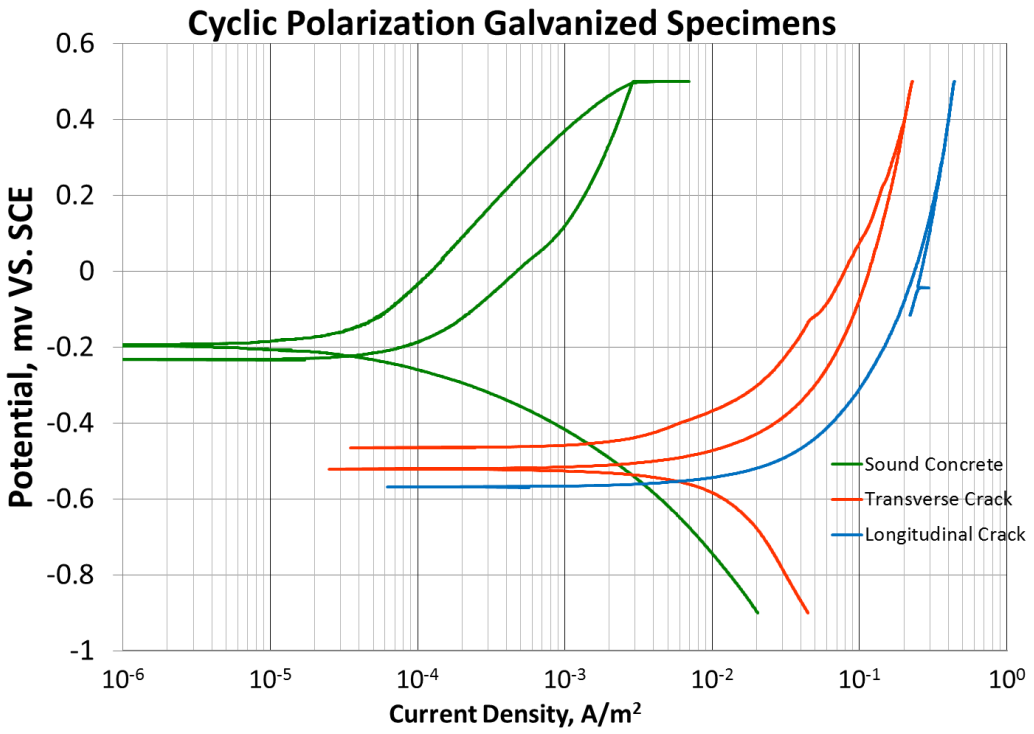

Figure 4-23: Cyclic polarization galvanized

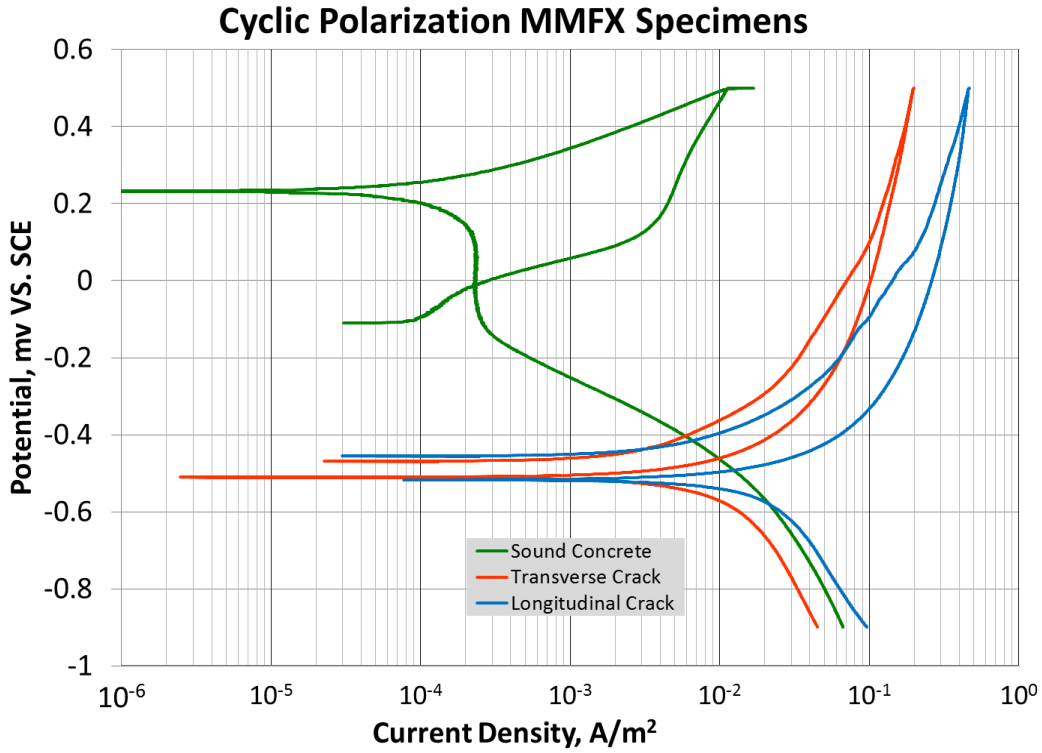

Figure 4-24: Cyclic polarization MMFX

4.3.2.2. Traditional and Recently Developed Stainless Steel Rebar

4.3.2.2.1. Sound Concrete

From the cyclic polarization curves, Figure 4-25 to Figure 4-31, note that all the steels exhibit passive behaviour, as the current density is lower when the potential is decreased from 500mV than on the positive potential sweep. The 316LN and 2205 steels have passive current densities (estimated by Tafel extrapolation) of $2x10^{-4}$ and $4x10^{-4}$ A/m^2, respectively, whereas those of the other stainless steels are much lower, namely between $2x10^{-5}$ and $8x10^{-5}$. This is in agreement with the GP and LPR measurements

4.3.2.2.2. Transversely Cracked Specimens

The initial open circuit potential of transversely cracked specimens in all cases are more cathodic than that of the bars in sound concrete specimens. The curves all show pitting potentials and, when the potential was decreased, all steels continued to actively corrode and exhibited a more cathodic open circuit potential than initially recorded.

4.3.2.2.3. Longitudinally Cracked Specimens

The initial open circuit potential of all the bars in the longitudinally cracked concrete, except Talley's XM28, were more cathodic than those of the bars in both the sound concrete and transversely cracked concrete. The potential of Talley's XM28 bar in the longitudinally cracked concrete was approximately 75mV more anodic then that of the bar in the transversely cracked concrete, and had a slightly lower corrosion current density at the maximum applied potential of 500mV vs SCE. It should also be noted that the 2304 had the highest corrosion current density (1 A/m^2) at a potential of 500mV, in the longitudinal specimen.

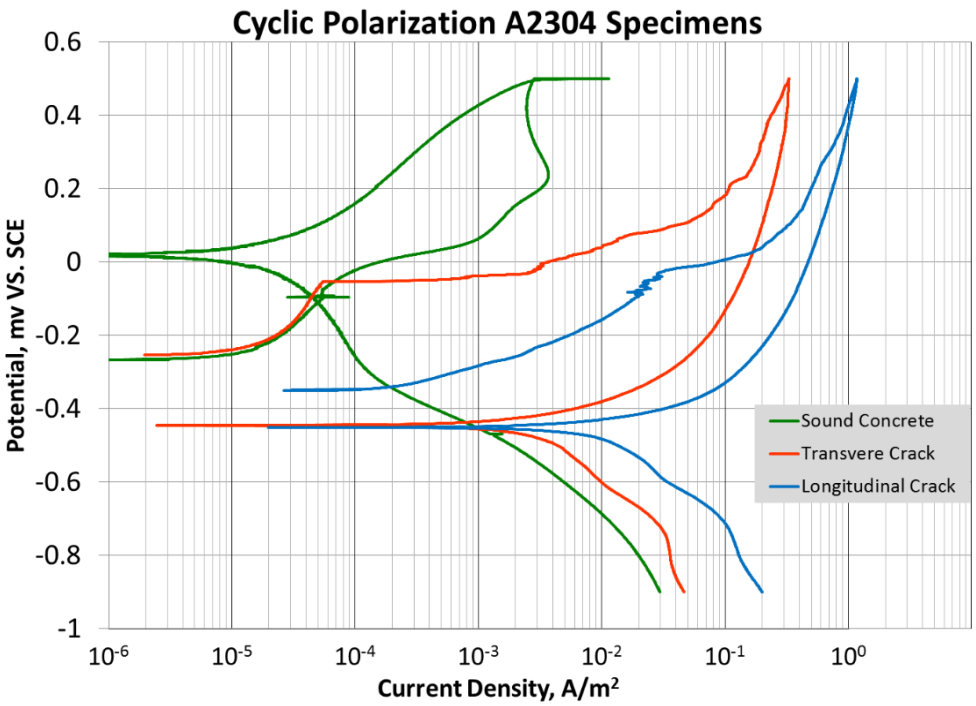

Figure 4-25: Cyclic polarization 2304

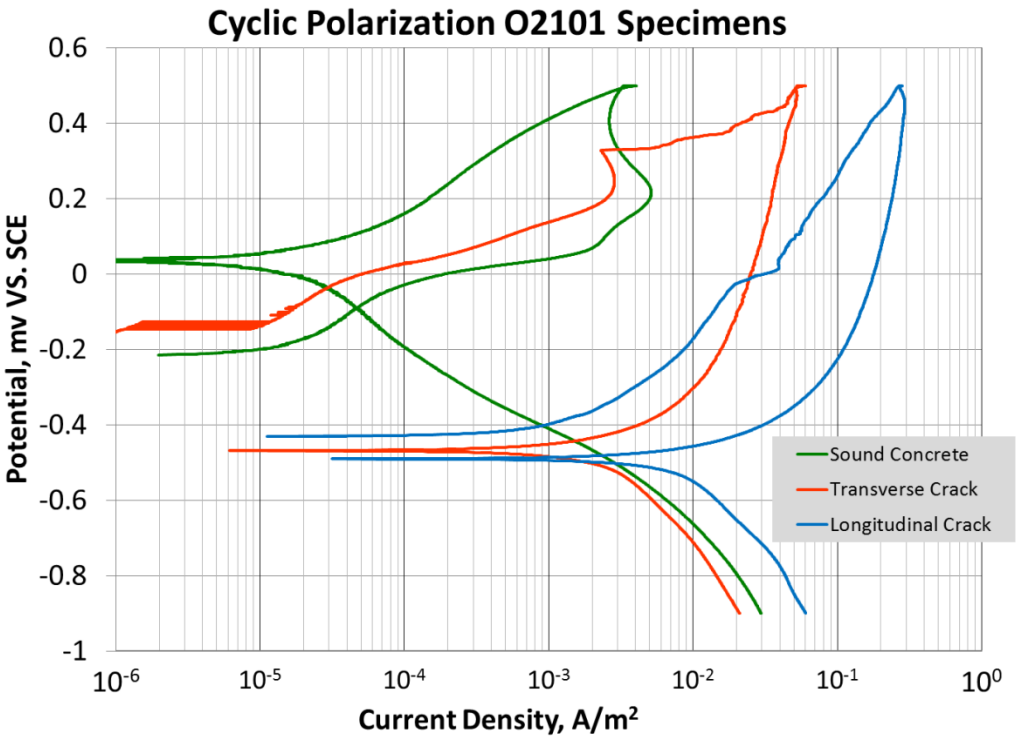

Figure 4-26: Cyclic polarization 2101

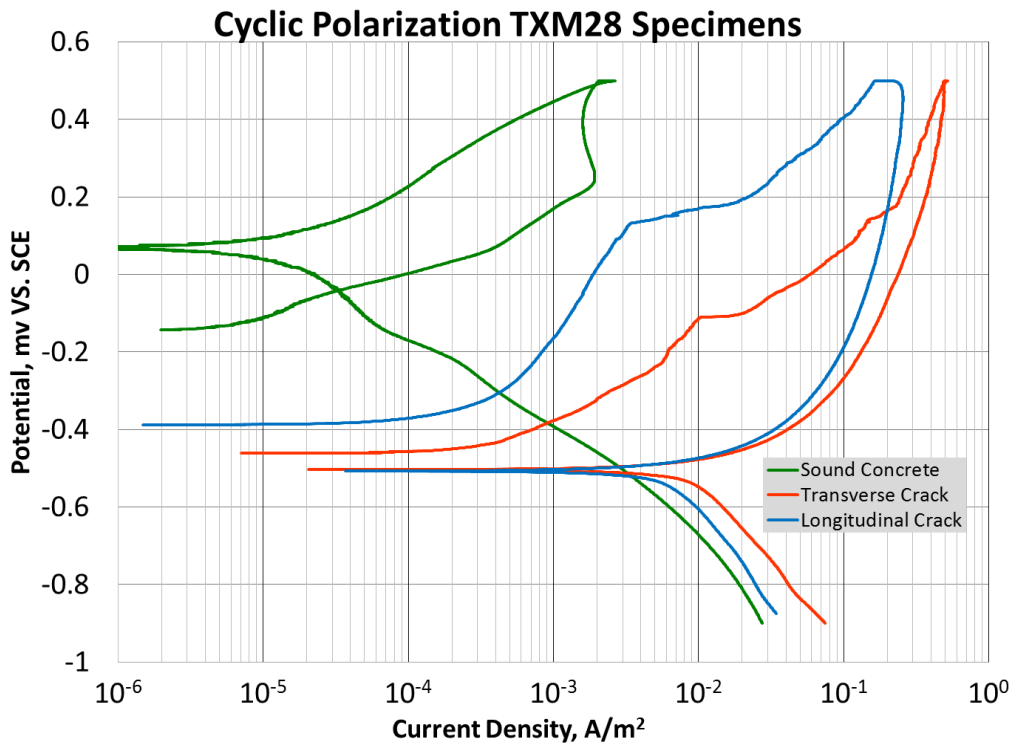

Figure 4-27: Cyclic polarization TXM28

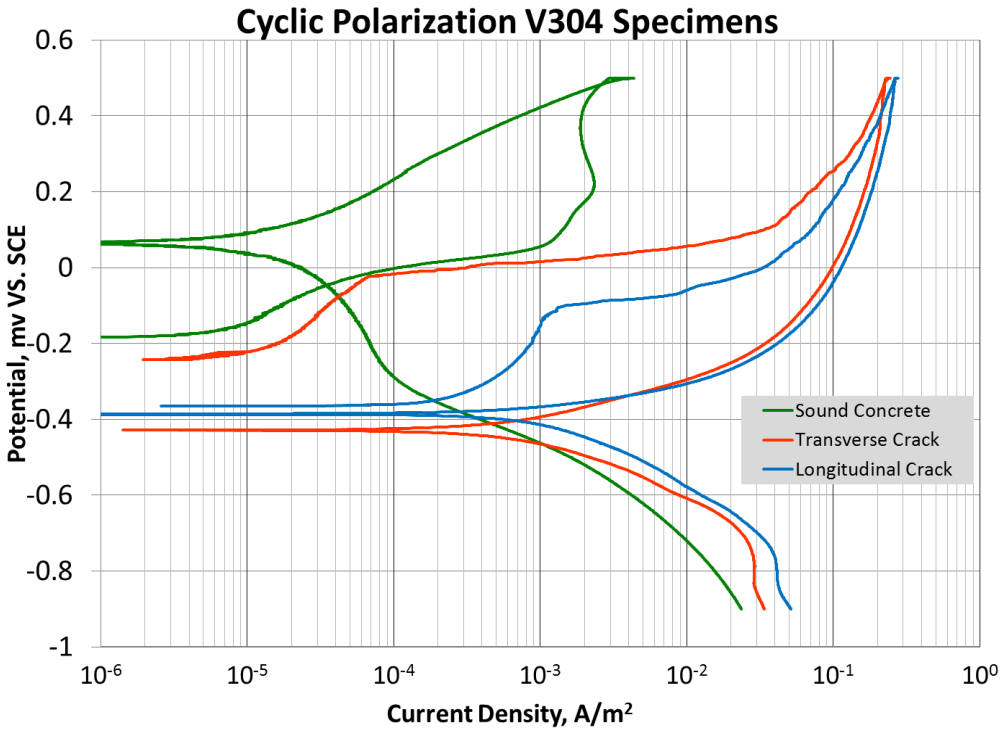

Figure 4-28: Cyclic polarization 304L

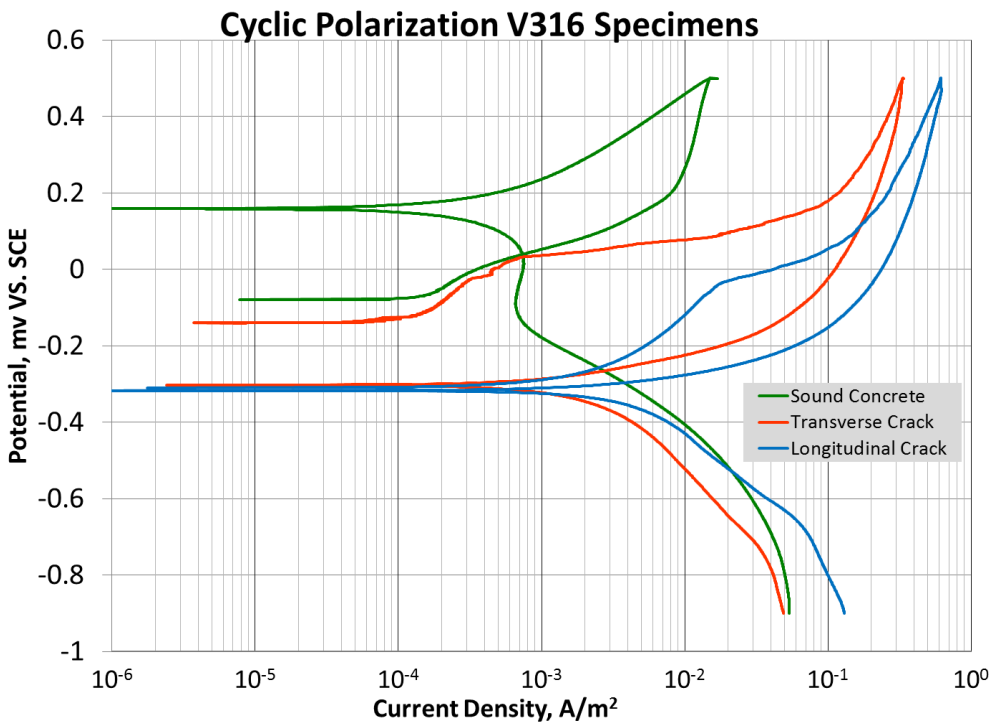

Figure 4-29: Cyclic polarization 316LN

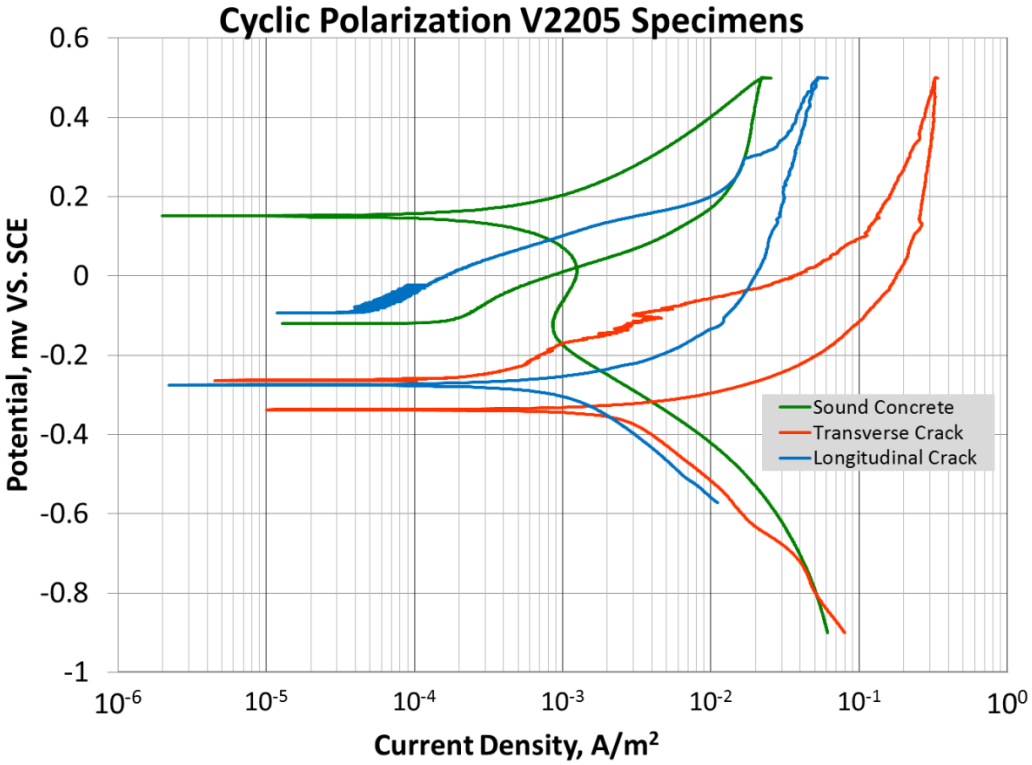

Figure 4-30: Cyclic polarization 2205

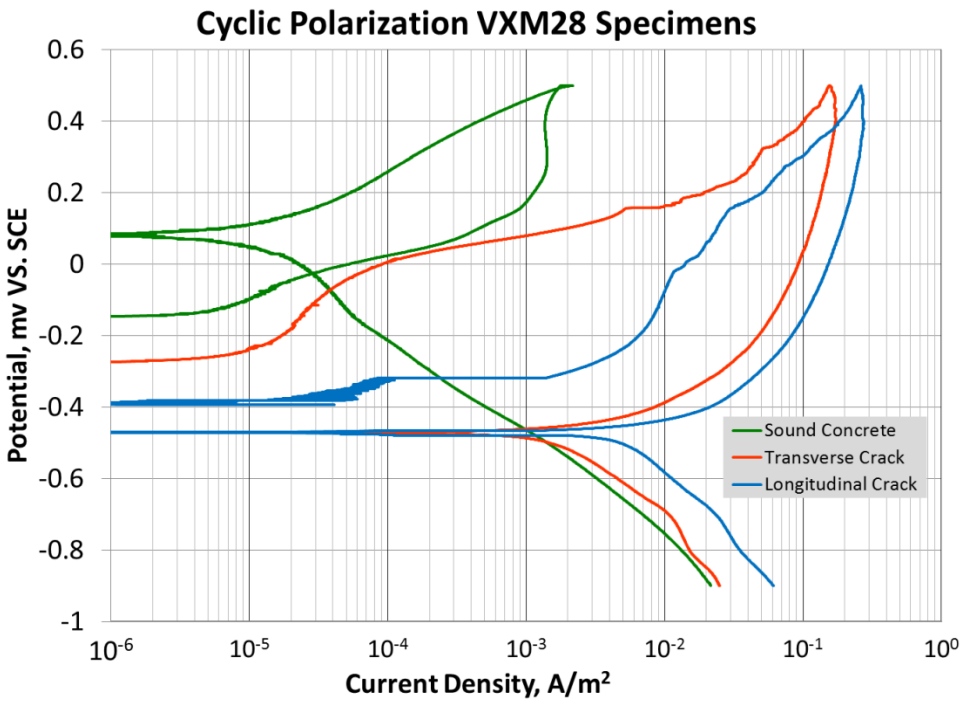

Figure 4-31: Cyclic polarization XM28

4.4. Autopsy Results

4.4.1. Transverse Specimens

In May 2014, after more than a year of electrochemical testing, one specimen of each rebar type in the transversely cracked concrete was autopsied. The specimens were chosen based on apparent corrosion rates, from electrochemical testing, to confirm that active corrosion had initiated and to determine the area of steel which has been affected. An example of the electrochemical i_{corr} results is displayed in Figure 4-32, to demonstrate why specimen number one of this grade of steel was chosen.

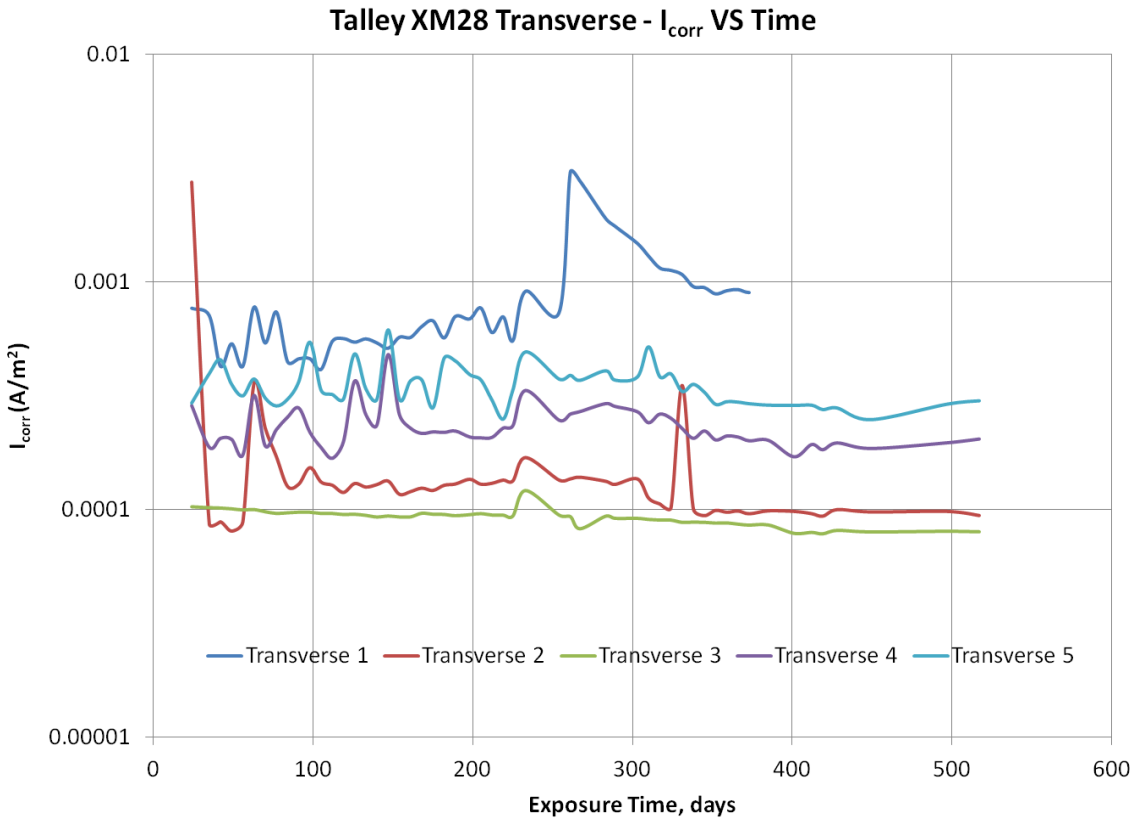

Figure 4-32: Talley XM28 transverse cracked i_{corr}

Once the specimens were removed from the multi-chloride brine, they were photographed to document any corrosion staining on the outside of the concrete, such as that shown in Figure 4-33. Note two observations: first, the 304 shims inserted to hold the crack open at 0.3 mm (top and bottom of the crack), did not survive the chloride and, second, it appears that corrosion product from the bar below is being driven out of the crack.

Figure 4-33: Example of a transversely cracked sample of Valbruna 304 before autopsy

The specimens were then autopsied by cutting the concrete on both sides to a depth of approximately 3mm (1/8 inch) above the steel, as to not detrimentally effect the surface of the rebar, or wash away corrosion products. One side of the sample was then compressed in a vice and levered to crack the prism in half. This allowed the surface of the rebar to be examined for corrosion, and the adjacent concrete to be examined to determine the migration of corrosion products, Figure 4-34.

Figure 4-34: A: Corrosion products migration demonstrated on the concrete surface adjacent to the steel; B: rebar surface corrosion on Valbruna XM28

It was noted that all the stainless steels, as well as the corrosion resistant steels exhibited corrosion to varying extents beginning directly under the crack with corrosion and corrosion products often migrating horizontally along the surface of the rebar, see summary and rank in Table 4-3. This is likely because of different crack widths and crack length providing different chloride concentrations to each specimen.

Table 4-3: Ranking of transversely cracked specimens by crack size and extent of visual corrosion

Bar	Crack Size (mm)	Extent and location of Corrosion Product	Rank
O2101-#2	0.2-0.4	1cm^2	1
V2205-#1	0.25-0.6	4 cm^2	2
V316-#3	0.15-0.33	Under end cap + strip along surface imperfection	3
A2304-#1	0.4-0.5	6cm^2	4
VXM28-#1	0.15-0.25	3 cm^2	5
V304-#1	0.25-0.5	13cm^2 + Under end cap	6
TXM28-#1	0.25-0.4	12cm^2	7
Galvanized	0.2-0.8	25cm^2 (Concrete exhibited severe cracking)	8
MMFX-#5	0.15-0.4	16cm^2 + severe pitting	9
Black	0.15-0.4	40 cm^2 - general corrosion	10

After the initial specimens were assessed, the remainder of the transversely cracked specimens were autopsied on January 5th, 2015, following the procedure outlined previously. The approximate crack size of each specimen was recorded, as well as the area of the corrosion product. Each specimen was given a score, Equation 5, and then the average score was used to rank the stainless steels,

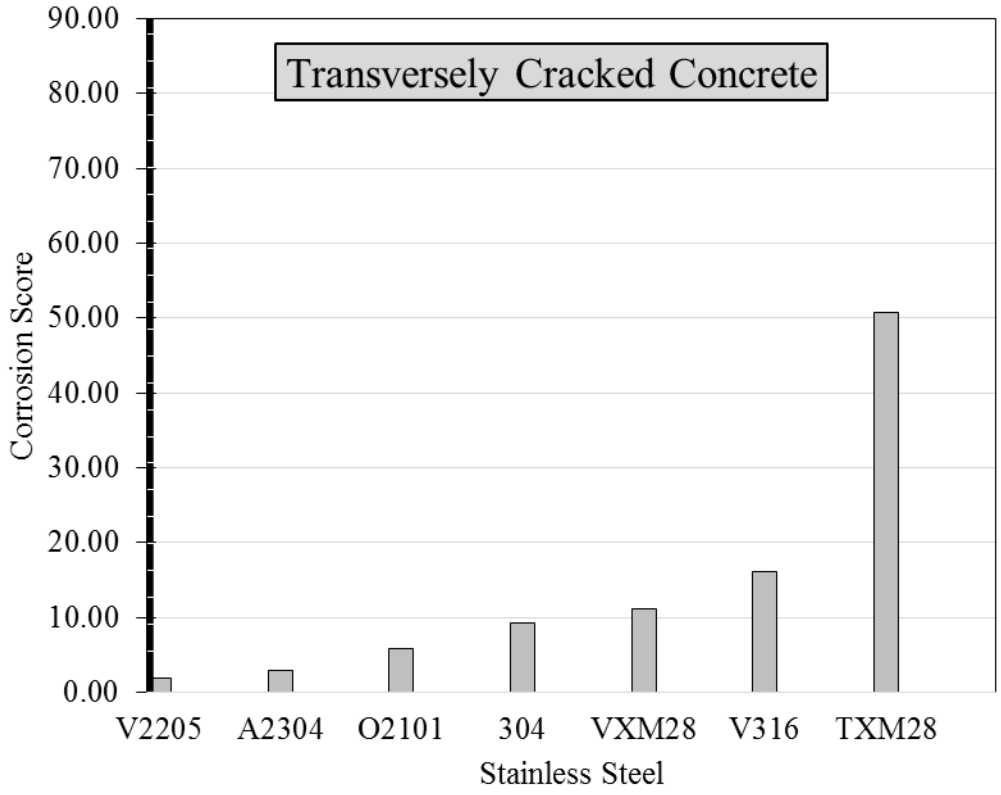

Figure 4-35, with the lowest score being the most corrosion resistant. The raw data has been placed in Appendix C.

$$Score = \frac{A_{Corrosion}}{W_k}$$ Equation 5

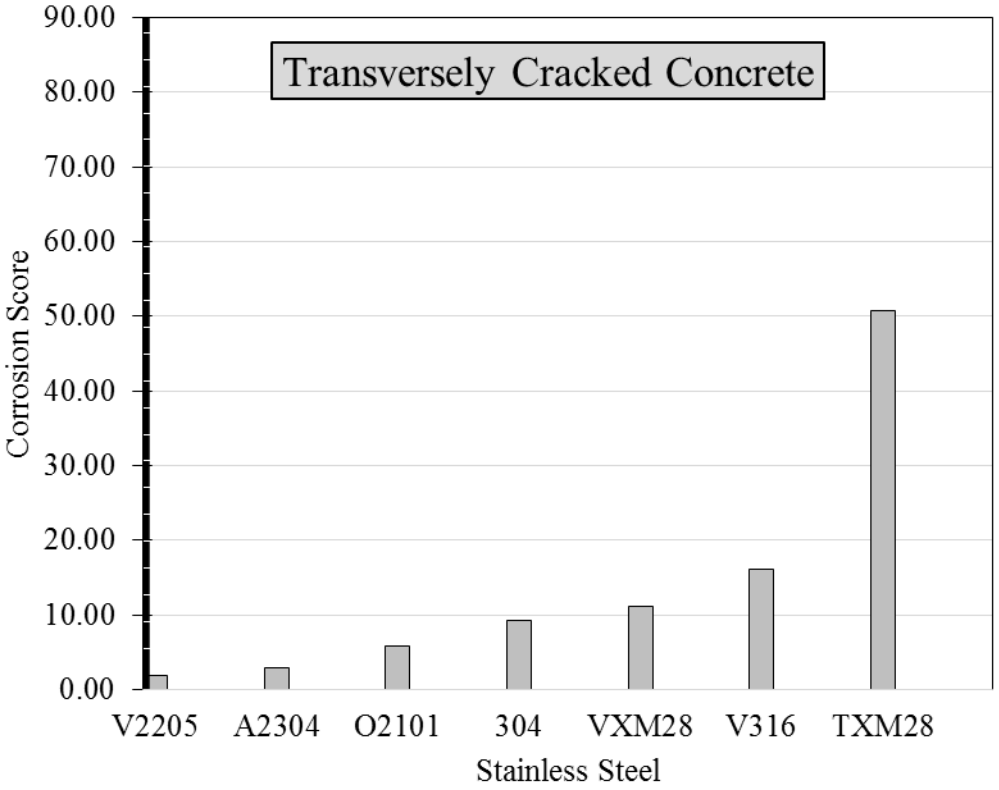

Figure 4-35: Corrosion score of transversely cracked concrete specimens

4.4.2. Longitudinal Specimens

In October of 2014, after 18 months exposure to multi chloride, one bar of every steel type was removed from the multi chloride bath and autopsied to confirm the results of the electrochemical testing. Since the geometries of these specimens were different from those of the transverse bars, the specimen selection was done based on the accessibility of bars, not the corrosion levels, which has provided some interesting results. Note due to accessibility issues an MMFX sample was not able to be removed from the tank. The average crack widths, amount of corrosion product, as well as rank are presented in Table 4-4, and i_{corr} results have been displayed in Figure 4-36.

Table 4-4: Crack widths of longitudinally autopsied specimens

Bar	Crack Size (mm)	Extent and location of Corrosion Product	Rank
V2205-#5	≈ 0.15	-No corrosion	1

O2101-#5	0.20-0.45	-corrosion under one end cap	2
V304-#4	0.20-0.40	-corrosion under one end cap	3
V316-#5	0.15-0.20	-corrosion under one end cap	4
VXM28-#5	≤ 0.15	-localized corrosion ≤1cm^2	5
TXM28-#5	≈ 0.15	-two localized corrosion ≈7cm^2	6
A2304-#5	0.25-0.33	-approximately 40% of exposed surface	7
Galvanized-#5	0.20-0.30	-approximately 25% of exposed surface	8
Black-#5	0.15-0.25	-approximately 40% of exposed surface	9

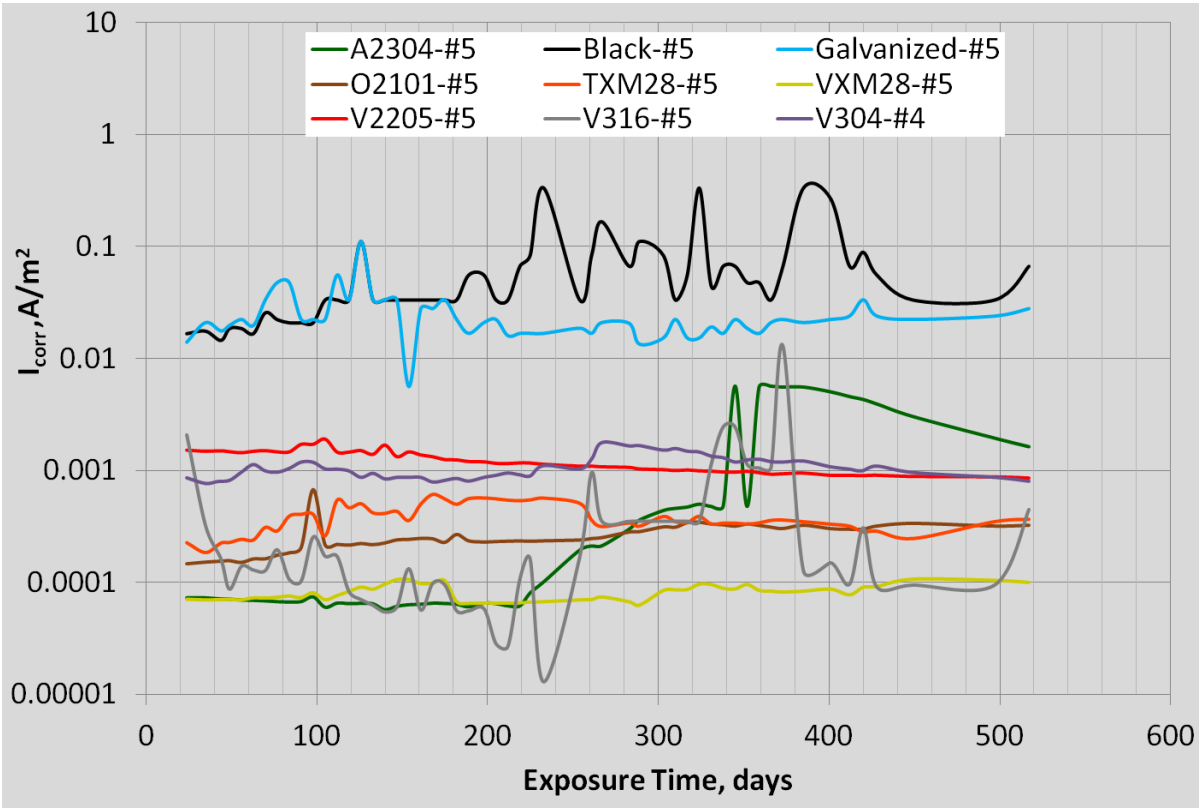

Figure 4-36: i_{corr} data for autopsied longitudinally cracked specimens

As the data suggest, both the galvanized and the black bar are corroding at a much higher rate than the stainless steels, even though the crack width falls within the Ministry of Ontario specifications. The 2304 has surface staining over approximately 40% of the exposed area, potentially because of

the larger crack widths. Both XM28 bars exhibited low surface staining suggesting that corrosion has just recently initiated, despite the smaller crack widths, and without much change in the i_{corr} values seen in Figure 4-36. The 304L, 316LN, and 2101 all exhibit small amounts of corrosion under the end cap. The fact that there is not any corrosion of the exposed surface can be expected from the 316, with the small crack widths and high corrosion resistance, but the fact that both 304 and 2101 have exhibited passive behaviour with cracks larger then Ministry specifications is rather surprising.

Approximately one month after the initial bars were autopsied, the remainder of the bars were removed from the chloride solution and autopsied, the crack widths and extent of corrosion have been presented in Appendix C. Although many of the bars have exhibited corrosion products on the surface of the rebar, and staining on the concrete, both of the XM28 bars exhibited a different surface staining pattern. While most corrosion product appears to be wet, with an expansion and delamination of the corroding steel, Figure 4-37, the XM28 corrosion product appeared dry and did not appear to stain the concrete, Figure 4-38.

Figure 4-37: Delaminated corrosion product on 2101 stainless steel

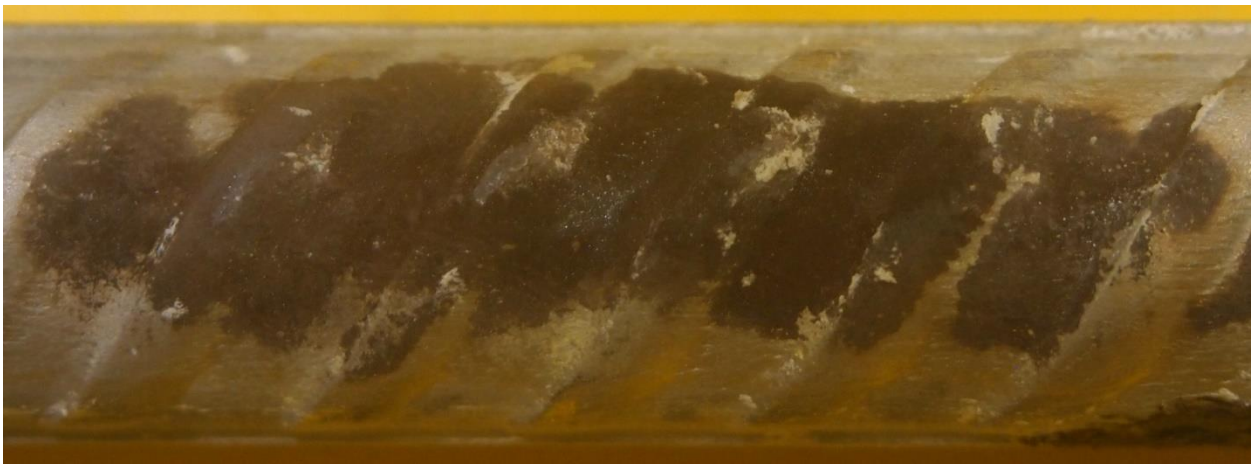

Figure 4-38: Adherent dry corrosion product on Valbruna XM28 stainless steel surface

Similarly to the transverse specimens, the longitudinally cracked specimens were scored using Equation 5, with the results displayed in Figure 4-39, with the raw data available in Appendix C.

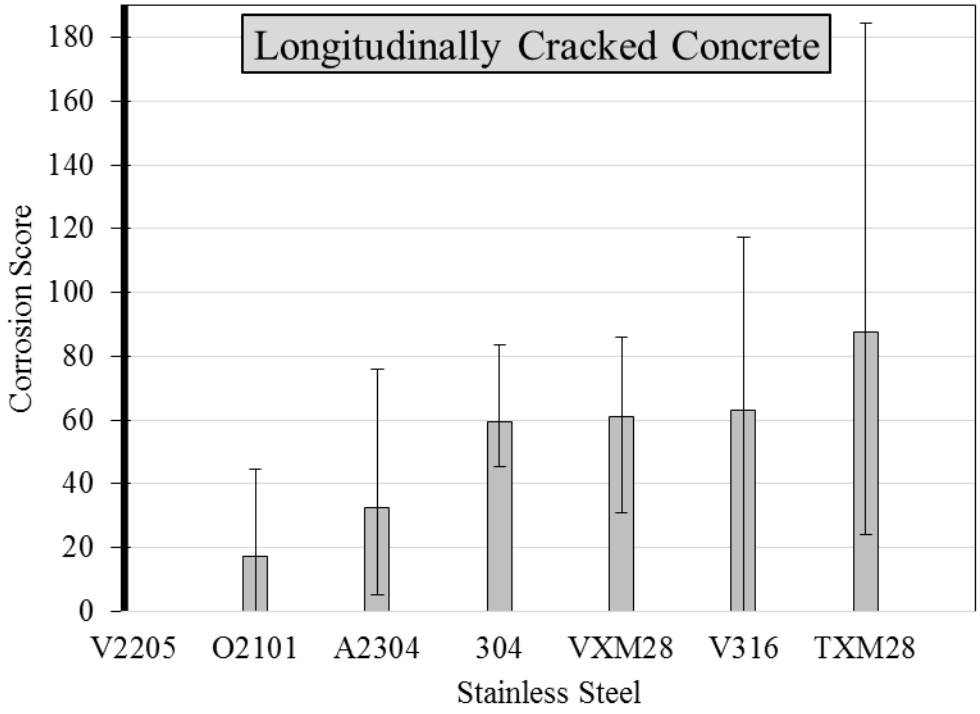

Figure 4-39: Corrosion score of longitudinally cracked concrete specimens

4.4.3. Comparison

In order to determine the ideal rebar for a specific exposure condition and price point, all the corrosion resistant rebar must initially be compared to the base black bar. Based on the results of a visual inspection of the bars in both the longitudinally and transversely cracked specimens, as well as work done by a colleague on rebar in pore solution and a modified European test, Table 4-5 was created.

Table 4-5: Comparison and ranking of rebar results from four different tests

	Modified EN: 480-14: 2006	Longitudinally cracked concrete	Transversely cracked concrete	Pore Solution Tests
S32205	1	1	1	1
S32101	2	2	3	4
S31653	3	6	6	5
S30403	NA	4	4	3
S32304	5	3	2	2
S24100-V	NA	5	5	6
S24100-T	4	7	7	7
Galvanized	NA	8	8	NA
MMFX	NA	9	9	8
Black	NA	10	10	9

The purpose of having several replicate specimens of each condition type was to determine the variability of the results, so that the data could be extrapolated to a 75 year design life. When comparing the results from Table 4-5, there is a lot of consistency across the modified EN: 480-14, longitudinally cracked, and transversely cracked result, while the pore solution results differ

slightly. Note, that the pore solution ranking was done by comparing the average chloride threshold values. The data suggest that the 2205 and 2101 are consistently the top performers, while 304L, Talley 24100, and 2304 round out the top five. While comparing the stainless steels to MMFX and galvanized rebar, it is interesting to note that galvanized bars tended to be more consistent than MMFX. Although limited corrosion was observed on the galvanized bar, it appears that the zinc coating, was performing as a sacrificial anode as it was designed to. Thus, this steel may be considered to be a viable option for high traffic municipal structures because of the price point and durability with soluble corrosion products.

4.5. Discussion

The electrochemical testing of the sound concrete samples does not indicate that any of the reinforcing bars have started to corrode verifying the low chloride diffusion rates of concrete with low water/cementitious material ratios and tightly controlled casting conditions. The data suggest that after nearly 600 days of chloride exposure, the chloride concentration at the depth of the rebar has not even exceeded the chloride threshold for black reinforcing bars, while the cracked specimens indicate the black rebar started to corrode within days of exposure, emphasising the need for corrosion models to include the effect of cracks.

When comparing the sound, transverse, and longitudinal concrete cyclic polarization data presented in Figure 4-22 to Figure 4-31, a number of interesting observations were made. In the sound concrete both the black and MMFX specimens reach a maximum current density of approximately $1.5x10^{-2}$ at 500mV vs SCE, slightly lower than the values for 2205 and 316LN which were approximately $2x10^{-2}$, while the galvanized reinforcing peaked at approximately $6x10^{-3}$, more similar to the other stainless steels. The trend of 2205 and 316LN having the highest passive corrosion current density of all the reinforcement tested in the sound concrete specimens was also observed by linear polarization resistance and galvanostatic pulse testing, Figure 4-9. When the longitudinal and transversely cracked concrete cyclic polarization data were compared, it was interesting to note that the corrosion current density of black, galvanized, and MMFX all peak around $5x10^{-1}$ A/m^2, which is a similar range to that of the stainless steels except the 2304. Which is counterintuitive, as the stainless steels should be more resistant to corrosion, thus having a lower corrosion current density. It is difficult to know why the 2205 and XM28 have higher

corrosion in the transversely cracked specimens rather than the longitudinal specimens, but it could be due to the width and depth of the crack, limiting the chloride diffusion in the longitudinally cracked specimens.

Chapter 5 Analysis

5.1. Deterioration Modelling

5.1.1. Sound Concrete

In order to investigate the life-cycle cost implications of choosing stainless as opposed to black steel reinforcing, a probabilistic corrosion model was developed, which combined elements of two existing models. First, Hartt's [1] service life projection model was utilized. This model uses Fick's second law, (Equation 1), to determine the time until corrosion initiation and the time until corrosion propagation results in concrete cracking and /or spalling. This model is described graphically in Figure 5-1[1], where t_i is the time to corrosion initiation, t_p is the "propagation" time from corrosion initiation until concrete spalling renders the structure unusable, and t_s is the total service life after which it is assumed that rehabilitation or replacement is required.

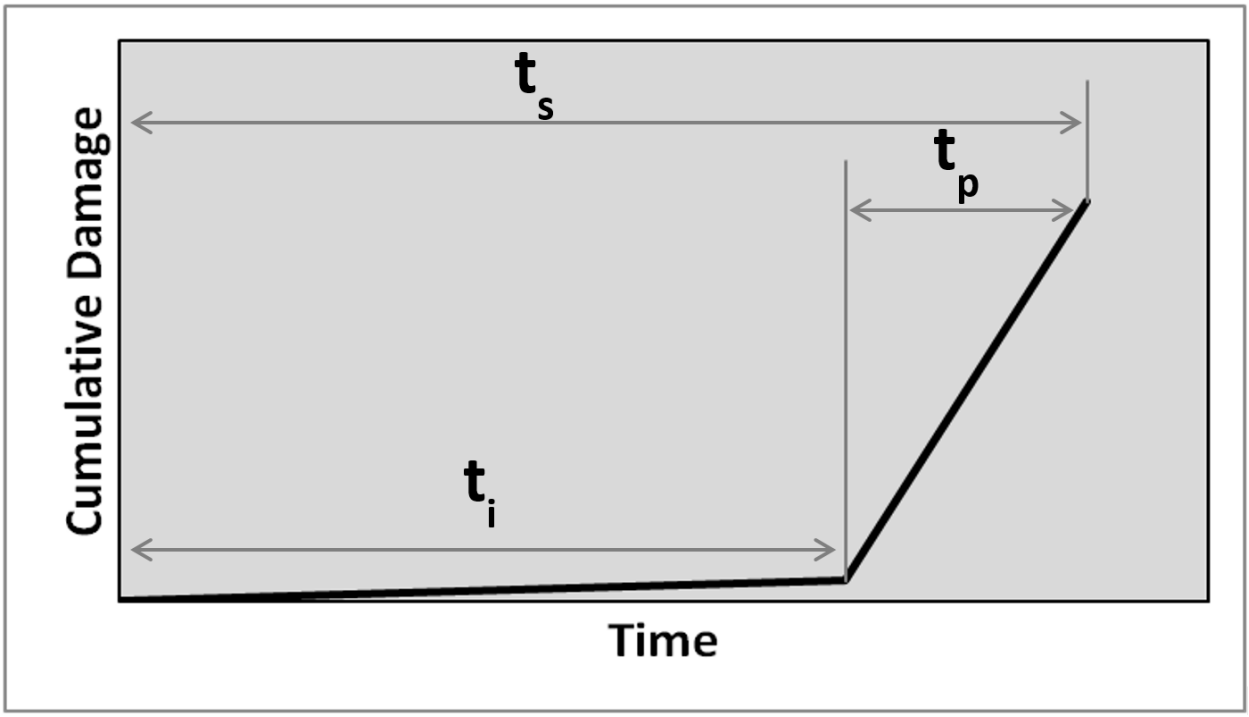

Figure 5-1: Hartt's graphical representation of the time scale of corrosion initiation, crack propagation, and time to failure of rebar in concrete structures [1]

Hartt calculates t_s as a statistical distribution, by defining the input parameters as statistical variables. He solves for this statistical distribution in a closed-form expression, which requires

integration over the ranges of the statistical variables. In the model developed for the current study, the same expression for t_s was used. However, Monte Carlo simulation (MCS) was employed rather than integration to determine the statistical distribution for t_s. Four input parameters were varied, namely: the surface chloride content (C_s in kg/m^3), the apparent diffusion coefficient (D in m^2/s), the concrete cover (x in m), and the chloride threshold level (C_T in wt% cementitious material). Once the chloride level is exceeded, corrosion is assumed to have initiated and the associated time, t_i has been determined. Next, t_p is determined by using Equation 6, where χ_{crit} is the critical corrosion section loss required to crack the concrete, and CR_{AVG} is the average corrosion rate over the whole rebar surface:

$$t_p = \frac{\chi_{Crit}}{CR_{AVG}} \qquad \text{Equation 6}$$

χ_{crit} is determined using Equation 7, where x is the concrete cover in metres, ϕ is the bar diameter in metres, and L is the bar length in metres (conservatively assumed to be infinite):

$$\chi_{Crit}(m) = 11*10^{-6}\left(\frac{x}{\phi}\right)\left(\frac{x}{L}+1\right)^2 \qquad \text{Equation 7}$$

Equation 7 was based on an experimental study by Sagues et al. [52]. As the rebar corrodes it experiences section loss. However, the corrosion product that results has a larger volume than the original metal. The result is that tensile stresses are introduced in the concrete, which eventually cause it to crack and spall. The level of section loss associated with spalling depends primarily on the bar diameter and cover, according to this model. Presumably the concrete strength also plays a role. However, the model does not consider this.

CR_{AVG} is determined using Equation 8, where ERF is the Gaussian error function, and D is the diffusion coefficient:

$$CR_{AVG} = 0.618\left[1.45C_s\left(1-\mathrm{ERF}\left(\frac{x}{2\sqrt{D\cdot T}}\right)\right)\right] \qquad \text{Equation 8}$$

This equation assumes that the chloride concentration at the rebar depth is varying according to Fick's law and the corrosion rate increases exponentially with the chloride concentration. Once t_i and t_p have been determined, the service life, t_s, is simply the sum of t_i and t_p.

5.1.2. Cracked Concrete

To incorporate the effect of concrete cracking, a model from Lu et al. [2] was used. Concrete cracking occurs in a number of ways, including but not limited to: impact damage, loading (i.e. structural cracks), and during concrete curing (i.e. shrinkage cracks). These shrinkage and structural cracks can go undetected until a detailed bridge assessment is conducted, greatly altering the corrosion initiation time estimates. If the extent of the cracking is known, Lu et al. [2] suggest a mathematical approach, whereby the combined diffusion rates in both the cracked and un-cracked regions are represented by a weighted average as shown in Equation 9:

$$D_{cc} = \frac{AD_a + A_{cr}D_{cr}}{A + A_{cr}} \qquad \text{Equation 9}$$

where D_{cc} is the combined chloride diffusion coefficient (m^2/s), D_a and D_{cr} are the apparent chloride diffusion coefficients of the sound concrete and the cracked concrete, respectively (m^2/s), and A_{cr} is the total area of the cracks. Lu et al. also provide equations for cracked concrete diffusion coefficients following the procedure of Djerbi et al. [53] (Equation 10) and equations for sound concrete with or without supplementary cementing materials (SCMs, Equation 11 to Equation 13):

$$D_{cr} = \begin{cases} (0.16w_k - 3)10^{-10} & 30\mu m \le w_k \le 100\mu m \\ 13 \cdot 10^{-10} & w_k \ge 100\mu m \end{cases} \qquad \text{Equation 10}$$

$$D_a = 10^{-6.77\left(\frac{w}{b}\right)^2 + 10.1\left(\frac{w}{b}\right) - 14.64} \text{ ... no SCMs} \qquad \text{Equation 11}$$

$$D_a = 10^{-0.79\left(\frac{w}{b}\right)^2 + 3.4\left(\frac{w}{b}\right) - 13.1} \text{ ... with SCMs} \qquad \text{Equation 12}$$

$$\frac{w}{b} = \frac{27}{f'c + 13.5} \qquad \text{Equation 13}$$

where f'_c is the compressive strength of a standard cylinder (MPa) and w_k is the crack width. In the model developed for the current study, Hartt's model is used, with D replaced by D_{cc} calculated using the formulas proposed by Lu et al. to consider the presence of cracks.

5.1.3. Surface Chloride Build Up

Since the different regions of North America encounter different amounts of snow and winter weather, the structures in these regions are exposed to a varying range of chlorides from anti-icing agents. To consider this, the chloride build-up rates assumed in the Life-365 software and shown in Figure 2-7, [41] were used to select a rate for the corridor from Windsor Ontario to Montreal Quebec. These rates are considered to be among the most severe rates in North America.

5.1.4. Input Parameters

The model described in the previous sections was used to determine the conditions under which the use of different stainless steel grades would be optimal from a life-cycle cost perspective. To do this, all of the model's input parameters were varied to represent "low", "medium", and "high" service conditions. A summary of the six input parameters, with their assumed means (μ) and standard deviations (σ), can be seen in Table 5-1. In this table, the standard deviations consider both the uncertainty and the natural variability of each parameter. It should be noted that the coefficient of variation (CoV) for each parameter was held constant and equal to the value assumed by Hartt [1], (where applicable), because of a lack of data available to assume otherwise.

Table 5-1: Input parameters for Monte Carlo simulation

Environmental Condition Severity			Low	Medium	High
Crack width	W_{struct} (μm)	μ	100	300	500
		σ	30	90	150
Crack density	D_{struct} (m/m^2)	μ	0.1	0.5	1.1
		σ	0.18	0.91	2
Chloride Threshold	Ct –stainless steel (wt% cem.)	μ	1.7	3	4.9
		σ	0.164	0.29	0.474
Concrete Cover	x (cm)	μ	3	5	7
		σ	0.3	0.5	0.7
Surface Chloride Concentration	Cs (wt% cem.)	μ	3	6	9
		σ	0.75	1.5	2.25
Chloride Diffusion Coefficient	D (m^2/s)	μ	1.00E-12	4.00E-12	7.00E-12
		σ	3.33E-13	1.33E-12	2.33E-12

5.2. Crack width and density

Since crack width (W_{struct}) and density (D_{struct}) are affected by many variables (concrete strength, reinforcement ratio, loading, etc.), the model must take this variability into consideration when trying to represent a wide variety of concrete structures in a variety of environments. For the crack widths, a lognormal distribution is assumed (since this distribution stops at zero and negative crack widths and densities are not possible), with mean values ranging from 100 μm to 500 μm. The 300 μm crack width was considered based on the Ministry of Transportation of Ontario (MTO) practice that crack widths larger than this must be sealed by the contractor [47]. The 100 μm crack width was considered to determine the effect of tighter crack control standards, and to see if it would improve the service life of black reinforcement. The 500 μm crack width was considered to determine if larger cracks would drastically reduce the service life of stainless steel. As for the crack densities, Darwin et al. [54] have presented a range of field data that show that crack densities can range from 0.1 m/m^2 to 1.06 m/m^2 depending on the type of girder connection, and the year and season of construction (dealing with changing concrete quality). The cumulative distribution

functions (CDFs) of the three analyzed scenarios for crack width and crack density are plotted in Figure 5-2 and Figure 5-3 respectively, with mean and standard deviations in parentheses.

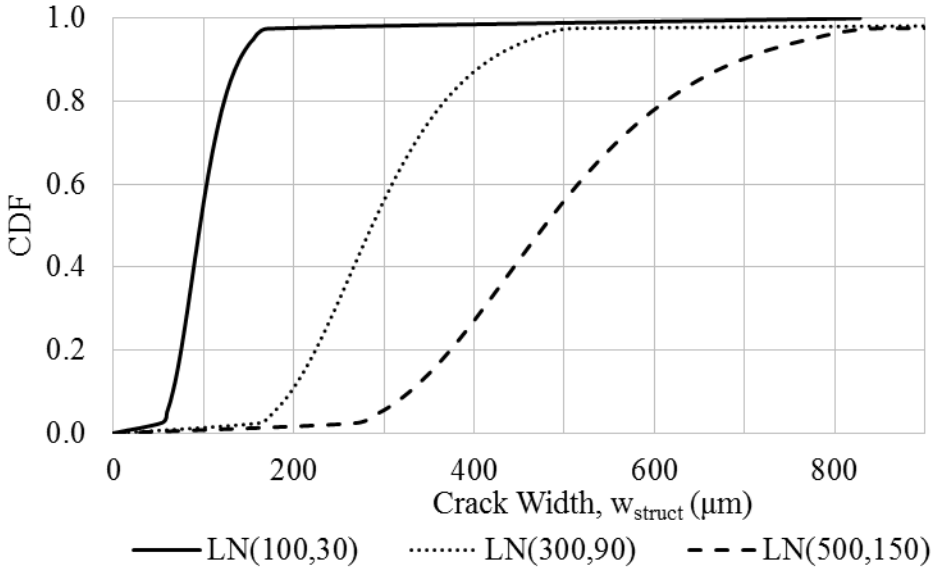

Figure 5-2: CDF's for 100, 300, and 500 μm crack widths

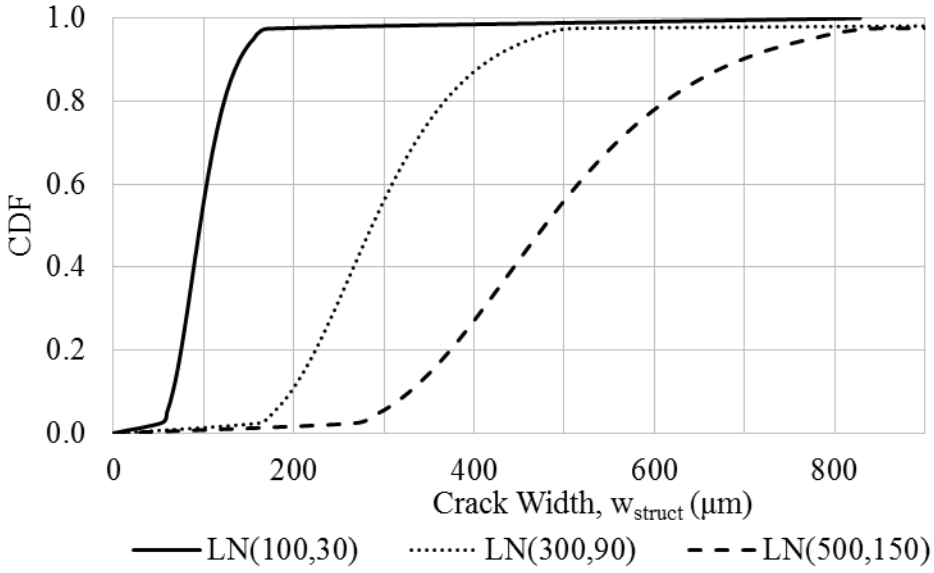

Figure 5-3: CDF's for 0.1, 0.5, and 1.1 m/m^2 crack densities

5.3. Chloride Threshold

When considering the variance in chloride threshold values for stainless steels, Randström et al. [31] have suggested it ranges between 2.5% and 11% in pore solution, as seen in Table 2-3. The chloride concentration in the pore solution is not equivalent to the chloride concentration by mass of cement, because some of it becomes chemically bound or physically trapped in the cement hydration products. Thus, the free chloride in the pore solution needs to be determined. When Anders et al. [55] analyzed the pore solution expressed from ordinary Portland cement paste with w/c = 0.50, they were able to plot the relationship in Figure 5-4, which correlated the chlorides in pore solution to known amounts of cast-in chlorides by mass of cement.

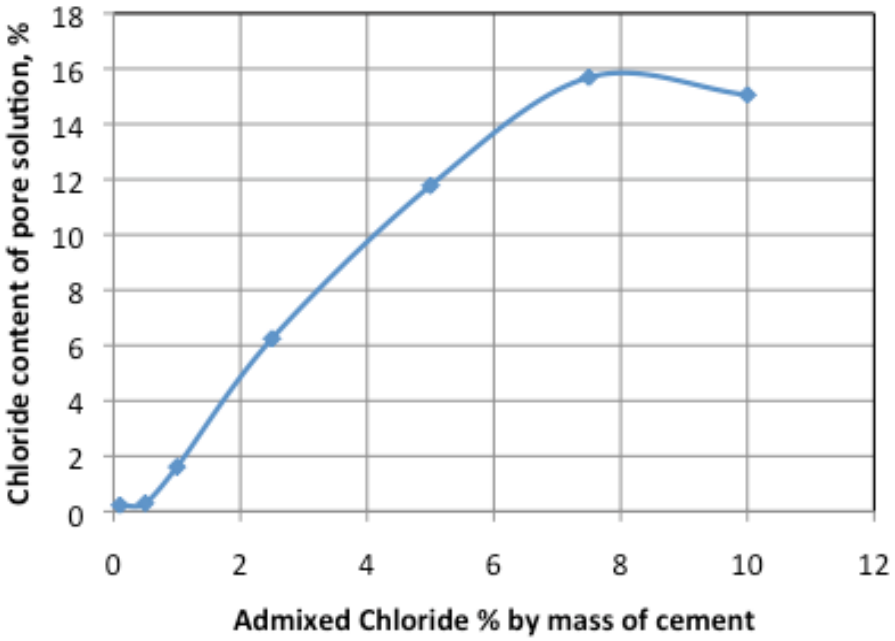

Figure 5-4: Chloride concentration of pore solution of pastes with admixed chlorides as NaCl [55]

Figure 5-4 suggests that 2.5% and 11% chloride in pore solution is equivalent to 1.7% and 4.9% respectively by mass of cement. The third value of 7% was used as a central value which correlates to approximately 3.0% by mass of cement. The cumulative distribution function (CDF) of the three lognormally distributed parameters analyzed is given in Figure 5-5.

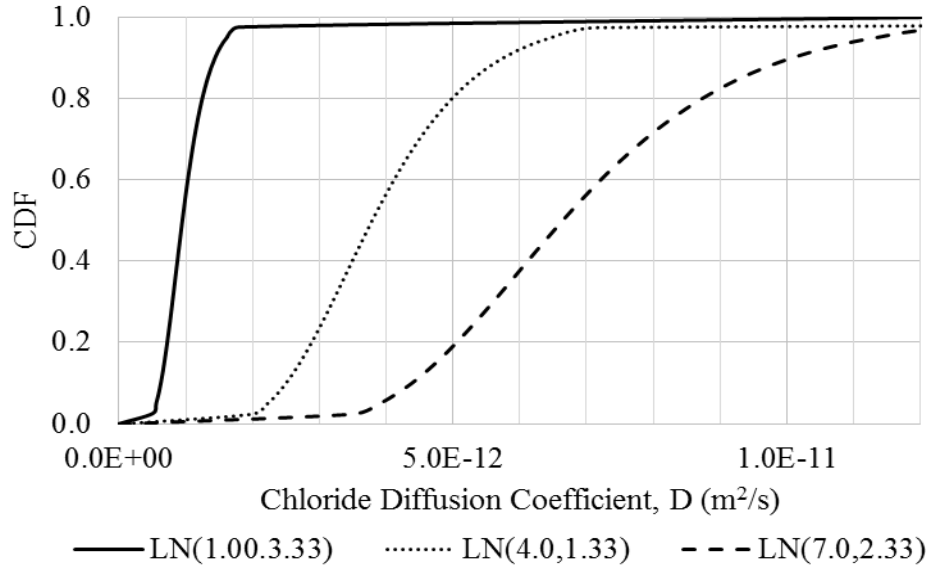

Figure 5-5: CDF's of 1.7, 3.0, and 4.9% chloride threshold by weight of cementitous material

5.4. Concrete Cover

When determining how the use of stainless steel, or corrosion resistant reinforcing could improve the durability of concrete structures, variations in concrete cover must be considered. The United Kingdom's Department of Transportation has proposed a 30 mm cover may be acceptable for structures where stainless steel is used if contractors can adequately ensure specifications are tightly met [42]. Alternatively, the New York State Department of Transportation [56] already allows for a concrete cover reduction of 1 inch (25 mm) from 3 inches to 2 inches (75 mm to 50 mm) if a solid stainless steel or stainless steel clad reinforcing bar is used in the top mat of the bridge deck. Lastly, a 70 mm concrete cover has been recommended in the Canadian Highway Bridge Design code [36] for structures using regular reinforcing. Regardless of which value is assigned for the nominal cover, cover is a parameter that is expected to vary considerably, due to the normal variations in construction tolerances. The cumulative distribution function (CDF) of the three lognormally distributed parameters analyzed is given in Figure 5-6.

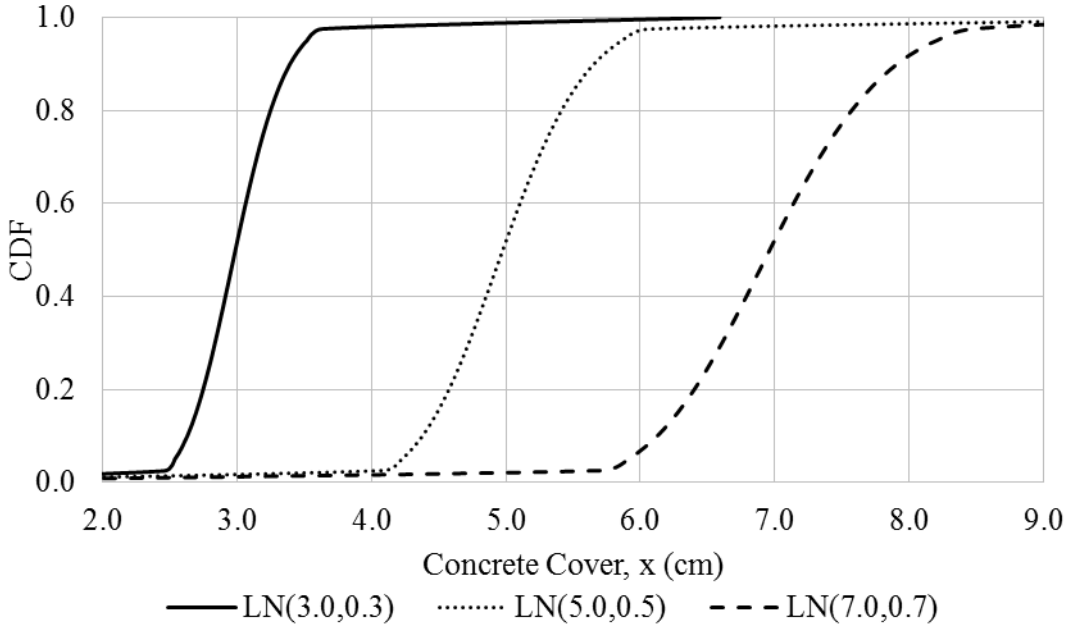

Figure 5-6: CDF's of 30, 50, and 70 mm concrete cover

5.5. Surface Chloride Content and Diffusion Coefficient

The surface chloride concentration of any concrete structure is dependent on the geographical location, the chloride exposure (i.e. splash zone, or water runoff zone), and when the content was measured (i.e. middle of the winter, after road cleaning, or after a rainfall). Ann et al. [57] suggest that since surface concrete is different from internal concrete, because there is more cement paste at the surface and areas adjacent to formwork, the chloride concentration millimetres below the surface may not be a true representation of the maximum chloride concentration over the life of the bridge. They also present data from a number of sources that suggest the highest surface chloride concentration for splash zones is approximately 5% by mass of cementitious materials, while tidal regions can have in excess of 12%. It should be noted that these papers are concerned with marine exposure and do not present de-icing salt data within Ontario, which Figure 2-7 suggests has the highest salting rates in North America. Thus, lognormally distributed parameters with mean values of 3%, 6%, and 9% have been used for the current study, with cumulative distributed functions as plotted in Figure 5-7.

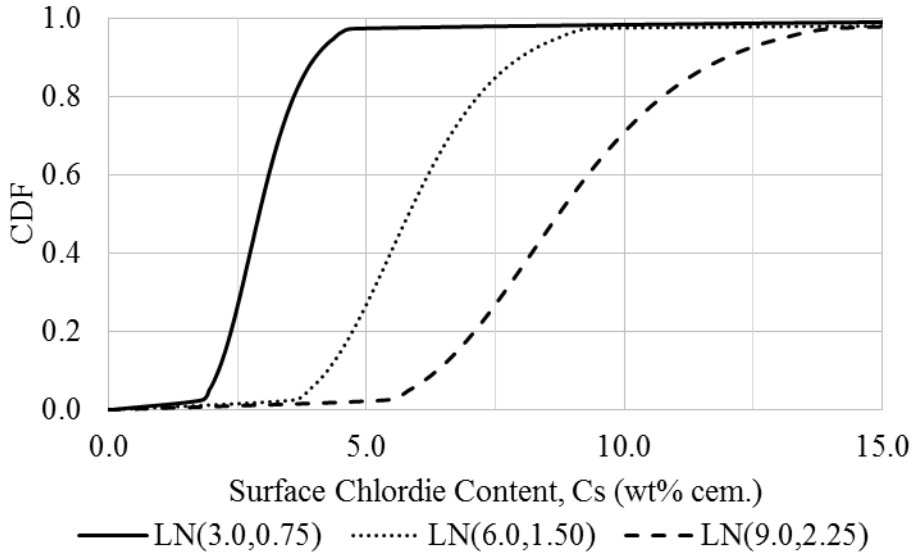

Figure 5-7: CDF's of 3.0, 6.0, and 9.0% surface chloride content, by weight of cementitious material

5.6. Diffusion Coefficient

The diffusion coefficient is largely affected by the mix design of the concrete (how much cement or other supplementary cementitious materials (SCM's) such as slag, fly ash, silica fume) and the curing and casting procedures. Thomas and Bamforth [58] studied the effect of the use of slag and fly ash as SCMs on the diffusion coefficient. Table 5-2 presents their mix designs and Table 5-3 presents the resulting diffusion coefficients compared with Portland cement (PC).

Table 5-2: Thomas and Bamforth [58] Folkestone concrete mix designs for ordinary Portland cement (PC), Portland cement with fly ash (P/PFA), and Portland cement with slag (P/GBS).

Mix Proportions (kg/m^3)			
Mix Designation	PC	P/PFA	P/GBS
Portland cement	288	227	110
Fly ash	-	98	-
Slag	-	-	255
Total cementitious content	288	325	365
w/*c* ratio	0.66	0.54	0.48
Stone	1240	1305	1240
Sand	660	585	600

Table 5-3: Best fit diffusion coefficients for Folkestone blocks, [58]

	Best Fit Diffusion Coefficients - D_a (10^{-12} m^2/s) Concrete Mix		
Age	PC Control	P/PFA	P/GBS
6 Months	9.5	4.3	7.5
1 Year	3.0	2.0	2.9
2 Years	7.6	1.9	1.9
3 Years	5.6	1.1	1.0
6 Years	10.0	0.8	1.0
8 Years	8.7	0.6	0.6

To fully utilize this information, the mix designs must be compared with Table 3-4. It can be observed from this comparison that their P/GBS design most closely resembles the mix used in the experimental part of this project, by containing slag and having the lowest water to cementitious material ratio. It should be noted that the their mix is 70% slag by mass of cementitious material, while the current mix is 25% slag by mass of cementitious material, so their

results must be analyzed in light of this. It can be noted that initially the diffusion coefficient was $7.5 \cdot 10^{-12}$ m^2/s, but decreased to a value of $0.6 \cdot 10^{-12}$ m^2/s after 8 years, presumably due to concrete curing. As such, the current parametric study has utilized lognormally distributed chloride diffusion coefficients with mean values of 1.0, 4.0, and $7.0 \cdot 10^{-12}$ m^2/s, as plotted in Figure 5-8.

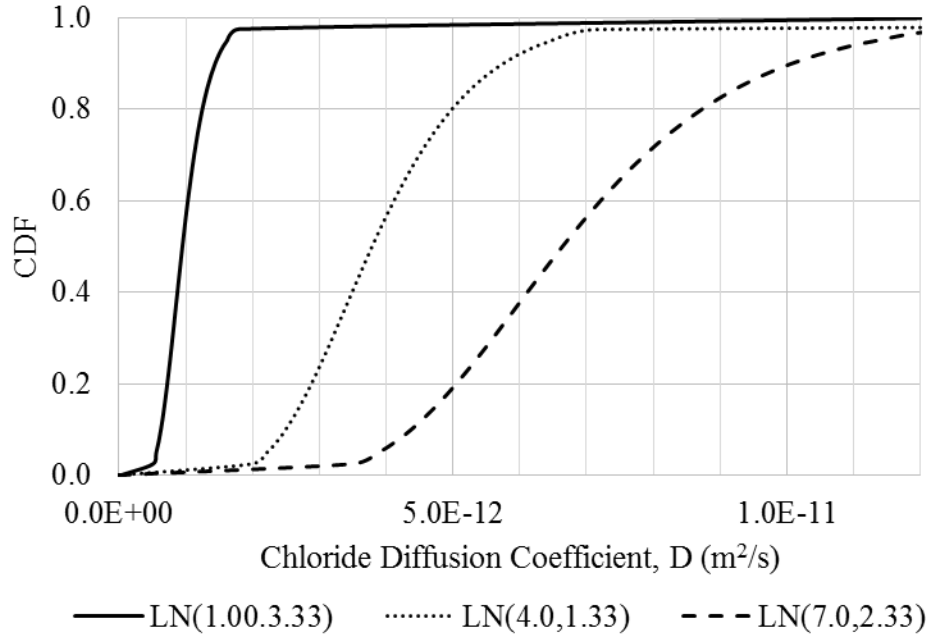

Figure 5-8: CDFs of 1.0, 4.0, and $7.0 \cdot 10^{-12}$ m^2/s chloride diffusion coefficients.

5.6.1. Parametric Study Results and Discussion

When determining the optimal way to present the results of the parametric study, which was performed by systematically varying each of the input parameters discussed in the previous section, it was determined that a cost ratio would be the most effective. The chosen cost ratio represents the premium that an infrastructure owner would be willing to pay for stainless steel (as opposed to black steel) under a given set of input parameters. As such, a higher cost ratio means that the owner should be willing to pay more to purchase stainless or corrosion resistant reinforcing bars. The advantage of this approach is that the owner can calculate the costs independently of the deterioration analysis and then simply compare the costs to the critical cost ratio obtained from the deterioration analysis to determine which steel grade is optimal. The way the critical cost ratio is calculated can be summarize as follows:

- First, an analysis of the black steel is completed to determine the number of times the structure containing black steel will need to be replaced during the analysis period. The net present value (NPV) of these replacements is then calculated using Equation 14 [59], where n is the number of replacements, γ is the discount rate, and t is the number of years since the first installation of the structure.
- Secondly, an analysis of the corrosion resistant rebar is completed, with all environmental and structural variables not affected by the steel grade unchanged, to determine the number of replacements of that structure using the corrosion resistant rebar.
- Thirdly, Equation 15 (which is based on Equation 14) is used to determine the cost that the owner or operator should be willing to pay for corrosion resistant alternative. In Equation 15, m is the number of replacements of the corrosion resistant alternative.
- Lastly, the critical cost ratio (CCR) is determined using Equation 16. It should be noted that the "cost" used in Equation 14 to Equation 16 could be the cost of the rebar alone, the owner's cost of replacing the reinforced concrete component or structure (of which the rebar cost is only a small part), or the cost of total structure replacement, including user delay costs, etc. This is a decision that the owner must make when calculating the actual cost ratio, which will be compared with the critical cost ratios determined in the current study, to assess whether or not the corrosion resistant alternative is superior from a life-cycle cost perspective. In general, the more costs that are included in the analysis, the better the case will be for the corrosion resistant alternative, since the tendency will be for the actual cost ratio to approach unity, as the significance of the rebar cost diminishes.

$$NPV_{bb} = Cost_{\text{bb}} \sum_{0}^{n-1} e^{-\gamma t_n} \qquad \text{Equation 14}$$

$$Cost_{\text{ss}} = \frac{NPV_{\text{bb}}}{\sum_{0}^{m-1} e^{-\gamma t_m}} \qquad \text{Equation 15}$$

$$CCR = \frac{Cost_{ss}}{Cost_{\text{bb}}} \qquad \text{Equation 16}$$

5.7. Chloride Diffusion Coefficient

To determine the effect of each input parameter on the critical cost ratio, a chloride diffusion versus critical cost ratio chart was created (Figure 5-9). It demonstrates the distribution of critical costs for the three different coefficients.

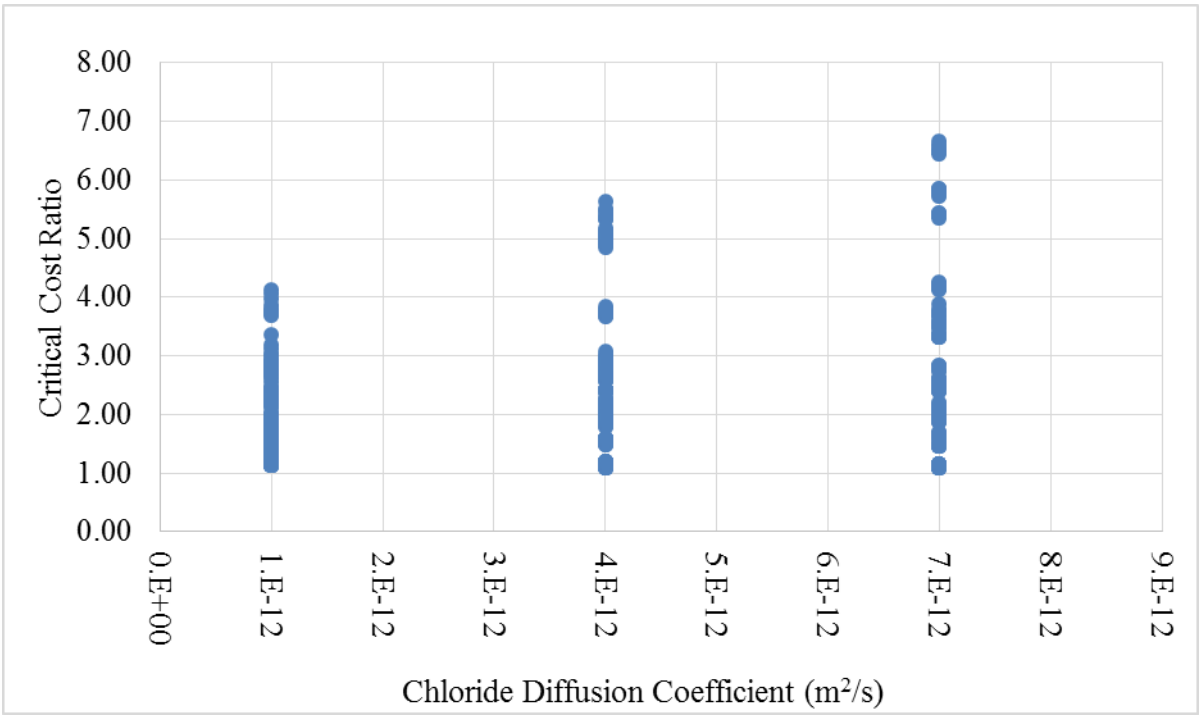

Figure 5-9: Chloride diffusion coefficient vs critical cost ratio for a 300 year service life

Initially the data presented appears logical, as it suggests that the higher the diffusion coefficient, the more likely the black bar is to corrode, and the more an owner is willing to spend initially. This graph is also interesting because it shows that there are conditions, based on material price alone, that suggest spending money on stainless steel reinforcement makes sense (2304 is reported to cost 4 times more than regular black steel [60]). However, instead of spending that money on a material with a higher chloride threshold value, that money could be used to offset the user costs associated with longer construction and detour times, to allow for longer wet curing, which has been shown to drastically decrease chloride diffusivity [61].

In order to provide a more practical graphical representation of how chloride diffusion affects the critical cost ratio, more analysis was conducted using a service life of 100 years. This analysis was done by varying the chloride diffusion rates between 1.00×10^{-12} and 7.00×10^{-12} m^2/s for three

different environmental aggression conditions (low, medium, high), then compared for three different chloride thresholds (1.7, 3.0, and 4.9 % cementitious material), see Figure 5-10 to Figure 5-12.

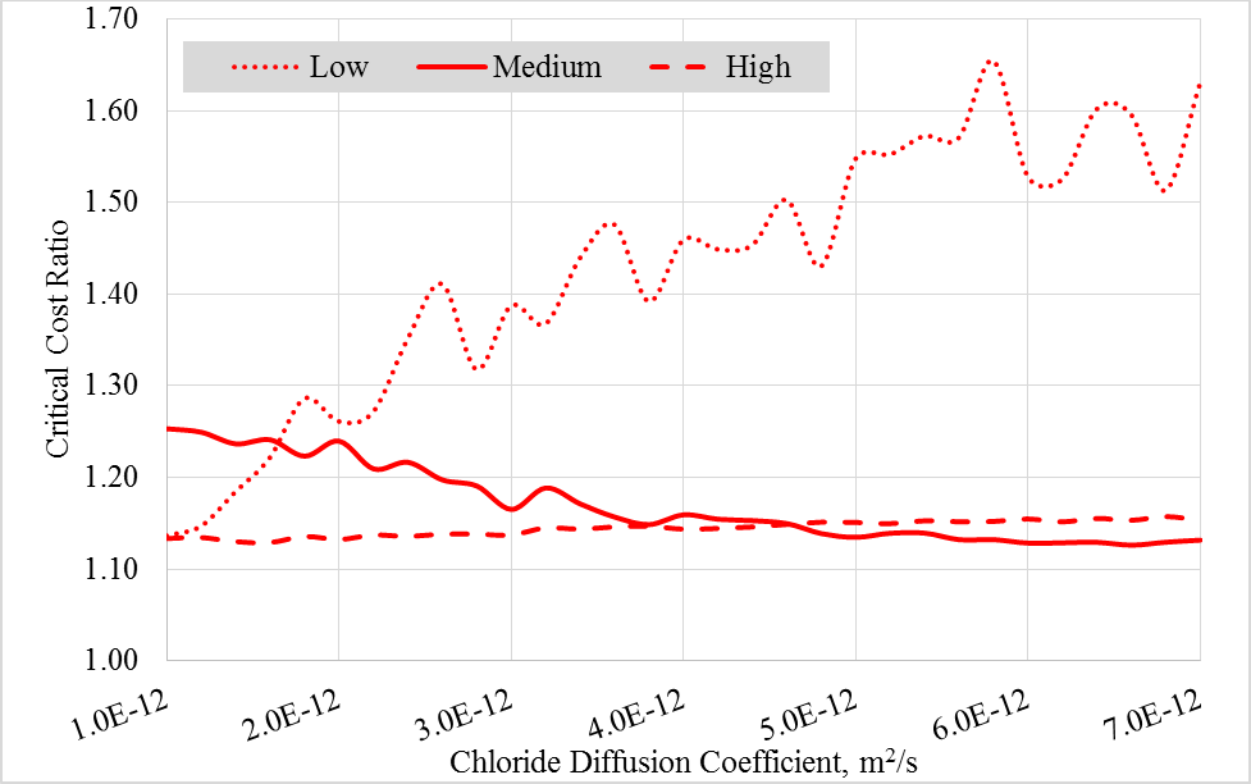

Figure 5-10: Critical cost ratio vs chloride diffusion for structure with 100 year service life, under three environmental conditions with a stainless steel chloride threshold of 1.7

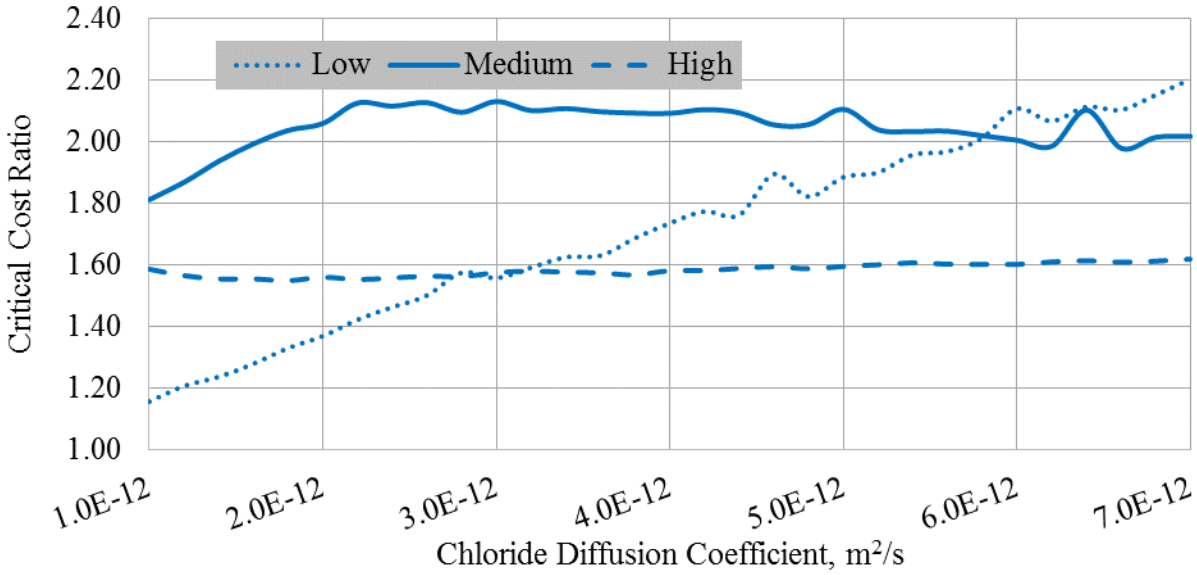

Figure 5-11: Critical cost ratio vs chloride diffusion for structure with 100 year service life, under three environmental conditions with a stainless steel chloride threshold of 3.0

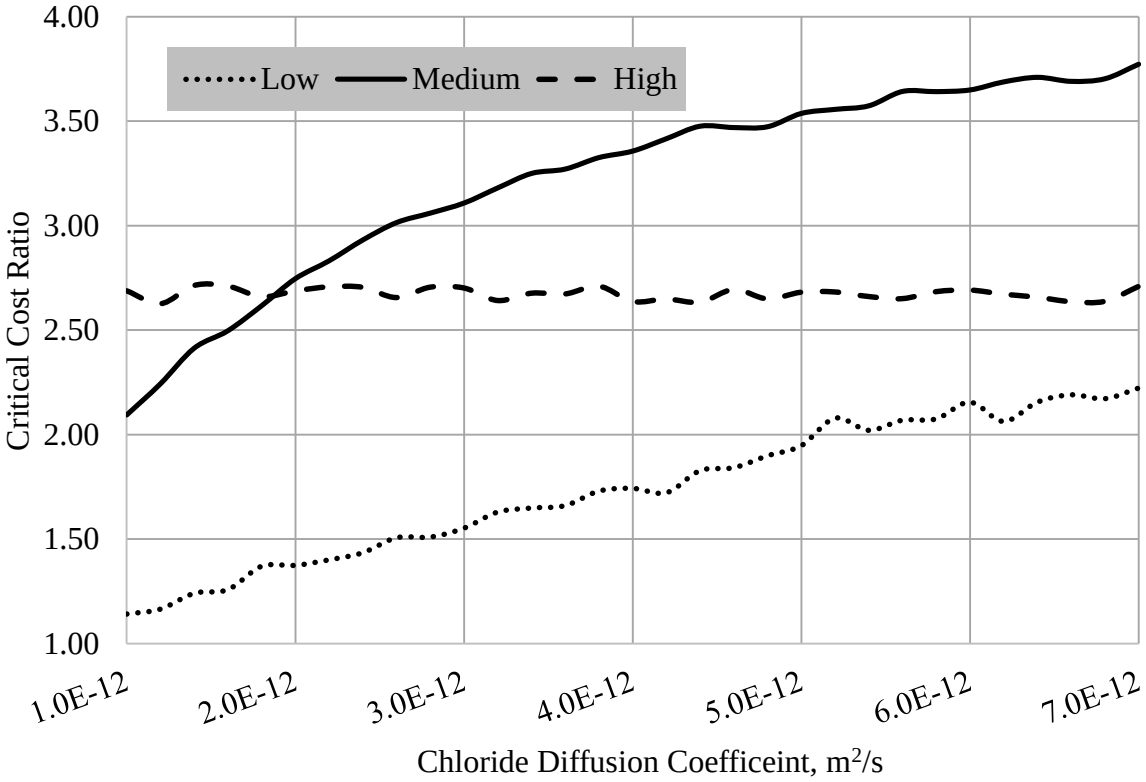

Figure 5-12: Critical cost ratio vs chloride diffusion for structure with 100 year service life, under three environmental conditions with a stainless steel chloride threshold of 4.9

What these results demonstrate is that the higher the chloride threshold level of the stainless steel rebar, the better (i.e. higher) the CCR. On the other hand, higher chloride threshold levels also typically translate into a higher rebar cost. These results also demonstrate the value of limiting the chloride diffusion. With a chloride diffusion rate of $1.0 \cdot 10^{-12}$ m^2/s, the CCR never exceeds 2.7, much less than the suggested cost of stainless at 4.0 times that of black reinforcing bar.

5.8. Concrete Cover

To analyse the effect of concrete cover on the critical cost ratio, Figure 5-13 was created. It appears from this figure that, as the concrete cover is increased, the CCR decreases, indicating a reduced willingness to pay for corrosion resistant rebar. This confirms what logic would suggest, as the thicker the concrete cover, the farther the chloride ions have to travel before initiating reinforcement corrosion. What the CCR does not take into account, however, is the reduction in load associated with the 40 mm lower concrete cover. This dead load reduction can save material in both the deck, as well as the support structure, which can help to reduce the initial cost associated with the more expensive corrosion resistant reinforcement. Essentially, in this analysis, it has been assumed that the effect of ignoring this cost is negligible. Further work may be advisable, however, to verify this assumption in a future study.

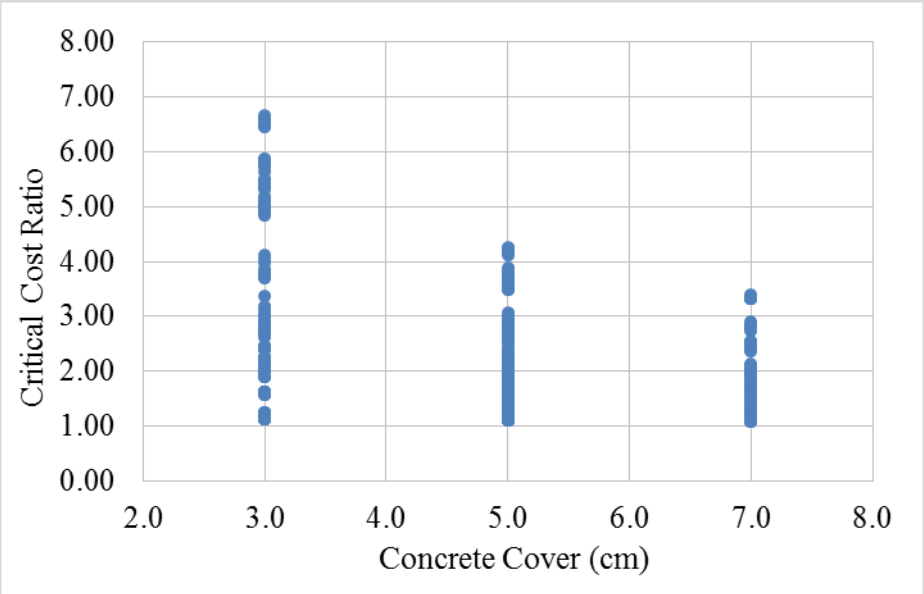

Figure 5-13: Concrete cover vs critical cost ratio for 300 year service life

To determine the optimal opportunity for structural designers to reduce the concrete cover and use stainless steel, a secondary analysis was conducted. This analysis was done by varying the concrete cover between 3.0 and 7.0 cm for three different environmental aggression conditions (low, medium, and high), then compared for three different chloride thresholds (1.7, 3.0, and 4.9 % cementitious material). The results, presented in Figure 5-14 to Figure 5-16, demonstrate the true value of stainless steel in average aggressive environments. When comparing the three figures note that the stainless steel critical cost ratio improves the most dramatically from 1.8 with a chloride threshold of 1.7 (% cem) to 4.5 with a chloride threshold of 4.9 (% cem), while the low and extreme curves remain relatively unchanged. What these curves also demonstrate is that in extreme environments, the chloride threshold is still too easily surpassed requiring stainless steel replacement, and thus lowering the critical cost ratio.

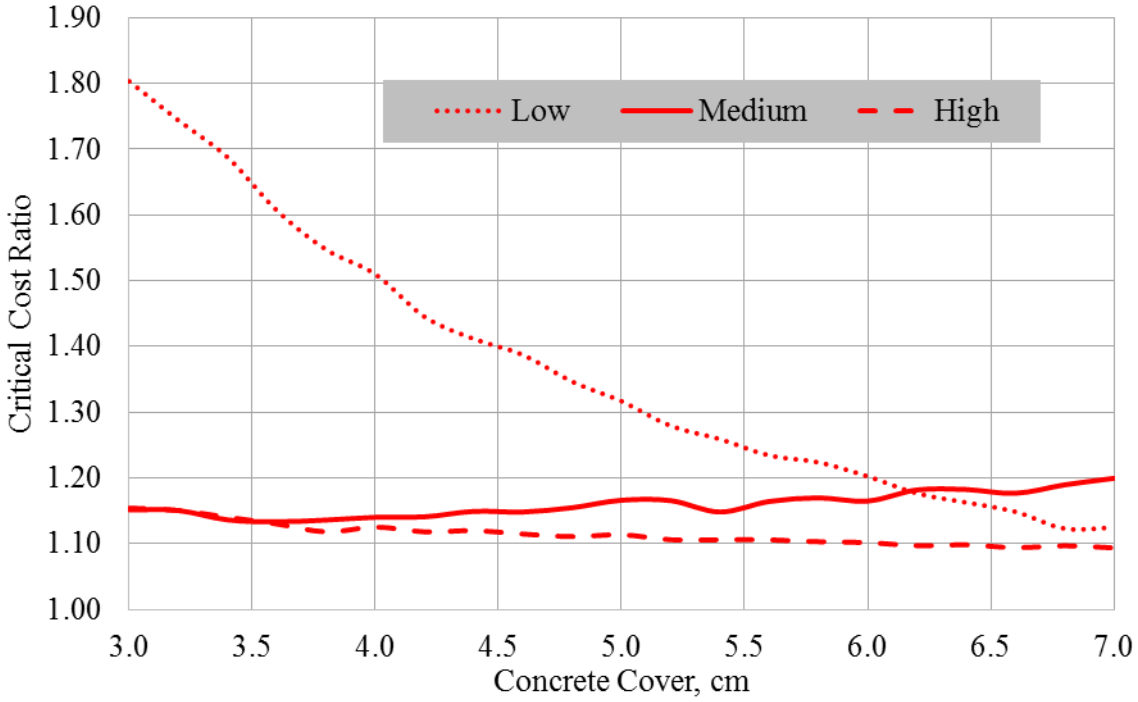

Figure 5-14: Critical cost ratio vs concrete cover for structures with 100 year service life, under three environmental conditions with a stainless steel chloride threshold of 1.7

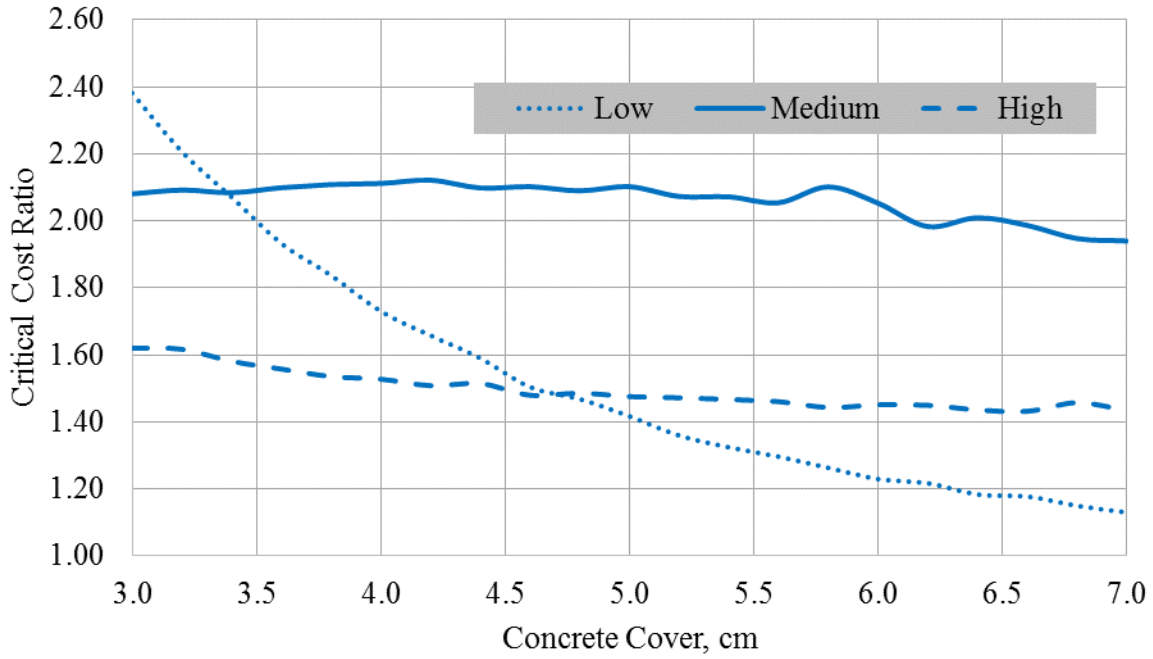

Figure 5-15: Critical cost ratio vs concrete cover for structures with 100 year service life, under three environmental conditions with a stainless steel chloride threshold of 3.0

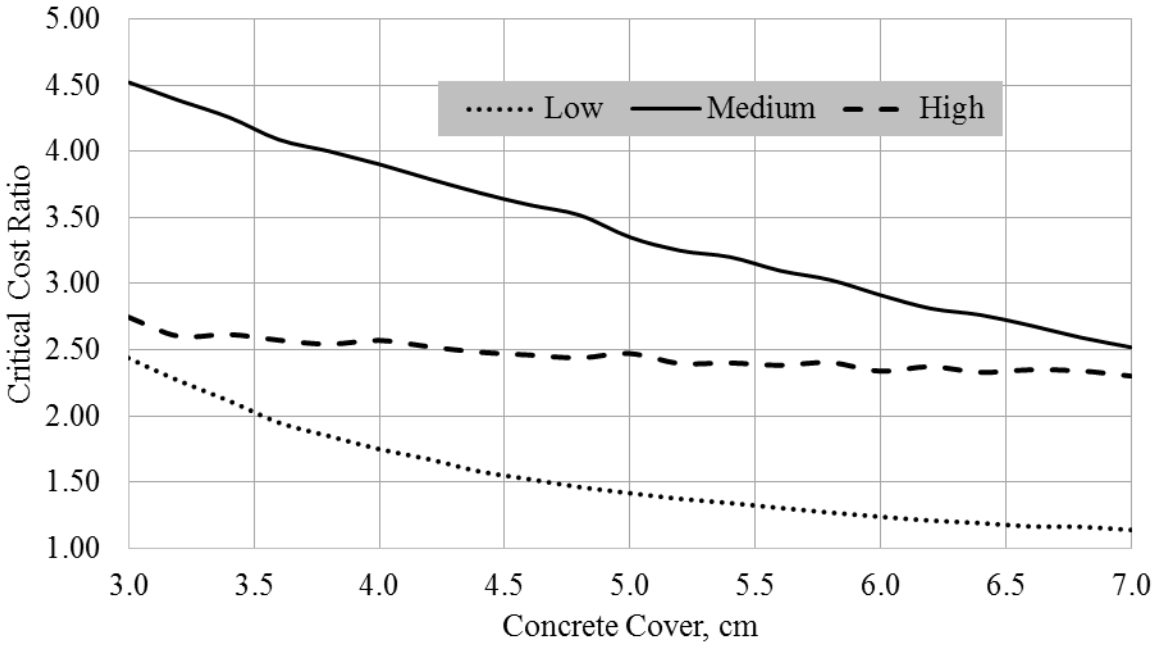

Figure 5-16: Critical cost ratio vs concrete cover for structures with 100 year service life, under three environmental conditions with a stainless steel chloride threshold of 4.9

5.9. Chloride Threshold

Varying the chloride threshold, and analysing the results is a little trickier than both the diffusion and concrete cover because they are easy to control. Theoretically, the analysis could be run to determine the optimal chloride threshold level, and steel created with that in mind, but that would be extremely experimentally rigorous and costly. The other alternative is to analyse and determine the chloride threshold level of all the commercially available stainless steel grades, and then re-run the parametric study using the mean and standard deviations determined and comparing the critical cost ratios with the actual known cost of the reinforcement. This is currently being undertaken by Timothy Bandura, with his results expected in the coming months, at which time the program will be re-run with the new parameters.

With the current parameters and results, Figure 5-17 was created. It demonstrates that the higher the chloride threshold of the corrosion resistant steel, the more the owners are willing to pay for the product. That being considered, the average critical cost ratio at a chloride threshold of 4.9% by weight of cementitious material is only 3.1, i.e. less than the current market value of 4 times the cost of black reinforcing for 2304.

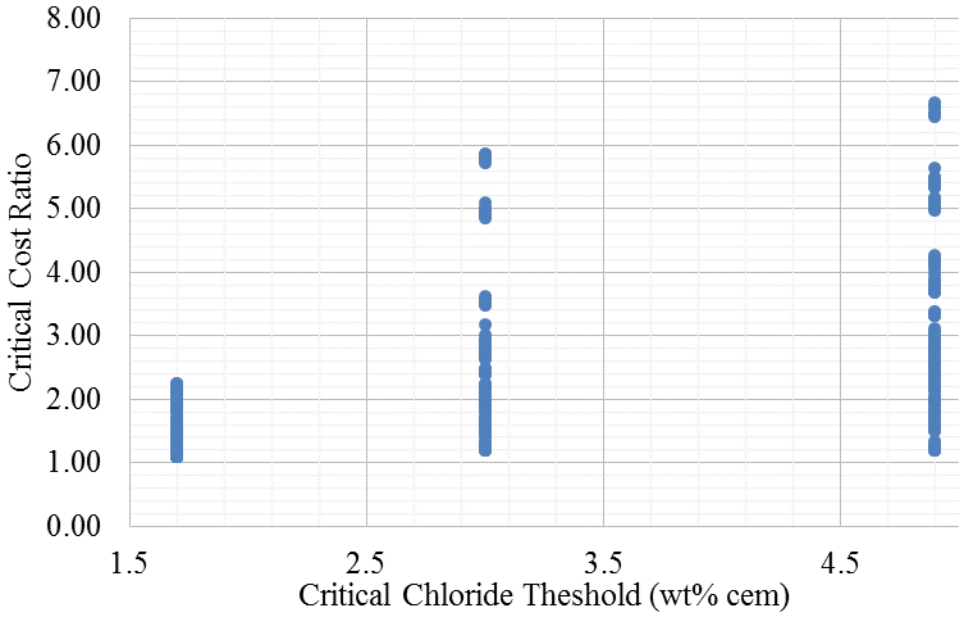

Figure 5-17: Chloride threshold vs critical cost ratio for a 300 year service life

Interesting to note are the results with a critical cost ratio for between 4.0 and 6.0 for a chloride threshold of 3.0%. These results represent extreme conditions, with high crack density, large crack widths, high chloride diffusion, and the lowest concrete cover of 3 centimeters. Based on these results, it could be more beneficial to use a leaner stainless (ie XM28) if the initial cost varies greatly from a more expensive 316LN or 2205.

When comparing chloride threshold values between 1.7 and 5.0 (wt% cementitious materials) for three environmental conditions, the results are very interesting, Figure 5-18. First, note that the low environmental condition curves stays very consistent at a critical cost ratio of approximately 2.5. This is due to the fact that under these conditions the number of replacements for the black bar is low, thus the improvement of stainless steel is limited. Using the same logic, the extreme environmental condition curve has such a low critical cost ratio because in this condition even the stainless steel requires numerous replacements. From the average condition it appears as if the critical cost ratio is leveling off between 4 and 4.5, making stainless steel a viable option at approximately 4 times that of black steel.

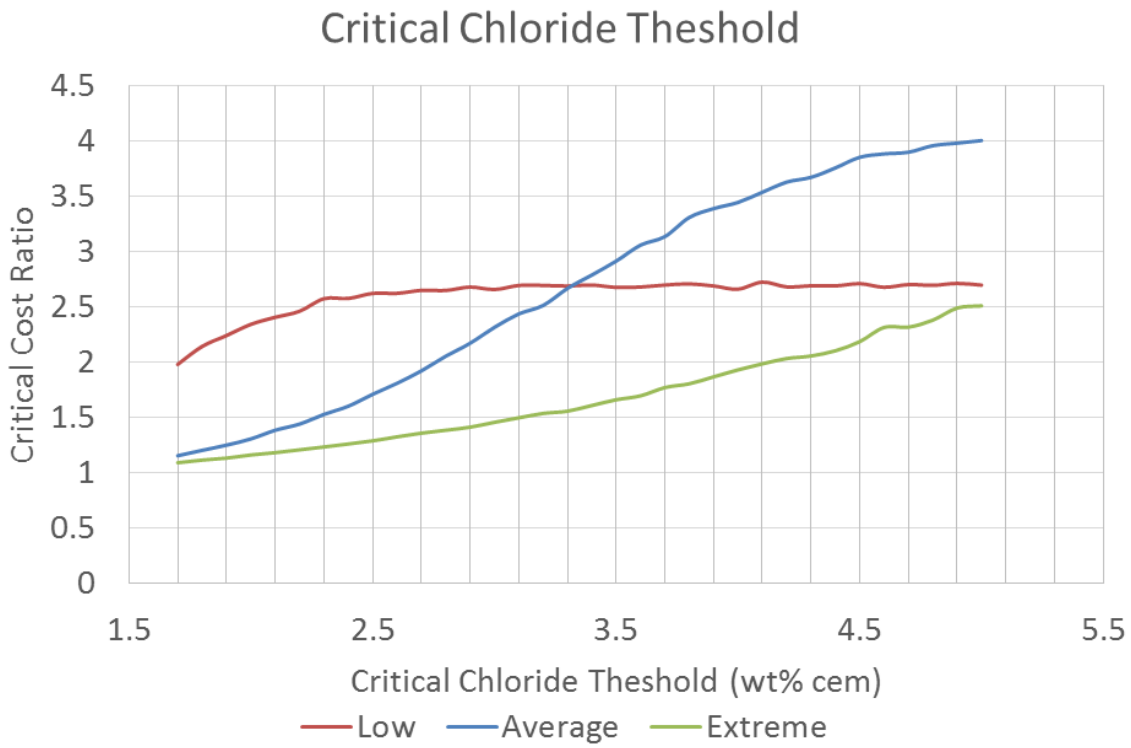

Figure 5-18: Chloride threshold for three environmental conditions

5.10. Crack Width and Crack Density

The crack width and crack density gave very interesting results, seen in Figure 5-19, which initially did not seem very logical. These results indicate that increasing crack density and crack width do not significantly correlate with an increase in cost. All crack widths and densities can represent any number of critical costs, all with an average around between 2.20 and 2.25. Upon further investigation the results can be explained as follows. Since the model uses the average chloride diffusion rate (between the sound and cracked portion of the structure) where the cracked concrete represents less than 1% of the area per square metre, the model suggests that the diffusion rate as a whole will not be largely affected by the cracked region. In reality, if the crack is above a reinforcing bar, the chloride will diffuse more quickly to that element, allowing corrosion to initiate, products to build up, and more cracks to form, speeding up the time to failure of the structure. It would be interesting to note the effect of cracks on concrete with a low diffusion rate, as the crack diffusion would likely have a larger impact.

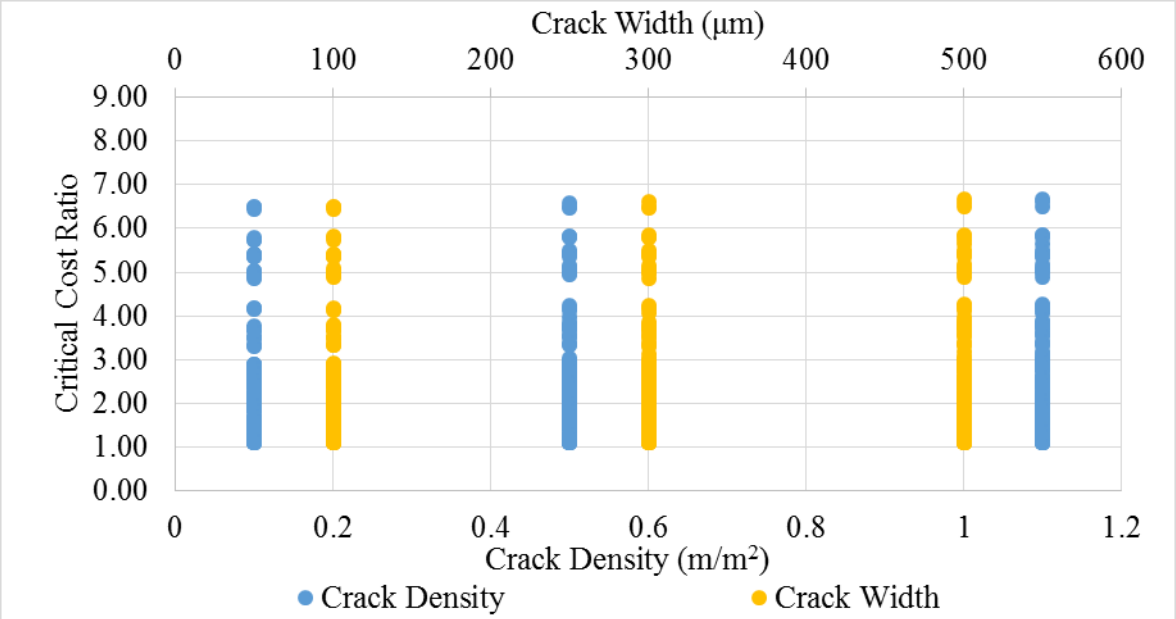

Figure 5-19: Crack width and density versus critical cost ratio for a 300 year service life

To determine if the results changed drastically over a shorter service life, with a varying crack width and crack density, the Monte Carlo simulations were conducted using a service life of 100 years. In this analysis the crack width varied between 100 µm and 500 µm, and the crack density between 0.1 m/m^2 and 2.0 m/m^2 for three different environmental aggression conditions (low,

medium, and high), then compared for three different chloride thresholds (1.7, 3.0, and 4.9 % cementitious material). The results are given in Figure 5-20 to Figure 5-25. Upon review of the figures, it can be noted that neither the crack width nor crack density tend to have a large effect on the critical cost ratio, as illustrated by a relatively level critical cost ratio. It appears as though only the environment in which the samples are placed affects their performance.

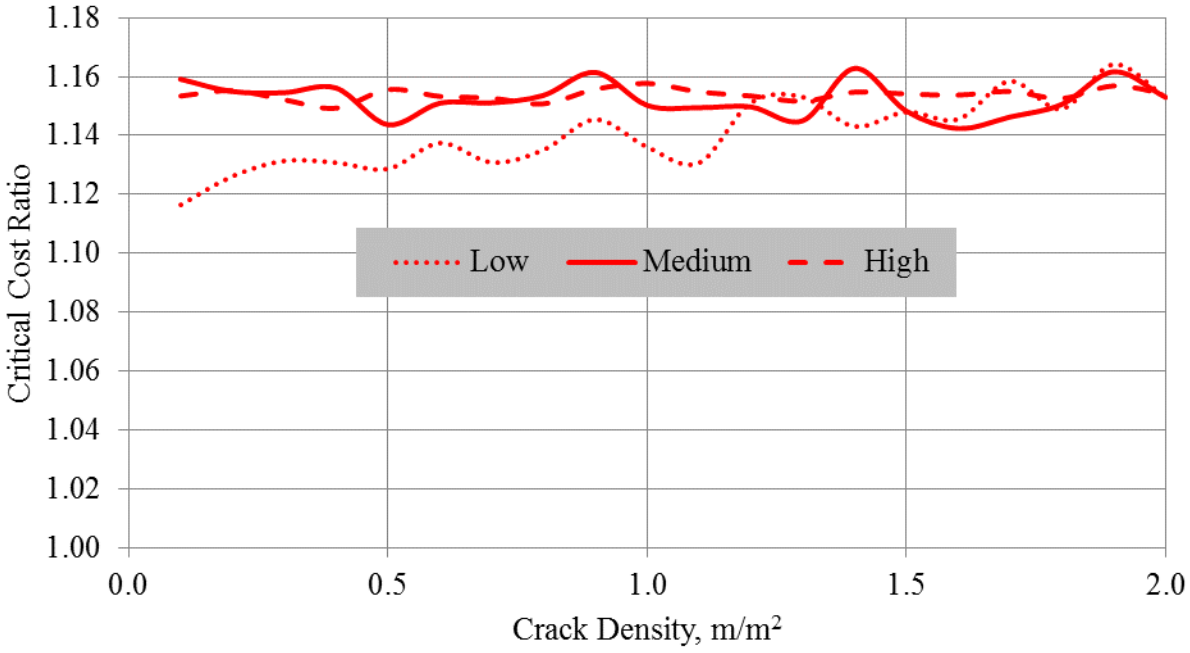

Figure 5-20: Critical cost ratio versus crack density for structures with 100 year service life, under three environmental conditions with a stainless steel chloride threshold of 1.7 (wt% cem)

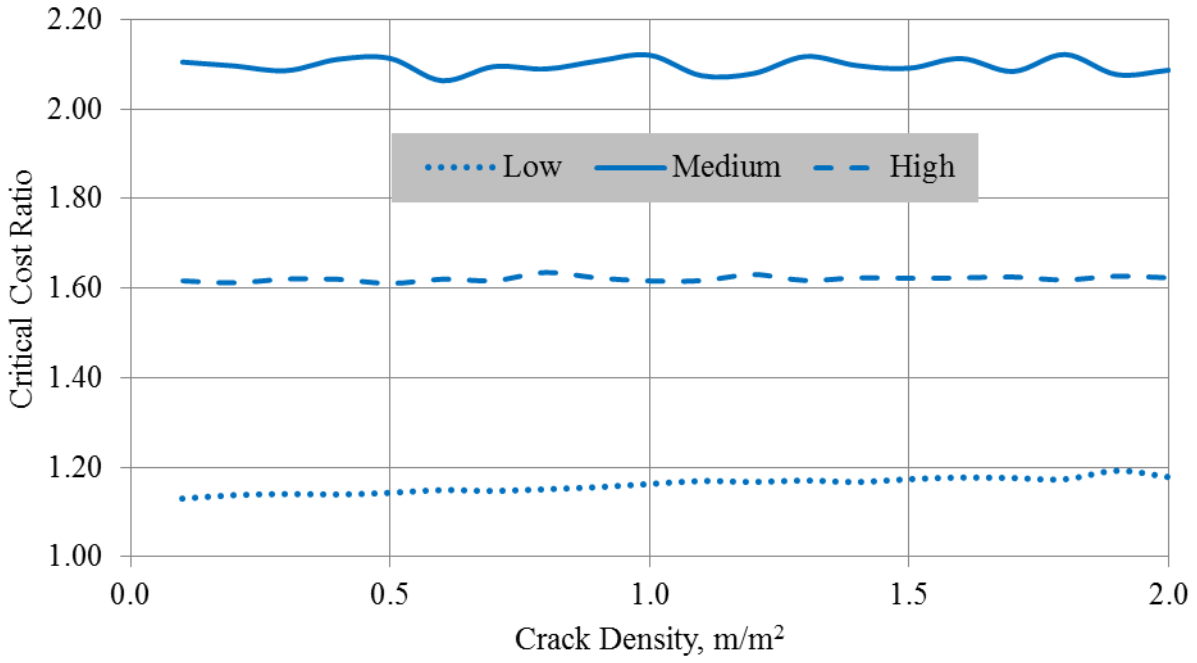

Figure 5-21 Critical cost ratio versus crack density for structures with 100 year service life, under three environmental conditions with a stainless steel chloride threshold of 3.0 (wt% cem)

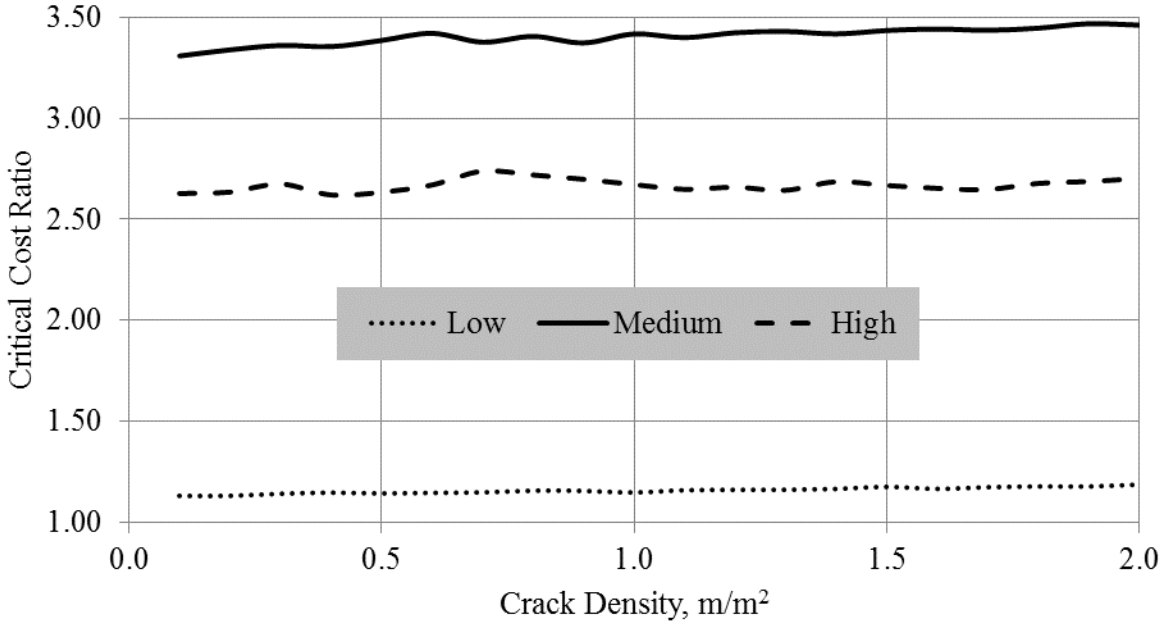

Figure 5-22: Critical cost ratio versus crack density for structures with 100 year service life, under three environmental conditions with a stainless steel chloride threshold of 4.9 (wt% cem)

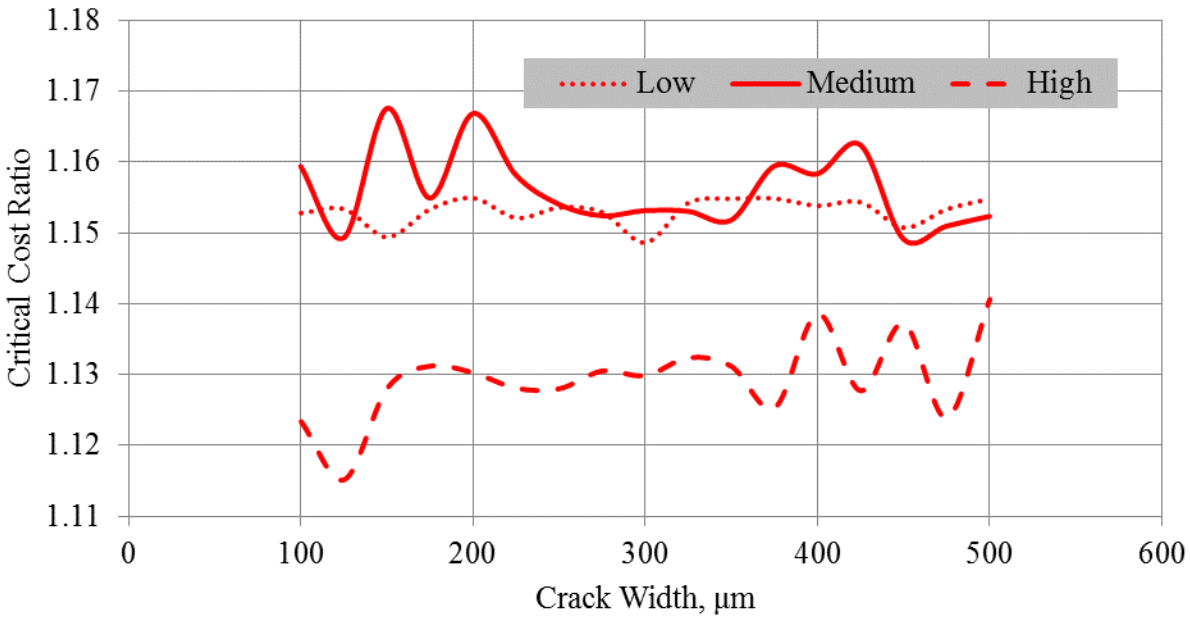

Figure 5-23 Critical cost ratio versus crack width for structures with 100 year service life, under three environmental conditions with a stainless steel chloride threshold of 1.7 (wt% cem)

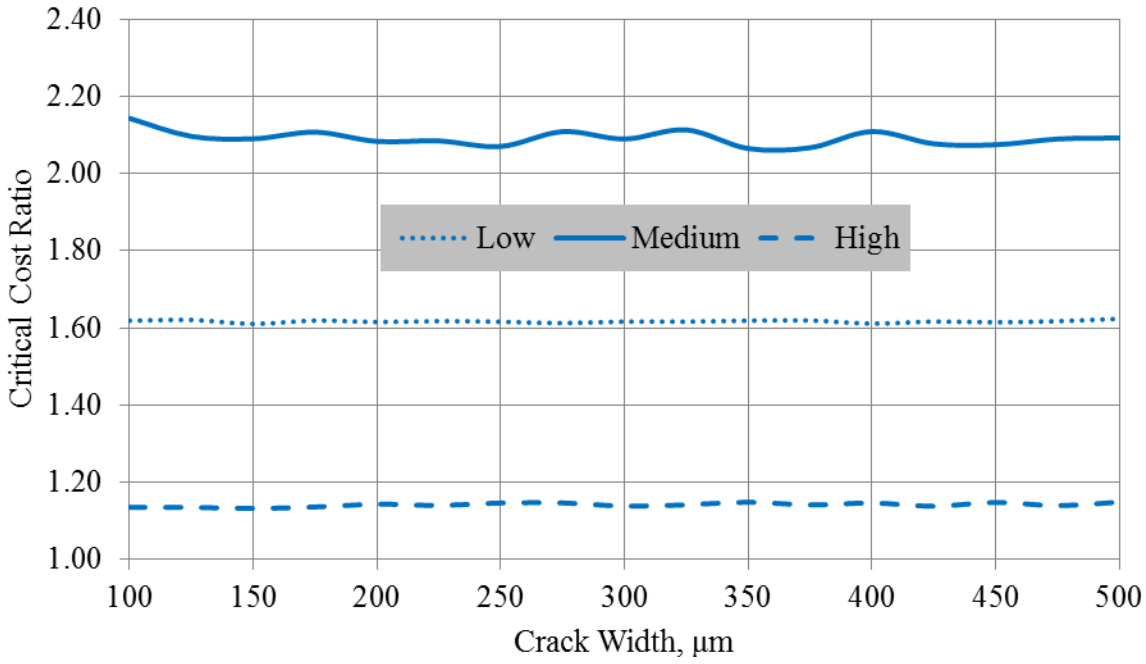

Figure 5-24: Critical cost ratio versus crack width for structures with 100 year service life, under three environmental conditions with a stainless steel chloride threshold of 3.0 (wt% cem)

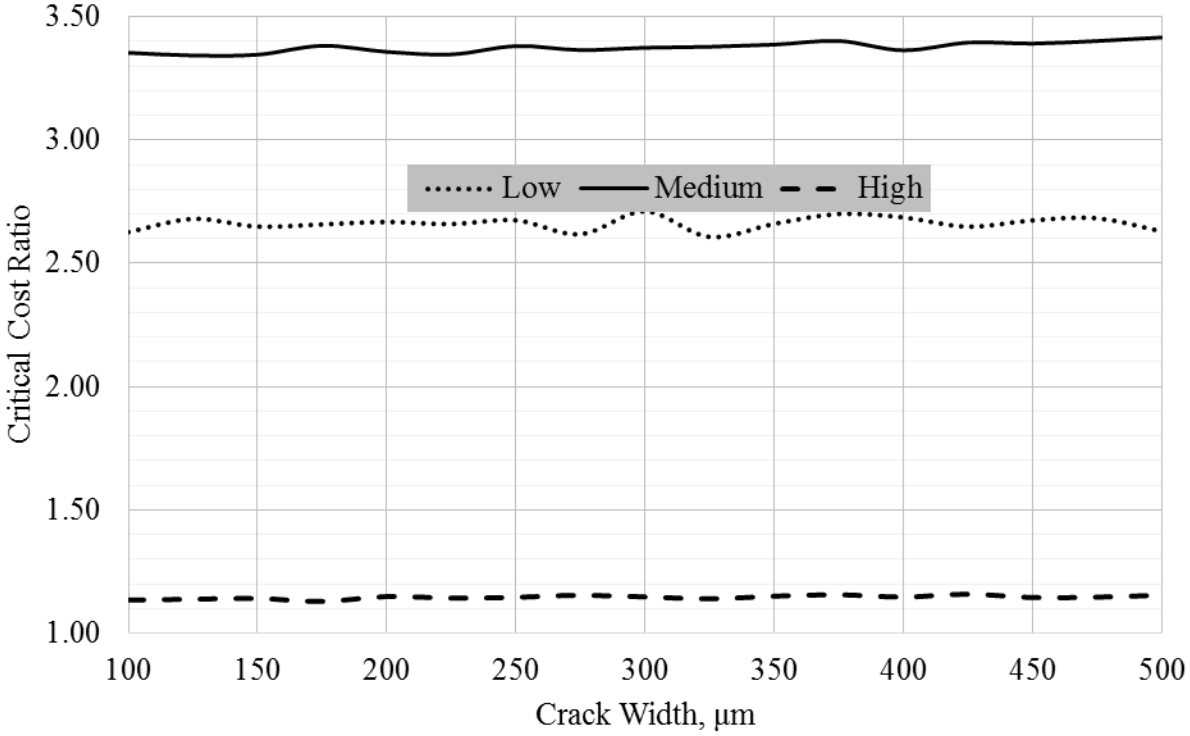

Figure 5-25: Critical cost ratio versus crack width for structures with 100 year service life, under three environmental conditions with a stainless steel chloride threshold of 4.9 (wt% cem)

5.11. Surface Chloride Content

When initially analyzing the results of the surface chloride content versus the critical cost ratio, the results were not intuitive. Figure 5-26 demonstrates that, as the surface chloride concentration increased, the amount that the owner or builder was willing to spend on the corrosion resistant reinforcing bars decreased. This can be explained by the fact that, although corrosion resistant bars have a much higher chloride threshold, as the surface chloride concentration increases, so does the chloride ingress, and the level of chloride experienced by the reinforcing bar. Thus, as the surface chloride level increases, there is a higher probability of active corrosion initiation in the corrosion resistant rebar, thereby increasing the number of repairs or replacements required and driving down the critical cost ratio.

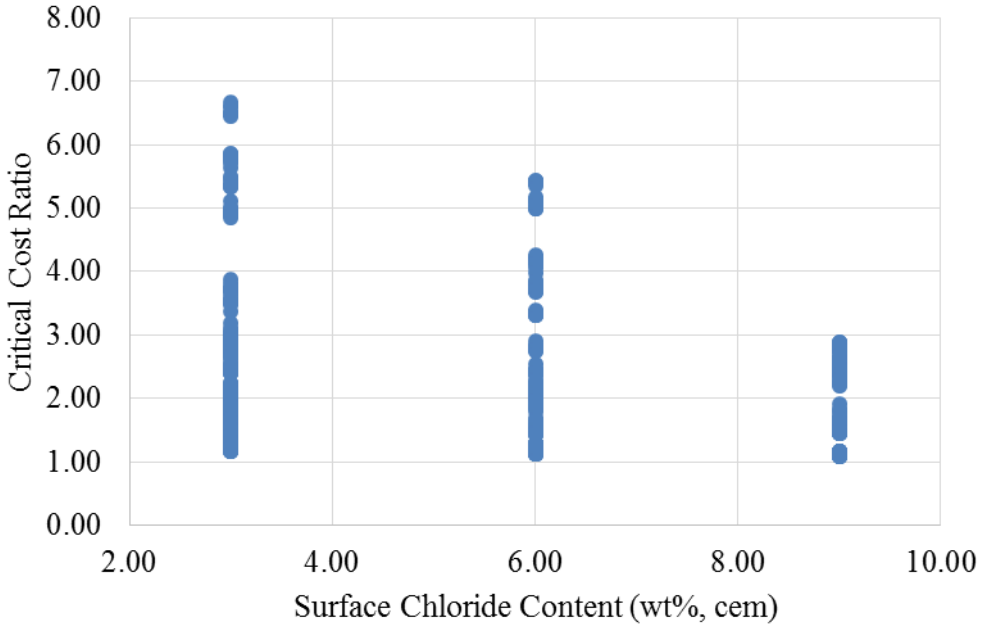

Figure 5-26: Surface chloride content versus critical cost ratio for a 300 year service life

To further investigate the effects of surface chloride on the critical cost ratio, a simulation was run under varying environmental exposure conditions, as described in Table 5-1, over a range of surface chloride conditions presented in Figure 5-27 to Figure 5-29. The data are interesting, because the effect of the surface chloride content dramatically affects the critical cost ratios in different environments. Note, when comparing the extreme conditions for the three different chloride contents that the ideal range, from a CCR perspective, for surface chloride values are between 3.0 and 4.0 by weight of cementituous material, which can have critical cost ratios of over 6.20. Logically, this suggests that poor concrete (highly cracked, high chloride diffusion rate) can still perform adequately if the chloride is continually removed from the surface, or if a membrane is applied to limit the surface chloride concentration.

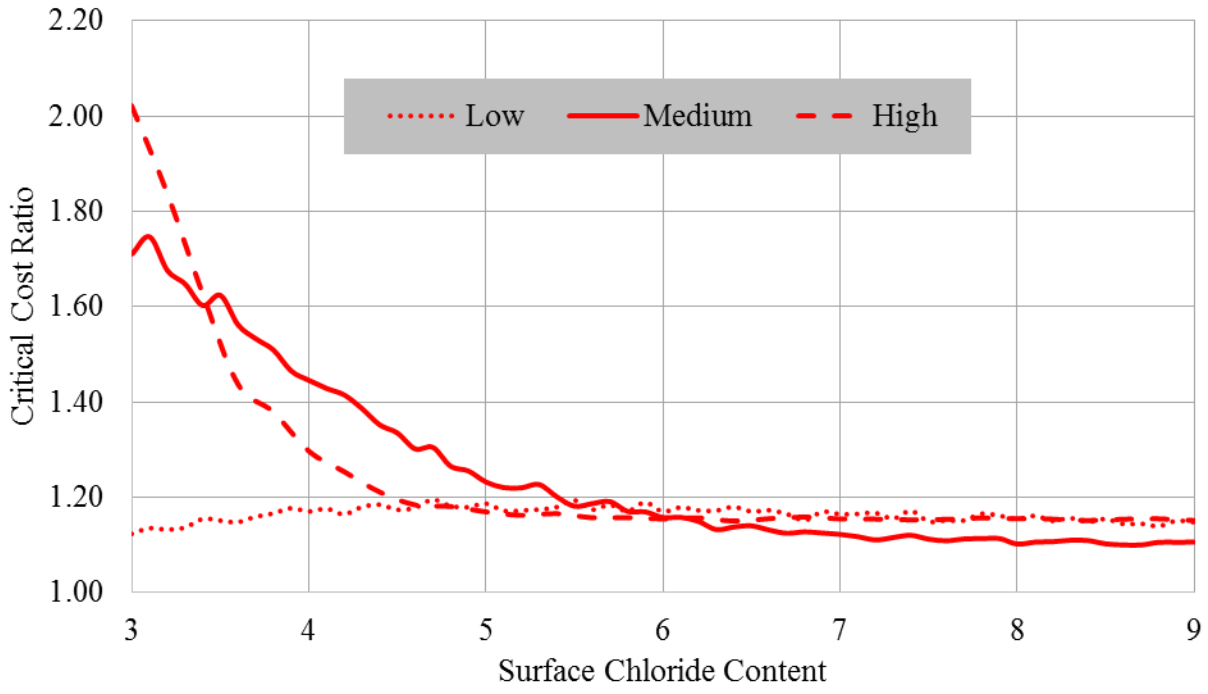

Figure 5-27: Critical cost ratio versus surface chloride content with 100 year service life, under three environmental conditions with a stainless steel chloride threshold of 1.7 (wt% cem)

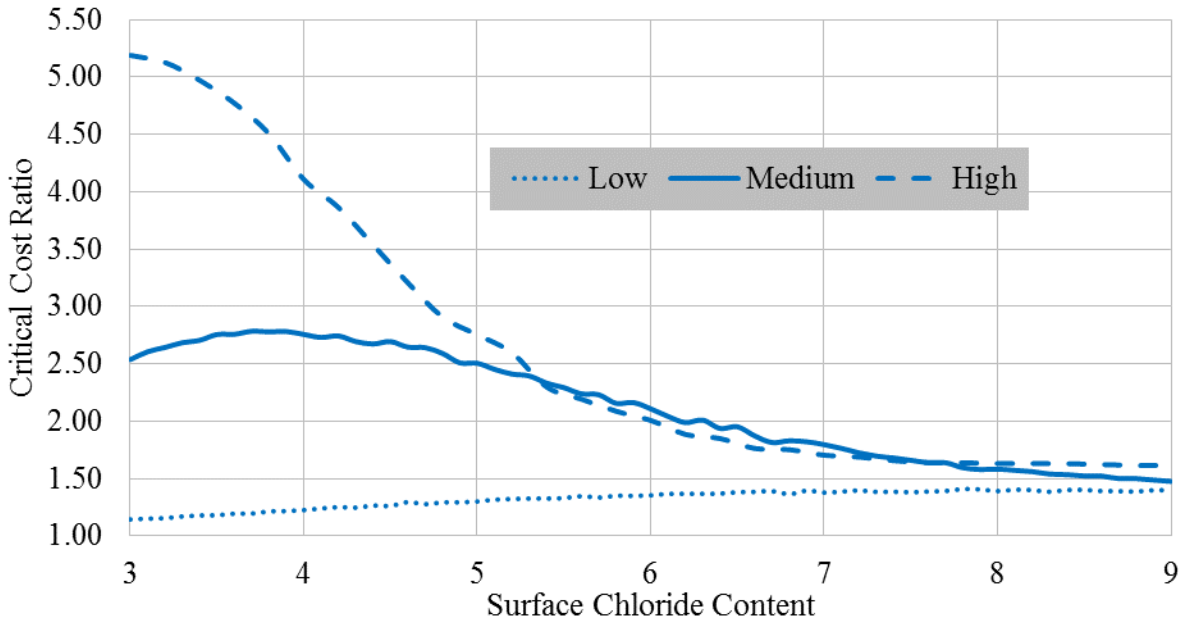

Figure 5-28: Critical cost ratio vs surface chloride content with 100 year service life, under three environmental conditions with a stainless steel chloride threshold of 3.0 (wt% cem)

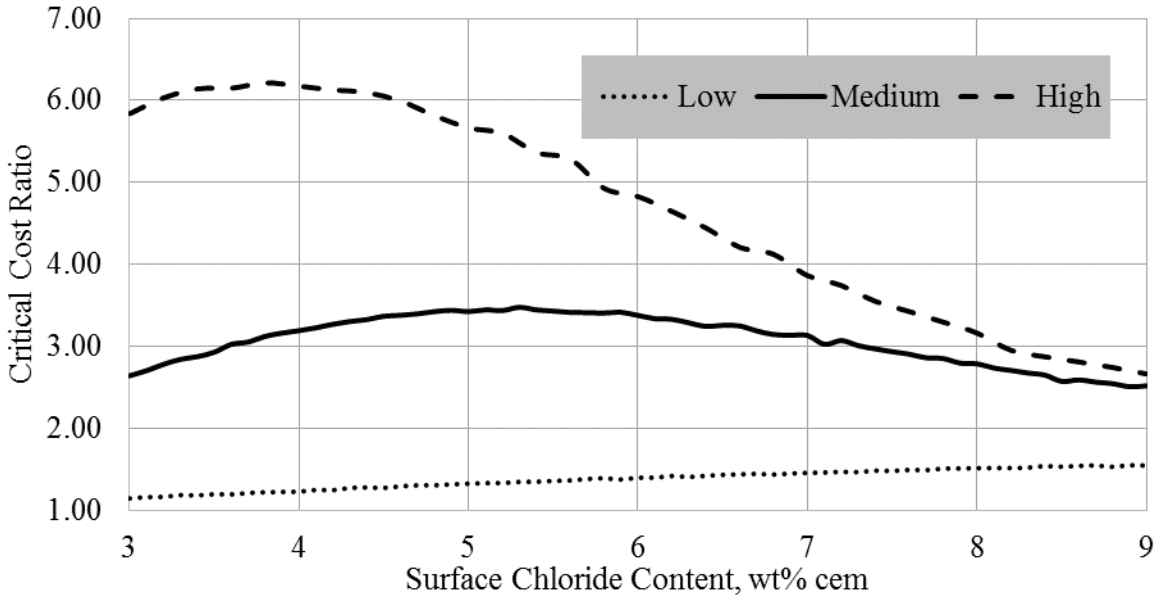

Figure 5-29: Critical cost ratio vs surface chloride content with 100 year service life, under three environmental conditions with a stainless steel chloride threshold of 4.9 (wt% cem)

5.11.1. Changing Service Life

Following the assumption made by Hartt [62], the Monte Carlo simulations were completed with a service life of 300 years. This produced a number of results with CCRs well above the expected cost of stainless steel, i.e. 4 times that of black reinforcement. However, the likelihood of a concrete structure's service requirements not changing over a 300 year lifetime seems remote, suggesting that although a 300 year service life provides exemplary results, a shorter (e.g. 100 year) service life is more realistic. With that in mind, more Monte Carlo simulations were conducted comparing CCRs over a range of analysis periods between 50 and 300 years for four different corrosion-resistant steel chloride threshold values (1.7, 3.0, 4.9, and 6.5 wt% cem), under low, medium, and severe environmental conditions as seen in Table 5-1. It should be noted that a chloride threshold level of 6.5 (wt% cem) was included in the simulation following the results of pore solution tests performed at the University of Waterloo by Tim Bandura. In order to determine the chloride threshold level of the different grades of stainless steel, he immersed five samples of each grade in synthetic pore solution. Each week he added a known increment of chlorides, and, after another week, measured the corrosion current density. The observed data for chloride

threshold levels were recorded in Table 5-4, and then converted to chlorides by mass of cementitious material using Figure 5-4, as shown in Table 5-5.

Table 5-4: Chloride threshold levels of reinforcing bars in synthetic pore solution with chlorides

Alloy	Bar Number				
	1	2	3	4	5
S24100T	11.5	6	6	6	8
S24100V	13	13	12		13
S30403	13		12		8
S31653	6	6	8	6	6
S32304			13.5		
S32205				14.5	
S32101	6, 13.5	6, 12.5	6, 13		13
Black	0.75	1	1	N/A	N/A

*N/A refers to when no bars were present, blank spaces represent bars that had not corroded

Table 5-5: Chloride threshold levels of reinforcing bars in concrete

Alloy	Bar Number				
	1	2	3	4	5
S24100T	5	2.5	2.5	2.5	3.25
S24100V	5.75	5.75	5	n/a	5.75
S30403	5.75	n/a	5	n/a	3.25
S31653	2.5	2.5	3.25	2.5	2.5
S32304			6		
S32205				6.5	
S32101	6	5.5	5.75		5.75
Black	0.5	0.75	0.75	N/A	N/A

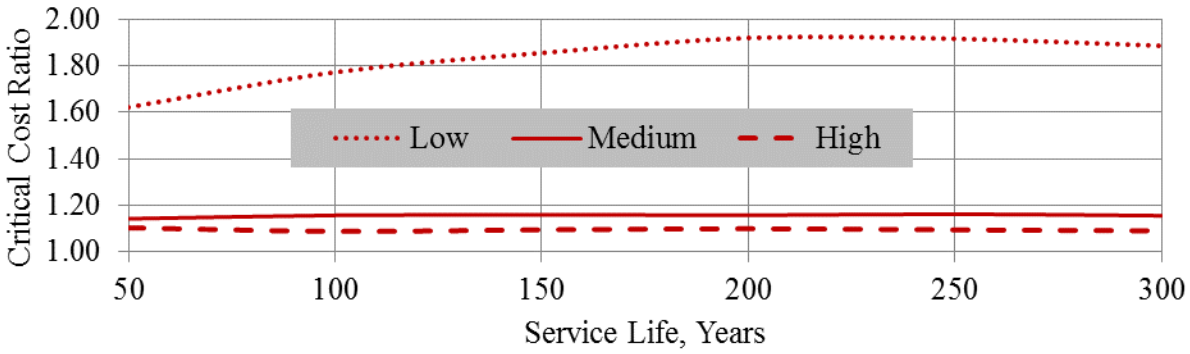

Figure 5-30: Critical cost ratio versus service life, under three environmental conditions with a stainless steel chloride threshold of 1.7 (wt% cem)

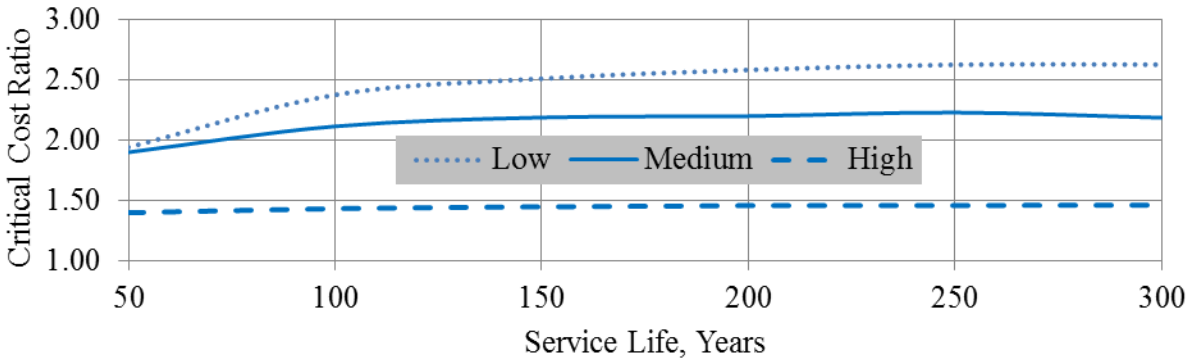

Figure 5-31: Critical cost ratio versus service life, under three environmental conditions with a stainless steel chloride threshold of 3.0 (wt% cem)

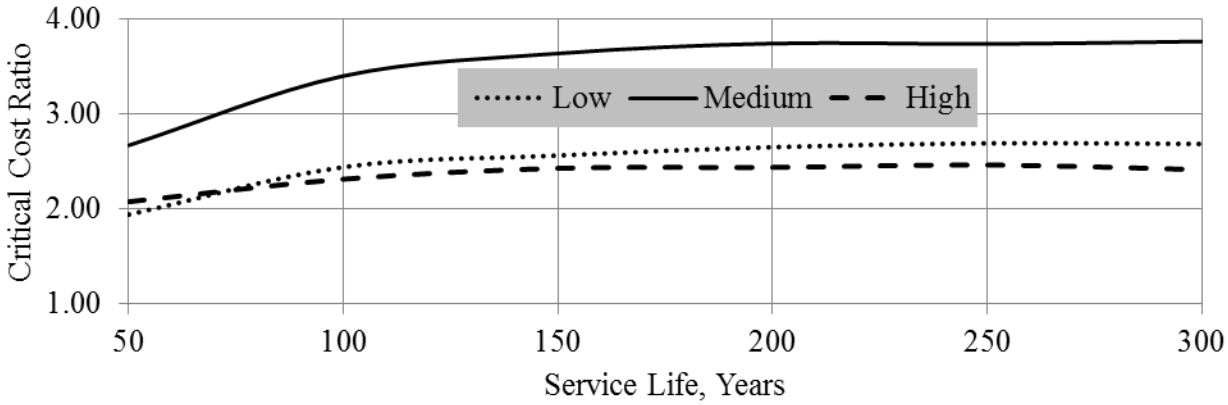

Figure 5-32: Critical cost ratio versus service life, under three environmental conditions with a stainless steel chloride threshold of 4.9 (wt% cem)

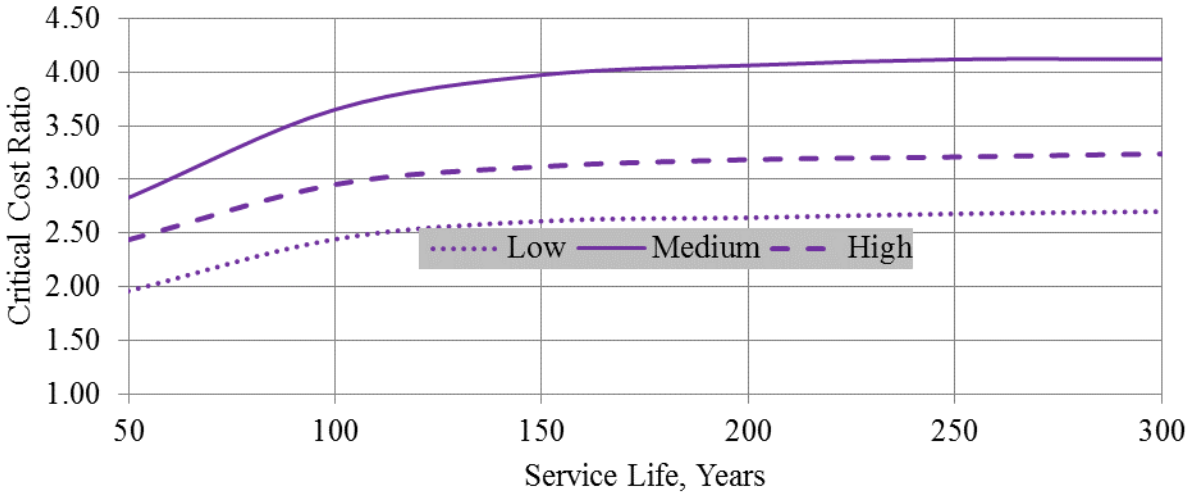

Figure 5-33: Critical cost ratio versus service life, under three environmental conditions with a stainless steel chloride threshold of 6.5 (wt% cem)

The results of this analysis show that the CCR generally increases with an increase in the service life of the structure. In general, however, the effect of the service life on the CCR is limited for service lives greater than 150 years. The CCR increases with an increase in the chloride threshold of the corrosion-resistant rebar. Concerning the environmental conditions, the highest CCRs in Figures 5-22 and 5-33 are interestingly seen under the "medium" conditions. It seems that under the mild environmental conditions, the black steel doesn't corrode, so there is no value in using stainless. In the most severe conditions, both the black steel and the stainless steel corrode rapidly, so again, the CCR is lower. There are a set of conditions in between, however, where the CCR is the highest, suggesting that stainless steel will be most effective.

Chapter 6 Conclusion and Recommendations

This chapter presents conclusions and recommendations based on the research presented in the previous chapters. Section 6.1 is divided into subsections summarizing the conclusions based on the experimental and the analytical research. The recommendations based on this research are presented in Section 6.2, which is divided into subsections summarizing the recommendations concerning industry practice and the recommendations for future research.

6.1. Conclusions

6.1.1. Based on Experimental Research

The bars in the sound concrete specimens to date have not produced any electrochemical data that indicates they are corroding. This indicates that the chloride diffusion rate has been slow enough that even the chloride threshold level of the black reinforcing bar has not been reached. This can be attributed to the excellent quality of the concrete. This is due to two factors: (i) the concrete mixture design with low water/cementitious materials ratio and the replacement of 25% of the cement with slag and (ii) the controlled casting conditions and increased curing time, which included 28 days of wet curing. These combined factors limit the amount of interconnected porosity through which the chlorides penetrate from the ponding solution and, thus, reduce the effective chloride diffusion rate Also, the size and reinforcing layout will have an effect, in this case limiting the micro shrinkage cracks.

Although there is a strong correlation between ambient temperature and the chloride diffusion rate [63], the extreme condition posed by year round exposure to multi-chloride ant-icing brine (containing 21% chloride) at a temperature of 20° - 25°C appears to have had no effect in inducing corrosion. This demonstrates the great benefits of increased wet curing for limiting diffusion rates.

To demonstrate the need for life cycle assessment programs to include the effects of cracks, the transversely and longitudinally cracked specimens were constantly exposed to multi-chloride brine. The effect of the cracks was demonstrated almost instantaneously, as electrochemical results suggest that some black bars under both crack conditions started to actively corrode almost immediately after the cracked concrete was exposed to the multi-chloride brine. Once the specimens were removed from the chloride bath and autopsied, the direct effect of the crack could

be physically seen as, for all grades of steel, the corrosion initiated in the vicinity of the crack, and propagated laterally along the surface of the reinforcement. The actual corrosion locations seen after pickling appear to only be on the upper half of the bar, and in the case of the transversely cracked concrete corrosion then moved laterally along the surface of the bar. In the longitudinally cracked specimen, corrosion appears to have begun under the widest section of the crack and then propagated laterally along the top of the bar as well.

Although the induced cracks varied in both depth and width, the results of the electrochemical testing and autopsied specimens allowed a comparative ranking to be completed. The chart below is a replica of one presented earlier in Section 4.4.1, and is repeated here to summarize the ranking of reinforcing under these conditions.

Table 6-1: Ranking of cracked specimens

	Longitudinally cracked concrete	Transversely cracked concrete
S32205	1	1
S32101	2	3
S32304	3	2
S30403	4	4
S24100-V	5	5
S36103	6	6
S24100-T	7	7
Galvanized	8	8
MMFX	9	9
Black	10	10

6.1.2. Based on Analytical Research

The research to date has demonstrated that under extreme conditions, the use of stainless steel or other corrosion resistant reinforcing can have a significant cost savings over the lifetime of the structure. The results of the parametric study are summarized as follows:

- The lower the chloride diffusion rate, the lower the relative cost owners are willing to pay for stainless steel: As such, to reduce the need for corrosion resistant reinforcing, owners should be willing to take more time to wet cure the concrete, either in the field or through the use of precast concrete, to reduce the chloride diffusion rate.
- The lower the concrete cover, the higher the critical cost ratio: This could be interpreted to mean that one can increase the concrete cover to reduce the need for stainless steel. It should be noted, however, that the analysis does not consider the increase in the concrete or reinforcing steel quantity that would be needed to increase the cover from a structural point of view. The effect of this simplification is expected to be small. However, future analyses can be envisioned where the change in material quantity is considered. In general, it is expected that this effect should favour the stainless steel alternative, however, since it is the one that does not require a cover increase.
- The higher the chloride threshold level of the stainless steel alternative, the higher the critical cost ratio: This is expected, as an increase in this chloride threshold level is intuitively something that one should be willing to pay for. Once the specific chloride threshold ranges of commercially available stainless steel are available, the parametric study should be re-run to determine which stainless steel has the best current price with respect to the critical cost ratio for its actual chloride threshold level.
- Crack width and crack density have a major effect on the performance of the bridge structure: The model shows that under extreme conditions, whether with small or large crack widths, or small or large crack densities, there are critical cost ratios that exceed six times that of the black reinforcing. If the goal is to negate the need to use stainless steel, the owner must make efforts to reduce the shrinkage cracks. This can be done through: the use of fibre reinforcement, prestressing, post tensioning, shrinkage reducing agents or longer wet curing times. It must be recognized, however, that flexural cracking is largely inevitable. The results also suggest that the maximum 0.3 mm crack width requirement by

the Ministry of Transportation of Ontario is not be strict enough, as even the smaller crack widths can lead to extremely high critical cost ratios.

- Surface chloride concentration has a major effect on the life of the structure and the diffusion of the chlorides: Along the corridor between Windsor and Montreal, the chloride application levels are the highest in North America, meaning that extreme surface chloride concentrations can be expected. The membrane applied to bridge decks along with spring surface cleaning will be beneficial, but concrete structures in the splash zones may require further considerations (e.g. increased maintenance or more durable design) to help limit surface chloride buildup.

6.2. Recommendations

6.2.1. Recommendations Based on Experimental and Analytical Results

The experimental results have demonstrated that stainless steel is a more corrosion resistant reinforcement then the traditional black bar. The extent to which it out performs the black bar is determined by its chemical composition and the environment and concrete quality in which it is being placed. Based purely on the experimental results, the 2205 reinforcing bar appears to be the least susceptible to chloride attack, slightly outperforming the cheaper 2101 and 2304. Therefore, if structural access, lane closures, and maintenance can all cause large user or social costs (eg. the Hwy 401 corridor), it is recommended that 2205 be specified.

Where information about the surface chloride concentration is known, along with statistical data providing average crack density, crack width, and chloride diffusion values based on specified structure and concrete designs, a more in depth decision matrix can be followed. The designers could either re-run a site specific analysis, for known stainless steel chloride values, or use the data presented in Figure 5-9 to Figure 5-33 to approximate a critical cost ratio for the use of a given stainless steel. If the comparative cost of the stainless steel to black steel is below the determined critical cost ratio, it would then be financially viable to use stainless steel.

6.2.2. Recommendations for Future Research

Although the conclusions presented here are based on the best information available at the time of writing, further work could be performed to enhance the value of the results. This work could include improvements to both the experimental design as well as the analytical model.

6.3. Improved Experimental Design

Certain experimental techniques could have been improved had there been more time to design the tests, but due to the time dependent nature of corrosion, especially in the case of stainless steel, this was impossible. Specific improvements are detailed in the following paragraphs.

6.4. Improved Mix Design and Curing Time

The mix design that was used was that to meet the specification of the Ministry of Transportation of Ontario for Ontario highway bridges. This mix design called for the use of 19 mm coarse aggregate. Due to the limited size of the specimens, with a 25 mm cover requirement, 12 mm stone was used in order to ensure adequate concrete compaction. Approximately 18 months after cast, after discussing the design with a member of Dufferin Concrete's quality assurance and mix design team, it was indicated that the use of the smaller aggregate required the addition of 20-30 kg/m^3 of cementitious material to provide the additional cement paste necessary for the increase in aggregate surface area. Since the extra cementitious material was not added to the experiment, the concrete mix may not represent in-situ concrete, which could have increased the permeability of the concrete although the increased wet curing likely limited this. If the permeability was reduced the concrete would binding less chloride and allowing higher chloride diffusion. If the experiment were to be re-conducted, the extra cementitious material should be added to more closely resemble in-situ concrete.

Another change that is recommended is the wet curing time of the specimens. The specimens in this experiment were cured in a humidity chamber for 28 days before the cracks were induced. Compared with the 4 day minimum specified by clause 904.07.10 of the Ontario Provincial Standard and Specifications for roads and bridges [45], this extended cure time would have decreased the chloride diffusivity of the concrete , increasing the time to corrosion initiation, and limiting the achievable results for a two year study period.

6.5. Improved Specimen Design

The specimens used had a number of flaws, which included: (i) shear cracks forming in the transversely cracked specimens because no stirrups were provided, and (ii) a large variance in crack width due to the brittle nature of concrete. To improve the cracking arrangement, and reduce the shear cracks, stress concentrations should be induced by reducing the cross section to the depth of the rebar at the desired location of the crack. Also a displacement transducer could be mounted across the reduced cross sectional location. Then by limiting the loading rate based on crack displacement, a more uniform crack width of 0.3 mm can be achieved in the specimens, allowing greater consistency and reproducibility in the replicate specimens.

6.6. Analytical Modelling

To improve the life cycle cost analysis the following additional information is needed:

- Consider site specific chloride type (e.g. calcium chloride, magnesium chloride, sodium chloride or multi-chloride) and average yearly application: This will help to ensure more accurate information at chloride buildup rates, as well as chloride diffusion rates, as different chlorides bind differently within the concrete paste.
- Consider site specific average annual daily traffic, AADT: This can be used to incorporate user delay costs into the critical cost ratio calculations
- Consider bridge demolition and construction costs: The current model only uses the cost to replace the material for the critical cost ratio, but demolition and reconstruction would be a much larger cost over the life of the project.
- Consider social and environmental costs associated with demolition and construction of highway bridge structures: These costs could include: pollution from traffic congestion, carbon dioxide emissions from concrete production; noise pollution as well as health and productivity of the delayed user.
- Develop a more realistic way to incorporate cracks into the chloride transportation model: Currently, the model utilizes a weighted average of the chloride diffusion rate of cracks, and the un-cracked region to determine when the chloride reaches the rebar. Cracks often appear above the rebar as stress concentrations occur in areas of effectively reduced concrete cover and are a direct conduit for chlorides.

- Incorporate experimentally determined chloride threshold levels for specific grades of stainless steels: Thus, once the critical cost ratio has been determined from the analysis it can be compared with the known cost of the specific reinforcing grade.

References

1. Hartt, W.H., *Service Life Projection for Chloride-Exposed Concrete Reinforced with Black and Corrosion Resistant Bars.* Corrosion, 2012. **68**(8): p. 754-761.
2. Lu, Z.-H., Y.-G. Zhao, Z.-W. Yu, and F.-X. Ding, *Probabilistic evaluation of initiation time in RC bridge beams with load-induced cracks exposed to de-icing salts.* Cement and Concrete Research, 2011. **41**(3): p. 365-372.
3. Oranowska, H. and Z. Szklarska-Smialowska, *An electrochemical and ellipsometric investigation of surface films grown on iron in saturated calcium hydroxide solutions with or without chloride ions.* Corrosion Science, 1981. **21**(11): p. 735-747.
4. Johannesson, B. and P. Utgenannt, *Microstructural changes caused by carbonation of cement mortar.* Cement and Concrete Research, 2001. **31**(6): p. 925-931.
5. Glass, G.K. and N.R. Buenfeld, *The Presentation of the Chloride Threshold Level for Corrosion of Steel in Concrete.* Corrosion Science, 1997. **39**(5): p. 1001-1013.
6. Canadian Standards Association, *Concrete Design Handbook*. 2006, Cement Association of Canada: Ottawa.
7. Koch, G.H., M. Brongers, N.G. Thomspon, Y.P. Virmani, and J.H. Payer, *Corrosion Cost and Preventive Strategies in the United States*. 2002, Research, Developmet, and Technology Turner-Fairbank Highway Research Center: 6300 Georgetown Pike McLean, VA 22101 -2296
8. Hansson, C.M., R. Haas, R. Green, R.C. Evers, O.K. Gepraegs, and R.A. Assar, *Corrosion Protection Strategies for Ministry Bridges*. 2000: Waterloo, Canada.
9. Adey, B.T., T. Herrmann, K. Tsafatinos, J. Lüking, N. Schindele, and R. Hajdin, *Methodology and base cost models to determine the total benefits of preservation interventions on road sections in Switzerland.* Structure and Infrastructure Engineering, 2010. **8**(7): p. 639-654.
10. Statista. *Gross Domestic Product (GDP) of the United States of America from 1990 to 2013*. 2014; Available from: http://www.statista.com/statistics/188105/annual-gdp-of-the-united-states-since-1990/.
11. Gagnon, M., V. Gaudreault, and D. Overton, *Age of Public Infrastructure: A Provincial Perspective*. 2007, Statistics Canada.
12. Thompson, P.D., R.M. Ellis, K. Hond, and T. Merlo, *Implementation of Ontario Bridge Management System*, in *9th Internation Bridge Management Conference*. 2003: Orlando Airport Marriott.
13. Canadian Standards Association, *Design of Highway Bridges*. 1988, Canadian Standards Association,: Rexdale, Ontario.
14. Canadian Standards Association, *Canadian Highway Bridge Design Code*. 2000, Canadian Standards Association, : Mississauga, Ontario, Canada.
15. Davis, S. and D. Goldberg, *The Fix We're in For: The State of Our Nation's Bridges 2013*. 2013, Transportation for America: Washington DC.
16. Knudesn, A., F.M. Jensen, O. Klinghoffer, and T. Skovsgaard. *Cost-effective Enhancement of Durability of Concrete Structures by Intelligent Use of Stainless Steel Reinforcement*. in *Corrosion and Rehabilitation of Reinfroced Concrete Structures*. 1998. Orlando: Federal Highway Administration.

17. American Society for Testing and Materials, *Standard Specification for Epoxy-Coated Prefabricated Steel Reinforcing Bars*. 2013: West Conshohocken, Pennsylvania United States.
18. Manning, D.G., *Corrosion performance of epoxy-coated reinforcing steel: North American experience.* Construction and Building Materials, 1995. **10**(5): p. 349-365.
19. Benmokrane, B., O. Chaallal, and R. Masmoudi, *GFRP rebar for concrete structures.* Construction and Building Materials, 1995. **9**(6): p. 353-364.
20. American Concrete Institute 440.1R-06, *Guide for the Design and Consruction of Structural Concrete Reinforced with FRP Bars*. 2006, American Concrete Institute: 38800 Country Club Dr. Farmington Hills, MI, USA.
21. Yeomans, S.R., *Applications of Galvanized Rebar in Reinforced Concrete Structures*. 2001, National Association of Corrosion Engineers,: Houston, TX, USA.
22. Galvanizing, C. *Custom Hot Dip Galvanizing*. 2003 [cited 2014 March 13].
23. Macias, A. and C. Andrade, *Corrosion of galvanized steel in dilute Ca(OH)2 solutions (pH 11·1–12·6).* British Corrosion Journal, 1987. **22**(3): p. 162-171.
24. Bautista, A. and J.A. González, *Analysis of the protective efficiency of galvanizing against corrosion of reinforcements embedded in chloride contaminated concrete.* Cement and Concrete Research, 1996. **26**(2): p. 215-224.
25. Pérez-Quiroz, J.T., J. Terán, M.J. Herrera, M. Martínez, and J. Genescá, *Assessment of stainless steel reinforcement for concrete structures rehabilitation.* Journal of Constructional Steel Research, 2008. **64**(11): p. 1317-1324.
26. Knudesn, A., O. Klinghoffer, and T. Skovsgaard, *Pier in Progreso, Mexico. Inspection Report.* 1999, Arminox Stainless,: Denmark. p. 40.
27. Baddoo, N.R., *Stainless steel in construction: A review of research, applications, challenges and opportunities.* Journal of Constructional Steel Research, 2008. **64**(11): p. 1199-1206.
28. Goñi, S. and C. Andrade, *Synthetic concrete pore solution chemistry and rebar corrosion rate in the presence of chlorides.* Cement and Concrete Research, 1990. **20**(4): p. 525-539.
29. Kouřil, M., P. Novák, and M. Bojko, *Threshold chloride concentration for stainless steels activation in concrete pore solutions.* Cement and Concrete Research, 2010. **40**(3): p. 431-436.
30. Alonso, C., C. Andrade, M. Castellote, and P. Castro, *Chloride threshold values to depassivate reinforcing bars embedded in a standardized OPC mortar.* Cement and Concrete Research, 2000. **30**(7): p. 1047-1055.
31. Randström, S., M. Almen, R. Pettersson, and M. Adair, *Reproducibility of critical chloride threshold levels for stainless steel reinforcement.*, in *Structural Faults*. 2010: Edinburgh, Scotland.
32. Bertonlini, L., F. Bolzoni, T. Pastore, and P. Pedeferri, *Behaviour of stainless steel in simulated concrete.* British Corrosion Journal, 1996. **31**(3): p. 218-222.
33. Bertolini L. and Gastaldi M. *Corrosion resistance of austenitic and low-nickel duplex stainless steel bars*. in *Corrosion from the Nanoscale to the Plant*. 2009. Nice, France.
34. Hurley, M.F. and J.R. Scully, *Threshold Chloride Concentrations of Selected Corrosion-Resistant Rebar Materials Compared to Carbon Steel.* Corrosion, 2006. **62**(10): p. 892-904.

35. Hansson, C.M. and B. Sørensen, *The Threshold Concentration of Chloride in Concrete for the Initiation of Reinforcement Corrosion*, in *Corrosion Rates of Steel in Concrete, Issue 1065*, N.S. Berke, V. Chaker, and D. Whiting, Editors. 1990, ASTM Internations. p. 3-17.
36. The Canadian Standards Association, *Canadian Highway Bridge Design Code*, in *8.11 Durability*. 2006, The Canadian Standards Association: Mississauga, Ontario, Canada.
37. Poulsen, E. and L. Mejlbro, *Diffusion of Chloride In Concrete: Theory and Application*. 2006, 270 Madison Ave, New York: Taylor and Francis.
38. Sagüés, A.A., K. Lau, R.G. Powers, and R.J. Kessler, *Corrosion of Epoxy-Coated Rebar in Marine Bridges—Part 1: A 30-Year Perspective.* Corrosion, 2010. **66**(6): p. 065001-065001-13.
39. Violetta, B., *Life-365 Service Life Prediction Model.* Concrete International, 2002. **24**(12): p. 53-57.
40. Ehlen, M., M. Thomas, and E. Bentz, *Life-365 Service Life Prediction Model Version 2.0.* Concrete International, 2009. **31**(5): p. 41-46.
41. Life-365™ Consortium III, *Life-365™ Service Life Prediction Model™ and Computer Program for Predicting the Service Life and Life-Cycle Cost of Reiforced Concrete Exposed to Chlorides*. 2014.
42. Scottish Executive Development Department, *Use of Stainless Steel Reinforcement in Highway Structures*, S.E.D. Department, Editor. 2002.
43. R. E. Schnell and M.P. Bergmann, *Use of advanced materials to extend bridge life and reduce initial cost: a case study of three projects in New York city*. 2010, Federal Highway Administration.
44. ASTM International, *Standard Specification for Stainless Steel Bars and Shapes*, in *A276-13*. 2013, ASTM International: West Conshohocken.
45. Ontario Provincial Standard Specification Provision 904, *Construction Specification for Concrete Structures*. 2012, Ontario Provincial Standard Specification.
46. Ontario Provincial Standard Specification Provision 1002, *Material Specification for Aggregates*, in *Concrete*. 2013, Ontario Provincial Standard Specification.
47. Ontario Provincial Standard Specification Provision 920, *Construction Specification for Deck Joint Assemblies, Preformed Seals, Joint Fillers, Joint Seals, Joint Sealing Compounds, and Waterstops - Structures*. 2008, Ontario Provincial Standard Specification.
48. Newton, C.J. and J.M. Sykes, *A galvanostatic pulse technique for investigation of steel corrosion in concrete.* Corrosion Science, 1988. **28**(11): p. 1051-1074.
49. Stern, M. and A.L. Geary, *Electrochemical Polarization - A Theoretical Analysis of the Shape of Polarization Curves.* Journal of the Electrochemical Society, 1957. **104**(1): p. 56-63.
50. ASTM international, *G59*, in *Conducting Potentiodynamic Polarization Resistance Measurements*. 2014, ASTM International,: West Conshohocken, PA.
51. ASTM International, *Standard Test Method for Corrosion Potentials of Uncoated Reinforcing Steel in Concrete*. 2009, ASTM International,: West Conshohocken, PA.
52. Andres, A.T.-A. and A.S. Alberto, *Concrete Cracking by Localized Steel Corrosion - Geometric Effects.* Materials Journal, 2004. **101**(6): p. 501-507.
53. Djerbi, A., S. Bonnet, A. Khelidj, and V. Baroghel-bouny, *Influence of traversing crack on chloride diffusion into concrete.* Cement and Concrete Research, 2008. **38**(6): p. 877-883.

54. Darwin, D., J. Browning, and W. Lindquist, *Control of Cracking in Bridge Decks Observations from the Field.* Cement, Concrete, and Aggregates, 2004. **26**(2).
55. Anders, K.A., B.P. Bergsma, and C.M. Hansson, *Chloride concentration in the pore solution of Portland cement paste and Portland cement concrete.* Cement and Concrete Research, 2014. **63**(0): p. 35-37.
56. New York State Department of Transportation, *Bridge Design Manual*, in *Section 5: Bridge Decks*. 2014, New York State Department of Transportation: New York.
57. Ann, K.Y., J.H. Ahn, and J.S. Ryou, *The importance of chloride content at the concrete surface in assessing the time to corrosion of steel in concrete structures.* Construction and Building Materials, 2009. **23**(1): p. 239-245.
58. Thomas, M.D.A. and P.B. Bamforth, *Modelling chloride diffusion in concrete: Effect of fly ash and slag.* Cement and Concrete Research, 1999. **29**(4): p. 487-495.
59. Walbridge, S., D. Fernando, and B. Adey, *Total Cost-Benefit Analysis of Alternative Corrosion Management Strategies for a Steel Roadway Bridge.* Journal of Bridge Engineering, 2012. **18**(4): p. 318-327.
60. Knapp, T., C.V. Niejenhuis, Editor. 2014.
61. Ramezanianpour, A.A. and V.M. Malhotra, *Effect of curing on the compressive strength, resistance to chloride-ion penetration and porosity of concretes incorporating slag, fly ash or silica fume.* Cement and Concrete Composites, 1995. **17**(2): p. 125-133.
62. Hartt, W.H., *Corrosion Initiation Projection for Reinforced Concrete Exposed to Chlorides: Part 2—Corrosion-Resistant Bars.* Corrosion, 2011. **67**(8).
63. Jones, M.R., R.K. Dhir, and J.P. Gill, *Concrete surface treatment: Effect of exposure temperature on chloride diffusion resistance.* Cement and Concrete Research, 1995. **25**(1): p. 197-208.

Appendix A Individual i_{corr} Values

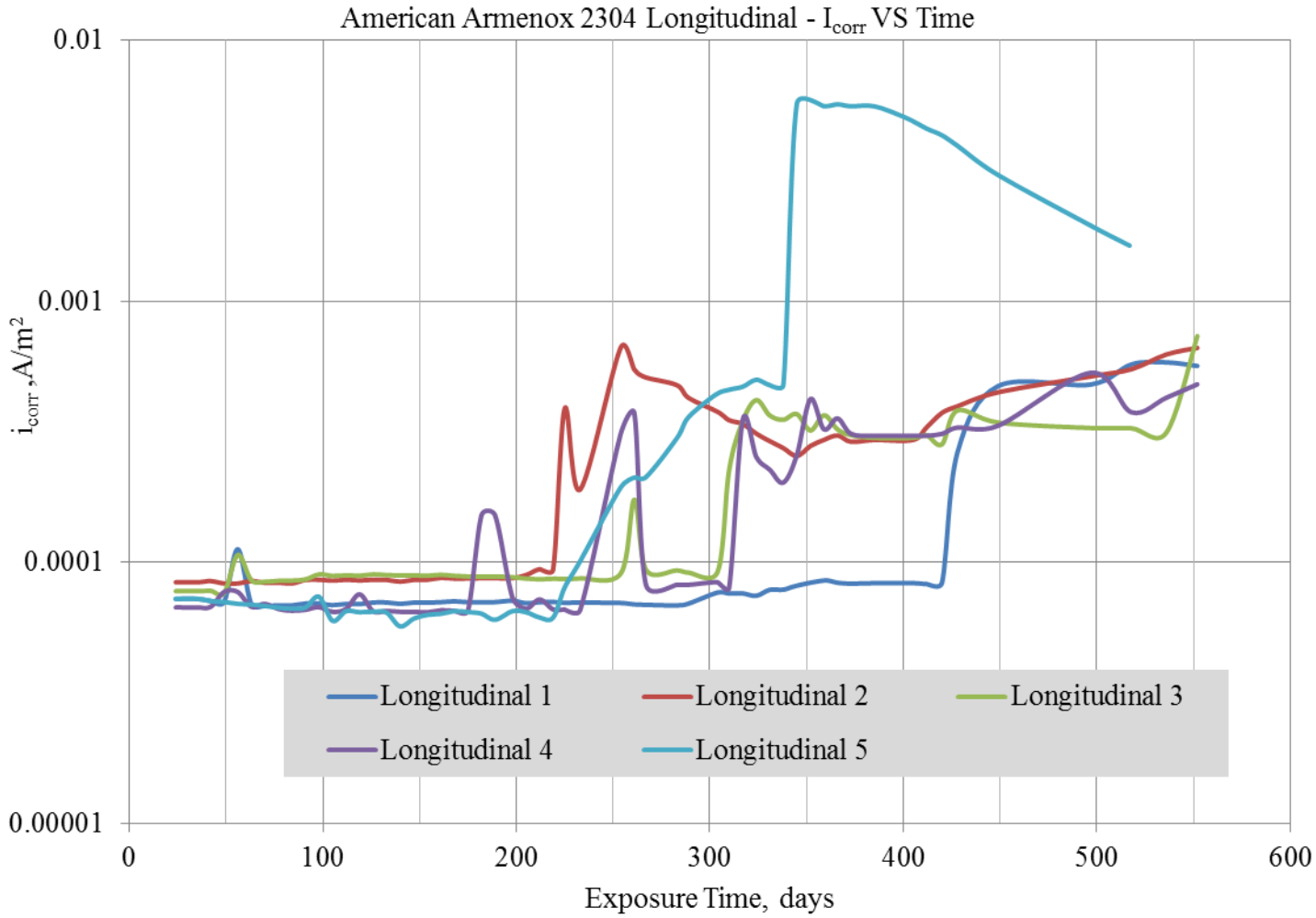

Figure A-1 Individual i_{corr} values for Armenox 2304 in longitudinally cracked concrete

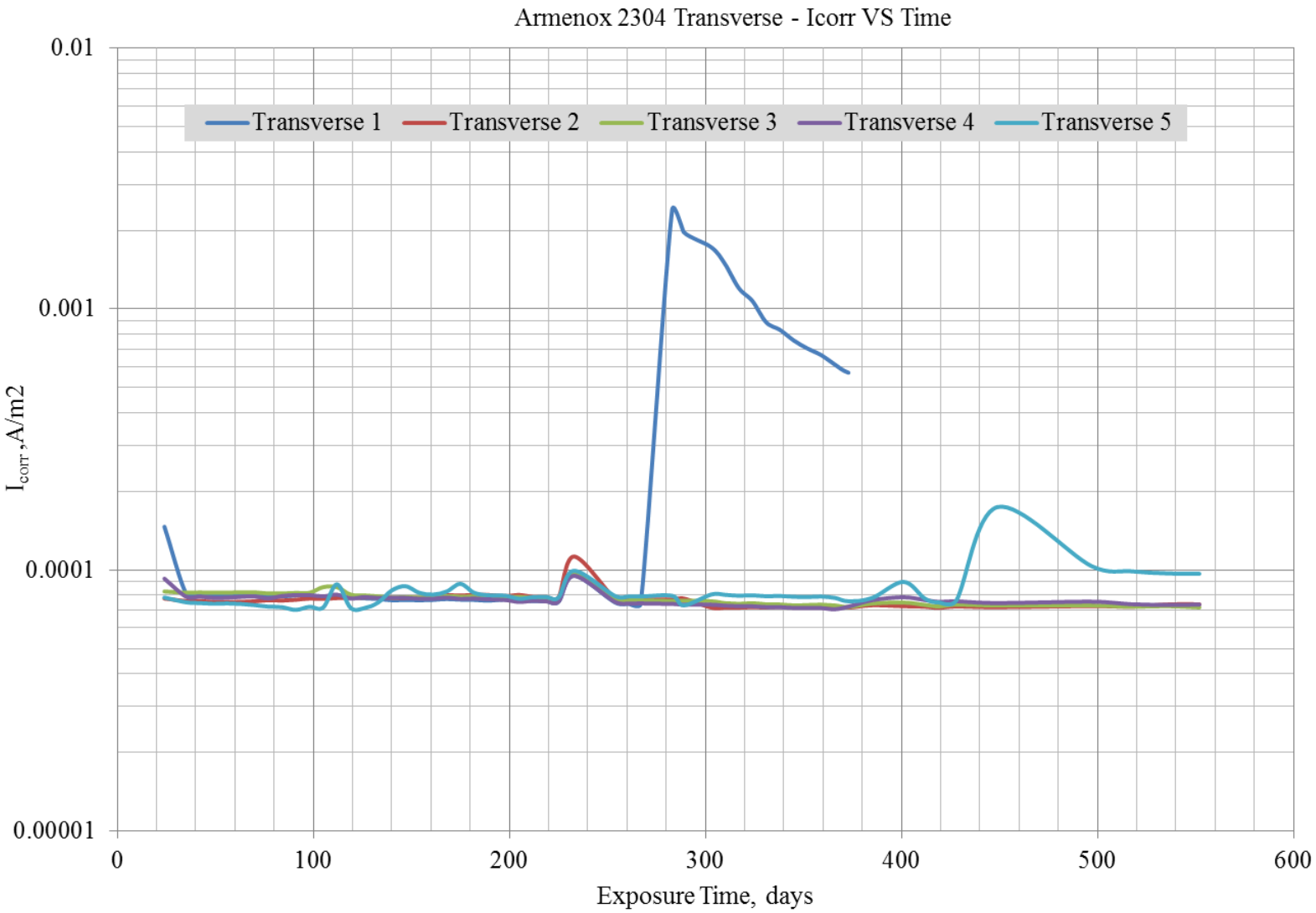

Figure A-2 Individual i_{corr} values for Armenox 2304 in transversely cracked concrete

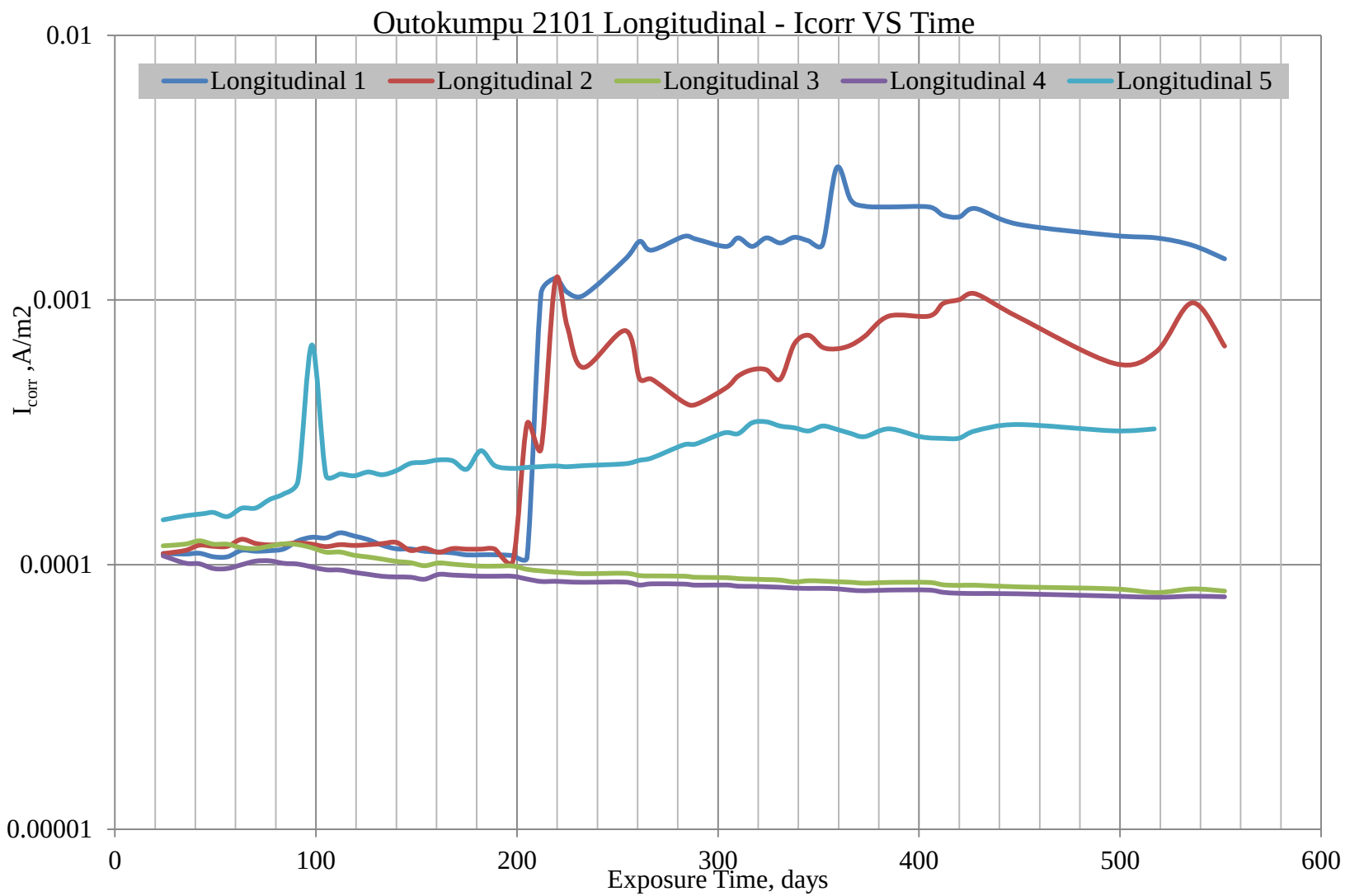

Figure A-3 Individual i_{corr} values for Outokumpu 2101 in longitudinally cracked concrete

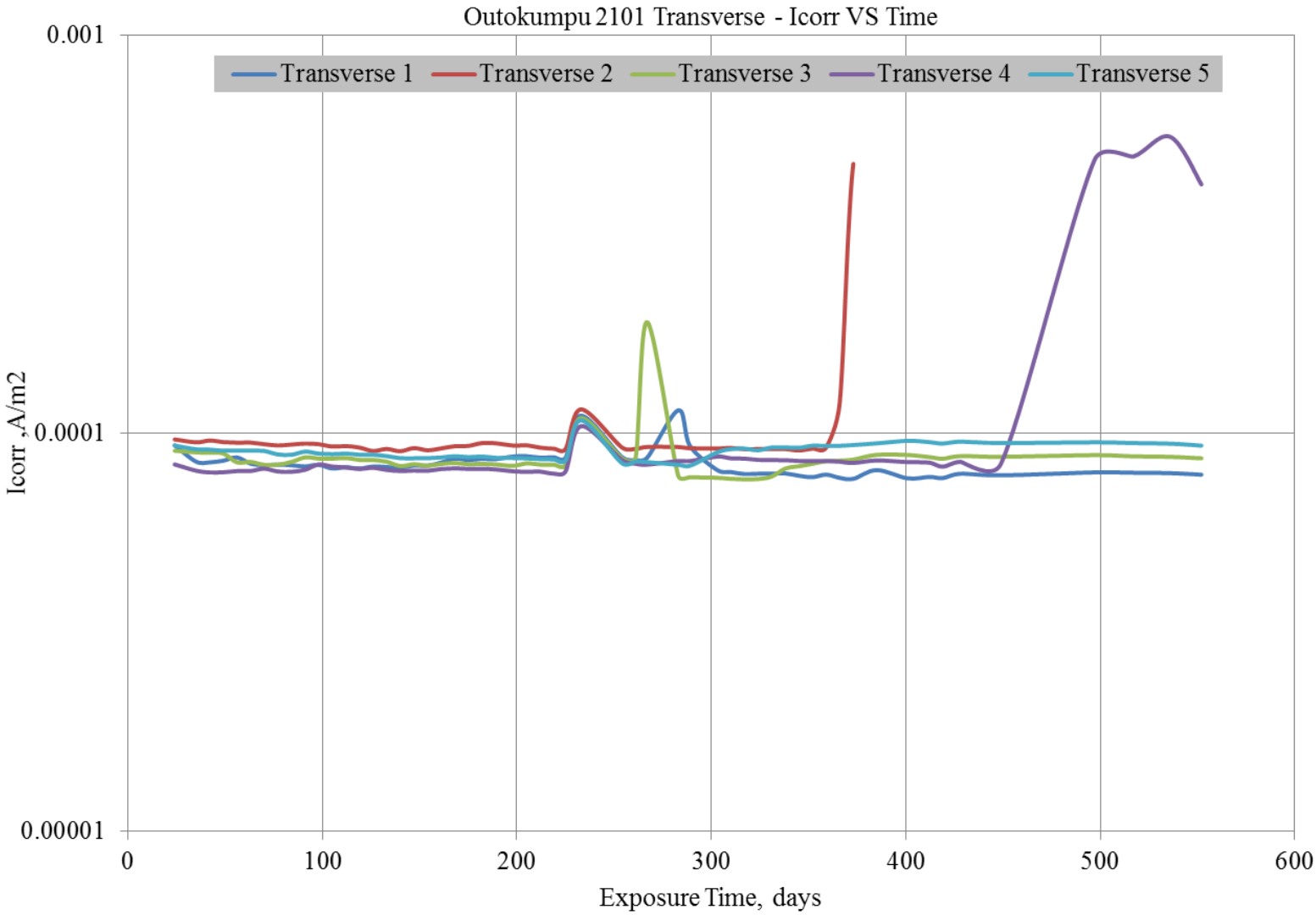

Figure A-4 Individual i_{corr} values for Outokumpu 2101 in transversely cracked concrete

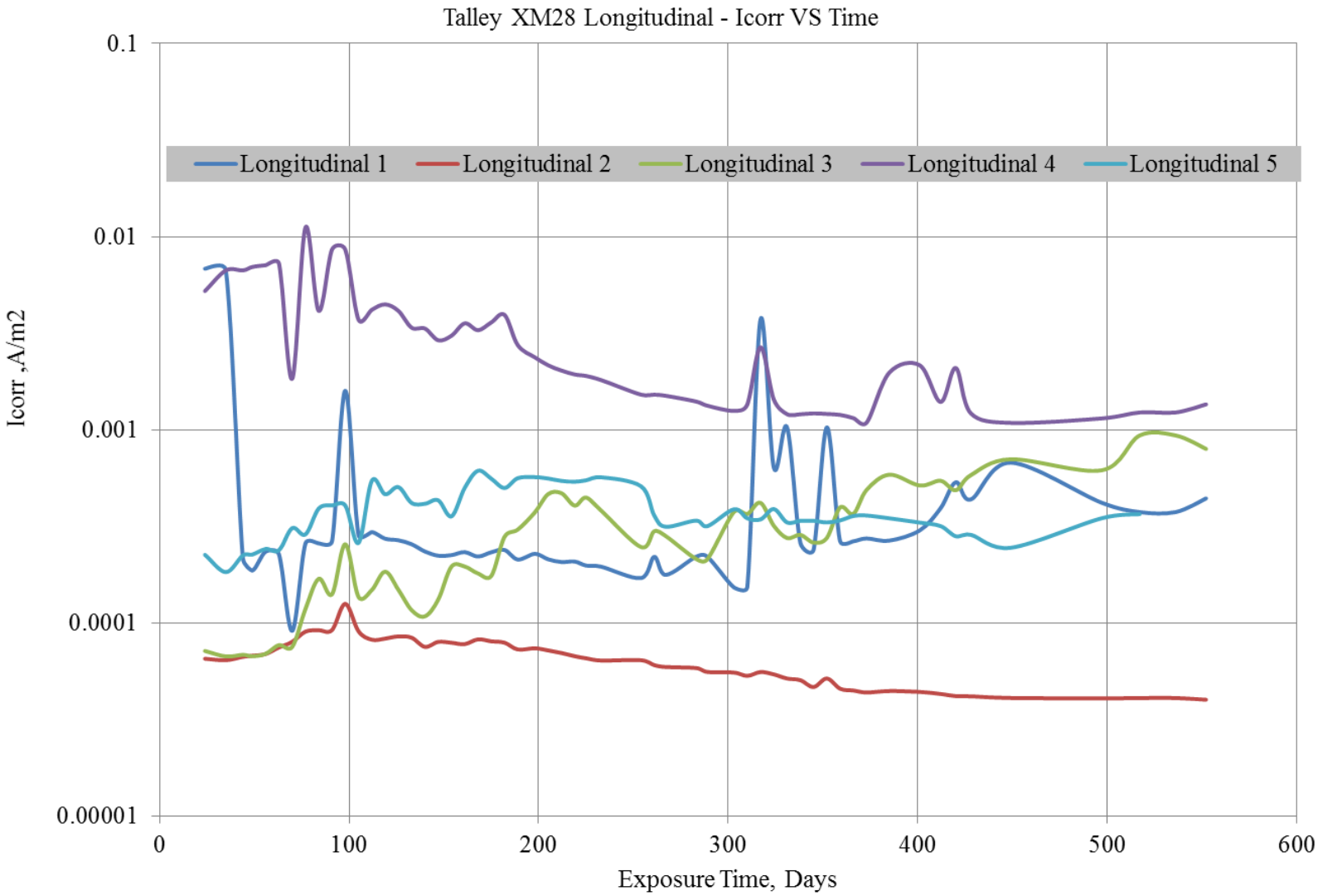

Figure A-5 Individual i_{corr} values for Talley XM28 in longitudinally cracked concrete

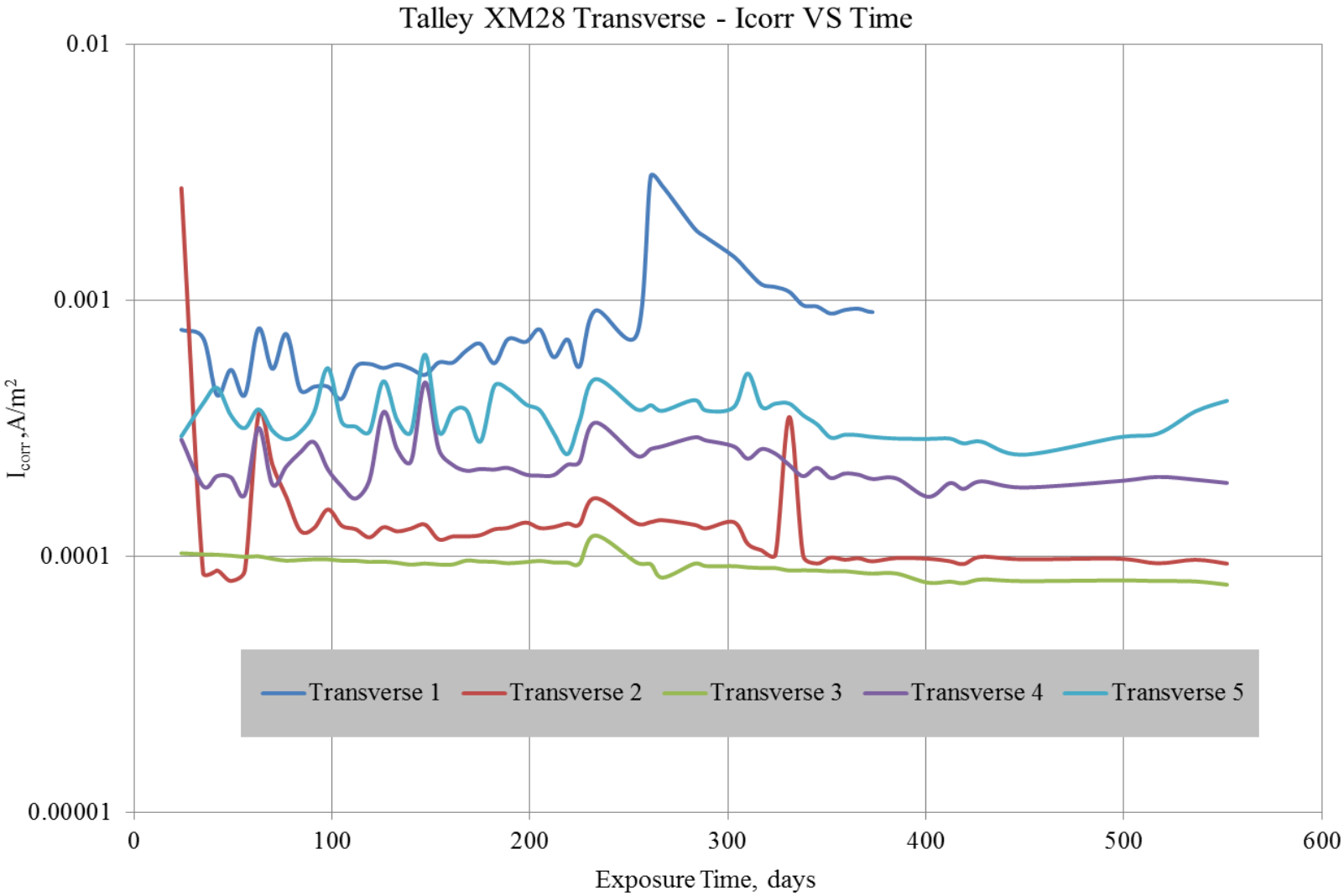

Figure A-6 Individual i_{corr} values for Talley XM28 in transversely cracked concrete

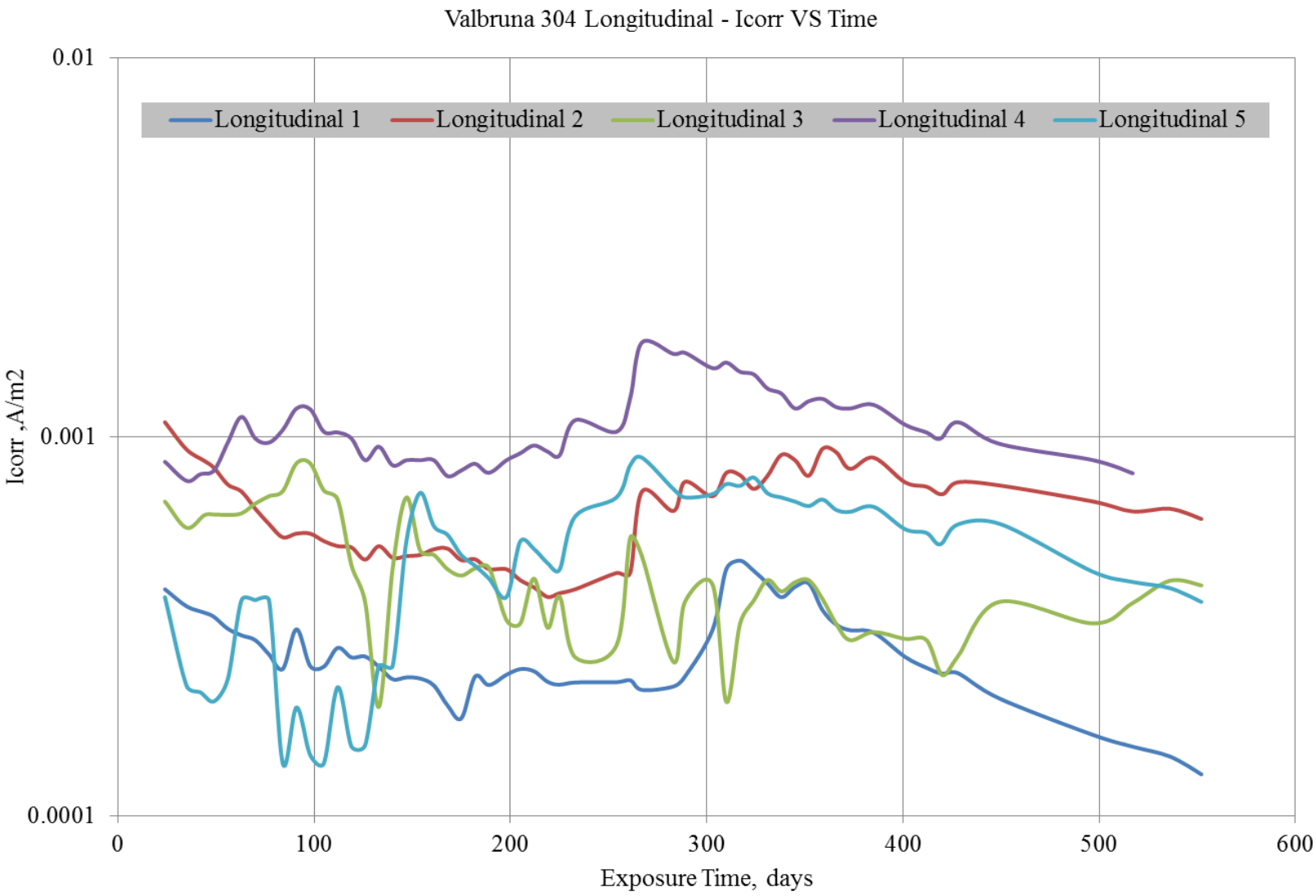

Figure A-7 Individual i_{corr} values for Valbruna 304 in longitudinally cracked concrete

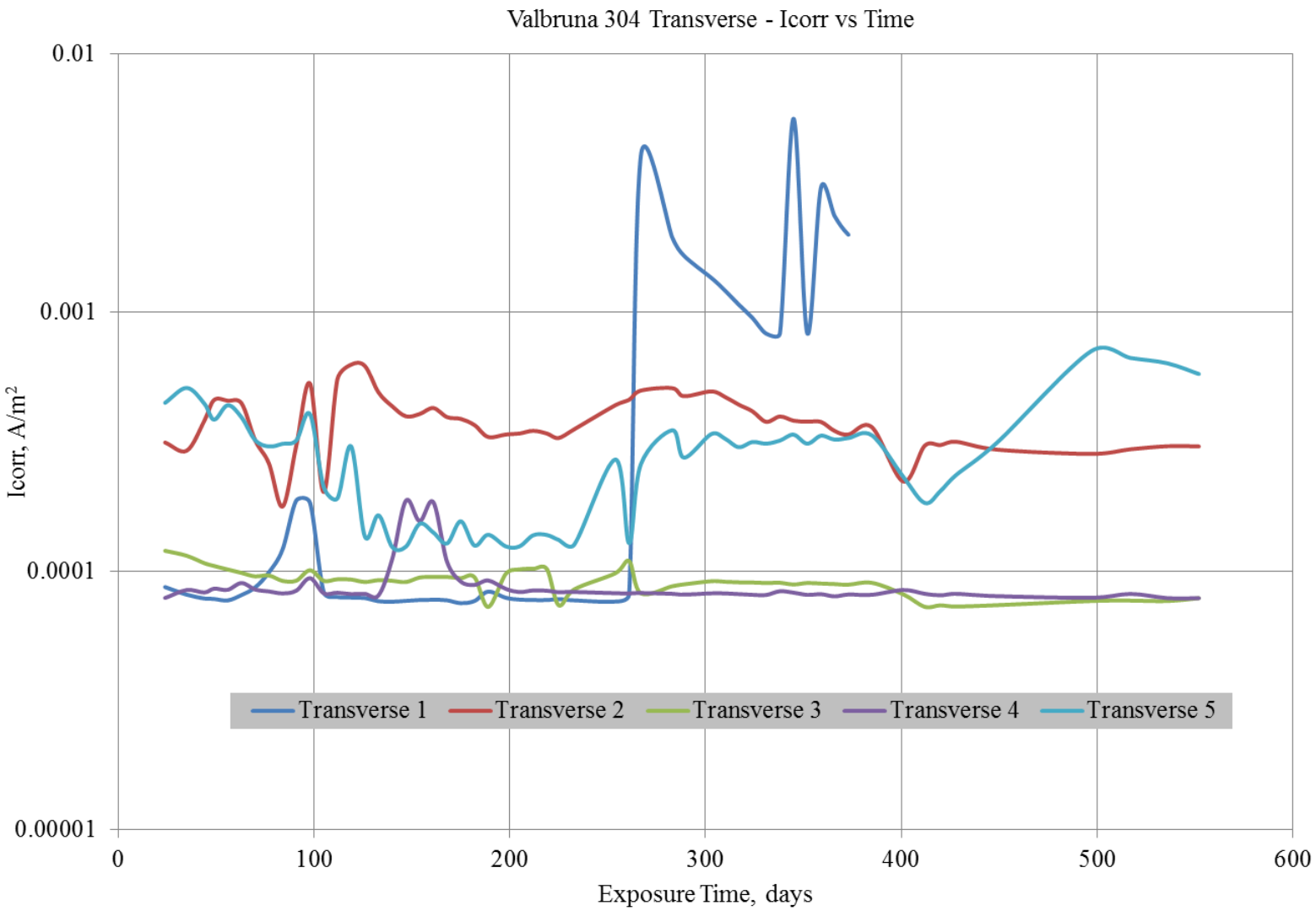

Figure A-8 Individual i_{corr} values for Valbruna 304 in transversely cracked concrete

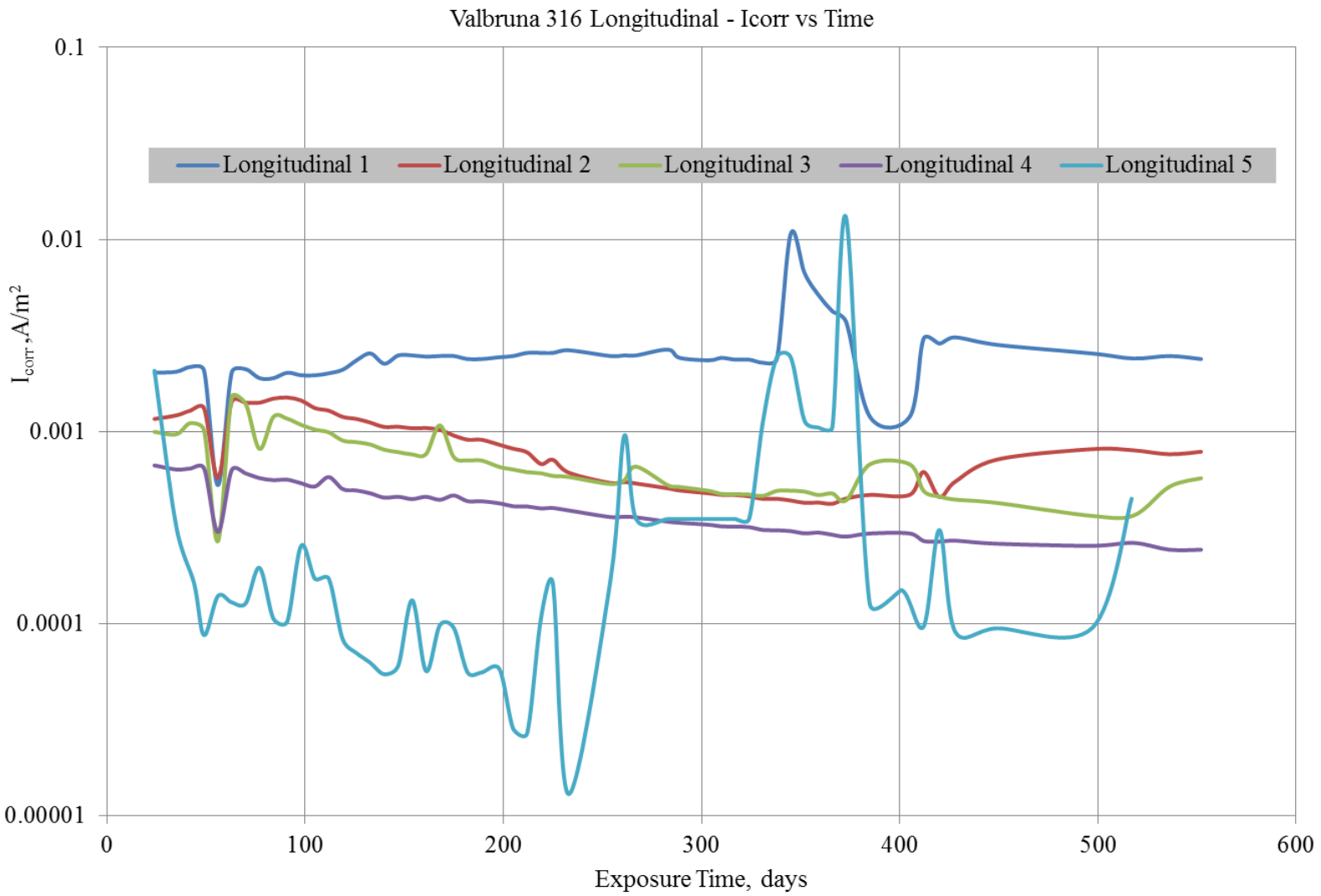

Figure A-9 Individual i_{corr} values for Valbruna 316 in longitudinally cracked concrete

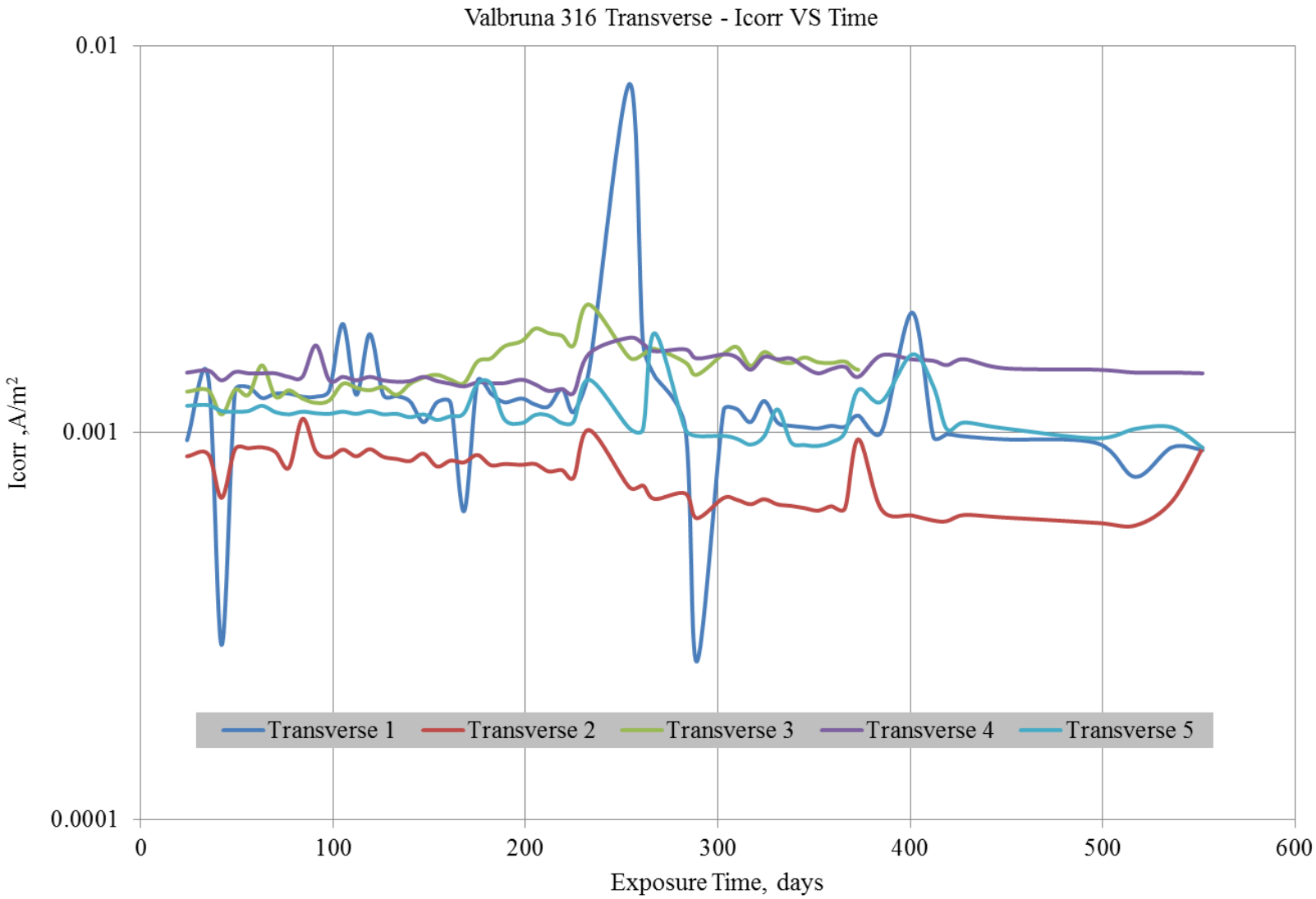

Figure A-10 Individual i_{corr} values for Valbruna 316 in transversely cracked concrete

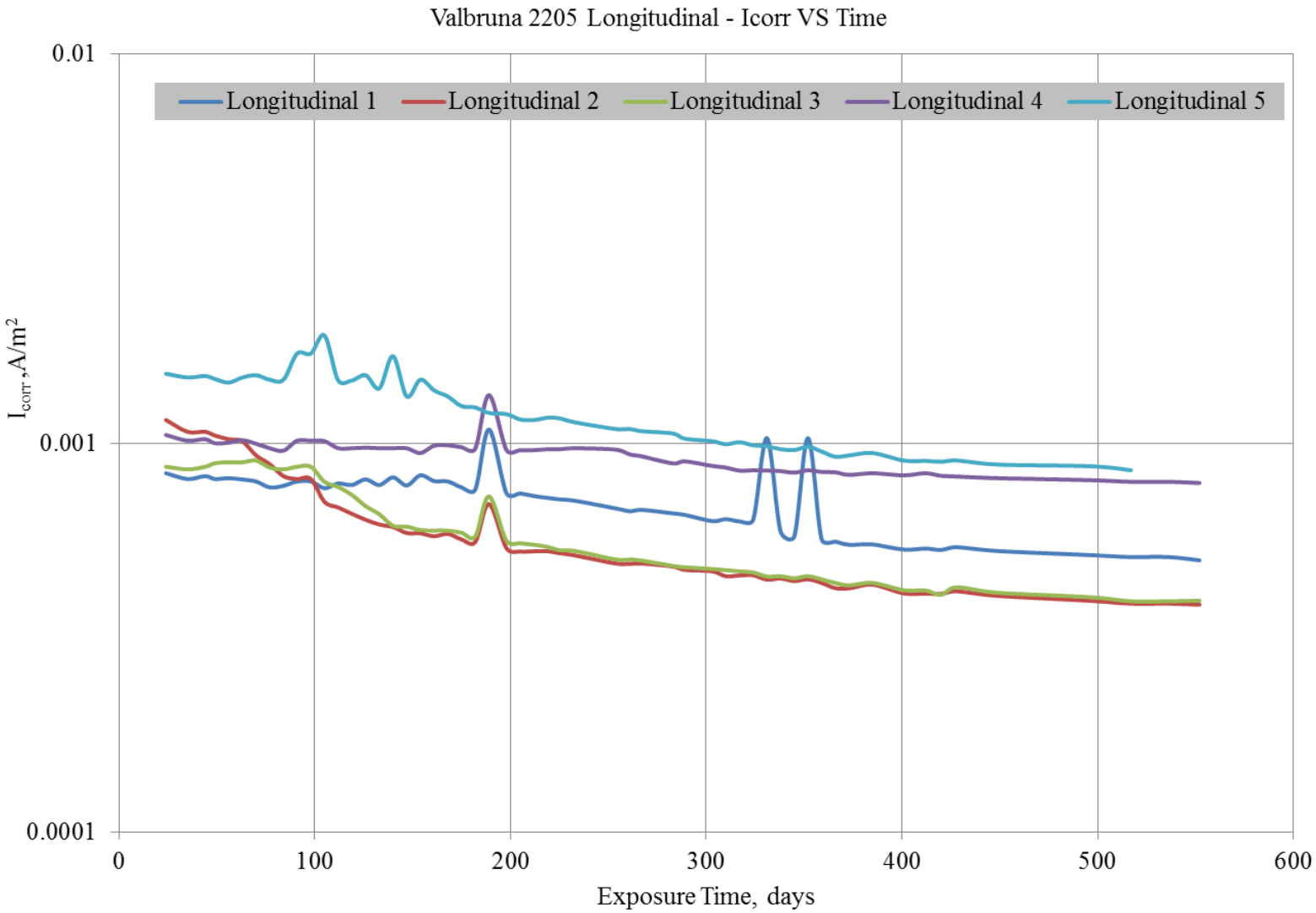

Figure A-11 Individual i_{corr} values for Valbruna 2205 in longitudinally cracked concrete

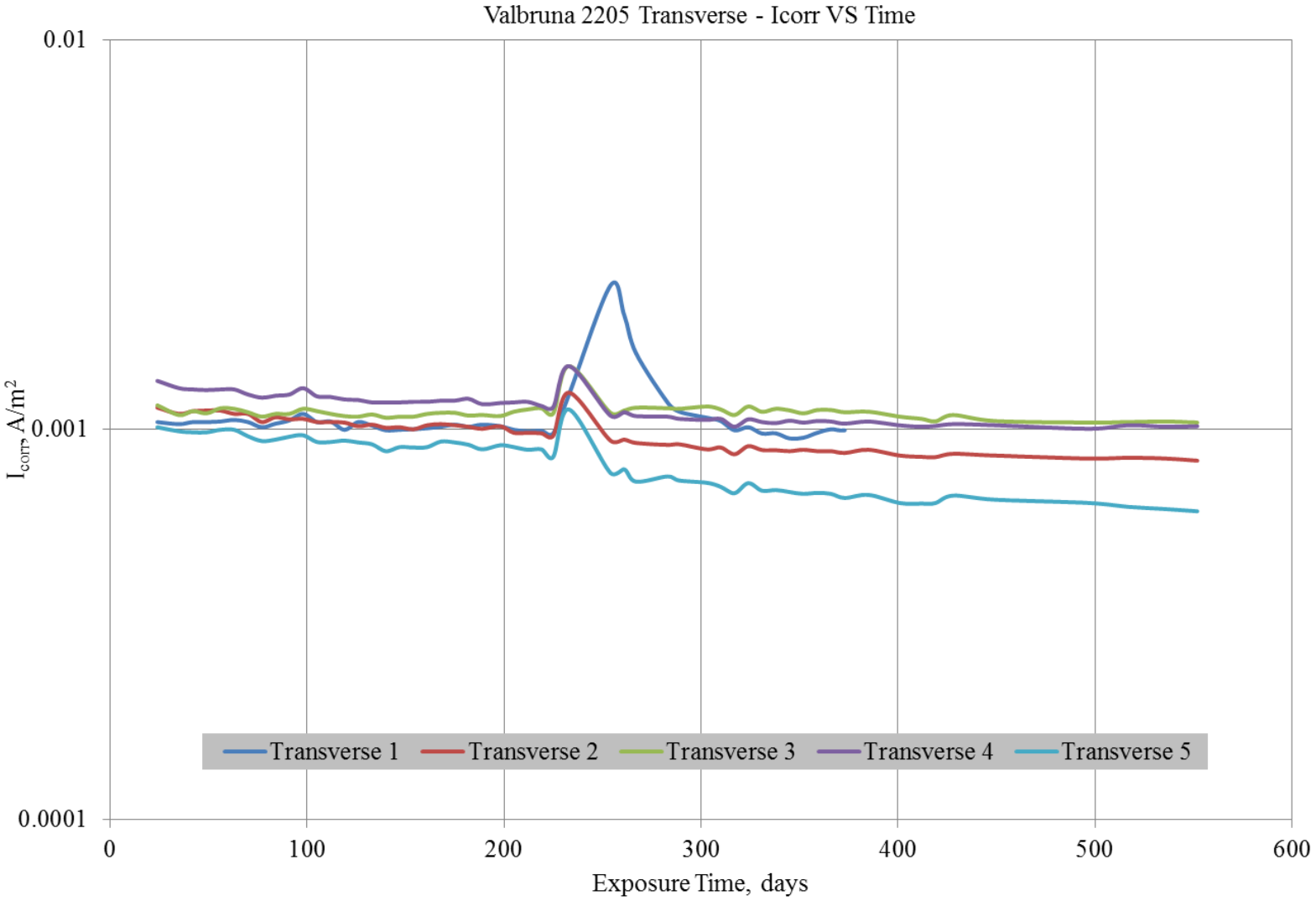

Figure A-12 Individual i_{corr} values for Valbruna 2205 in transversely cracked concrete

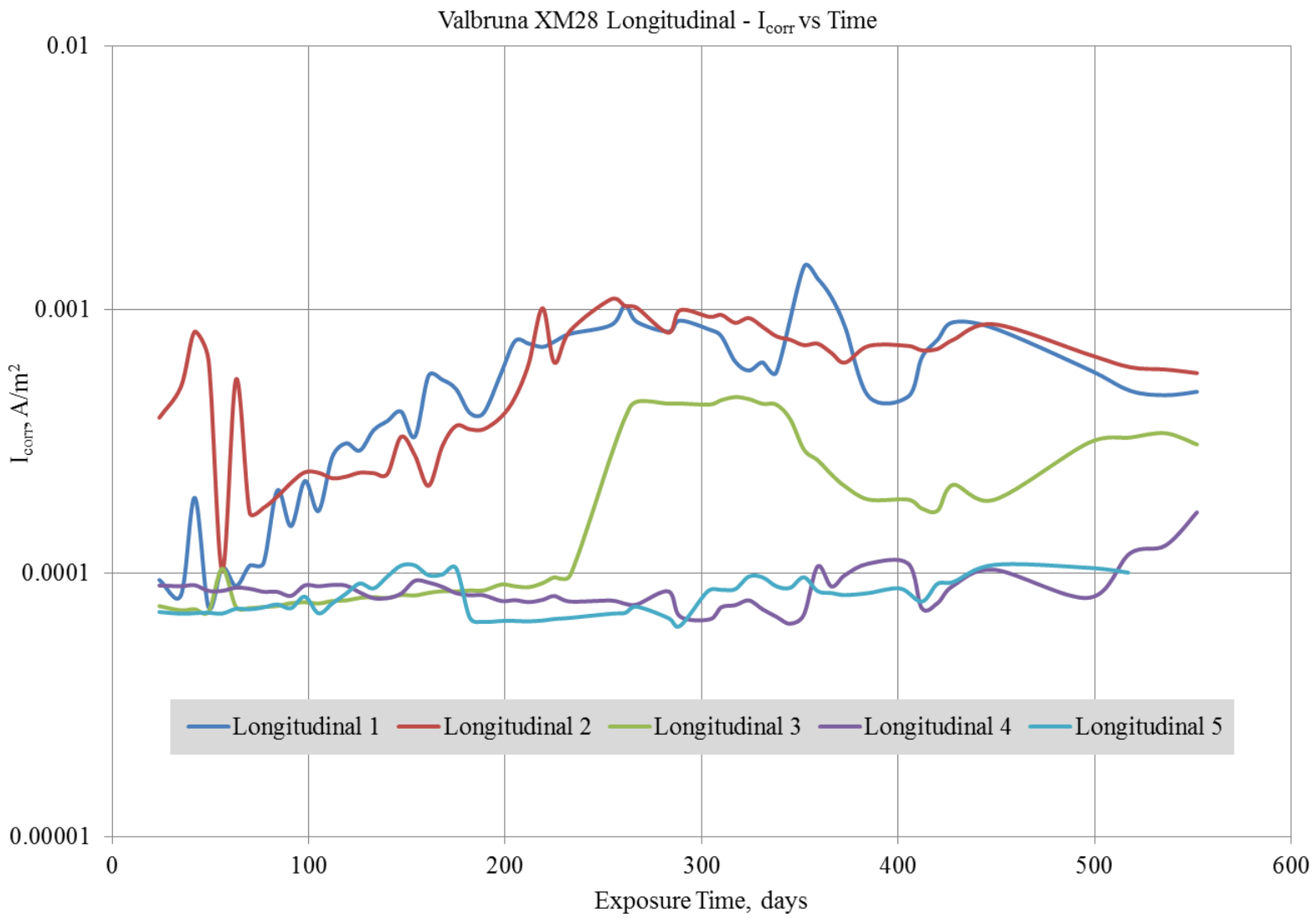

Figure A-13 Individual i_{corr} values for Valbruna XM28 in longitudinally cracked concrete

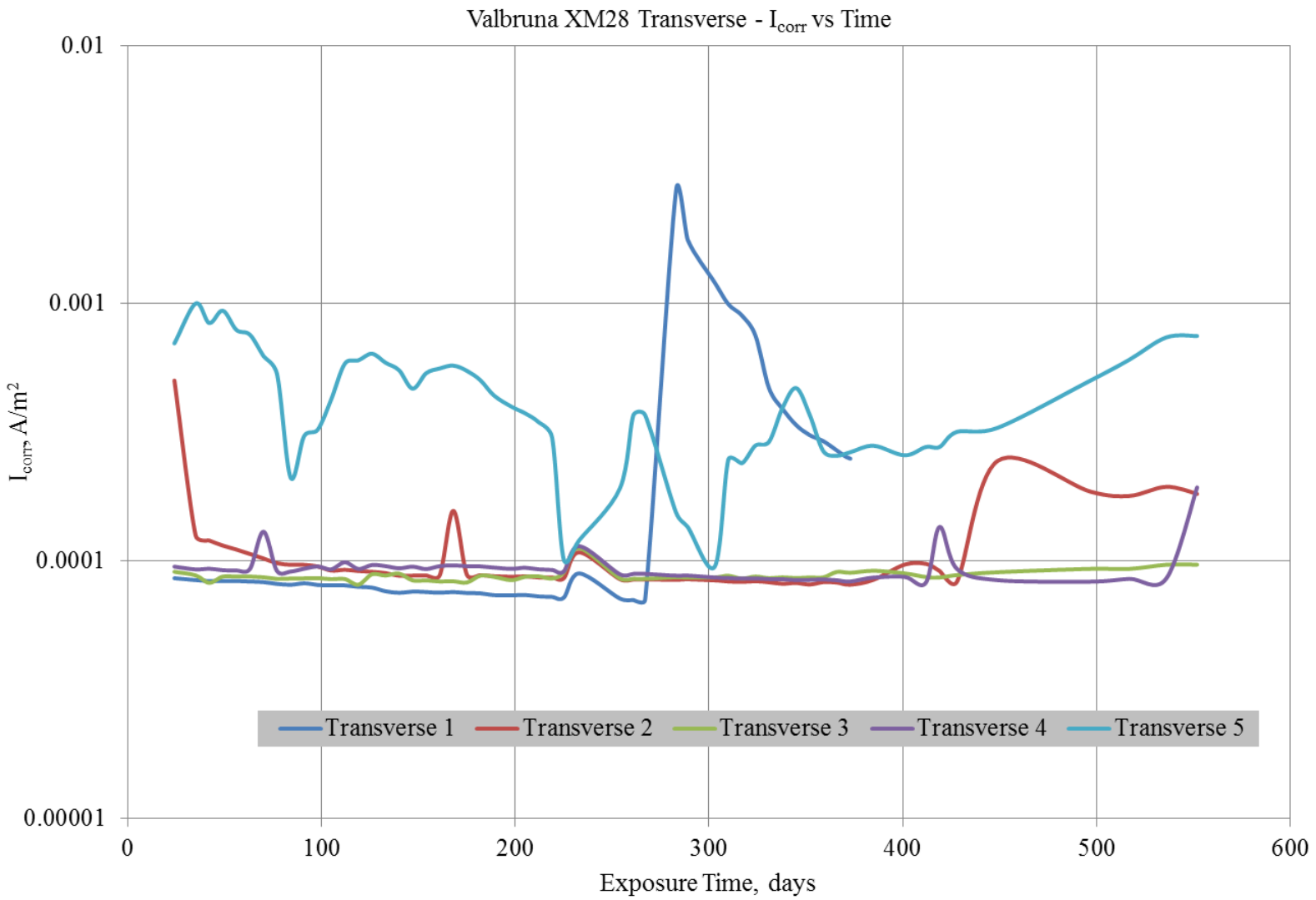

Figure A-14 Individual i_{corr} values for Valbruna XM28 in transversely cracked concrete

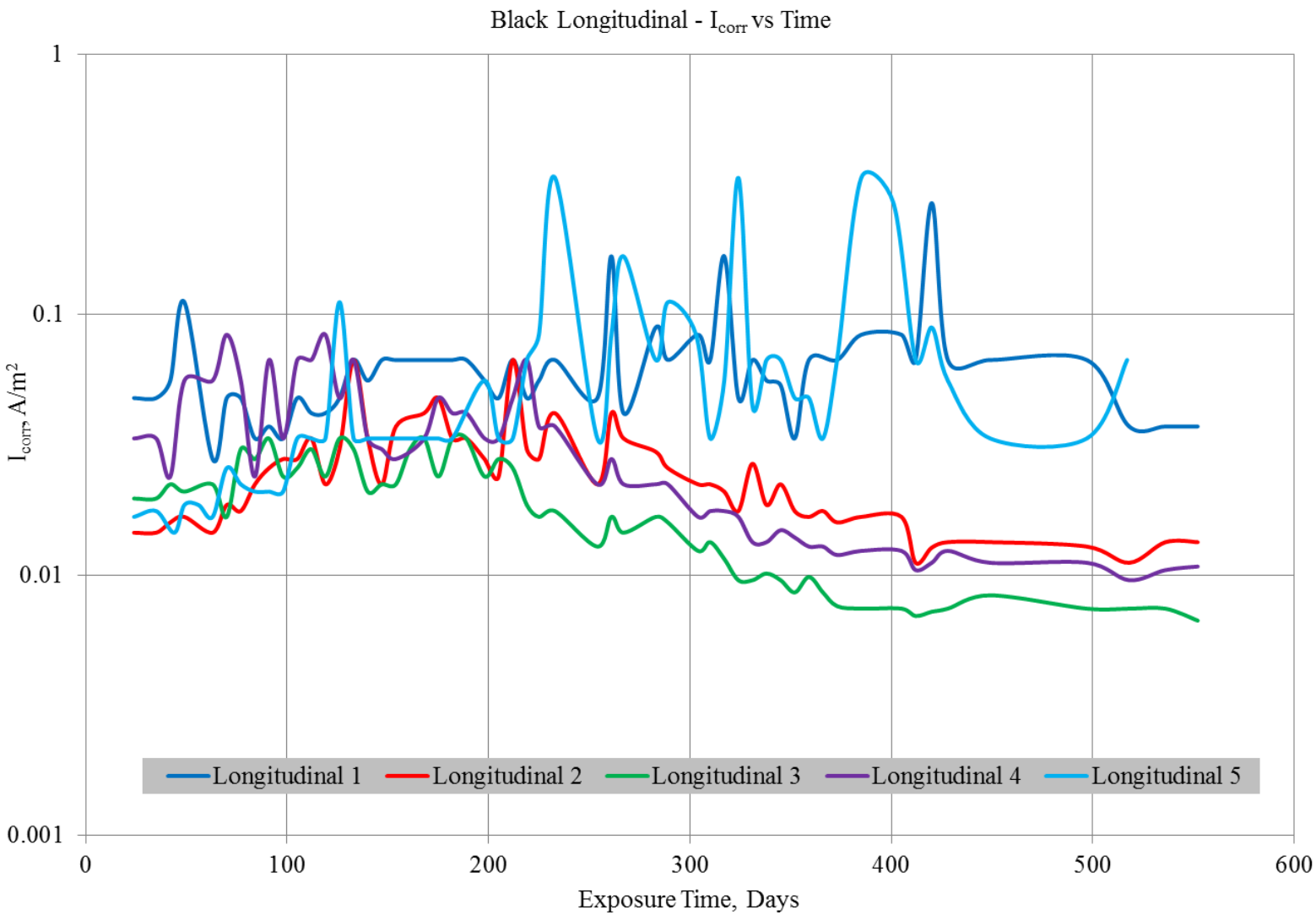

Figure A-15 Individual i_{corr} values for black steel in longitudinally cracked concrete

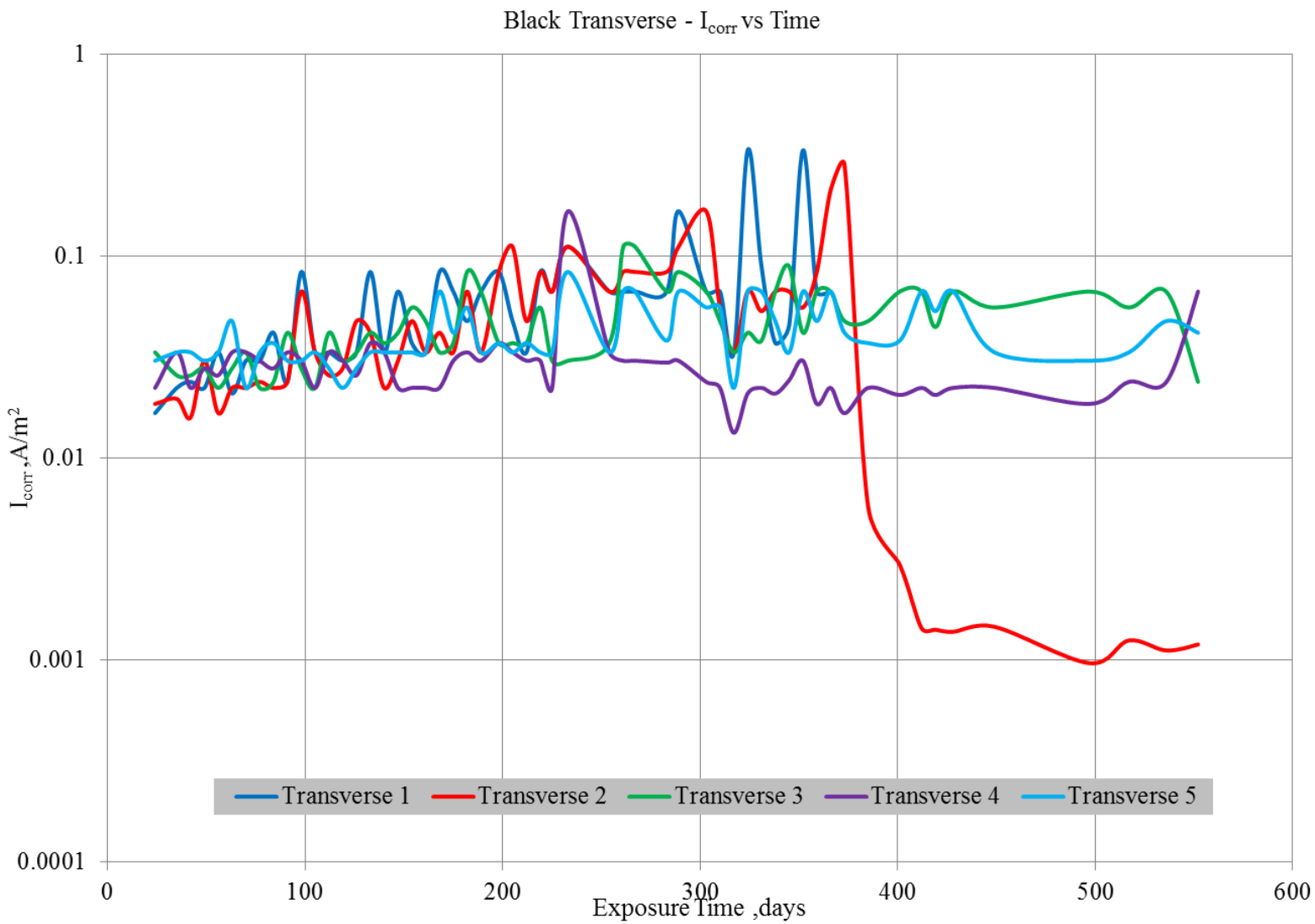

Figure A-16 Individual i_{corr} values for black steel in transversely cracked concrete

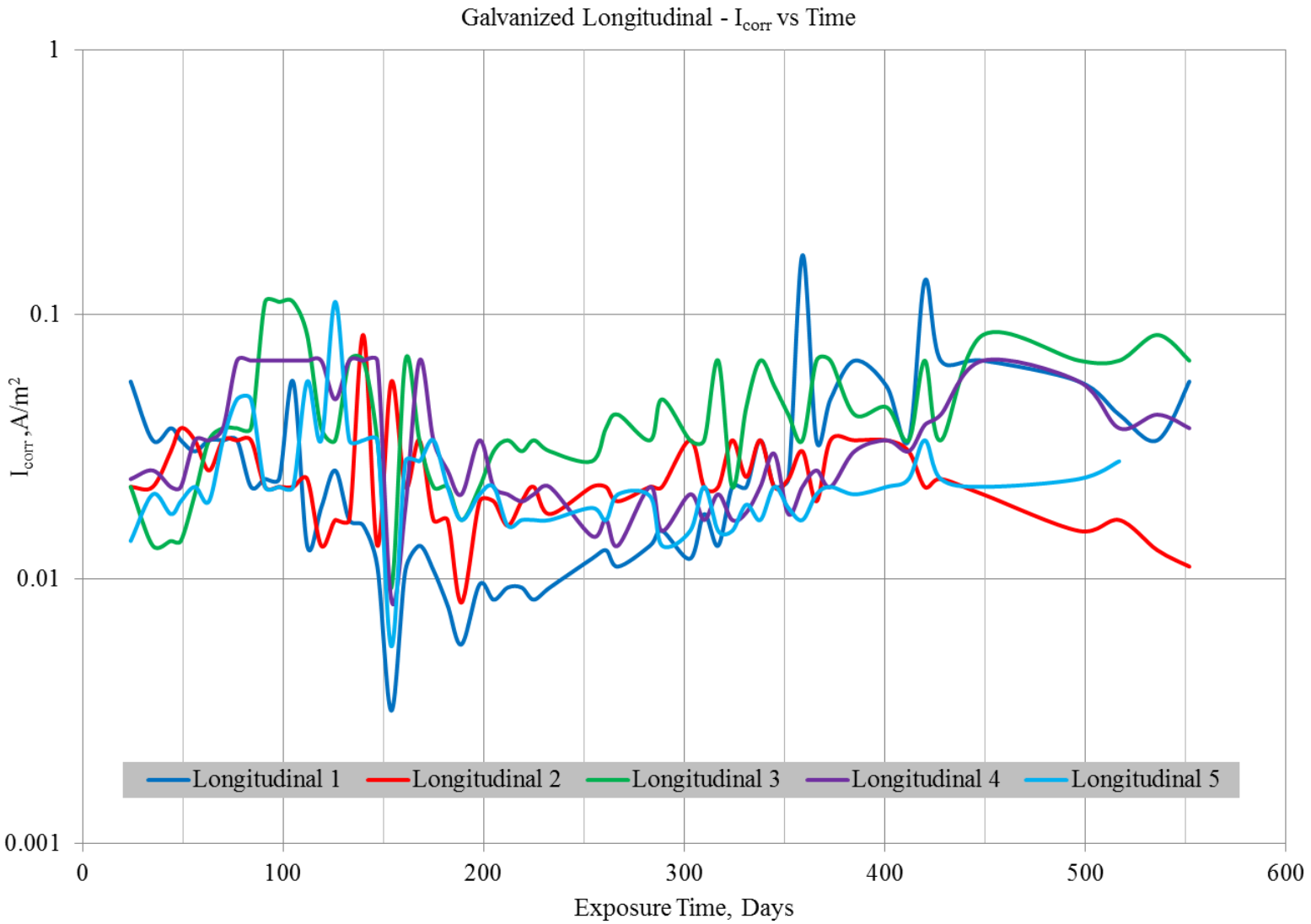

Figure A-17 Individual i_{corr} values for galvanized steel in longitudinally cracked concrete

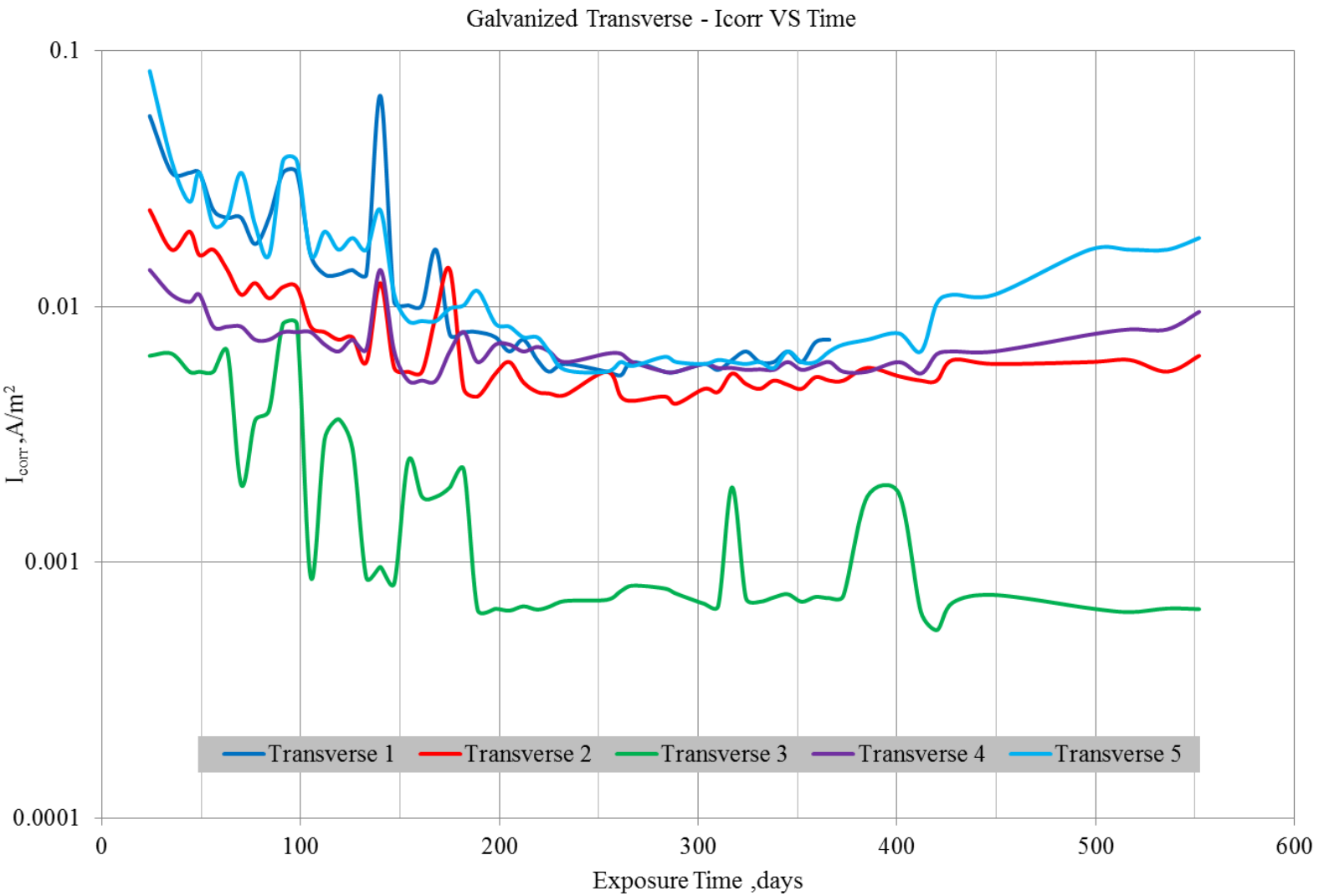

Figure A-18 Individual i_{corr} values for galvanized steel in transversely cracked concrete

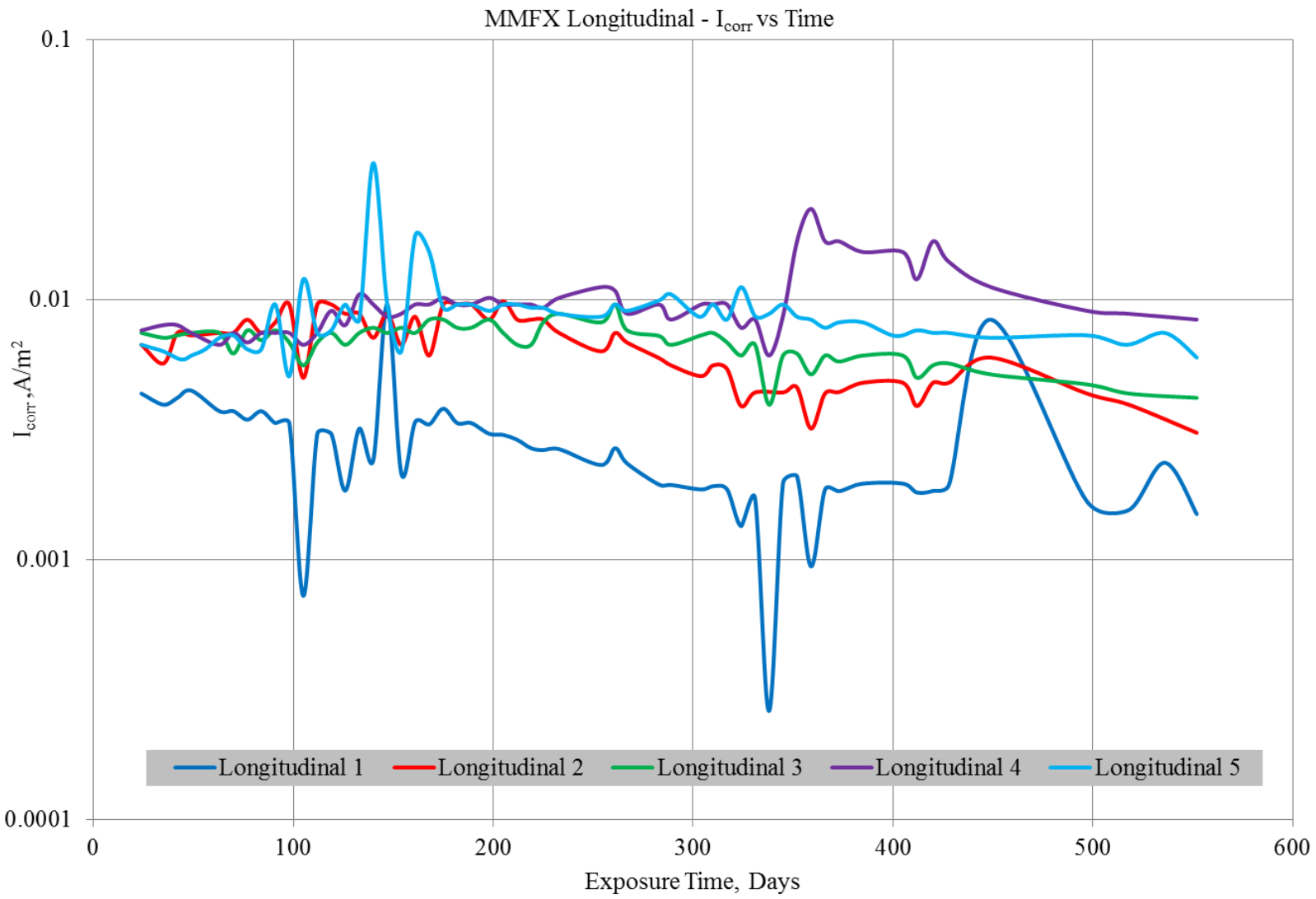

Figure A-19 Individual i_{corr} values for MMFX steel in longitudinally cracked concrete

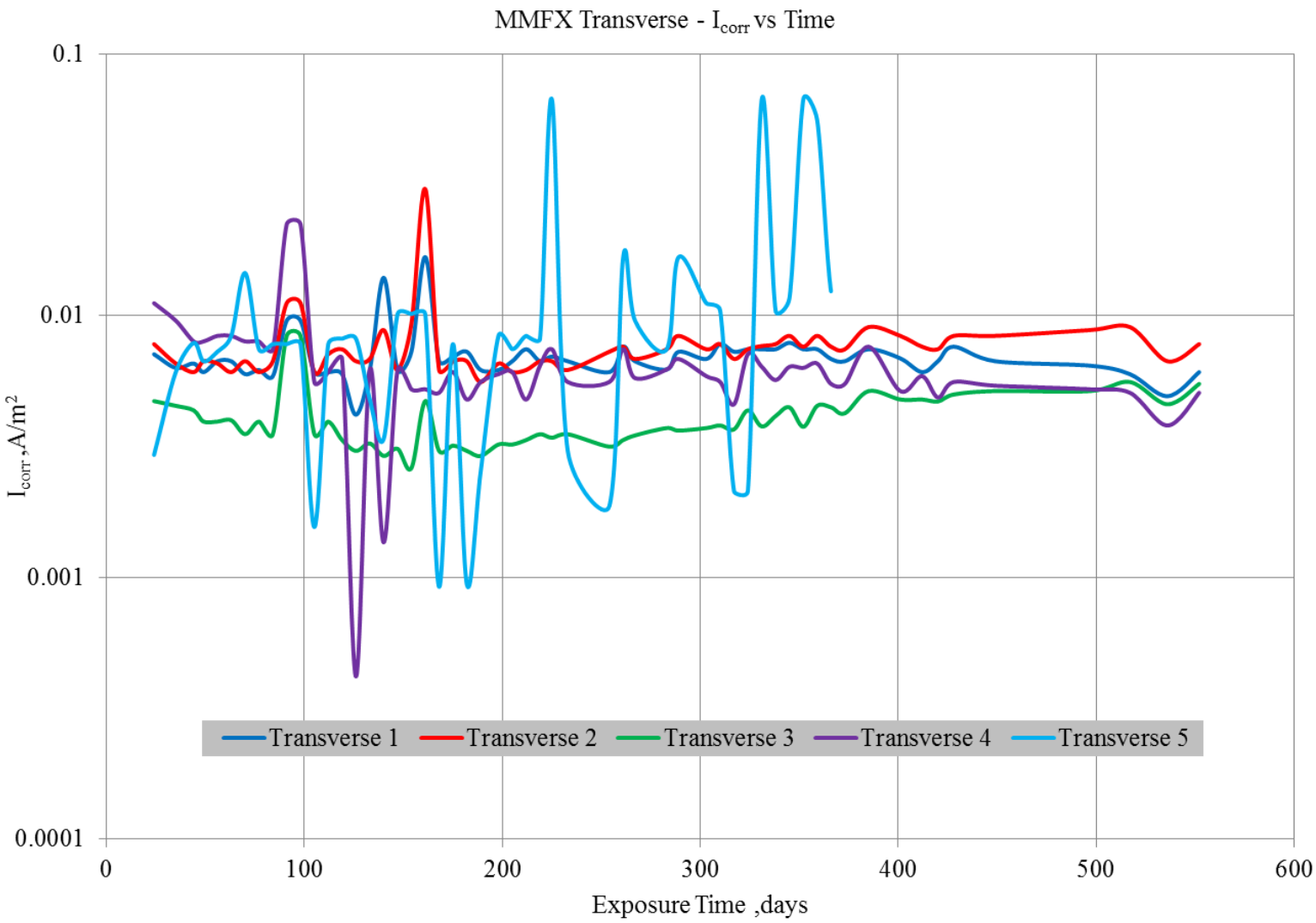

Figure A-20 Individual i_{corr} values for MMFX in transversely cracked concrete

Appendix B Individual E_{corr} Values

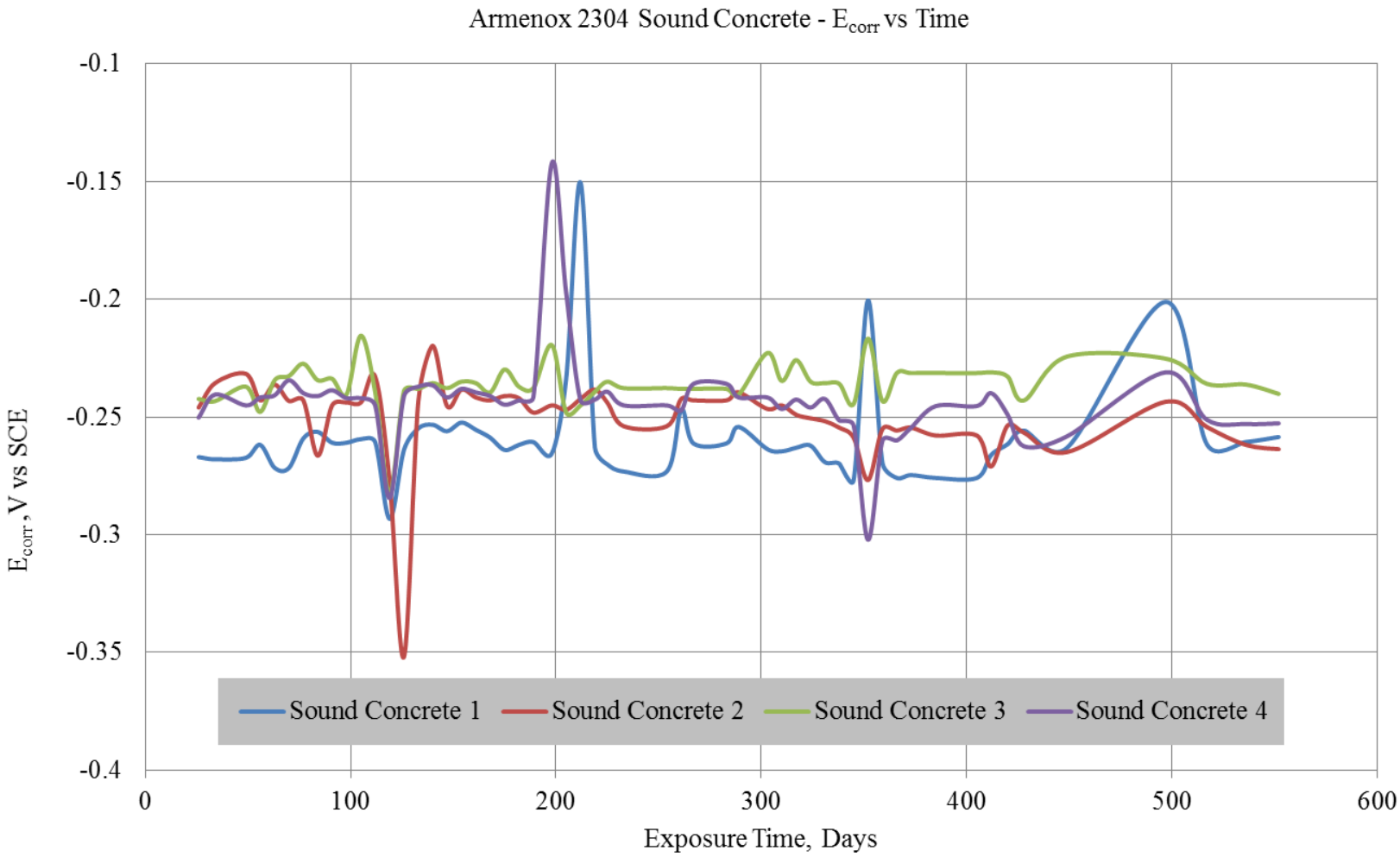

Figure B-1 Individual E_{corr} values for American Amrinox 2304 in sound concrete

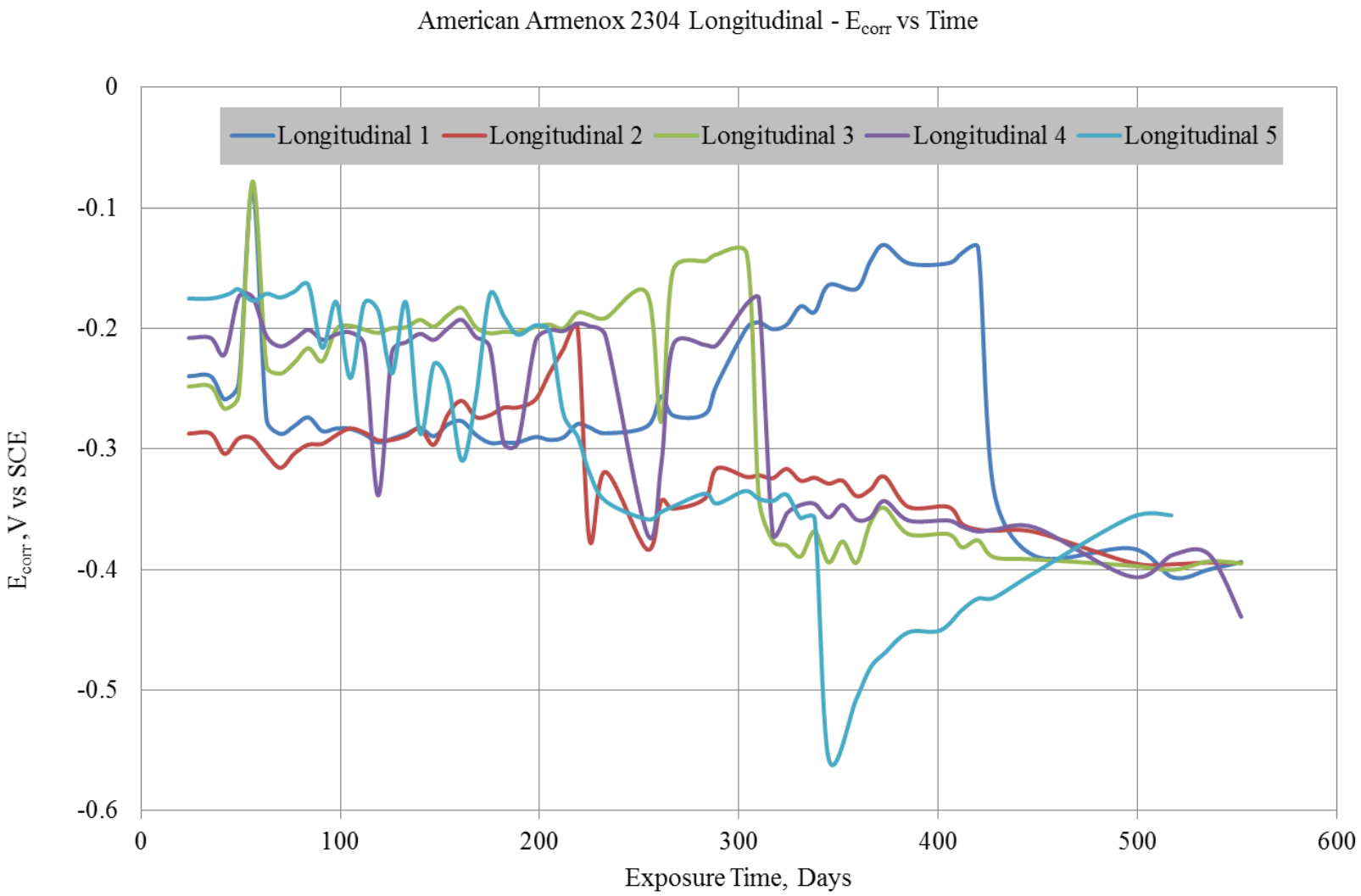

Figure B-2 Individual E_{corr} values for American Amrinox 2304 in longitudinally cracked concrete

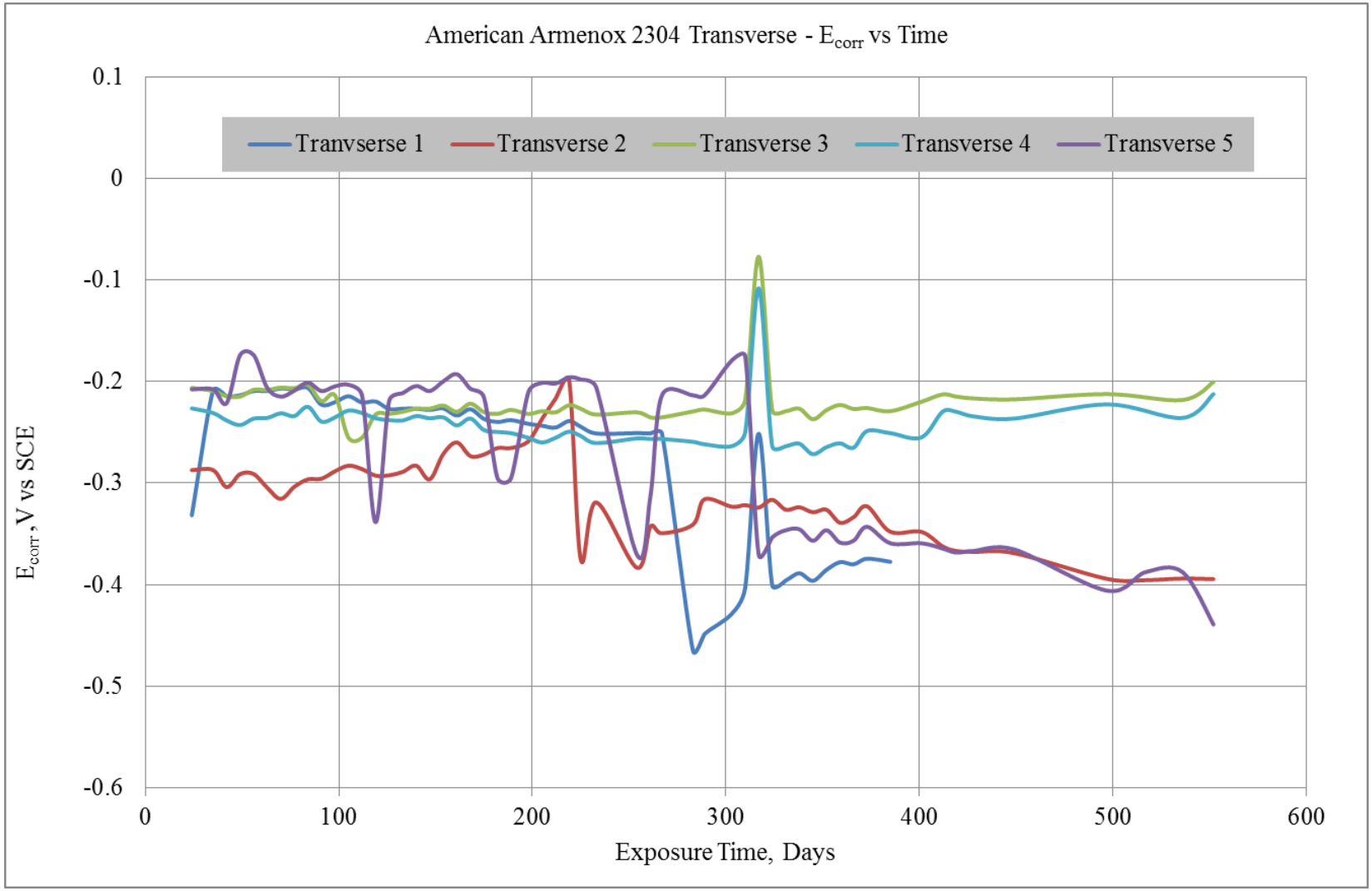

Figure B-3 Individual E_{corr} values for American Amrinox 2304 in transversely cracked concrete

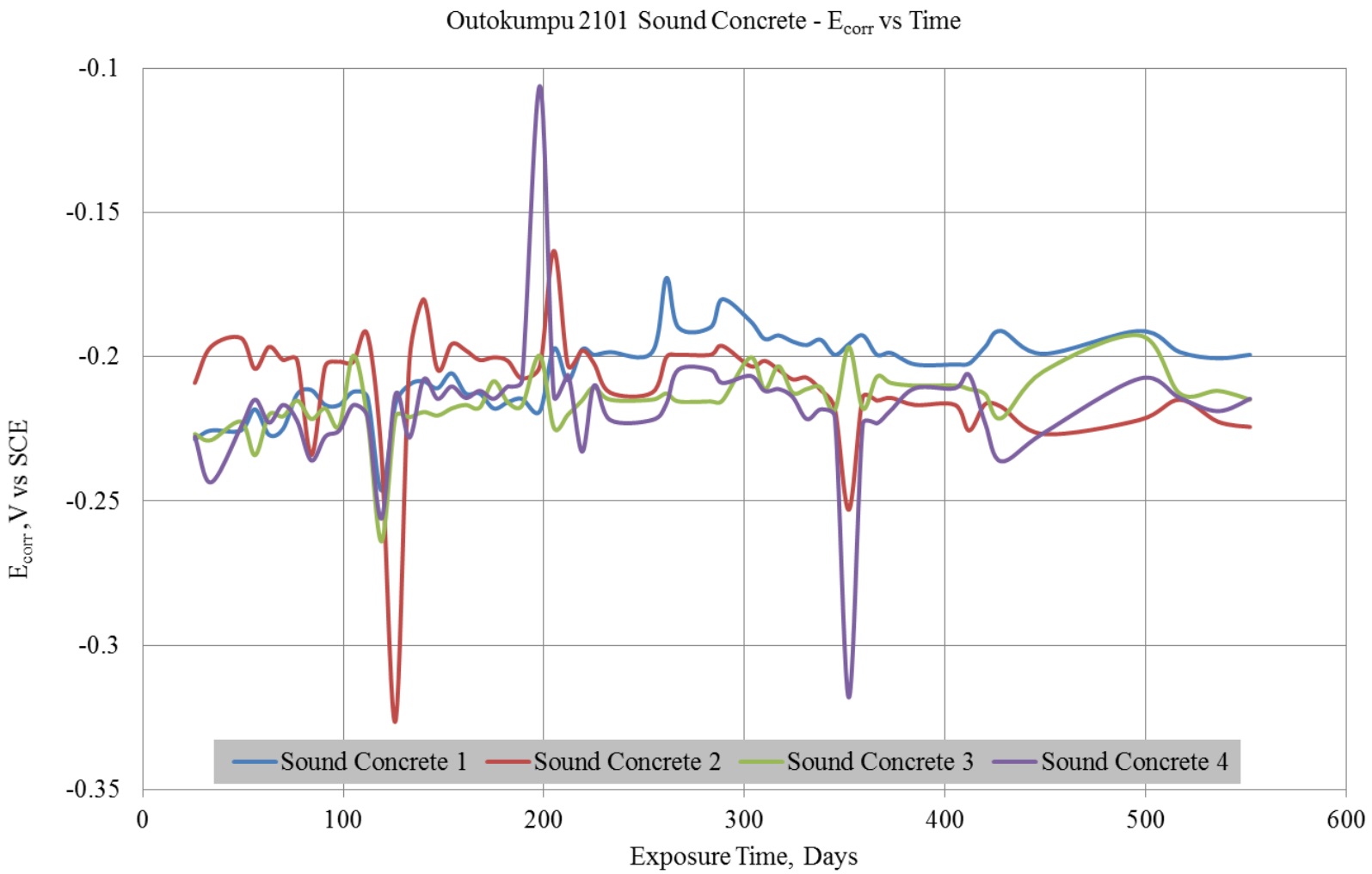

Figure B-4 Individual E_{corr} values for Outokumpu 2101 in sound concrete

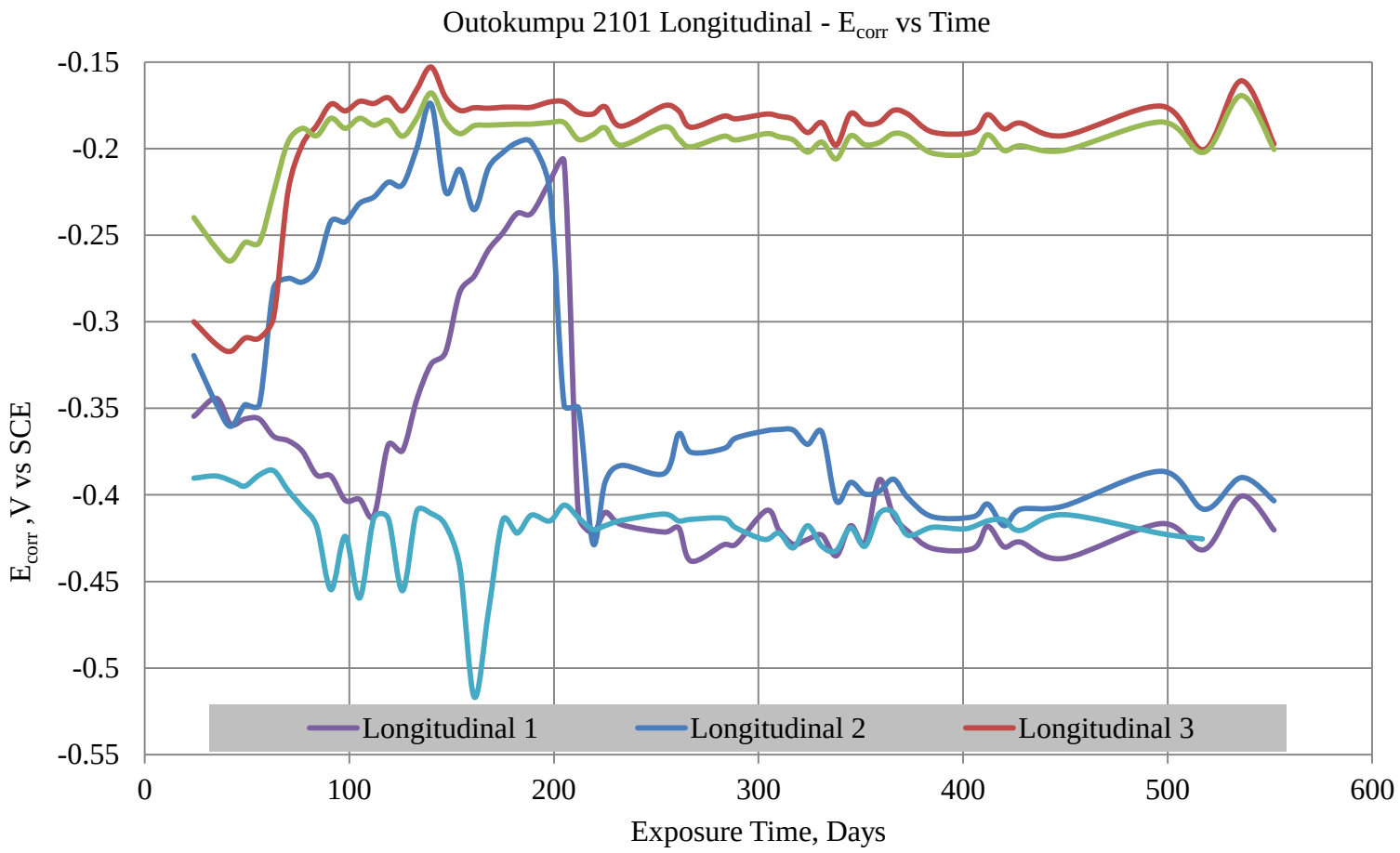

Figure B-5 Individual E_{corr} values for Outokumpu 2101 in longitudinally cracked concrete

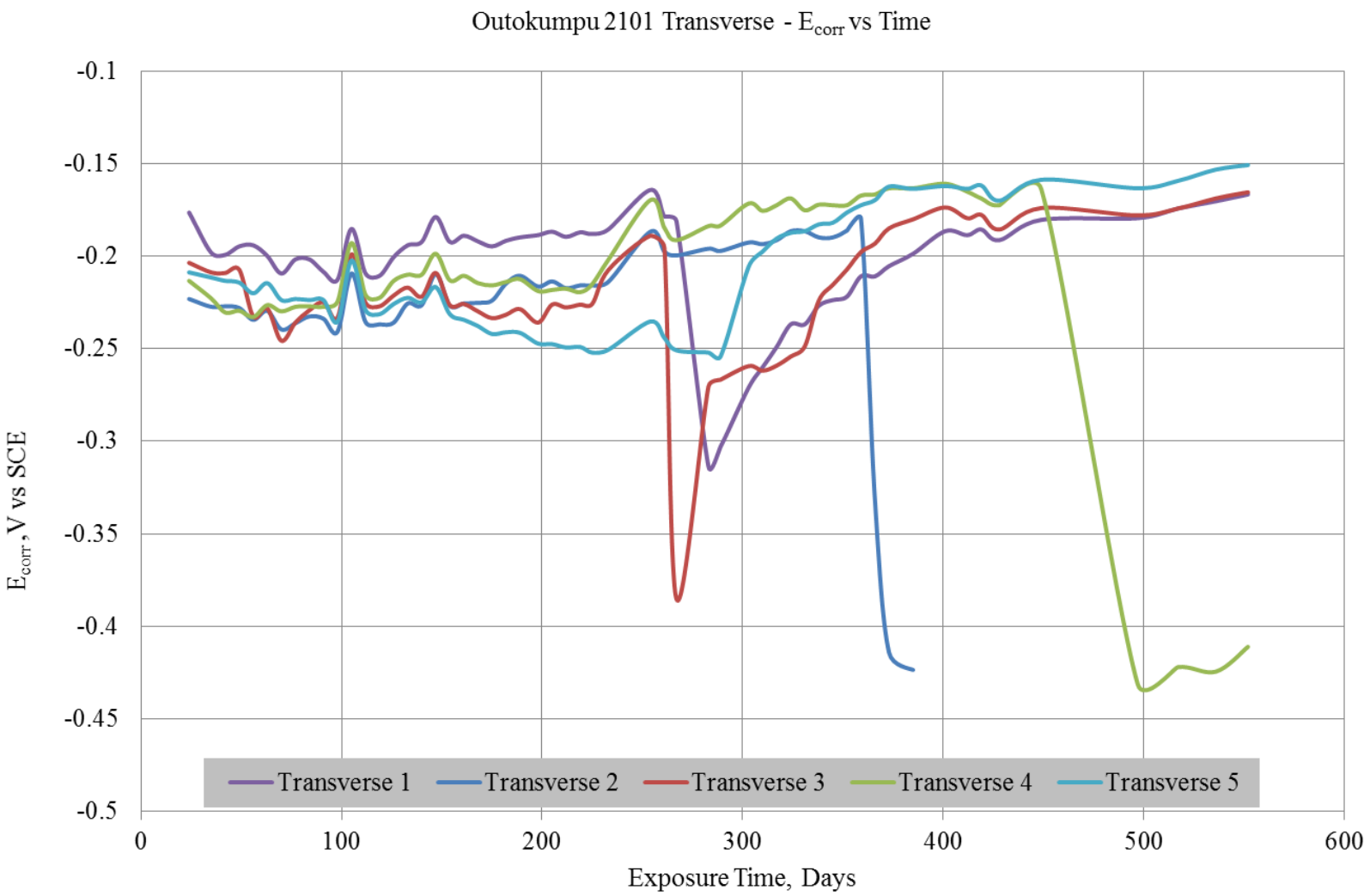

Figure B-6 Individual E_{corr} values for Outokumpu 2101 in transversely cracked concrete

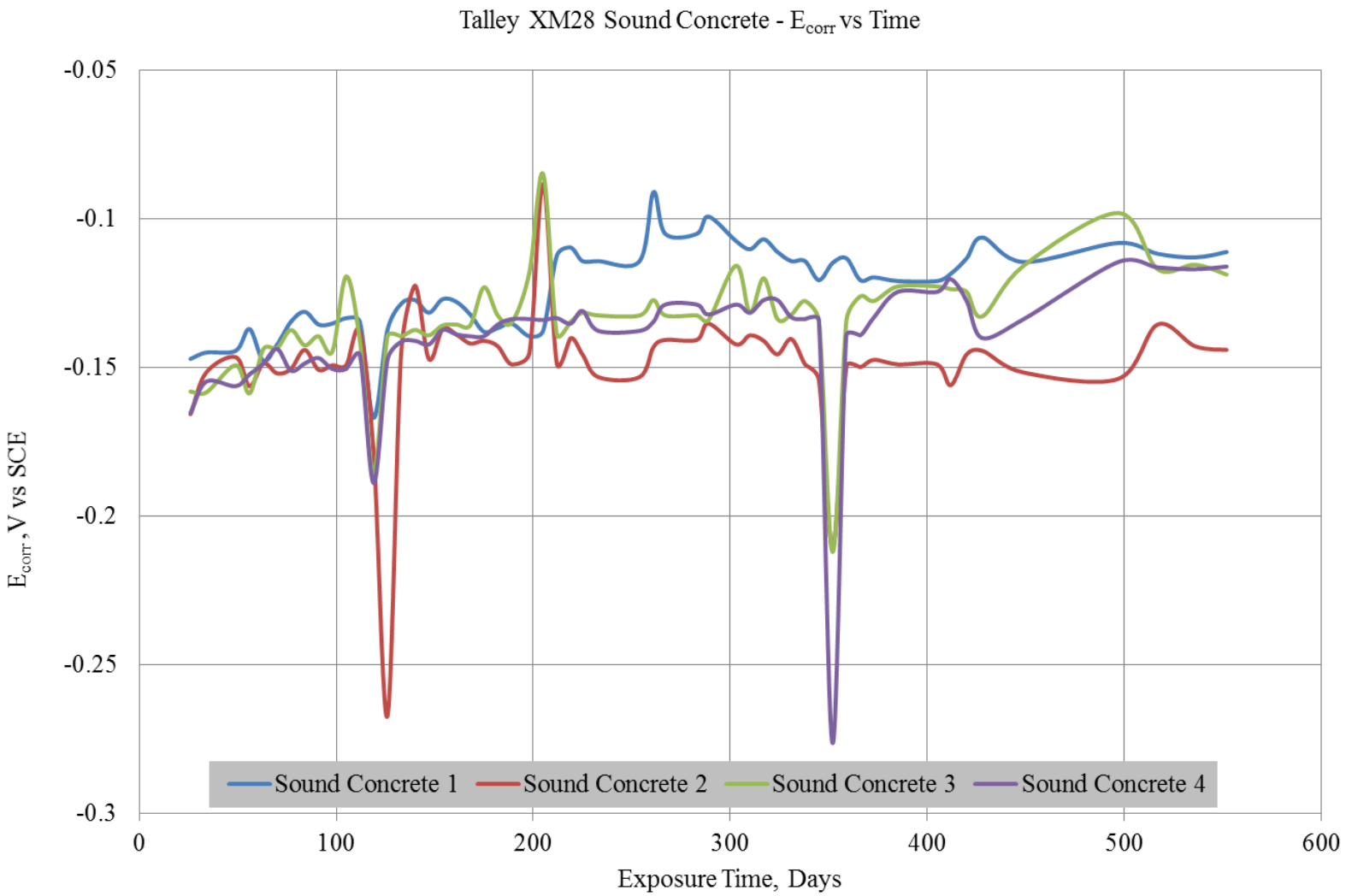

Figure B-7 Individual E_{corr} values for Talley XM28 in sound concrete

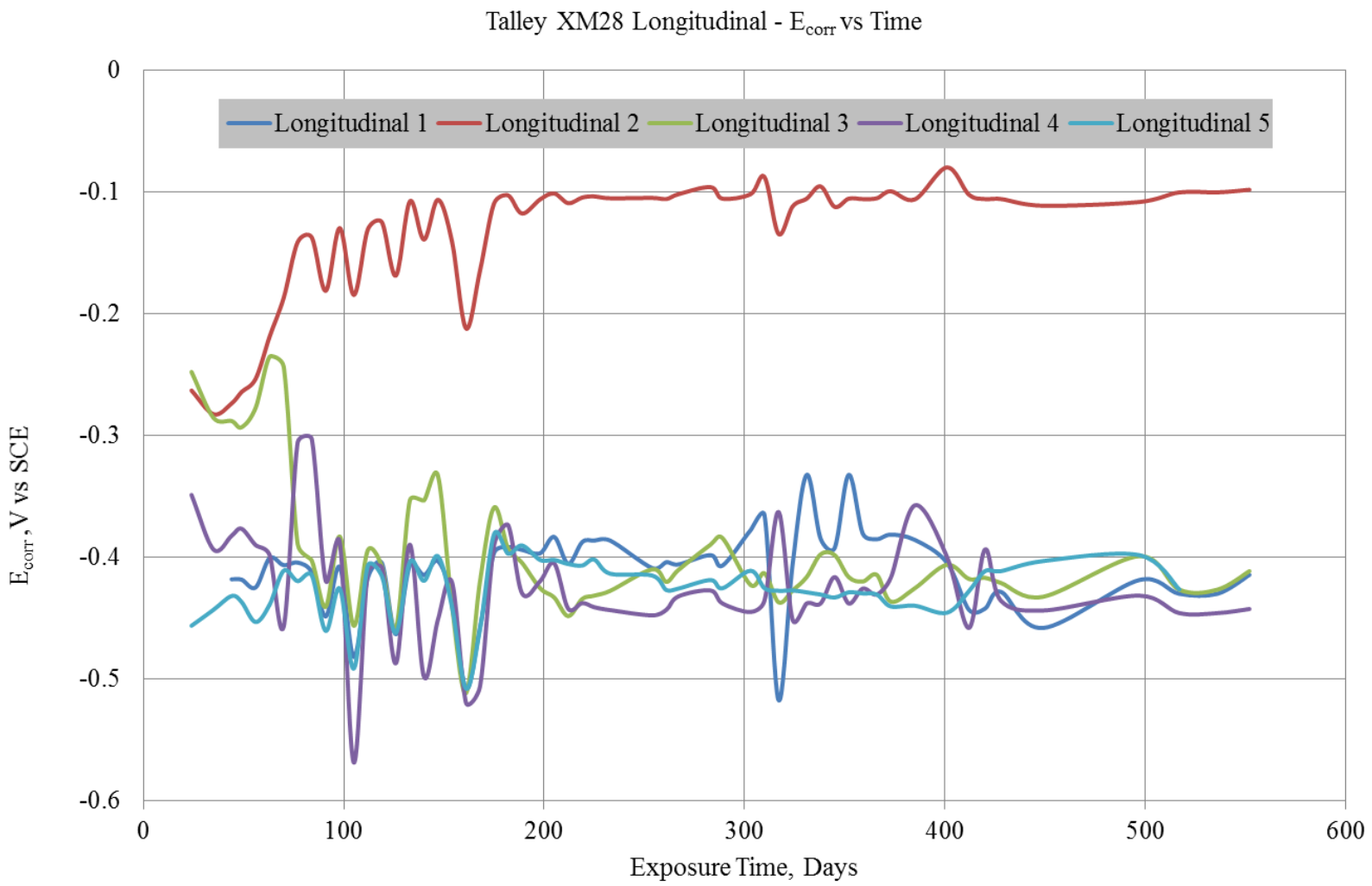

Figure B-8 Individual E_{corr} values for Talley XM28 in longitudinally cracked concrete

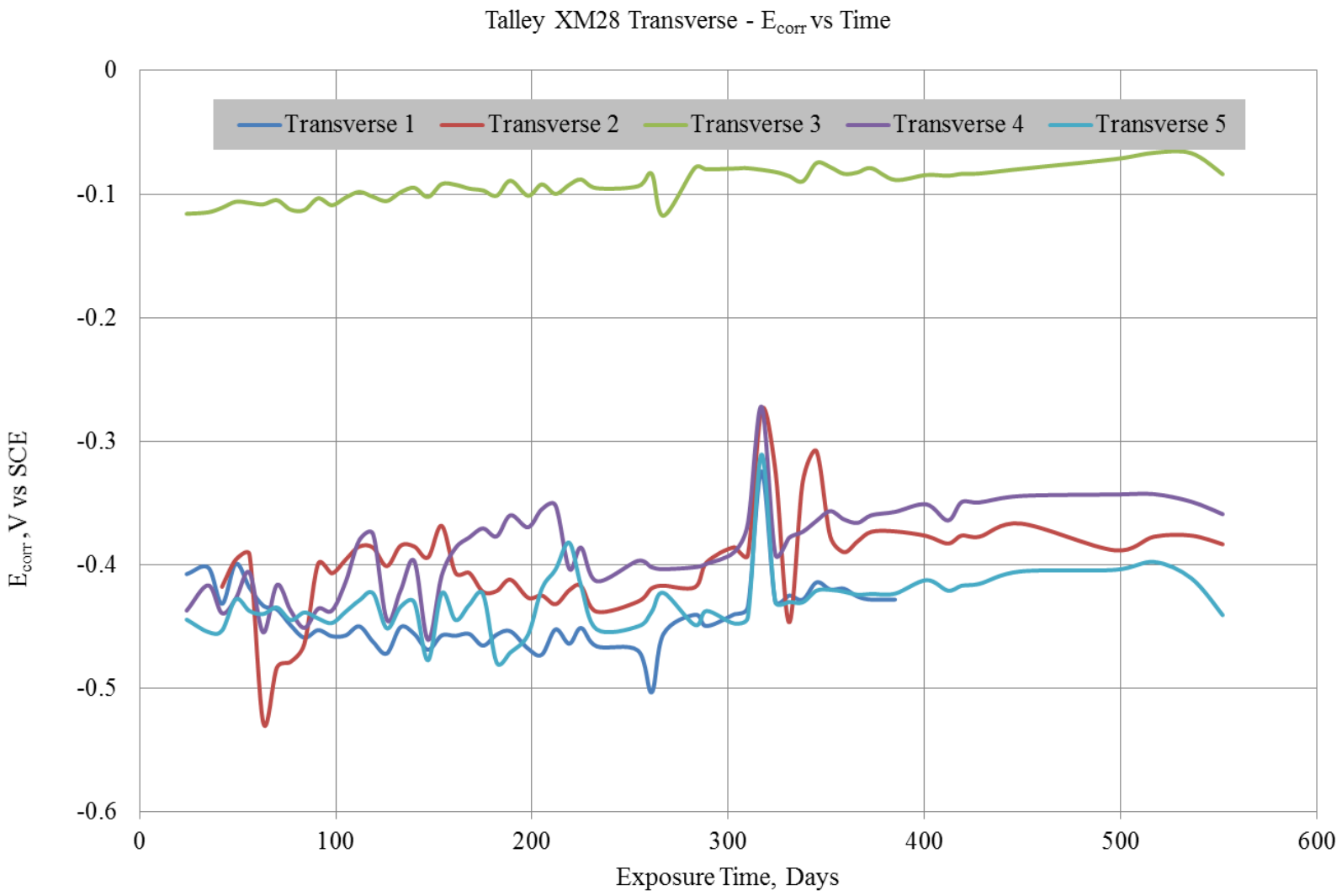

Figure B-9 Individual E_{corr} values for Talley XM28 in transversely cracked concrete

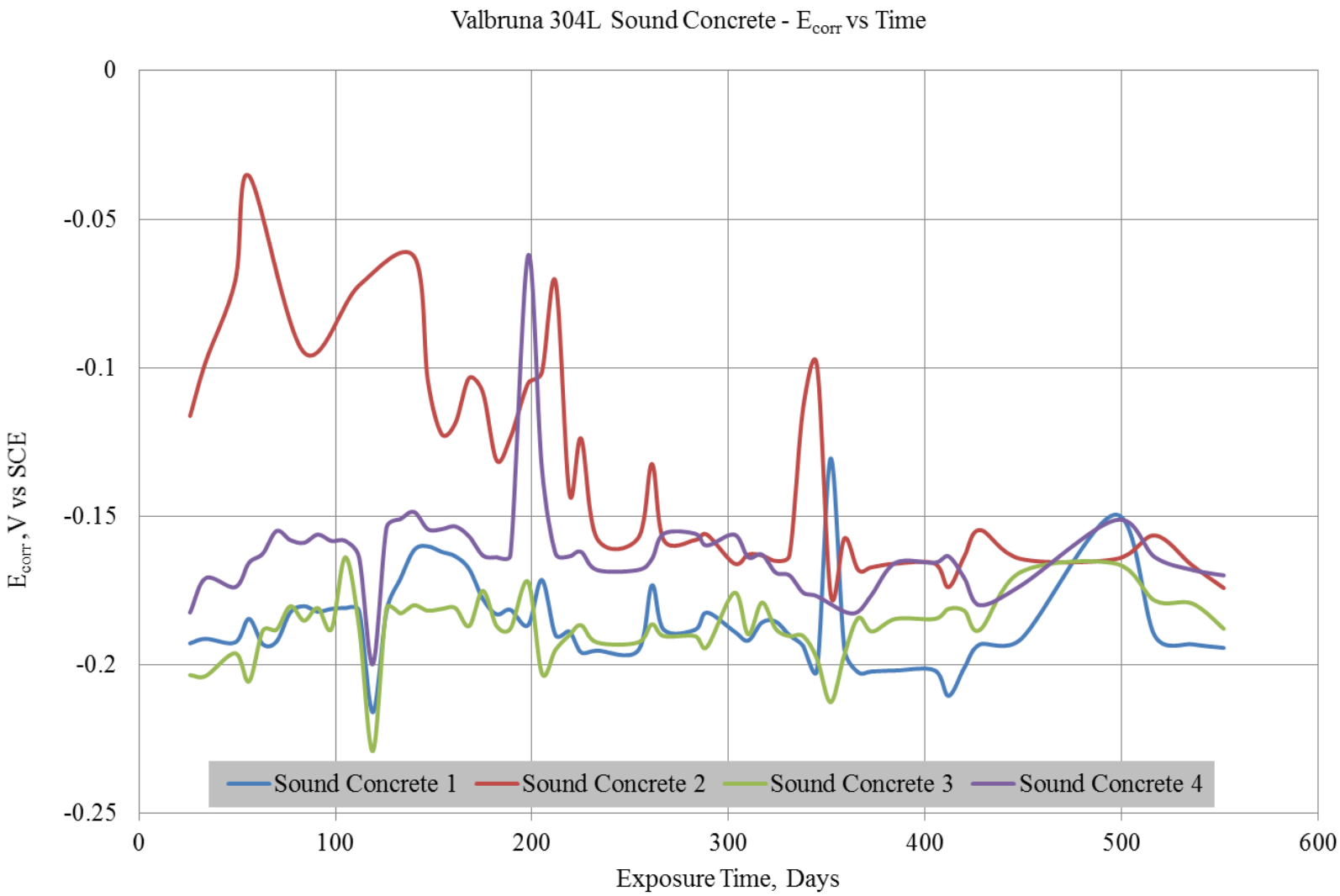

Figure B-10 Individual E_{corr} values for Valbruna 304L in sound concrete

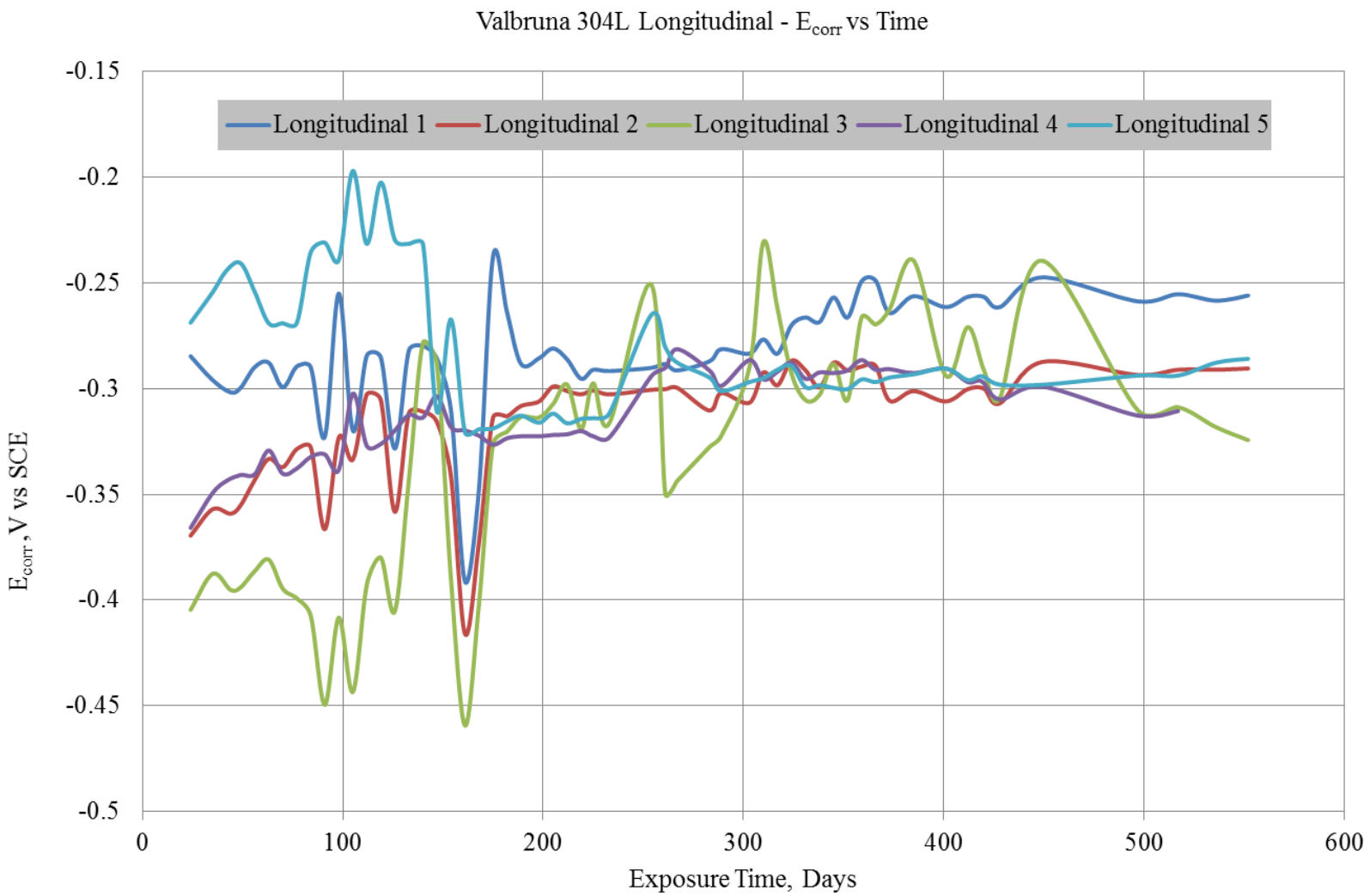

Figure B-11 Individual E_{corr} values for Valbruna 304L in longitudinally cracked concrete

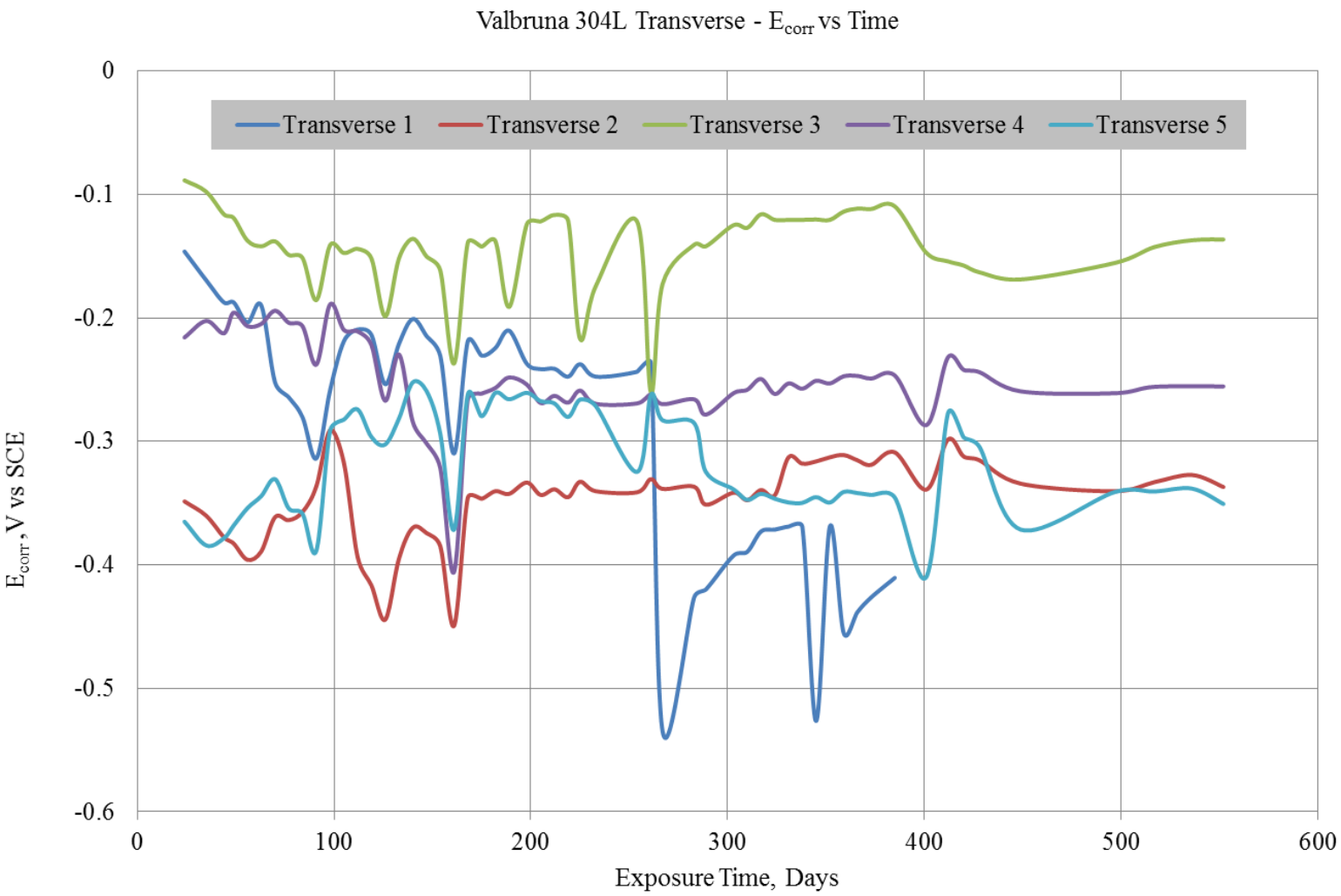

Figure B-12 Individual E_{corr} values for Valbruna 304L in transversely cracked concrete

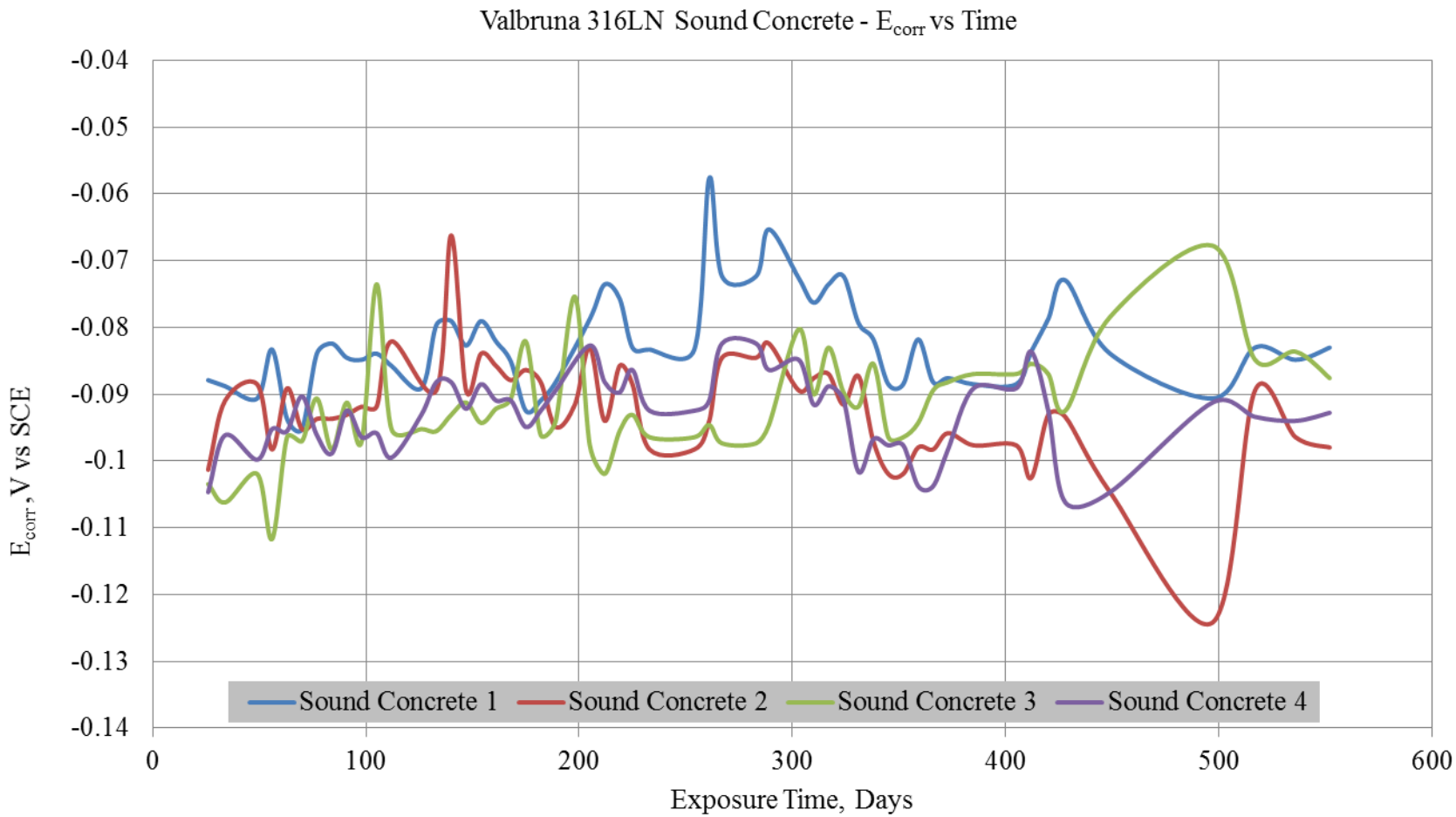

Figure B-13 Individual E_{corr} values for Valbruna 316LN in sound concrete

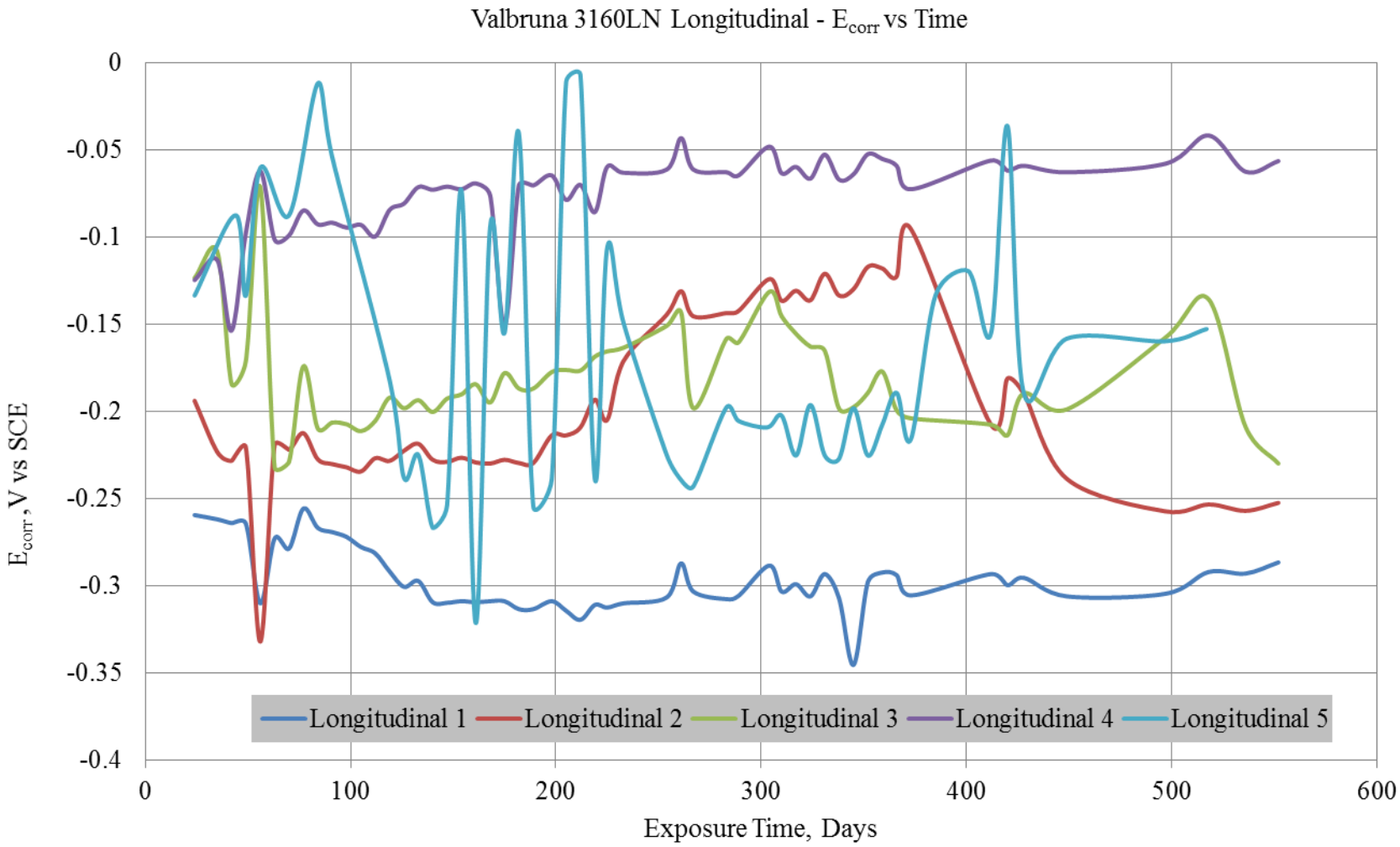

Figure B-14 Individual E_{corr} values for Valbruna 316LN in longitudinally cracked concrete

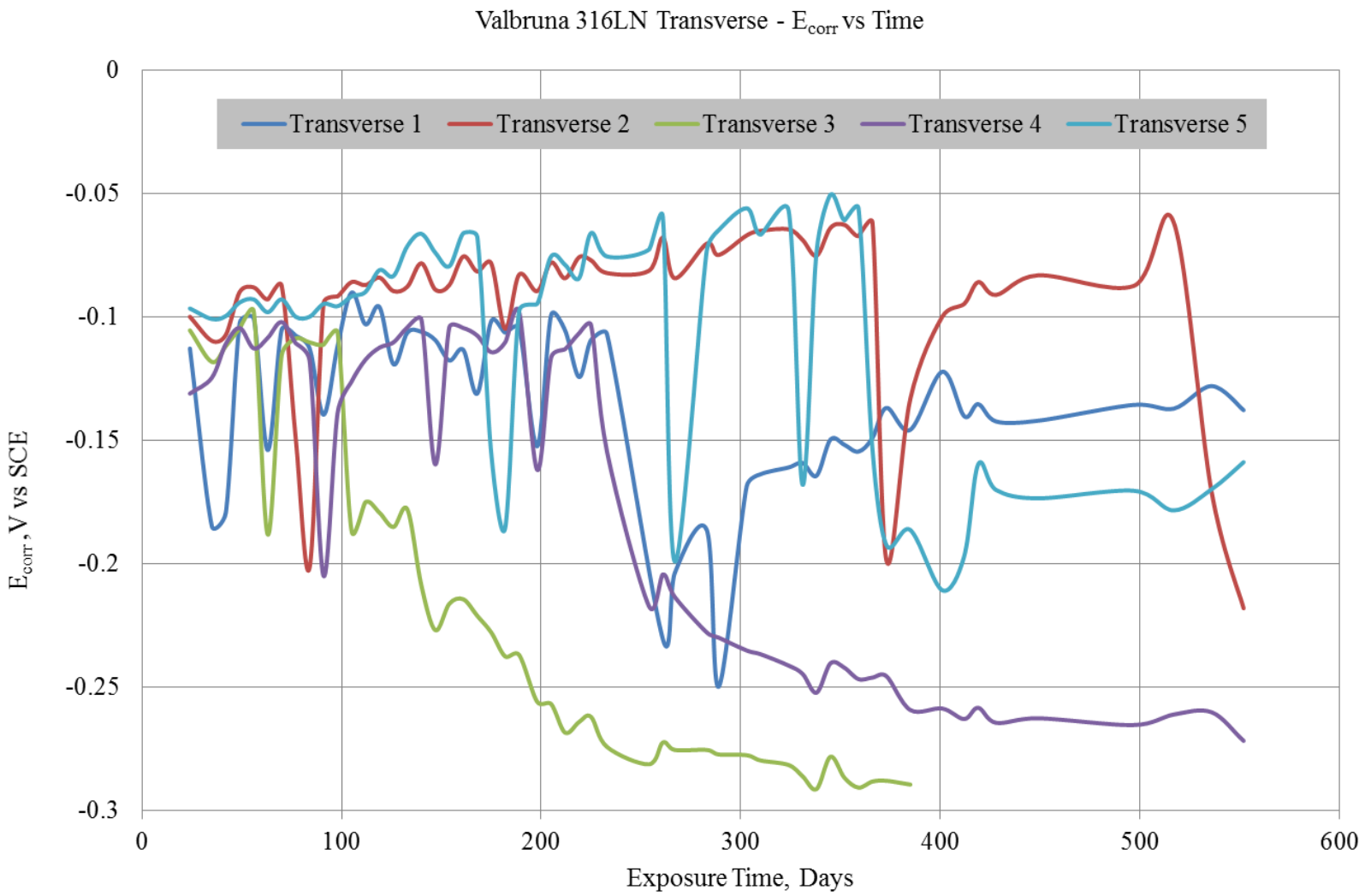

Figure B-15 Individual E_{corr} values for Valbruna 316LN in transversely cracked concrete

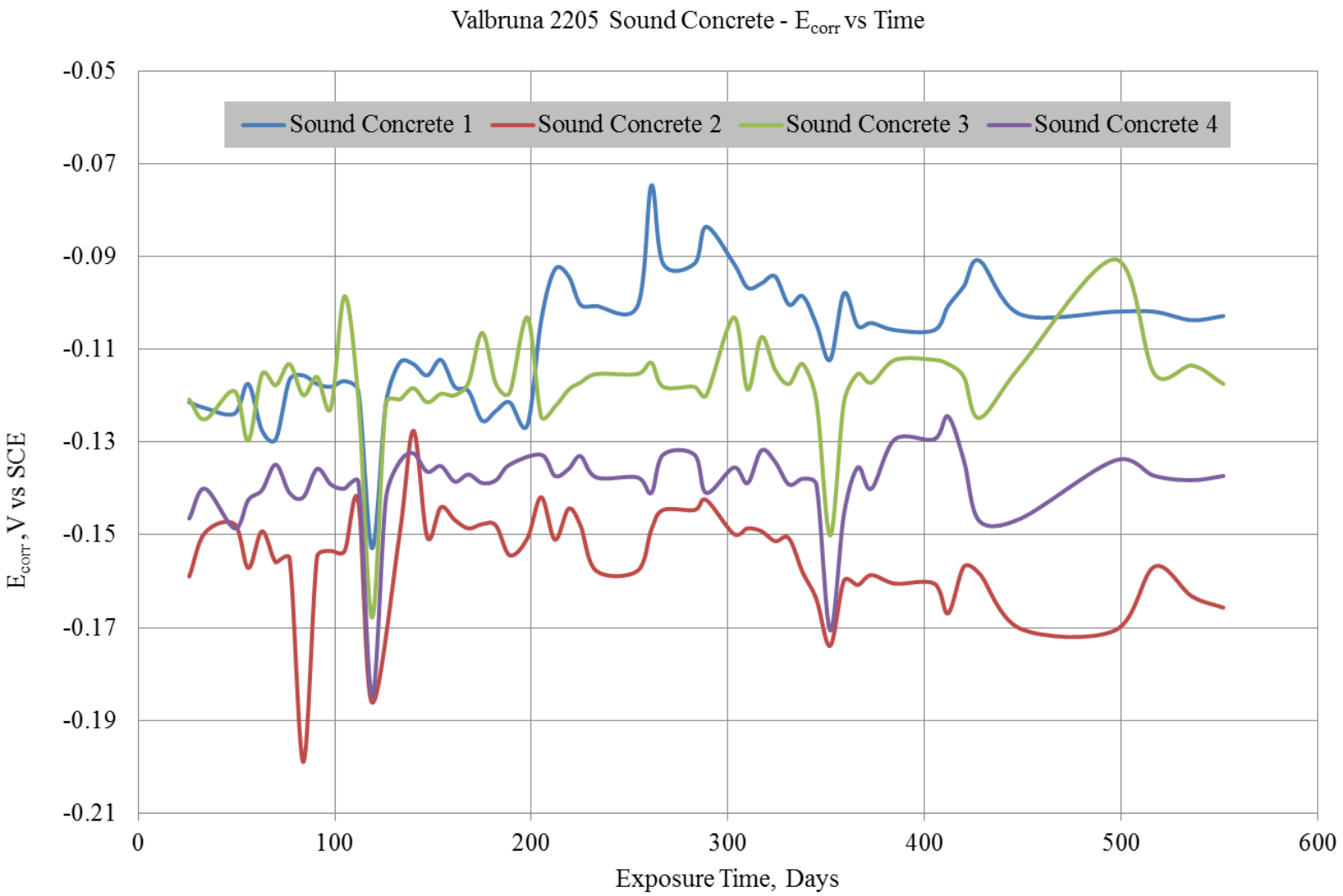

Figure B-16 Individual E_{corr} values for Valbruna 2205 in sound concrete

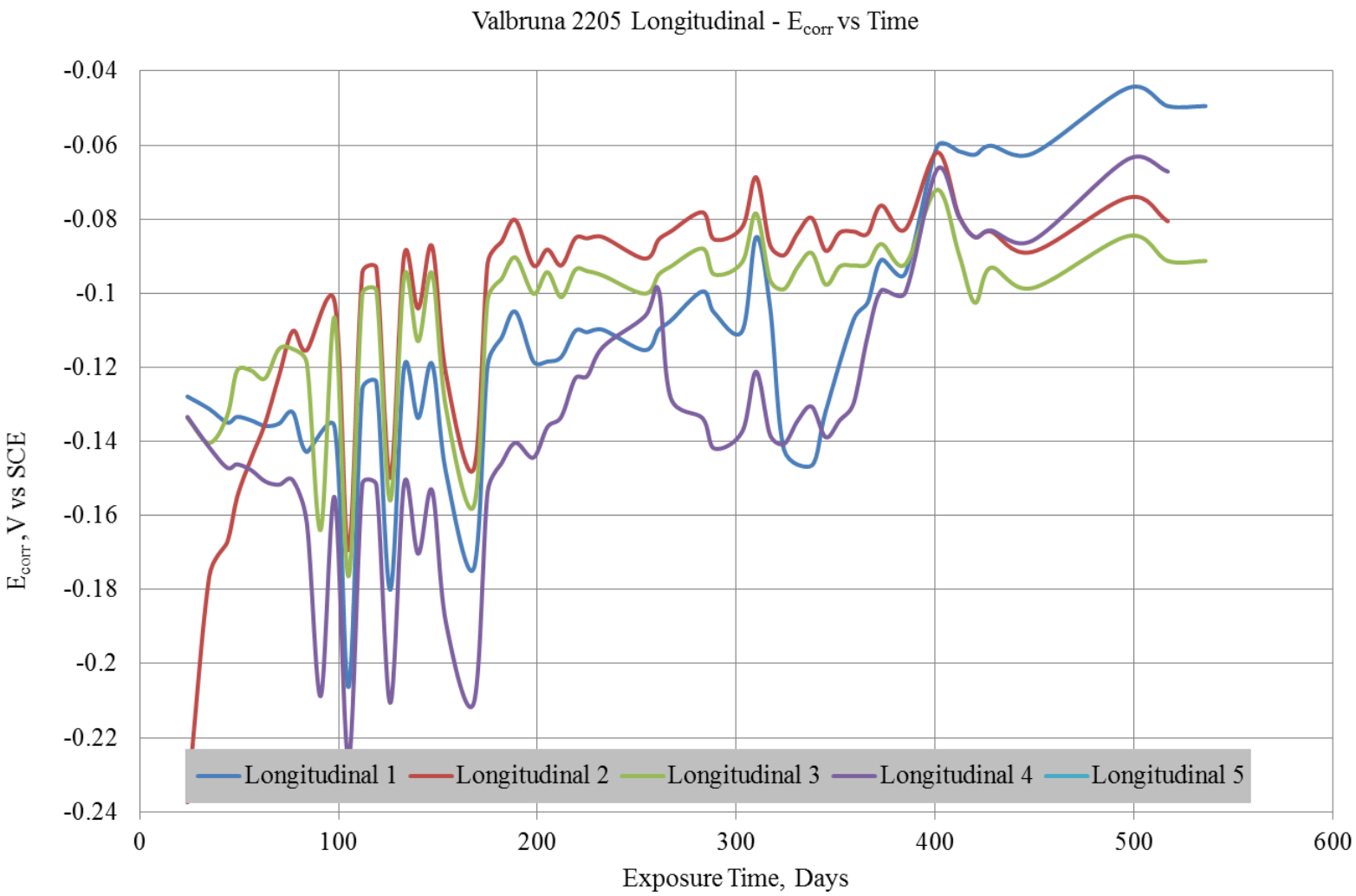

Figure B-17 Individual E_{corr} values for Valbruna 2205 in longitudinally cracked concrete

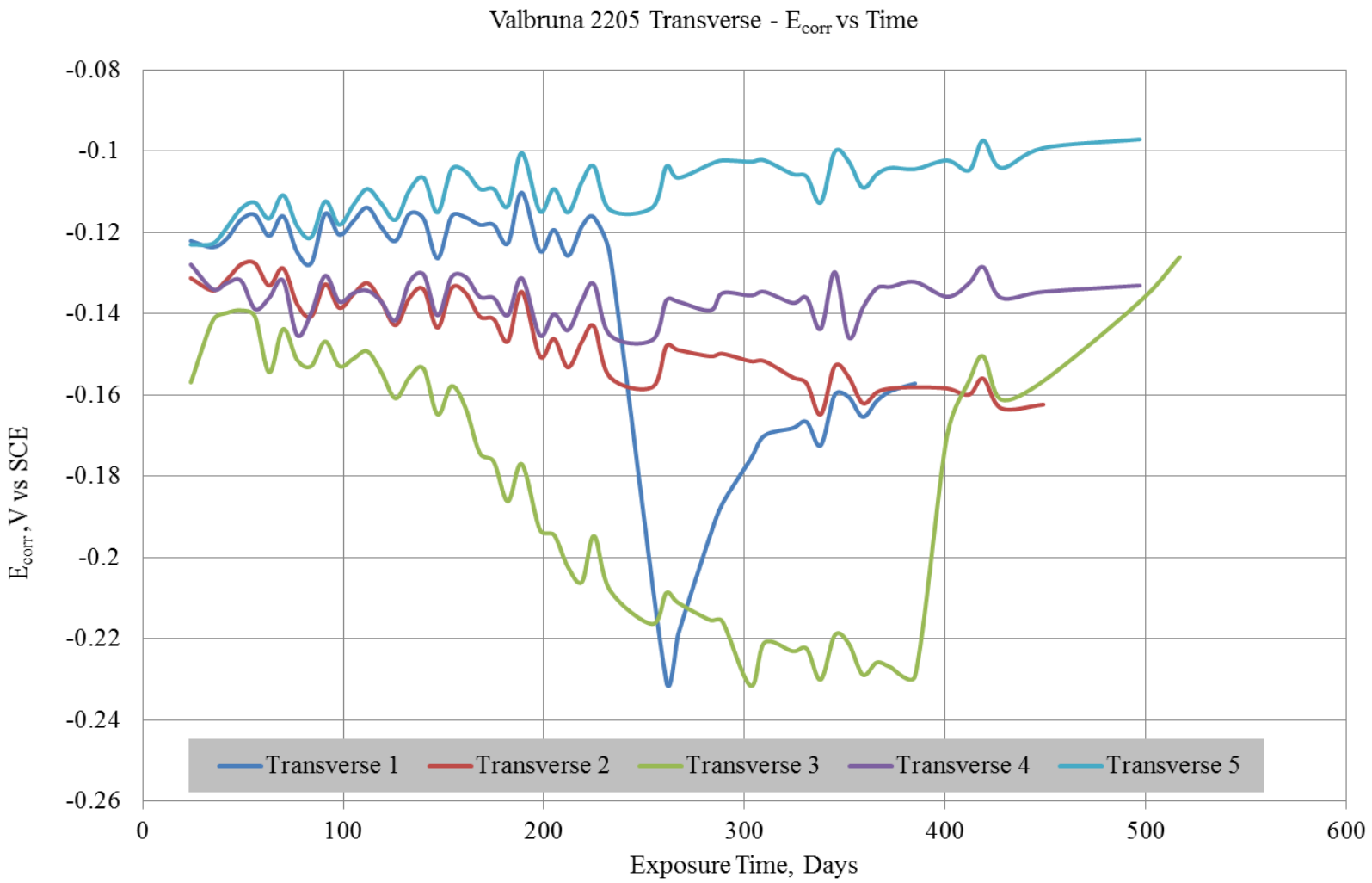

Figure B-18 Individual E_{corr} values for Valbruna 2205 in longitudinally cracked concrete

Appendix C Results of Transverse and Longitudinal Autopsy

Corrosion Results of Transversely Cracked Specimens						
Bar	#	Area (cm^2)	Crack Width	Score	Score	Rank
V2205	1	4.00	0.25mm-0.6mm	9.41	1.96	1st
	2	0.09	0.2mm - 0.4mm	0.30		
	3	0.00	0.2mm - 0.4mm	0.00		
	4	0.04	0.25mm - 0.5mm	0.11		
	5	0.00	0.3mm - 0.4mm	0.00		
A2304	1	6.00	0.4mm-0.5mm	13.33	2.94	2nd
	2	0.00	0.25mm - 0.4mm	0.00		
	3	0.25	0.25mm - 0.4mm	0.77		
	4	0.20	0.25mm - 0.4mm	0.62		
	5	0.00	0.25mm - 0.4mm	0.00		
O2101	1	2.25	0.15mm - 0.25mm	11.25	5.87	3rd
	2	1.00	0.2mm-0.4mm	3.08		
	3	1.00	0.15mm - 0.25mm	5.00		
	4	4.00	0.3mm - 0.5mm	10.00		
	5	0.00	0.15mm - 0.3mm	0.00		
304	1	13.00	0.25mm-0.5mm	34.67	9.24	4th
	2	2.25	0.15mm - 0.4mm	8.18		
	3	0.09	0.15mm - 0.3mm	0.40		
	4	0.25	0.15mm - 0.33mm	1.04		
	5	1.00	0.25mm - 0.8mm	1.90		
VXM28	1	3.00	0.25mm - 0.4mm	9.23	11.15	5th
	2	7.54	0.3mm - 0.5mm	18.85		
	3	3.50	0.25mm - 0.4mm	10.77		
	4	2.00	0.25mm - 0.33mm	6.90		
	5	2.00	0.15mm-0.25mm	10.00		
V316	1	11.31	0.15mm - 0.33mm	47.12	16.13	6th
	2	1.00	0.15mm-0.33mm	4.17		
	3	1.00	0.1mm -0.15mm	8.00		
	4	6.28	0.3mm - 0.5mm	15.71		
	5	1.50	0.2mm - 0.33mm	5.66		
TXM28	1	12.00	0.25mm-0.4mm	36.92	50.79	7th
	2	15.08	0.15mm - 0.2mm	86.17		
	3	0.25	0.15mm - 0.2mm	1.43		
	4	15.08	0.2mm - 0.3mm	60.32		
	5	27.65	0.3mm - 0.5mm	69.12		

Corrosion Results of Longitudinally Cracked Specimens						
Bar	#	Area (cm^2)	Crack Width	Score	Score	Rank
V2205	1	0.00	0.10mm-0.20mm	0.0	0	1st
	2	0.00	0.10mm-0.25mm	0.0		
	3	0.00	0.10mm-0.20mm	0.0		
	4	0.00	0.15mm-0.30mm	0.0		
	5	0.00	0.10mm-0.15mm	0.0		
O2101	1	6.70	0.15mm-0.40mm	24.4	17.3	2nd
	2	10.05	0.15mm-0.30mm	44.7		
	3	0.25	0.10mm-0.15mm	2.0		
	4	0.00	0.10mm-0.15mm	0.0		
	5	5.03	0.20mm-0.45mm	15.5		
A2304	1	5.03	0.20mm-0.33mm	19.0	32.7	3rd
	2	15.08	0.20mm-0.33mm	56.9		
	3	1.50	0.20mm-0.25mm	6.7		
	4	2.00	0.30mm-0.50mm	5.0		
	5	22.00	0.25mm-0.33mm	75.9		
304	1	9.42	0.15mm-0.20mm	53.9	59.6	4th
	2	15.71	0.20mm-0.30mm	62.8		
	3	13.57	0.20mm-0.40mm	45.2		
	4	15.71	0.20mm-0.40mm	52.4		
	5	12.57	0.10mm-0.20mm	83.8		
VXM28	1	10.05	0.25mm-0.40mm	30.9	60.9	5th
	2	15.08	0.20mm-0.33mm	56.9		
	3	15.08	0.15mm-0.20mm	86.2		
	4	7.54	0.10mm-0.20mm	50.3		
	5	10.05	0.10mm-0.15mm	80.4		
V316	1	20.11	0.25mm-0.80mm	38.3	63.2	6th
	2	17.59	0.10mm-0.20mm	117.3		
	3	17.59	0.10mm-0.20mm	117.3		
	4	0.00	0.10mm-0.15mm	0.0		
	5	7.54	0.15mm-0.20mm	43.1		
TXM28	1	32.67	0.15mm-0.30mm	145.2	87.6	7th
	2	3.00	0.10mm-0.15mm	24.0		
	3	23.05	0.10mm-0.15mm	184.4		
	4	10.05	0.25mm-0.40mm	30.9		
	5	6.70	0.10mm-0.15mm	53.6		